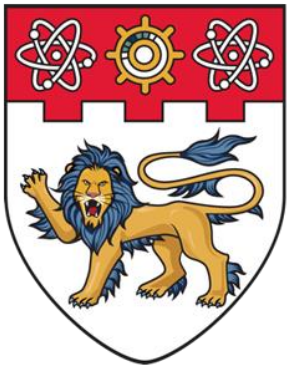

NANYANG TECHNOLOGICAL UNIVERSITY
SINGAPORE

DIRECT C-H ARYLATION AS A TOOL FOR SYNTHESIS OF CONJUGATED POLYMERS: FROM 1D LINEAR POLYMERS TO 2D/3D POROUS NETWORKS

HASSAN BOHRA

SCHOOL OF CHEMICAL AND BIOMEDICAL ENGINEERING

2018

A thesis submitted to Nanyang Technological University in fulfilment of the requirement for the degree of Doctor of Philosophy

Statement of Originality

I hereby certify that the work embodied in this thesis is the result of original research, is free of plagiarised materials, and has not been submitted for a higher degree to any other University or Institution.

6 Mar. 2019
Date

HASSAN BOHRA
Name and Signature

Authorship Attribution Statement

This thesis contains material from 5 papers published in the following peer-reviewed journals in which I am listed as an author.

Parts of Chapter 1 are published as Bohra, H.; Wang, M. Direct C-H Arylation: A "Greener" Approach Towards Facile Synthesis of Organic Semiconducting Molecules and Polymers. *J. Mater. Chem. A* **2017**, *5*, 11550-11571. DOI: 10.1039/c7ta00617a

The contributions of the co-authors are as follows:

- Prof. Wang provided the direction for the review article and revised the manuscript drafts.
- I prepared the manuscript drafts.

Chapter 2 is published as Bohra, H.; Shao, J.; Huang, S.; Wang, M. Facile Synthesis of Naphthodithiophenediimide Based Small Molecules and Polymers Via Direct Arylation Coupling. *Tetrahedron Lett.* **2016**, *57*, 1497-1501. DOI: 10.1016/j.tetlet.2016.02.081

The contributions of the co-authors are as follows:

- Prof. Wang directed the project, designed the experiments, discussed the results and revised the manuscript.
- I wrote the manuscript and analyzed the data. The manuscript was revised together with Dr. Shao.
- I performed all the material synthesis, carried out chromatography experiments, conducted NMR spectroscopy, UV-visible and fluorescence spectroscopy and collected cyclic voltammetry data.
- Dr. Shao assisted in the synthesis of precursors for Naphthodithiophenediimide.
- Dr. Shuo assisted in thermogravimetric analysis and differential scanning calorimetry experiments.

Chapter 3 is published as Bohra, H.; Chen, H.; Peng, Y.; Efrem, A.; He, F.; Wang, M. Direct arylation polymerization toward efficient synthesis of benzo[1,2-c:4,5-c'] dithiophene-4,8-dione based donor-acceptor alternating copolymers for organic

optoelectronic applications. *J. Polym. Sci. A: Polym. Chem.*, **2018**, 56, 2554-2564. DOI: 10.1002/pola.29235

The contributions of the co-authors are as follows:

- Prof. Wang directed the project, designed the experiments, discussed the results and revised the manuscripts.
- I designed the experiments, analyzed the data, and wrote the manuscript. The manuscript was revised together with Dr. Chen and Prof. He.
- I performed all the material synthesis, carried out chromatography experiments, conducted NMR, UV-visible, and fluorescence spectroscopy and collected cyclic voltammetry, thermogravimetric analysis, and differential scanning calorimetry data.
- I fabricated organic field-effect transistor devices and tested their performance.
- Dr. Chen fabricated organic solar cell devices and tested their performance.
- Ms. Peng performed atomic force microscopy experiments.
- Dr. Efrem synthesized 3,3'''-dioctyl-2,2':5',2'':5'',2'''-quaterthiophene.

Chapter 4 is published as Bohra, H.; Tan, S. Y.; Shao, J.; Yang, C.; Efrem, A.; Zhao, Y.; Wang, M. Narrow Bandgap Thienothiadiazole-Based Conjugated Porous Polymers: From Facile Direct Arylation Polymerization to Tunable Porosities and Optoelectronic Properties. *Polym. Chem.* **2016**, *7*, 6413-6421. DOI: 10.1039/c6py01453d

The contributions of the co-authors are as follows:

- Prof. Wang directed the project, designed the experiments, discussed the results and revised the manuscripts.
- I designed the experiments, analyzed the data, and wrote the manuscript. The manuscript was revised together with Prof. Zhao.
- I performed all the material synthesis, carried out chromatography experiments, conducted solution-state NMR spectroscopy, UV-visible-NIR and fluorescence spectroscopy, infrared spectroscopy, and scanning electron microscopy and collected cyclic voltammograms, X-ray diffractograms and thermogravimetric analysis data.

- Dr. Tan conducted solid-state NMR spectroscopy and collected N_2 adsorption isotherms.
- Dr. Shao synthesized the precursors to Thienothiadiazole.
- Dr. Yang assisted with transmission electron microscopy experiments.

Chapter 6 is published as Bohra, H.; Li, P.; Yang, C.; Zhao, Y.; Wang, M. "Greener" and Modular Synthesis of Triazine-Based Conjugated Porous Polymers Via Direct Arylation Polymerization: Structure–Function Relationship and Photocatalytic Application. *Polym. Chem.* **2018**, *9*, 1972-1982. DOI: 10.1039/c8py00025e

The contributions of the co-authors are as follows:

- Prof. Wang directed the project, designed the experiments, discussed the results and revised the manuscripts.
- I designed the experiments, analyzed the data, and wrote the manuscript. The manuscript was revised together with Prof. Zhao.
- I performed all the material synthesis and photocatalysis experiments, carried out chromatography experiments, conducted solution-state NMR spectroscopy, UV-visible and fluorescence spectroscopy, infrared spectroscopy, and scanning electron microscopy and collected cyclic voltammograms, X-ray diffractograms, N_2 adsorption isotherms, and thermogravimetric analysis data.
- Dr. Li conducted solid-state NMR spectroscopy.
- Dr. Yang assisted with transmission electron microscopy.

6 Mar. 2019
Date

HASSAN BOHRA
Name and Signature

Supervisor Declaration Statement

I have reviewed the content and presentation style of this thesis and declare it is free of plagiarism and of sufficient grammatical clarity to be examined. To the best of my knowledge, the research and writing are those of the candidate except as acknowledged in the Author Attribution Statement. I confirm that the investigations were conducted in accord with the ethics policies and integrity standards of Nanyang Technological University and that the research data are presented honestly and without prejudice.

6 Mar, 2019
Date

WANG Mingfeng
Supervisor's Name and Signature

ACKNOWLEDGEMENT

First and foremost, I would like to thank my supervisor, Prof. Mingfeng Wang for giving me the opportunity to pursue a Ph.D. degree. His scientific acumen, innovative insight and patient guidance have helped me grow as a researcher. His assistance in all aspects of my work from experiment design, to analysis of results has been a tremendous encouragement to pursue scientific research of the highest quality.

I am also indebted to Dr. Jinjun Shao, whose mentorship made me a competent organic chemist. His patience as a tutor and cordiality as a colleague helped me get through some challenging times.

I would like to thank the following collaborators for aiding with my research:

Prof. Yanli Zhao, Dr. Si Yu Tan, Dr. Peizhou Li and Mr. Wee Kong Ong for their help with solid-state ^{13}C NMR spectroscopy.

Prof. Feng He and Dr. Hui Chen for their help with fabrication and testing of organic solar cells.

Prof. Rong Xu for providing access to diffuse-reflectance UV-Vis spectrometer.

I am also grateful for the financial support provided by Nanyang Technological University, Singapore and Ministry of Education, Singapore. I would like to especially thank my colleagues – Dr. Kai Wang, Dr. Amsalu Efrem, Dr. Cangjie Yang and Dr. Shuo Huang for providing insightful discussion on my research.

Lastly, I would like to thank my father – Zakiuddin Bohra, my mother – Yasmeen Bohra and my sister, Tasneem Bohra. Their love and support has given me the strength to persevere through the many vicissitudes of life, and to them, I dedicate this thesis.

Many thanks.

TABLE OF CONTENTS

ABSTRACT

Organic π-conjugated linear and network polymers, owing to their large synthetic variety of finely tunable structures and properties, are promising semiconducting materials for optoelectronic devices and light harvesting applications. A vast library of such π-conjugated systems has been synthesized through conventional tools of coupling (e.g. Suzuki coupling, Stille coupling) which involves tedious preactivation of C-H bonds using highly toxic and flammable reagents. In recent years an emerging synthetic technique called direct C–H arylation has been extensively studied as a facile, atom-efficient and environmentally benign pathway for the synthesis of conjugated polymers and small molecules. In this thesis, direct arylation has been applied to rationally chosen monomers to produce conjugated small molecules, linear polymers as well as 2D/ 3D porous polymers that exhibit performances comparable with those made from conventional reactions.

In this thesis, we use naphthodithiophenediimide (NDTI) – a new electron-accepting building block that has shown high performance in ambi-polar organic field-effect transistors to synthesize polymers and small molecules by direct arylation. To examine its regioselectivity, NDTI was used to synthesize small molecules by coupling with 2-bromo-9,9-dihexylfluorene. Two NDTI-based narrow bandgap polymers, one with benzothiadiazole and the other with 9,9-dioctylfluorene, were synthesized via polymerization (DAP). The chemical structures and optoelectronic properties of these molecules and polymers were characterized.

Benzo[1,2-c:4,5-c′]dithiophene-4,8-dione (BDTD) is another electron-accepting building block which has demonstrated outstanding performance in organic bulk heterojunction (BHJ) solar cells. We use DAP to synthesize a series of wide bandgap D-A copolymers with a common acceptor building block of BDTD and study the structure-property relationship in these polymers. We also present the device performances of these polymers in both thin-film field-effect

transistors and organic solar cells using BDTD-based polymers as the electron donors and fullerene derivatives as the electron acceptors.

In this thesis, we have also demonstrated direct arylation as an efficient synthetic tool for conjugated porous polymers (CPPs). A series of narrow bandgap conjugated porous polymers have been synthesized by facile direct arylation polymerization of thiophene-flanked thienothiadiazole (TTD) with multi-brominated monomers with different geometries. The polymer products show strong light absorption in the near infrared region, corresponding to narrow optical bandgaps below 1.3 eV. Under the same polymerization conditions, the morphologies, porosities and optoelectronic properties of the resulting polymers are determined by the chemical structures of the aryl bromides.

In order to extend the library of thiophene-containing CPPs synthesized by direct arylation, we chose three thiophene-flanked monomers – bithiophene **(**BT**)**, 4,7-di(thiophen-2-yl)benzo[c][1,2,5]thiadiazole (DTBT**)** and 2,5-bis(2-octyldodecyl)-3,6-di(thiophen-2-yl)-2,5-pyrrolo[3,4-c]pyrrole-1,4(2H,5H)-dione (DPP) with active C-H bonds and polymerized them with tri- and tetra-brominated monomers. This modular design has allowed us to study the effect of thiophene monomers on the morphology, porosity and optical properties of the CPPs.

In our final research work, we present the direct arylation synthesis of a new series of conjugated porous polymers (CPPs) containing triazine. We used 2,4,6-(tri-2-thienyl)-1,3,5-triazine (TTT) to synthesize a series of robust triazine-core polymers by with DAP without need for preactivating the C–H bonds in the arene monomers. The resulting triazine-core polymers were used to catalyze the photo-oxidation of benzylamines and the polymers containing the highest fraction of triazine units showed > 99% conversion with a relatively low loading of the catalyst.

1. Introduction

1.1 Conjugated polymers: a brief overview

Organic π-conjugated small molecules and polymers have been investigated extensively in recent years for their applications in light emitting diodes (LEDs)[1-3], field effect transistors (FETs)[4-6], organic solar cells (OSCs)[7-9] and sensors.[10-11] The discovery of conductivity in polyacetylene by Heeger, MacDiarmid, and Shirakawa[12] in 1977 opened a new era of organic electronics where the optoelectronic properties of semiconductors can now be integrated with solution processability, mechanical flexibility and synthetic variety[13] of conjugated molecules and polymers. With advances in the field, focus shifted from insoluble powders like polyacetylene and polyaniline (PANI) to solution processable, high-performance semiconducting polymers such as MEH-PPV[14-16] and P3HT [17-20] (**Scheme 1.1**). As a result, a large library of organic building blocks and semiconductive polymers has been established. π-blocks such as thiophene,[21] fluorene and its core extended derivatives,[22-23] diketopyrrolopyrroles and its derivatives,[24] rylene diimides and their derivatives[25-26] (**Figure 1.1**) have been synthesized, their chemical and physical properties tuned for applications in domains ranging from optoelectronics, bio-imaging and light harvesting to catalysis and gas adsorption.

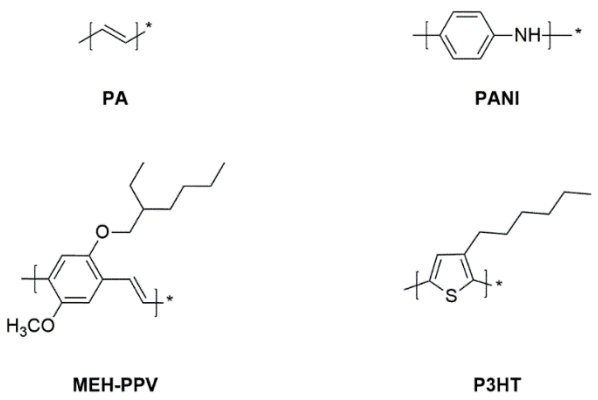

Scheme 1.1 Structures of early semiconducting polymers.

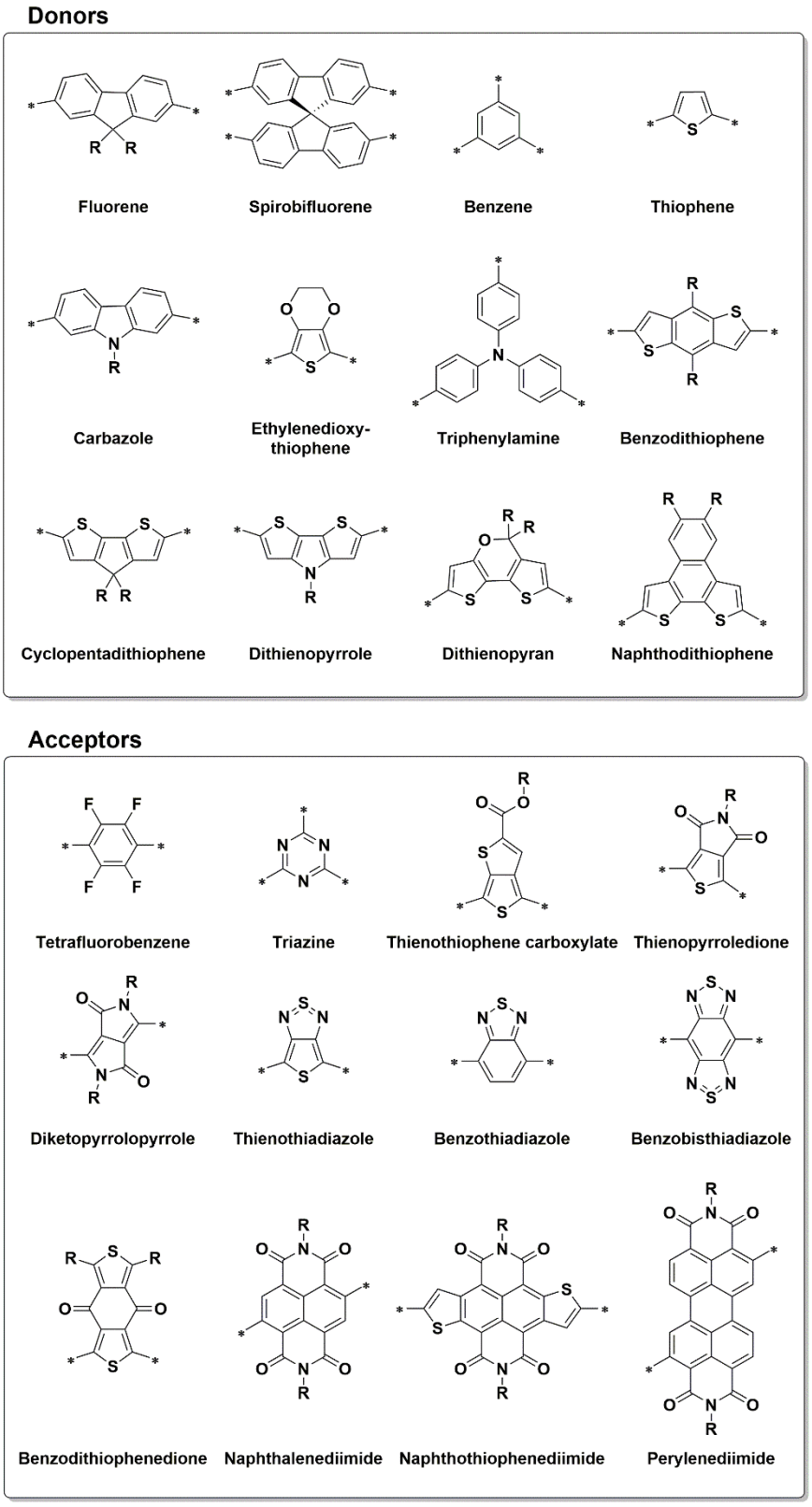

Figure 1.1 Structures of selected donor and acceptor building blocks used in the synthesis of π-conjugated donor-acceptor (D-A) polymers.

Several design strategies to tailor the properties of conjugated polymers for specific applications have been studied.[7, 27-28] An important example is the donor-acceptor (D-A) strategy in which electron-rich (donors) and electron-deficient (acceptors) moieties are used to tune the electrochemical properties and bandgap of the resulting material.[29-31] This approach has been successful in producing polymers with charge-carrier mobilities as high as 14.4 $cm^2 V^{-1} s^{-1}$ in OFETs[32] and power conversion efficiencies (PCE) as high as 14% in OSCs.[33]

1.2 C-C coupling reaction – gateway to new conjugated polymers

Synthesis of π-conjugated molecules and polymers relies on efficient C-C bond formation between two sp^2 carbons.[34] To this end cross couplings such as Stille,[35-36] Suzuki-Miyaura,[37-38] and Kumada[39] have been developed for the coupling of heteroaryl-halides with organometallic-heteroarenes. These reactions are most commonly catalyzed by organometallic complexes of palladium[40] and nickel.[41] These transition metal catalyzed reaction schemes not only allow the formation of functional polymers from conventional monomers but also the help in the synthesis of new conjugated building blocks by facilitating Csp^2- Csp^2 and Csp- Csp^2 bond formations.[42]

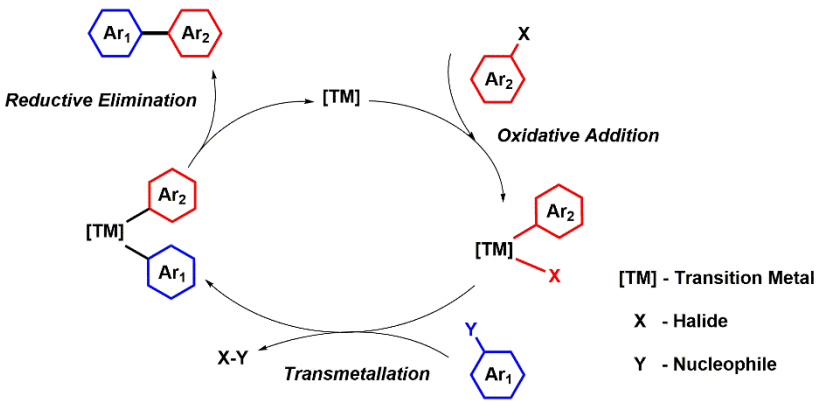

Scheme 1.2 Mechanism for transition metal catalysed cross-coupling reaction.

A metal catalysed coupling reaction occurs in three steps as depicted in **Scheme 1.2**. The reaction begins with 1) oxidative addition of an electrophilic organic halide to a metal catalyst across the C-X bond followed by the 2)

transmetallation of the nucleophilic segment of the second reactant placing both the coupling partners across the metal center. Finally, by 3) reductive elimination of the coupled species from the metal complex, the catalyst is regenerated, and the coupled product is released. A brief description of cross-coupling reactions most commonly used for the synthesis of conjugated polymers is given below.

1.2.1 Migita-Stille Reaction

Stille reaction is an important C-C coupling reaction between nucleophilic organostannanes and organohalides or pseudo halides. The Stille reaction is accessible to a variety of organic groups – the nucleophiles can be alkenyl, alkynyl or aryl stannanes whereas the halides are not limited to chlorides, bromides, and iodides but also include triflates and sulfonates. Mechanism of palladium catalysed stille coupling is like most C-C coupling reactions (**Figure 1.2a**). Oxidative addition of the halide to the Pd (0) forms a Pd (II) complex. This is followed by the transmetalation of the organostannane whereby the organic moiety of the stannane replaces the halide on Pd. The final product is obtained by the reductive elimination of the coupled product. Although Stille reaction has been extensively used for the synthesis of conjugated polymers for organic electronic applications,[43] the need for prefunctionalization with toxic stannyl compounds remains its major drawback.

1.2.2 Suzuki-Miyaura Reaction

Suzuki coupling involves the reaction of an organoborane with an organohalide to give the coupled product in a palladium catalyzed reaction. Recent development in catalytic conditions has expanded the scope of reactions from aryls to alkyls, alkenyls, and alkynyls. One difference between the Suzuki mechanism and that of the Stille Coupling is that the boronic acid must be activated, for example with base (**Figure 1.2b**). After the oxidative addition of organohalide to Pd (0), a molecule of the hydroxide or alkoxide base replaces the halide on the palladium complex, while another adds to the organoborane to form a borate regent making its organic group more nucleophilic. Transmetalation with the borate then follows where its organic group replaces the halide anion on the

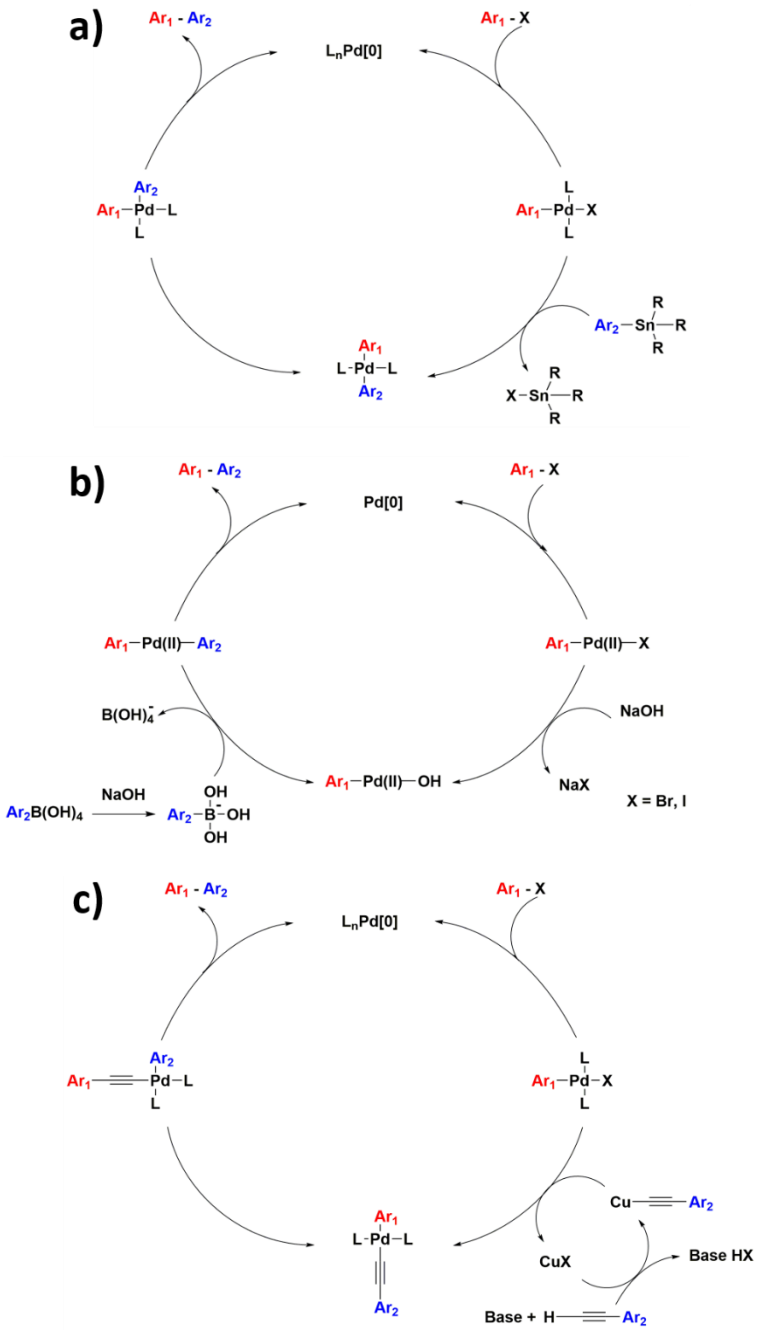

Figure 1.2 Mechanism for palladium catalysed a) Stille coupling of an aryl stannane with an aryl halide, b) Suzuki coupling of an aryl boronic acid with an aryl halide and c) an aryl alkyne with an aryl halide.

palladium complex. This activation of the boron atom enhances the polarisation of the organic ligand and facilitates transmetalation.

Although, the Suzuki reaction has been widely used for the synthesis of conjugated systems for organic electronics, studies comparing polymers synthesised by the Suzuki reaction with direct arylation have found that, the rate of structural defects in Suzuki-synthesised polymers is higher or comparable to that of direct arylation, specially defects arising from the homocoupling of two aryl bromides.[44]

1.2.3 Sonogashira-Hagihara Reaction

Sonogashira coupling is the reaction of an aryl or vinyl halide with a terminal alkyne to form enynes and arylalkynes. The reaction is most commonly catalyzed by a palladium catalyst in the presence of a copper (CuI) co-catalyst and an amine base. Mechanism of the Sonogashira reaction, like other C-C coupling reactions, begins with the oxidative addition of the aryl halide on Pd (0) (**Figure 1.2c**). In a concurrent co-catalyst cycle, the alkyne forms a π-complex with copper which is then deprotonated by the amine base. The deprotonated alkyne in the form of copper acetylide replaces the halide on the palladium complex and regenerates the copper catalyst in the transmetalation step. The coupled product is formed by the reductive elimination from the PdL_2 complex. Due to its ability to form strong C(sp)-C-(sp^2) bonds under relatively mild conditions and a vast library of available arylalkyne monomers, Sonogashira reaction has been widely used for the synthesis of conjugated macromolecules including conjugated microporous polymers (CMPs).[45] Most notably, Cooper and workers have used Sonogashira polymerization extensively to create a variety of CMPs with high Brunauer-Emmet-Teller (BET) surface areas.[46-47]

1.2.4 Mizori-Heck Reaction

Heck reaction undergoes between an unsaturated halide (or triflate) with an alkene in the presence of a base and a palladium catalyst to form a substituted alkene (**Scheme 1.3).** The oxidative addition of the aryl halide to Pd(0) gives a σ-aryl–palladium(II) halide, trans-ArPdXL2, which first coordinates to the alkene after dissociation of one phosphine and then undergoes a syn insertion of the alkene, leading to a σ-alkyl–palladium(II) halide. An internal C-C bond

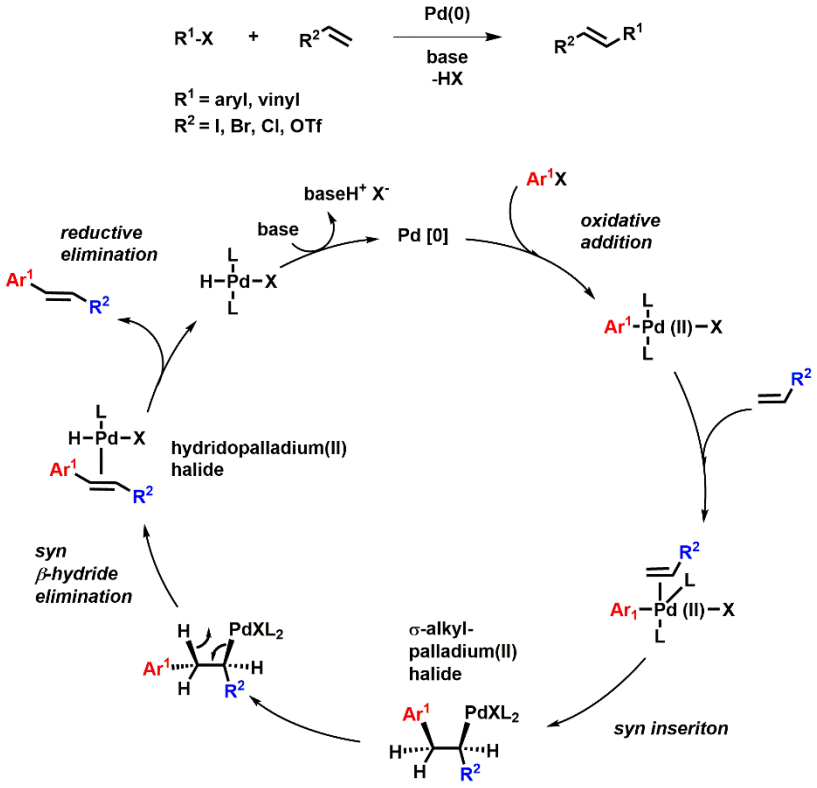

Scheme 1.3 General scheme for and mechanism of palladium catalysed Heck coupling.

rotation in the σ-alkyl–palladium(II) halide brings an sp^3- bonded β-hydrogen in a syn position relative to the palladium atom. A syn β-hydride elimination gives a hydridopalladium(II) halide ligated to the arylated alkene. After dissociation from the arylated alkene, the hydridopalladium(II) halide undergoes a reversible reductive elimination to regenerate the active Pd(0) complex. The base shifts this equilibrium towards the Pd(0) catalyst by quenching the hydrogen halide. The reactivity order of aryl halides in Mizoroki–Heck reactions is usually: ArI > ArBr > ArCl, suggesting that the oxidative addition is rate determining for the less reactive aryl halides. Besides the usual parameters of all reactions (temperature, solvent, and concentration), other parameters may be varied (Pd precursors, ligands, bases, additives, etc.) to optimize Mizoroki–Heck reactions.

1.3 Direct C-H Arylation

1.3.1 Introduction

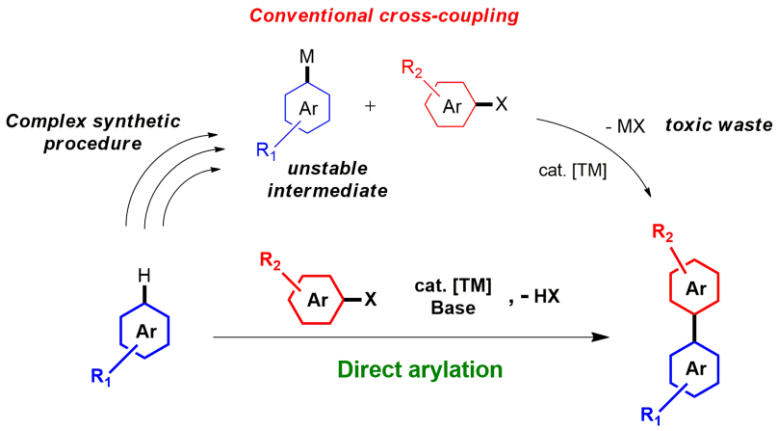

Scheme 1.4 General comparison of conventional cross-coupling reactions with direct arylation.

Aryl-aryl cross coupling is crucial to the development of several pharmaceutical products, biological agents and organic electronic materials Hence, great effort has been devoted to developing new and efficient methods for C-C bond formation. While these traditional coupling methods have been effective to synthesize a broad range of π-conjugated systems, they often require tedious preactivation of C-H bonds using organometallic reagents that are flammable (e.g. butyl lithium), nonstable, and/or highly toxic (e.g. organostannane). Over the last decade, an emerging synthetic tool called direct C-H arylation, which enables facile direct coupling of aryl halides with non-substituted heteroaryls without the need of preactivating the sp^2 C-H bonds (**Scheme 1.4**), has been studied extensively.[48-59] As a result, a variety of π-conjugated molecules and polymers could be synthesized via direct C-H arylation in fewer synthetic steps, without involving highly flammable reagents such as butyl lithium and highly toxic agents such as organotin that are often used in Stille coupling. In recent years, our group has also explored direct arylation as a

greener synthetic tool for conjugated small molecules, linear polymers, and porous networks.[60-69]

1.3.2 Development of direct C-H arylation

Discovery of new aryl-aryl coupling reactions has been driven by the need for efficient pathways to synthesize new materials for organic electronics. Poly(thiophenes) are a class of such materials that had been studied extensively by researchers mainly owing to their good electric conductivity, thermal stability and solution processability.[70-71] Direct arylation was first reported by Lemaire and coworkers[72] in 1999 as an alternative to commonly used routes such as Kumada-Corriu reaction,[73] for synthesis of polythiophenes. 2-Iodo-3-octylthiophene was polymerized under Heck-type reaction conditions using $Pd(OAc)_2$ and tetrabutylammonium bromide as the catalytic system to yield poly(3-octylthiophene) with a molecular weight (M_n) of 3 kDa and regioregularity of ~90%. Even though this route circumvented the need for prefunctionalization of thiophene monomers, the oligomeric products obtained made it a poor choice for synthesizing polythiophenes. In 2010, Ozawa's group reported the direct arylation synthesis of poly(3-hexylthiophenes) using Hermann-Beller catalyst instead of $Pd(OAc)_2$ to obtain high molecular weight (M_n = 30.6 kDa) polymers with a regioregularity as high as 98%.[74] Several phosphine ligands were tested and tris(2-dimethylaminophenyl)phosphine in combination with cesium carbonate as the base was found to give the best results.

In a 2012 paper, Leclerc and coworkers optimized the direct arylation polymerization of a donor-acceptor polymer synthesized from a C-H active acceptor molecule – thienopyrroledione (TPD) and a brominated bithiophene derivative.[75] Best results were obtained when Pd(OAc)(*o*-Tol) and tris(*o*-methoxyphenyl)phosphine were used as the catalyst ligand to give a molecular weight of 56 kDa and polydispersity of 2.6. C-H activation of TPD not only demonstrated DAP to be the more efficient choice for synthesis of TPD-based donor acceptor polymers[76] but also inspired the synthesis of high performance TPD-based organic photovoltaic materials.[77] Other noteworthy contributions to the development of DAP were made by Kanbara's research group which reported

conditions for the C-H activation of 1,2,4,5-tetrafluorobeneze.[78] Polymerization with dibromooctylfluorene using palladium acetate as the catalyst yielded polymers with M_n as high as 31 kDa after a reacting for 48 hours.

1.3.3 Mechanism of Direct Arylation Coupling

The mechanism of direct arylation coupling has been the subject of several experimental[79-80] and computational reports[81-82] in the past two decades. Two pathways that have been widely studied are the electrophilic aromatic substitution and concerted metalation deprotonation (CMD). In 2000, Sakaki and coworkers reported a computational study of the C-H activation of benzene by palladium.[83] They concluded that the heterolytic cleavage of the C-H bond in benzene occurs when an oxygen from bisformate complex decoordinates from the palladium center to form an O-H bond, while the benzene C simultaneously coordinates with palladium, leading to the formation of a six-centered transition state. Over the next decade, Fagnou[84-85] and coworkers corroborated these results and demonstrated the applicability of the CMD pathway to a wide range of heteroarenes.

Scheme 1.5 describes the common mechanism of direct heteroarylation by the CMD pathway for both carboxylate-mediated[86] and carboxylate-free catalytic models.[87] The reaction begins with the oxidative addition of the aryl halide bond (Ar_1-Br) to the Pd (0) complex with bidentate ligands (L) to form an aryl-halo complex (1). Depending on the catalytic model, a carboxylate or carbonate ion coordinates with the aryl-halo complex to deprotonate Ar_2 while simultaneously forming the Ar_2-Pd bond, hence leading to the formation of the transition state. The concerted-metalation and deprotonation step distinguishes direct C-H arylation from the conventional C-C coupling. It should be noted that while most arenes follow the CMD pathway, the exact mechanism depends on the nature of substrates, ligands and solvents involved.[88-90] The final product is formed by the reductive elimination of Ar_1-Ar_2 from palladium.

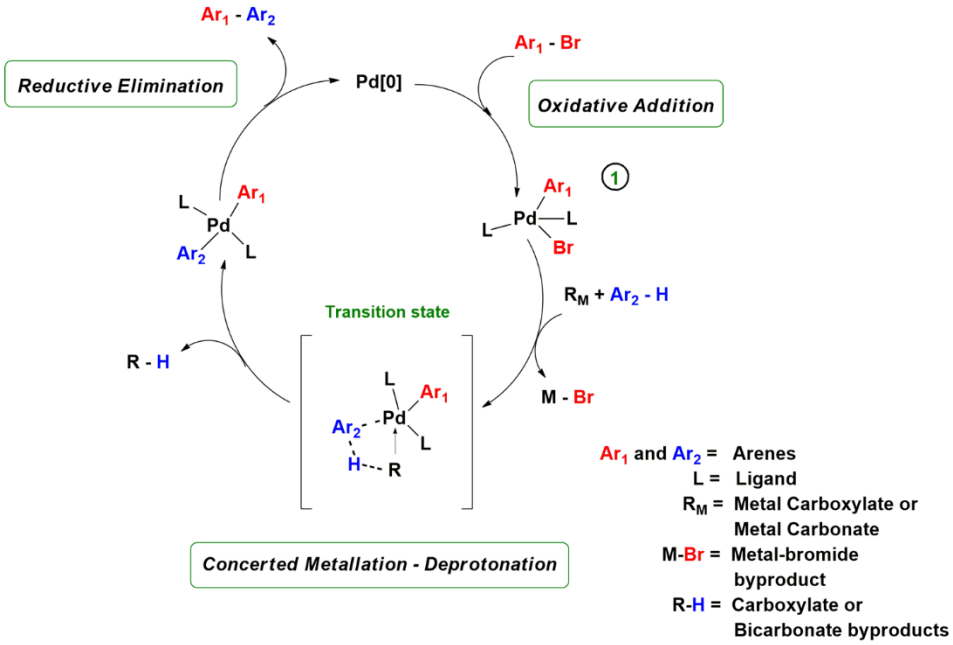

Scheme 1.5 General mechanism of direct arylation via the concerted metalation-deprotonation (CMD) pathway.

1.4 Direct Arylation for the synthesis of linear polymers for applications in organic electronics

1.4.1 Recent progress in high-performance materials synthesized by direct arylation

Conjugated polymers have been intensively studied as functional materials for organic electronics such as light emitting diodes (LEDs), organic field effect transistors (OFETs) and organic solar cells (OSCs) in the past two decades.[91] However, in recent years, the sustainable development of these materials by using eco-friendly methods such as DAP has garnered interest in the research community and to that end several polymers exhibiting impressive performances in OFETs and OSCs have been reported.[34, 92] A class of macromolecules that has consistently shown high performance in thin film transistors is DPP-based polymers[93-94] and a significant contribution to DPP polymers and small molecules synthesized by DAP has been made by Leclerc's

group. Polymer **P4 (Figure 1.3)** synthesized by Pouliot et al. exhibited ambipolar behaviour with dominant p-type character (μ_h = 0.92 cm^2 V^{-1} s^{-1}) in top-gate bottom-contact devices.[95] Recently, Gao et al. synthesized a donor acceptor polymer **PDPP-4FTVT**, consisting of fluorinated thiophene units in the polymer chain.[96] Electron and hole mobilities of 4.19 and 3.4 cm^2 V^{-1} s^{-1} respectively have been reported for this polymer, which are the highest mobilities for polymers synthesized via DAP. Fewer NDI polymers synthesized via DAP in OFETs have been studied in OFETs compared to DPP polymers, though some significant contributions towards n-type polymers have been made. For example, Sommer's group achieved electron mobility as high as 3 cm^2 V^{-1} s^{-1} for an NDI-bithiophene polymer[97] (**PNDIT2**), which was comparable to the mobility of the same type of polymers synthesized via Stille coupling.

In recent years, DPP-based polymer solar cells have been optimized to exhibit PCEs approaching 10%. However, very few of these polymers have been synthesized by DAP.[98] In a recent report, Guérette et al. reported the synthesis of a phenanthridone-based random terpolymer, **P3** by DAP that exhibited PCEs as high as 6.3%.[99] Several TPD polymers synthesized by DAP[100-101] have also been used to fabricate solar cells however the PCEs obtained are moderate compared to the ones obtained from Stille polymerization.[102-103] Farinola and coworkers recently published a comparative study of the synthesis and OPV characteristics of a benzodithiophene-*alt*-TPD polymer (**P_{DHAP}, Figure 1.3**) synthesized by DAP and Stille polymerization.[104] Higher molecular weights were obtained from the DAP protocol (12 kDa vs. 10 kDa from Stille polymerization) and the PCEs for the polymer made by DAP were also found to be higher in various fabrication conditions.

Facchetti, Marks, and coworkers reported a series of high-performance D-A alternating copolymers synthesized through a robust synthetic scheme of DAP using Pd_2dba_3/P(*o*-$MeOC_6H_4)_3$ as the catalyst/ligand pair and 2,2-diethylhexanoic acid (denoted as DEHA) as the additive.[105] The bulkier nature of DEHA compared to pivalic acid, a more commonly used acidic derivative in DAP, played a crucial role to improve the C-H selectivity while not

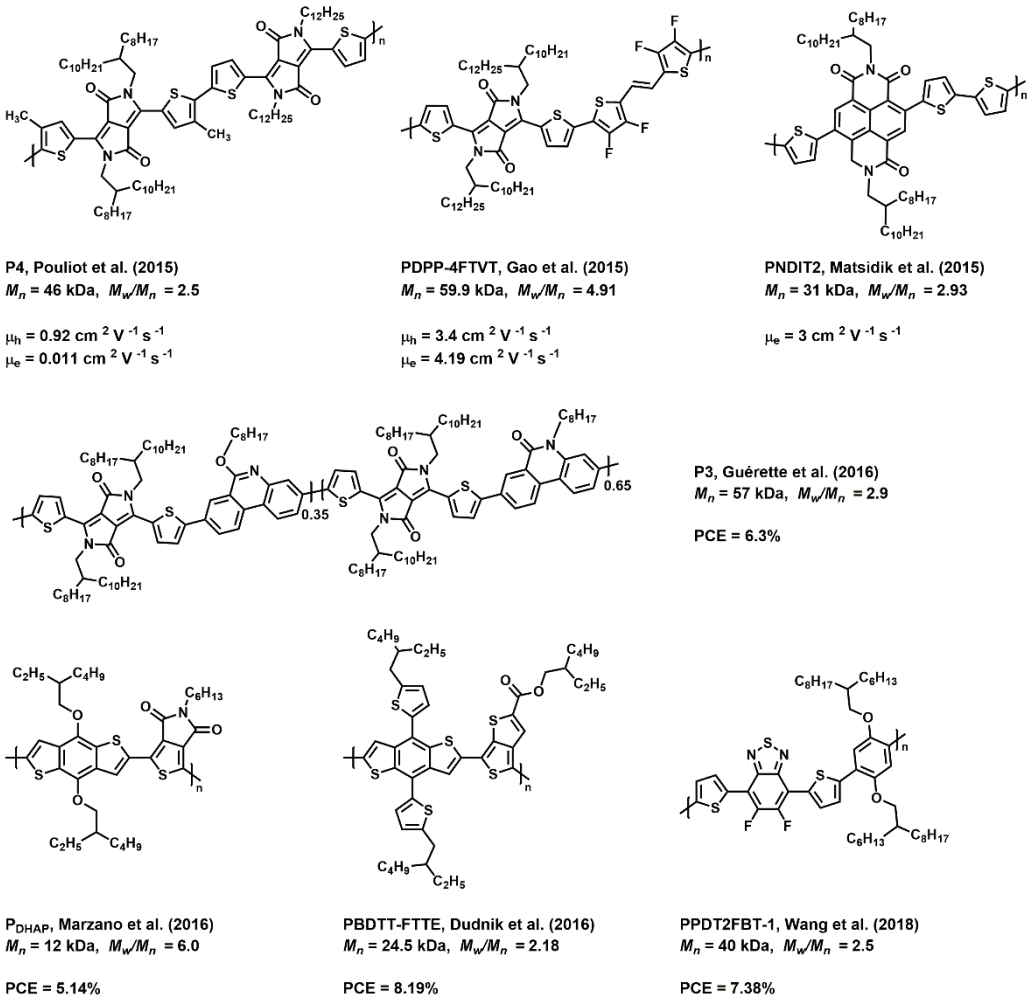

Figure 1.3 Structures of polymers synthesized by direct arylation polymerization for applications in OFETs and OSCs.

compromising the C-H reactivity. **PBDTT-FTTE** synthesized under the optimized condition of DAP showed a remarkably high PCE of 8.19% in bulk heterojunction (BHJ) photovoltaic devices, which is not only comparable to the PCE (8.24%) obtained for its Stille counterpart but also the highest reported for a DAP copolymer. Very recently, Wang and coworkers reported the direct arylation synthesis of **PPDT2FBT-1**[69] (**Figure 1.3**) – a fluorinated polymer containing benzothiadiazole and alkoxy substituted benzene which exhibits tight interchain packing owing to strong intramolecular non-covalent interactions. Power conversion efficiencies up to 7.3% were obtained from **PPDT2FBT-1**

based devices which are comparable to the performance of a similar polymer synthesized by Stille polymerization.[106] These results cleared the prejudice that DAP produces conjugated polymers with inferior structural quality and device performances compared to those synthesized via conventional Suzuki or Stille polymerizations.

1.4.2 Scope of direct arylation for efficient synthesis of high-performance linear polymers

Despite the recent advances in optimizing direct arylation conditions to produce high molecular weight polymers with performances comparable to their counterparts synthesized by conventional coupling reactions, the majority of benchmark polymers applied in BHJ organic solar cells have been synthesized by Stille coupling. For instance, a new acceptor molecule – benzo[1,2-c:4,5-c′]dithiophene-4,8-dione (BDTD) has been recently employed, most notably by Hou's[107-110] and Sun's[111-113] groups to synthesize wide bandgap donor-acceptor polymers via Stille polymerization. BDTD-based polymers have been reported to yield power conversion efficiencies as high as 14%, which is among the highest values ever reported (**Figure 1.4a**).[110] The fused benzodithiophene core of BDTD results in planar polymer chains which enhance π–π stacking in polymer films while the wide bandgap of polymer provides deeper highest molecular orbital energy levels which are crucial for high open circuit voltages.

Another example of a core extended acceptor molecule that has demonstrated high performance in organic electronics is naphtho[2,3-*b*:6,7-*b*′]dithiophenediimides (NDTI). Synthesis of α,β-unsubstituted NDTI was first reported by Takimiya's group by annulation of thiophene on 1,4,5,8-naphthalenediimide.[114] Like BDTD, NDTI's fused structure enhances rigid packing necessary for charge transport. Moreover, the LUMO levels of NDTI-based donor-acceptor polymers and triads have been found to remain constant around -4 eV over a wide range of donors which has facilitated the fabrication of several high-performance air-stable OFETs (**Figure 1.4a**).[115-117] From a synthetic standpoint, unsubstituted α-position on NDTI allows the expansion of the

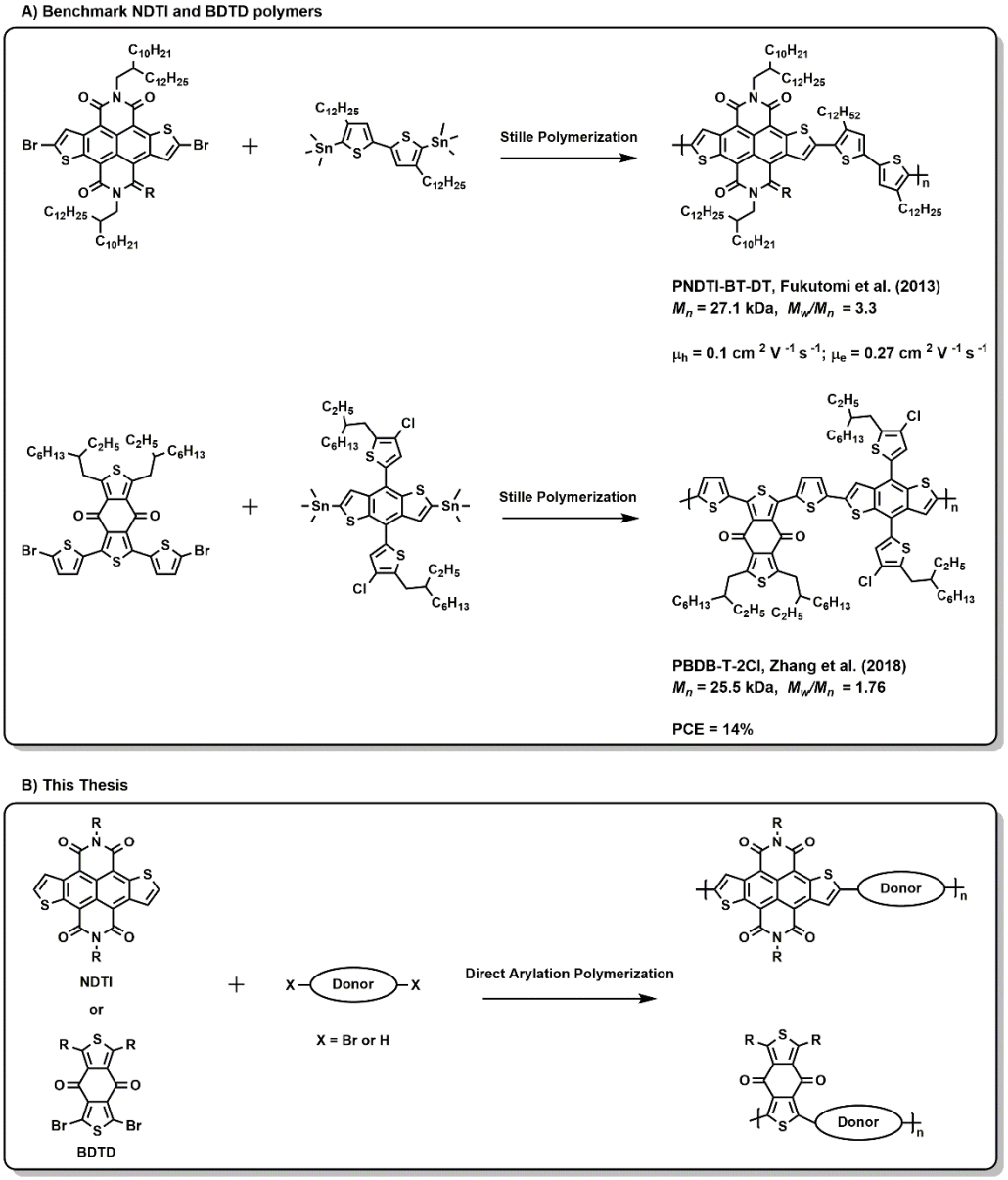

Figure 1.4 a) Examples of benchmark NDTI- and BDTD-based polymers reported in the literature. b) Schematic representation of the direct arylation scheme used to synthesise NDTI- and BDTD-based polymers in this thesis.

conjugated backbone either by pre-functionalization with reactive nucleophiles or by direct C-H activation.

In this thesis, we apply the chemistry of direct arylation to high performance building blocks such as NDTI and BDTD to synthesize new materials for optoelectronics (**Figure 1.4b**). Details of experiments highlighting

the optimization reactions and electro-optical characterizations of NDTI and BDTD based polymers is presented in **Chapter 2** and **3** respectively. Device performance of BDTD-based polymers in BHJ organic solar cells is also presented. These results demonstrate that rational optimization of reaction conditions in DAP is a cost-effective and eco-friendly synthetic approach that can lead to high-quality polymers with large molecular weights, minimal structural defects, and thus high performances in optoelectronic devices.

1.5 Direct arylation as a synthetic tool for 2D/3D conjugated porous polymers (CPPs)

1.5.1 Recent progress in the synthesis of CPPs by direct arylation

Conjugated porous polymers (CPPs)[46-47] are a class of organic polymers characterized by large specific surface area, remarkable chemical stability and excellent electronic properties that have found applications in gas storage and catalysis.[46-47, 118] Electrochemical properties of CPPs can be tuned by proper selection of monomers from a vast library of π-blocks, but the synthetic approach to these polymers has been limited to conventional coupling reactions.[119] Direct arylation, which has only recently been studied in the context of CPPs, allows for the facile synthesis of porous networks by reacting non-functionalized, C-H active monomers with multi-halogenated heteroaryls.

Han and coworkers published the first report of the CPPs synthesized by direct arylation polymerization.[120] 1,2,4,5-tetrafluorobenzene was used to synthesize polymers with 1,3,5-tribromobenzene and tetrakis(4-bromophenyl)methane under DAP conditions optimized by Kanbara.[78] The resulting polymers **FPOP-1** and **FPOP-2** (**Scheme 1.6**), showed Brunauer-Emmet-Teller (BET) surface areas of 1170 and 1020 $m^2 g^{-1}$, respectively, which remain the highest values of BET specific surface areas for polymers synthesized by DAP till date. Feng and coworkers synthesized a polymer, **FPSBF** with 2,2′,7,7′-Tetrabromo-9,9′-spirobifluorene under Kanbara's conditions which exhibited a surface area of 700 $m^2 g^{-1}$.[121] Recently, Koizumi's group used higher

catalyst loading and an extended reaction time to obtain a polymer **CMP1** that exhibited BET surface area of 258 m^2 g^{-1}.[122]

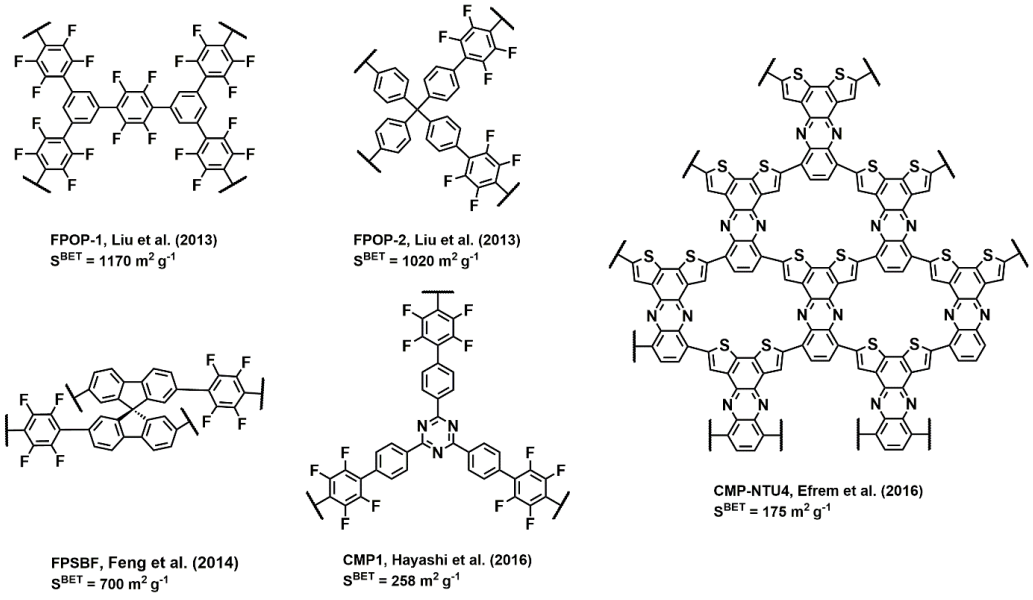

Scheme 1.6 Structures of conjugated porous polymers synthesized by direct arylation.

Very recently, Wang's group reported the synthesis of narrow bandgap CPPs via DAP involving thiophene-based monomers. Specifically, porous homopolymers[66] – **NTU-CMPs** (**Scheme 1.6**) were obtained via a facile one-step DAP involving 8,11-dibromodithieno[3,2-a:2',3'-c]phenazine as a single monomer building block under the catalytic condition with Pd_2dba_3 and P(*o*-$MeOC_6H_4)_3$ as the catalyst-ligand pair that was previously optimized in the C-H activation of benzo[1,2-b:4,5-b′]dithiophene.[60] Conjugated polymer networks with a narrow bandgap of 1.5 eV and hierarchical porous structures were obtained.

Applications of conjugated porous polymers broadly include gas storage, heterogeneous catalysis and energy storage owing to their high microporosity, large interfacial area, tunable electronic structure, and distinct morphology. A comprehensive discussion of design strategies and application of CPPs in the aforementioned areas is presented in reviews by Jiang[47] and Antonietti.[118] The

first synthesis of CPPs via DAP[120] (reported by Liu et al.) exhibited high BET surface areas greater than 1000 m^2 g^{-1} which are comparable to values of polymers obtained by conventional coupling reactions. **FPOP-1** and **FPOP-2** showed moderate values for uptake of carbon dioxide and hydrogen while a methane uptake capacity of 3.3 % (by weight) was obtained for **FPOP-2** which is higher than several highly porous materials. **FPOP-2** also exhibited impressive toluene adsorption (10.6 mmol g^{-1}) due to strong host-guest interactions. Sorption properties of polymers reported by Koizumi[122] were also tested. However, the BET surface area, as well as CO_2 adsorption were much lower compared to benchmark polymers.[123] Application of CPPs as heterogeneous catalysts for organic syntheses either by encapsulation of metal co-catalysts in their pores or post-synthetic modification of polymer structure has also been extensively studied.[124] Conjugated porous polymers allow for the rational design of organic catalysts by selection of appropriate building blocks, thereby providing greater control on the optoelectronic properties. These features make CPPs promising alternatives to inorganic catalysts (e.g. platinum) that have been the standard.[125-126]

1.5.2 Limitations of conventional synthesis and scope of direct arylation as a greener alternative for synthesizing new CPPs

Despite the versatile applications of CPPs in CO_2 capture, energy storage, and catalysis, these polymers have been most commonly synthesized under thermally and chemically harsh reaction conditions which are often energy intensive and require corrosive reagents. For instance, the majority of thiophene-based CPPs reported in the literature have been synthesized by conventional C-C coupling reactions such as ferric chloride catalyzed oxidative coupling,[30, 127-131] and Sonogashira-Hagihara polymerization.[132-134] Despite its moderate reaction conditions, the oxidative coupling has been reported to yield chlorinated polymers[128] with residual iron salts.[135] whereas Sonogashira polymerization requires pre-functionalization of C-H bonds with toxic and flammable reagents like organosilanes and is limited to monomers containing terminal ethynyl groups. Triazine-containing CPPs are another class of nitrogen-rich porous

material have been promising for versatile applications in catalysis and gas storage.[136-137] However, ionothermal[138] and solvothermal[139-140] cyclotrimerization of aryl nitriles has been used most commonly for the synthesis of triazine frameworks.[47, 141] Ionothermal reactions require high temperatures and stoichiometric amounts of $ZnCl_2$ which are difficult to remove from the polymer while solvothermal reactions are carried out in highly corrosive 'superacids' such as triflic acid.

We have been exploring a "greener" C-C coupling approach so called direct arylation polymerization (DAP) for facile synthesis of a broad scope of π-conjugated small molecules, linear donor-acceptor alternating copolymers, and 2D/3D networks. In contrast to Suzuki coupling and Stille coupling, DAP does not require tedious pre-activation of C-H bonds in arene monomers and does not involve flammable organometallic agents such as butyl lithium and highly toxic stannyl agents that are often used in Stille coupling. Nevertheless, DAP has been rarely used for the synthesis of triazine-containing 2D/3D networks as a new type of π-conjugated porous polymers.

1.6 Research objectives

DAP has only recently emerged as a promising synthetic technique for conjugated polymers owing to the high products yields that are obtainable with minimal monomer functionalization. Significant progress in terms of reaction optimization for high yields and developing a DAP synthesized library of highly functional polymers has been done in the last five years alone.[57, 59]

In this thesis,

1) we aim to, synthesize new linear using rationally selected π-conjugated building blocks. Polymers containing naphthodithiophenediimide (NDTI) NDTI and benzodithiophenedione (BDTD, refer **Figure 1.4**) have consistently shown high-performance in OFETs and OSCs but their synthesis has been carried out exclusively by conventional coupling reactions such like Stille and Suzuki coupling. The planar structure of NDTI and BDTD monomers leads to the efficient packing of polymer chains which consequently enhances charge

transport. Moreover, BDTD has been reported to form wide bandgap polymers with deep HOMO levels which are crucial for increasing V_{oc} in OSCs whereas NDTI-based small molecules and polymers[114] have been reported to possess low lying LUMO levels necessary for fabricating air-stable OFETs. Despite their excellent structural and electrochemical properties, NDTI- and BDTD-based polymers have never been synthesized by direct arylation. In this thesis, we use pre-optimized direct arylation conditions[60] to synthesize a series of NDTI- and BDTD-based polymers and investigate their structural, optical and electrochemical properties. OFET and OSC device characterization of BDTD polymers is also presented. These results signify that direct arylation is a facile alternative to conventional reactions for obtaining high-performance polymers as it allows for the incorporation of a wide variety of tunable building blocks in the polymer backbone while overcoming the need for tedious preactivation with toxic reagents.

2) We also aim to extend the scope of direct arylation from synthesis of conjugated linear polymers to conjugated 2D/3D porous networks. Much like, linear conjugated polymers, the vast majority of conjugated porous polymers (CPPs) have been synthesized by conventional reactions which either require preactivation of monomers (eg. Suzuki coupling) or are limited to monomers containing specific functional groups (eg. Sonogashira-Hagihara coupling, Schiff-base condensation). In fact, direct arylation has been used to synthesize CPPs only recently. In this thesis, we present a systematic approach towards the direct arylation synthesis of a library of CPPs with good control on structural, optical, morphological and surface properties. We present the first example of thienothiadiazole-based narrow bandgap CPPs synthesized by direct arylation. Although previously reported CPPs synthesized by direct arylation showed specific surface areas as high as 1170 $m^2 g^{-1}$,[120] their wide bandgaps limited light absorption in visible and near infrared (NIR) regions which is crucial for polymers used in energy conversion as well as other light harvesting applications. We further investigate the structure-function relationships in CPPs by synthesizing a series of polymers from thiophene-flanked monomers with active C-H bonds. Finally, we use 2,4,6-(tri-2-thienyl)-1,3,5-triazine (TTT) to

synthesize a series of triazine based polymers. Although triazine-based functional materials have been used in a wide variety of applications due to their high electron deficiency, planar structure, and high nitrogen content, they have been commonly synthesized under chemically harsh conditions. In this thesis, we present the first report of triazine-based CPPs synthesized by direct arylation and demonstrate their application in photocatalysis. Excellent control on morphology and porosity can be obtained by controlling the monomer ratio. These results suggest direct arylation is an efficient tool to synthesise robust CPPs that can incorporate a wide array of monomers and their intrinsic functionality in the polymer network.

1.7 Organization of the thesis

This thesis presents experiments carried out in five research projects connected with a unifying theme: direct arylation polymerization (DAP). DAP presents as an environmentally benign and economically feasible alternative to conventional cross-coupling reactions for the synthesis of conjugated polymers. In this thesis, we introduce the concept of conjugated polymers and highlight the need for a sustainable alternative synthetic route such as direct arylation. In the subsequent chapters, we present the experimental results of the synthesis and characterization of novel conjugated linear and network polymers and demonstrate their potential applications.

Chapter 1 provides a brief introduction to conjugated polymers and the various techniques utilized for the design and synthesis of these polymers. Subsequently, the chemistry of direct arylation is introduced and a brief review of linear and 2D/3D polymers synthesized by direct arylation is presented. Finally, the importance of direct arylation in the context of functional conjugated polymers is discussed and scope for new research is highlighted.

In **Chapter 2**, direct arylation is used to synthesize naphthodithiophenediimide (NDTI) based polymers. NDTI as a new electron-accepting building block has been used to synthesize narrow bandgap small molecules and polymers for ambi-polar organic field-effect transistors and

organic solar cells. Herein, the first application of direct arylation coupling to synthesize a series of NDTI based small molecules and polymers is presented. The regioselectivity is examined in the direct arylation coupling of NDTI with 2-bromo-9,9 dihexylfluorene. Two NDTI-based narrow bandgap polymers, one with benzothiadiazole and the other with 9,9-dioctylfluorene, are synthesized via direct arylation polymerization. The chemical structures and optoelectronic properties of these molecules and polymers are characterized.

In **Chapter 3**, direct arylation is applied to another electron-accepting building block – benzo[1,2-c:4,5-c′]dithiophene-4,8-dione (BDTD). Donor-acceptor (D-A) alternating copolymers consisting BDTD have demonstrated outstanding performances in OSCs but the synthesis of these polymers has been largely limited to Stille-coupling based polycondensations. Herein, a direct arylation route to a series of wide bandgap D-A copolymers with a common acceptor building block of BDTD is reported. Structure-property relationship in these polymers is characterized and the device performances of these polymers in both thin-film OFETs and bulk-heterojunction OSCs involving BDTD-based polymers as the electron donors and fullerene derivatives as the electron acceptors are studied.

In **Chapter 4**, direct arylation is used to synthesize narrow bandgap small molecules and conjugated porous polymers (CPPs) from thiophene-flanked thienothiadiazole (TTD). TTD-based small molecules serve as a model reaction for the polymerization of TTD with multi-brominated monomers. Morphologies, porosities and optoelectronic properties of the resulting polymers are studied. The synthetic protocol of direct arylation polymerization and the structure–property relationship established in these narrow bandgaps conjugated porous polymers will be important for rational material design towards applications such as gas separation/storage and photocatalysis.

In **Chapter 5**, a series of CPPs containing thiophene-flanked monomers are synthesized. Building blocks containing bithiophene, benzothiadiazole and diketopyrrolopyrrole are incorporated in the porous polymer structure by polymerization with tri- and tetra-brominated monomers under direct arylation

conditions like those used to synthesize TTD-based CPPs. Effect of monomer size and geometry on the porosity, morphology and optical properties of CPPs is studied.

Chapter 6 presents the direct arylation synthesis of triazine containing CPPs is presented. Previous synthetic approaches such as the ionothermal and solvothermal cyclotrimerization of aryl nitriles to these CPPs are limited to monomers that are stable against high temperatures (≥ 400 °C) or strong acids. Herein, a milder direct arylation approach towards a new series of robust triazine-core polymers by coupling 2,4,6-(tri-2-thienyl)-1,3,5-triazine (TTT) with multi-brominated monomers of varying geometries. The direct C–H activation of TTT enables the facile incorporation of the triazine unit into multidimensional polymeric structures while the choice of comonomers gives good synthetic control of the morphologies, porosities and optoelectronic properties of triazine-core CPPs. The resulting triazine-core polymers were used to catalyse the photo-oxidation of benzylamines.

Finally, a conclusion to the experimental work carried out in this thesis is presented in **Chapter 7**. Limitations of direct arylation in terms of scalability and economy of reaction conditions are discussed. To overcome these challenges, an outlook for the future of direct arylation as a greener alternative for synthesizing conjugated linear and 2D/3D polymers is proposed

1.8 References

1. Gather, M. C.; Kohnen, A.; Meerholz, K. *Adv. Mater.* **2011,** *23*, 233-48.
2. Xiao, L.; Chen, Z.; Qu, B.; Luo, J.; Kong, S.; Gong, Q.; Kido, J. *Adv. Mater.* **2011,** *23*, 926-52.
3. Xu, R.-P.; Li, Y.-Q.; Tang, J.-X. *J. Mater. Chem. C* **2016,** *4*, 9116-9142.
4. Facchetti, A. *Chem. Mater.* **2011,** *23*, 733-758.
5. Mei, J.; Diao, Y.; Appleton, A. L.; Fang, L.; Bao, Z. *J. Am. Chem. Soc.* **2013,** *135*, 6724-6746.
6. Sirringhaus, H. *Adv. Mater.* **2014,** *26*, 1319-35.

7. Bian, L.; Zhu, E.; Tang, J.; Tang, W.; Zhang, F. *Prog. Polym. Sci.* **2012,** *37*, 1292-1331.

8. Kang, H.; Lee, W.; Oh, J.; Kim, T.; Lee, C.; Kim, B. J. *Acc. Chem. Res.* **2016,** *49*, 2424-2434.

9. Jin, Y.; Chen, Z.; Dong, S.; Zheng, N.; Ying, L.; Jiang, X. F.; Liu, F.; Huang, F.; Cao, Y. *Adv. Mater.* **2016,** *28*, 9811-9818.

10. Magliulo, M.; Manoli, K.; Macchia, E.; Palazzo, G.; Torsi, L. *Adv. Mater.* **2015,** *27*, 7528-51.

11. Zhang, C.; Chen, P.; Hu, W. *Chem. Soc. Rev.* **2015,** *44*, 2087-107.

12. Chiang, C. K.; Fincher, C. R.; Park, Y. W.; Heeger, A. J.; Shirakawa, H.; Louis, E. J.; Gau, S. C.; MacDiarmid, A. G. *Phys. Rev. Lett.* **1977,** *39*, 1098-1101.

13. Chueh, C.-C.; Li, C.-Z.; Jen, A. K. Y. *Energy Environ. Sci.* **2015,** *8*, 1160-1189.

14. Burroughes, J. H.; Bradley, D. D. C.; Brown, A. R.; Marks, R. N.; Mackay, K.; Friend, R. H.; Burns, P. L.; Holmes, A. B. *Nature* **1990,** *347*, 539.

15. Gustafsson, G.; Cao, Y.; Treacy, G. M.; Klavetter, F.; Colaneri, N.; Heeger, A. J. *Nature* **1992,** *357*, 477.

16. Granström, M.; Petritsch, K.; Arias, A. C.; Lux, A.; Andersson, M. R.; Friend, R. H. *Nature* **1998,** *395*, 257.

17. Sirringhaus, H.; Brown, P. J.; Friend, R. H.; Nielsen, M. M.; Bechgaard, K.; Langeveld-Voss, B. M. W.; Spiering, A. J. H.; Janssen, R. A. J.; Meijer, E. W.; Herwig, P.; de Leeuw, D. M. *Nature* **1999,** *401*, 685.

18. Ong, B. S.; Wu, Y.; Liu, P.; Gardner, S. *J. Am. Chem. Soc.* **2004,** *126*, 3378-3379.

19. Zhuoying, C.; Henrik, L.; Sebastian, A. S.; Mario, C.; Meedom, N. M.; Martin, H.; Weimin, Z.; Iain, M.; Henning, S. *Adv. Mater.* **2010,** *22*, 2371-2375.

20. Guangjin, Z.; Youjun, H.; Yongfang, L. *Adv. Mater.* **2010,** *22*, 4355-4358.

21. F., P. I.; F., P. D.; H., M.; F., W. *Adv. Mater.* **2005,** *17*, 2281-2305.

22. Li, C.; Liu, M.; Pschirer, N. G.; Baumgarten, M.; Müllen, K. *Chem. Rev.* **2010,** *110*, 6817-6855.

23. Xie, L.-H.; Yin, C.-R.; Lai, W.-Y.; Fan, Q.-L.; Huang, W. *Prog. Polym. Sci.* **2012,** *37*, 1192-1264.

24. Marek, G.; T., G. D. *Adv. Opt. Mater.* **2015,** *3*, 280-320.

25. Zhan, X.; Facchetti, A.; Barlow, S.; Marks Tobin, J.; Ratner Mark, A.; Wasielewski Michael, R.; Marder Seth, R. *Adv. Mater.* **2010,** *23*, 268-284.

26. Guo, X.; Tu, D.; Liu, X. *J. Energy Chem.* **2015,** *24*, 675-685.

27. Guo, X.; Baumgarten, M.; Müllen, K. *Prog. Polym. Sci.* **2013,** *38*, 1832-1908.

28. Duan, L.; Qiao, J.; Sun, Y.; Qiu, Y. *Adv. Mater.* **2011,** *23*, 1137-1144.

29. Wu, J.-S.; Cheng, S.-W.; Cheng, Y.-J.; Hsu, C.-S. *Chem. Soc. Rev.* **2015,** *44*, 1113-1154.

30. Yali, L.; Buyi, L.; Wei, W.; Kangbing, W.; Bien, T. *Adv. Mater.* **2012,** *24*, 5703-5707.

31. Beaujuge, P. M.; Amb, C. M.; Reynolds, J. R. *Acc. Chem. Res.* **2010,** *43*, 1396-1407.

32. Kim, G.; Kang, S.-J.; Dutta, G. K.; Han, Y.-K.; Shin, T. J.; Noh, Y.-Y.; Yang, C. *J. Am. Chem. Soc.* **2014,** *136*, 9477-9483.

33. Li, S.; Ye, L.; Zhao, W.; Yan, H.; Yang, B.; Liu, D.; Li, W.; Ade, H.; Hou, J. *J. Am. Chem. Soc.* **2018,** *140*, 7159-7167.

34. Marrocchi, A.; Facchetti, A.; Lanari, D.; Petrucci, C.; Vaccaro, L. *Energy Environ. Sci.* **2016,** *9*, 763-786.

35. Milstein, D.; Stille, J. K. *J. Am. Chem. Soc.* **1978,** *100*, 3636-3638.

36. Carsten, B.; He, F.; Son, H. J.; Xu, T.; Yu, L. *Chem. Rev.* **2011,** *111*, 1493-1528.

37. Miyaura, N.; Suzuki, A. *J. Chem. Soc., Chem. Commun.* **1979**, 866-867.

38. Sakamoto, J.; Rehahn, M.; Wegner, G.; Schlüter, A. D. *Macromol. Rapid Commun.* **2009,** *30*, 653-687.

39. Tamao, K.; Sumitani, K.; Kumada, M. *J. Am. Chem. Soc.* **1972,** *94*, 4374-4376.

40. Johansson Seechurn, C. C. C.; Kitching, M. O.; Colacot, T. J.; Snieckus, V. *Angew. Chem. Int. Ed.* **2012,** *51*, 5062-5085.

41. Tasker, S. Z.; Standley, E. A.; Jamison, T. F. *Nature* **2014,** *509*, 299-309.

42. Cheng, Y.-J.; Luh, T.-Y. *J. Organomet. Chem.* **2004,** *689*, 4137-4148.

43. Marzano, G.; Ciasca Cosimo, V.; Babudri, F.; Bianchi, G.; Pellegrino, A.; Po, R.; Farinola Gianluca, M. *Eur. J. Org. Chem.* **2014,** *2014*, 6583-6614.

44. Hendriks, K. H.; Li, W. W.; Heintges, G. H. L.; van Pruissen, G. W. P.; Wienk, M. M.; Janssen, R. A. J. *J. Am. Chem. Soc.* **2014,** *136*, 11128-11133.

45. Chinchilla, R.; Nájera, C. *Chem. Soc. Rev.* **2011,** *40*, 5084-5121.

46. Dawson, R.; Cooper, A. I.; Adams, D. J. *Prog. Polym. Sci.* **2012,** *37*, 530-563.

47. Xu, Y.; Jin, S.; Xu, H.; Nagai, A.; Jiang, D. *Chem. Soc. Rev.* **2013,** *42*, 8012-31.

48. Facchetti, A.; Vaccaro, L.; Marrocchi, A. *Angew. Chem. Int. Ed. Engl.* **2012,** *51*, 3520-3.

49. Mercier, L. G.; Leclerc, M. *Acc. Chem. Res.* **2013,** *46*, 1597-1605.

50. Wang, K.; Wang, M. *Curr. Org. Chem.* **2013,** *17*, 999-1012.

51. Okamoto, K.; Zhang, J.; Housekeeper, J. B.; Marder, S. R.; Luscombe, C. K. *Macromolecules* **2013,** *46*, 8059-8078.

52. Kowalski, S.; Allard, S.; Zilberberg, K.; Riedl, T.; Scherf, U. *Prog. Polym. Sci.* **2013,** *38*, 1805-1814.

53. Théveau, L.; Schneider, C.; Fruit, C.; Hoarau, C. *ChemCatChem* **2016,** *8*, 3183-3194.

54. Suraru, S.-L.; Lee, J. A.; Luscombe, C. K. *ACS Macro Lett.* **2016,** *5*, 724-729.

55. Rossi, R.; Lessi, M.; Manzini, C.; Marianetti, G.; Bellina, F. *Tetrahedron* **2016,** *72*, 1795-1837.

56. Bura, T.; Blaskovits, J. T.; Leclerc, M. *J. Am. Chem. Soc.* **2016,** *138*, 10056-71.

57. Pouliot, J. R.; Grenier, F.; Blaskovits, J. T.; Beaupre, S.; Leclerc, M. *Chem. Rev.* **2016,** *116*, 14225-14274.

58. Yu, S.; Liu, F.; Yu, J.; Zhang, S.; Cabanetos, C.; Gao, Y.; Huang, W. *J. Mater. Chem. C* **2017,** *5*, 29-40.

59. Bohra, H.; Wang, M. *J. Mater. Chem. A* **2017,** *5*, 11550-11571.

60. Wang, X.; Wang, M. *Polym. Chem.* **2014,** *5*, 5784-5792.

61. Wang, X.; Wang, K.; Wang, M. *Polym. Chem.* **2015,** *6*, 1846-1855.

62. Shao, J.; Wang, G.; Wang, K.; Yang, C.; Wang, M. *Polym. Chem.* **2015,** *6*, 6836-6844.

63. Huang, J.; Wang, K.; Gupta, S.; Wang, G.; Yang, C.; Mushrif, S. H.; Wang, M. *J. Polym. Sci., Part A: Polym. Chem.* **2016,** *54*, 2015-2031.

64. Wang, K.; Wang, G.; Wang, M. *Macromol. Rapid Commun.* **2015,** *36*, 2162-70.

65. Bohra, H.; Tan, S. Y.; Shao, J.; Yang, C.; Efrem, A.; Zhao, Y.; Wang, M. *Polym. Chem.* **2016,** *7*, 6413-6421.

66. Efrem, A.; Wang, K.; Amaniampong, P. N.; Yang, C.; Gupta, S.; Bohra, H.; Mushrif, S. H.; Wang, M. *Polym. Chem.* **2016,** *7*, 4862-4866.

67. Bohra, H.; Shao, J.; Huang, S.; Wang, M. *Tetrahedron Lett.* **2016,** *57*, 1497-1501.

68. Wang, K.; Wang, M. *J. Polym. Sci., Part A: Polym. Chem.* **2017,** *55*, 1040-1047.

69. Wang, K.; Chen, H.; Wei, X.; Bohra, H.; He, F.; Wang, M. *Dyes Pigm.* **2018,** *158*, 183-187.

70. Chan, H. S. O.; Ng, S. C. *Prog. Polym. Sci.* **1998,** *23*, 1167-1231.

71. D., M. R. *Adv. Mater.* **1998,** *10*, 93-116.

72. Se´vignon, M.; Papillon, J.; Schulz, E.; Lemaire, M. *Tetrahedron Lett.* **1999,** *40*, 5873-5876.

73. Yamamoto, T.; Sanechika, K.; Yamamoto, A. *J. Polym. Sci., Part A: Polym. Chem.* **1980,** *18*, 9-12.

74. Wang, Q.; Takita, R.; Kikuzaki, Y.; Ozawa, F. *J. Am. Chem. Soc.* **2010,** *132*, 11420-11421.

75. Berrouard, P.; Najari, A.; Pron, A.; Gendron, D.; Morin, P. O.; Pouliot, J. R.; Veilleux, J.; Leclerc, M. *Angew. Chem. Int. Ed.* **2011,** *51*, 2068-2071.

76. Allard, N.; Najari, A.; Pouliot, J.-R.; Pron, A.; Grenier, F.; Leclerc, M. *Polym. Chem.* **2012,** *3*, 2875-2879.

77. Dudnik, A. S.; Aldrich, T. J.; Eastham, N. D.; Chang, R. P. H.; Facchetti, A.; Marks, T. J. *J. Am. Chem. Soc.* **2016,** *138*, 15699-15709.

78. Lu, W.; Kuwabara, J.; Kanbara, T. *Macromolecules* **2011,** *44*, 1252-1255.

79. Gorelsky, S. I. *Organometallics* **2012,** *31*, 4631-4634.

80. Wakioka, M.; Nakamura, Y.; Wang, Q.; Ozawa, F. *Organometallics* **2012,** *31*, 4810-4816.

81. Lapointe, D.; Fagnou, K. *Chem. Lett.* **2010,** *39*, 1118-1126.

82. Balcells, D.; Clot, E.; Eisenstein, O. *Chem. Rev.* **2010,** *110*, 749-823.

83. Biswas, B.; Sugimoto, M.; Sakaki, S. *Organometallics* **2000,** *19*, 3895-3908.

84. Gorelsky, S. I.; Lapointe, D.; Fagnou, K. *J. Am. Chem. Soc.* **2008,** *130*, 10848-10849.

85. Gorelsky, S. I.; Lapointe, D.; Fagnou, K. *J. Org. Chem.* **2012,** *77*, 658-668.

86. Lafrance, M.; Fagnou, K. *J. Am. Chem. Soc.* **2006,** *128*, 16496-16497.

87. Ackermann, L. *Chem. Rev.* **2011,** *111*, 1315-45.

88. Colletto, C.; Islam, S.; Juliá-Hernández, F.; Larrosa, I. *J. Am. Chem. Soc.* **2016,** *138*, 1677-1683.

89. Ueda, K.; Yanagisawa, S.; Yamaguchi, J.; Itami, K. *Angew. Chem. Int. Ed.* **2010,** *49*, 8946-8949.

90. Alberico, D.; Scott, M. E.; Lautens, M. *Chem. Rev.* **2007,** *107*, 174-238.

91. Dou, L.; Liu, Y.; Hong, Z.; Li, G.; Yang, Y. *Chem. Rev.* **2015,** *115*, 12633-65.

92. Burke, D. J.; Lipomi, D. J. *Energy Environ. Sci.* **2013,** *6*, 2053.

93. Holliday, S.; Donaghey, J. E.; McCulloch, I. *Chem. Mater.* **2014,** *26*, 647-663.

94. Kanimozhi, C.; Yaacobi-Gross, N.; Chou, K. W.; Amassian, A.; Anthopoulos, T. D.; Patil, S. *J. Am. Chem. Soc.* **2012,** *134*, 16532-16535.

95. Pouliot, J.-R.; Sun, B.; Leduc, M.; Najari, A.; Li, Y.; Leclerc, M. *Polym. Chem.* **2015,** *6*, 278-282.

96. Gao, Y.; Zhang, X.; Tian, H.; Zhang, J.; Yan, D.; Geng, Y.; Wang, F. *Adv. Mater.* **2015,** *27*, 6753-9.

97. Matsidik, R.; Komber, H.; Luzio, A.; Caironi, M.; Sommer, M. *J. Am. Chem. Soc.* **2015,** *137*, 6705-11.

98. Li, W.; Hendriks, K. H.; Wienk, M. M.; Janssen, R. A. J. *Acc. Chem. Res.* **2016,** *49*, 78-85.

99. Guérette, M.; Najari, A.; Maltais, J.; Pouliot, J.-R.; Dufresne, S.; Simoneau, M.; Besner, S.; Charest, P.; Leclerc, M. *Adv. Energy Mater.* **2016,** *6*, 1502094.

100. Jo, J.; Pron, A.; Berrouard, P.; Leong, W. L.; Yuen, J. D.; Moon, J. S.; Leclerc, M.; Heeger, A. J. *Adv. Energy Mater.* **2012,** *2*, 1397-1403.

101. Wang, D. H.; Pron, A.; Leclerc, M.; Heeger, A. J. *Adv. Funct. Mater.* **2013,** *23*, 1297-1304.

102. Cabanetos, C.; El Labban, A.; Bartelt, J. A.; Douglas, J. D.; Mateker, W. R.; Fréchet, J. M. J.; McGehee, M. D.; Beaujuge, P. M. *J. Am. Chem. Soc.* **2013,** *135*, 4656-4659.

103. Chu, T.-Y.; Lu, J.; Beaupré, S.; Zhang, Y.; Pouliot, J.-R.; Zhou, J.; Najari, A.; Leclerc, M.; Tao, Y. *Adv. Funct. Mater.* **2012,** *22*, 2345-2351.

104. Marzano, G.; Carulli, F.; Babudri, F.; Pellegrino, A.; Po, R.; Luzzati, S.; Farinola, G. M. *J. Mater. Chem. A* **2016,** *4*, 17163-17170.

105. Dudnik, A. S.; Aldrich, T. J.; Eastham, N. D.; Chang, R. P.; Facchetti, A.; Marks, T. J. *J. Am. Chem. Soc.* **2016,** *138*, 15699-15709.

106. Nguyen, T. L.; Choi, H.; Ko, S. J.; Uddin, M. A.; Walker, B.; Yum, S.; Jeong, J. E.; Yun, M. H.; Shin, T. J.; Hwang, S.; Kim, J. Y.; Woo, H. Y. *Energy Environ. Sci.* **2014,** *7*, 3040-3051.

107. Maojie, Z.; Xia, G.; Wei, M.; Harald, A.; Jianhui, H. *Adv. Mater.* **2015,** *27*, 4655-4660.

108. Zhang, S.; Qin, Y.; Uddin, M. A.; Jang, B.; Zhao, W.; Liu, D.; Woo, H. Y.; Hou, J. *Macromolecules* **2016,** *49*, 2993-3000.

109. Zhao, W.; Li, S.; Yao, H.; Zhang, S.; Zhang, Y.; Yang, B.; Hou, J. *J. Am. Chem. Soc.* **2017,** *139*, 7148-7151.

110. Zhang, S.; Qin, Y.; Zhu, J.; Hou, J. *Adv. Mater.* **2018,** *30*, 1800868.

111. Huo, L.; Liu, T.; Sun, X.; Cai, Y.; Heeger Alan, J.; Sun, Y. *Adv. Mater.* **2015,** *27*, 2938-2944.

112. Tao, L.; Lijun, H.; Xiaobo, S.; Bingbing, F.; Yunhao, C.; Taehyo, K.; Young, K. J.; Hyosung, C.; Yanming, S. *Adv. Energy Mater.* **2016,** *6*, 1502109.

113. Tao, L.; Xuexue, P.; Xiangyi, M.; Yu, L.; Donghui, W.; Wei, M.; Lijun, H.; Xiaobo, S.; Ho, L. T.; Minjuan, H.; Hyosung, C.; Young, K. J.; H., C. W. C.; Yanming, S. *Adv. Mater.* **2017,** *29*, 1604251.

114. Fukutomi, Y.; Nakano, M.; Hu, J.-Y.; Osaka, I.; Takimiya, K. *J. Am. Chem. Soc.* **2013,** *135*, 11445-11448.

115. Nakano, M.; Osaka, I.; Takimiya, K. *Macromolecules* **2015,** *48*, 576-584.

116. Hu, J.-Y.; Nakano, M.; Osaka, I.; Takimiya, K. *J. Mater. Chem. C* **2015,** *3*, 4244-4249.

117. Nakano, M.; Osaka, I.; Hashizume, D.; Takimiya, K. *Chem. Mater.* **2015,** *27*, 6418-6425.

118. Vilela, F.; Zhang, K.; Antonietti, M. *Energy Environ. Sci.* **2012,** *5*, 7819.

119. Liu, Q.; Tang, Z.; Wu, M.; Zhou, Z. *Polym. Int.* **2014,** *63*, 381-392.

120. Liu, D.-P.; Chen, Q.; Zhao, Y.-C.; Zhang, L.-M.; Qi, A.-D.; Han, B.-H. *ACS Macro Lett.* **2013,** *2*, 522-526.

121. Feng, L.-J.; Guo, J.-W.; Zhong, X.; Sun, Z.-Y. *J. Macromol. Sci., Part A: Pure Appl. Chem.* **2014,** *51*, 604-609.

122. Hayashi, S.; Togawa, Y.; Ashida, J.; Nishi, K.; Asano, A.; Koizumi, T. *Polymer* **2016,** *90*, 187-192.

123. Zhu, Y.; Long, H.; Zhang, W. *Chem. Mater.* **2013,** *25*, 1630-1635.

124. Kaur, P.; Hupp, J. T.; Nguyen, S. T. *ACS Catal.* **2011,** *1*, 819-835.

125. Li, L.; Cai, Z.; Wu, Q.; Lo, W. Y.; Zhang, N.; Chen, L. X.; Yu, L. *J. Am. Chem. Soc.* **2016,** *138*, 7681-6.

126. Sprick, R. S.; Jiang, J. X.; Bonillo, B.; Ren, S.; Ratvijitvech, T.; Guiglion, P.; Zwijnenburg, M. A.; Adams, D. J.; Cooper, A. I. *J. Am. Chem. Soc.* **2015,** *137*, 3265-70.

127. Xue, W.; Chong, Z.; Yunfeng, X.; Qian, H.; Pan, M.; Yu, C.; Jinghui, Z.; Feng, W.; Jia-Xing, J. *Macromol. Chem. Phys.* **2018,** *219*, 1700524.

128. Sun, C.-J.; Wang, P.-F.; Wang, H.; Han, B.-H. *Polym. Chem.* **2016,** *7*, 5031-5038.

129. Sun, C.-J.; Zhao, X.-Q.; Wang, P.-F.; Wang, H.; Han, B.-H. *Sci. China Chem.* **2017,** *60*, 1067-1074.

130. Liu, H.; Li, Q.; Li, Q.; Jin, W.; Li, X.; Hameed, A.; Qiao, S. *Polym. Chem.* **2017,** *8*, 6733-6740.

131. Palma-Cando, A.; Brunklaus, G.; Scherf, U. *Macromolecules* **2015,** *48*, 6816-6824.

132. Feng, R.; Fei, W.; Yu, P.; Hanxue, S.; Zhaoqi, Z.; Chonghua, M.; Chaohu, X.; Weidong, L.; Lihua, C.; An, L. *Macromol. Mater. Eng.* **2018,** *303*, 1700619.

133. Ren, F.; Zhu, Z.; Qian, X.; Liang, W.; Mu, P.; Sun, H.; Liu, J.; Li, A. *Chem. Commun.* **2016,** *52*, 9797-9800.

134. Qin, L.; Xu, G.-j.; Yao, C.; Xu, Y.-h. *Polym. Chem.* **2016,** *7*, 4599-4602.

135. Vangeneugden, D. L.; Vanderzande, D. J. M.; Salbeck, J.; van Hal, P. A.; Janssen, R. A. J.; Hummelen, J. C.; Brabec, C. J.; Shaheen, S. E.; Sariciftci, N. S. *J. Phys. Chem. B* **2001,** *105*, 11106-11113.

136. Hug, S.; Stegbauer, L.; Oh, H.; Hirscher, M.; Lotsch, B. V. *Chem. Mater.* **2015,** *27*, 8001-8010.

137. Puthiaraj, P.; Lee, Y.-R.; Zhang, S.; Ahn, W.-S. *J. Mater. Chem. A* **2016,** *4*, 16288-16311.

138. Bhunia, A.; Vasylyeva, V.; Janiak, C. *Chem. Commun.* **2013,** *49*, 3961-3963.

139. Wang, X.; Zhang, C.; Zhao, Y.; Ren, S.; Jiang, J.-X. *Macromol. Rapid Commun.* **2016,** *37*, 323-329.

140. Ren, S.; Bojdys, M. J.; Dawson, R.; Laybourn, A.; Khimyak, Y. Z.; Adams, D. J.; Cooper, A. I. *Adv. Mater.* **2012,** *24*, 2357-2361.

141. Feng, X.; Ding, X.; Jiang, D. *Chem. Soc. Rev.* **2012,** *41*, 6010-6022.

Parts of Chapter 1 are published as Bohra, H.; Wang, M., Direct C-H Arylation: A "Greener" Approach Towards Facile Synthesis of Organic Semiconducting Molecules and Polymers. *J. Mater. Chem. A* 2017, *5*, 11550-11571. DOI: 10.1039/C7TA00617A

2. Synthesis and characterization of naphthodithiophenediimide small molecules and polymers by direct arylation

2.1 Introduction

Among the various π-conjugated building blocks utilized for organic optoelectronic devices, naphthalene diimide (NDI) is one of the most widely studied electron-accepting species in the rylene diimide family.[1-2] Core-extended NDI derivatives[3-4] have found great potential as building blocks for high electron mobility n-type[5-7] as well as ambi-polar thin film transistors (TFTs).[8] In particular, a new core-expanded NDI derivative called naphtho[2,3-*b*:6,7-*b*]-dithiophenediimide (NDTI) was recently reported by Takimiya and co-workers.[9] NDTI provides several advantages over other core-extended NDI derivatives: (i) the fused thiophene groups improve the planarity of the molecule as opposed to flanked thiophenes that form an out of plane angle with the NDI core,[10] (ii) the rigidity and overall long range ordering is conducive to extensive p-orbital overlap which consequently facilitates charge transport.

Most of the reported NDI-based small molecules and polymers have been synthesized through conventional coupling methods such as Suzuki coupling and Stille coupling, both of which involve tedious C–H pre-activation using organometallic reagents that suffer from high flammability (e.g., butyllithium), high toxicity (e.g., stannyl reagents) and poor stability. To that end, C–H direct arylation has emerged as a new efficient and green method that enables the facile synthesis of p-conjugated molecules and polymers in fewer steps, without the need for C–H bond pre-activation or involvement of toxic stannyl reagents. Although C–H direct arylation has been extensively studied in the organometallic community for the synthesis of a variety of organic small molecules for applications such as pharmaceutics,[11-13] its application to synthesis of π-

conjugated systems (both small molecules and polymers) with tunable optoelectronic properties has until recently not attracted much attention.[14-23]

To date, a variety of π-conjugated small molecules,[24-25] homopolymers[26-28] and donor–acceptor copolymers[29-34] have been synthesized using C–H direct arylation coupling. For example, Sommer and co-workers recently reported the synthesis of donor–acceptor–donor (D–A–D) type NDI building blocks and polymers using highly efficient direct arylation routes.[35-36] Moreover, core expansion on the lateral edges of NDI derivatives for fine tuning of electrical and optical properties can now be realized by the activation of the C–H bond of simple unsubstituted heteroaryls such as thiophene.[37] More recently, a NDI-tetrafluorobenzene polymer (P(ThNDIThF4)) was synthesized by direct arylation polymerization (DAP) and the polymer showed an electron mobility as high as 1.3 $cm^2 V^{-1} s^{-1}$ in top-gate, bottom contact field effect transistors.[10] To the best of our knowledge, C–H direct arylation coupling has never been used in the synthesis of NDTI based polymers and small molecules. Recently, we have reported the synthesis of donor–acceptor (D–A) type copolymers via direct-arylation cross coupling polycondensation.[29-31, 38] We found that in the high-boiling-point, non-polar aromatic solvent 1,2-dimethylbenzene (*o*-xylene), Pd_2dba_3/(*o*-$MeOC_6H_4)_3P$, potassium carbonate and pivalic acid as an additive, serves as an efficient catalyst system to obtain high quality polymers.[30-31]

Herein, we present the synthesis and characterization of a novel NDTI polymer (**PNDTI-OF**) containing the electron-rich co-monomer unit 9,9-dioctylfluorene, and an analogous NDTI triad (denoted as **NDTI-2HF**) with containing 9,9-dihexylfluorene, by direct arylation. A narrow bandgap polymer — **PNDTI-BTz**, consisting of alternating NDTI and benzothiadiazole, which was synthesized by Stille coupling in an earlier report,[39] was also synthesized under the scheme of DAP.

2.2 Synthesis and structural characterization

In contrast to previous reports of polymerization with NDTI where conventional coupling methods such as Suzuki coupling and Stille coupling were

utilized to obtain high molecular weight polymers, we investigated the previously devised DAP route using the NDTI monomer to synthesize small molecule derivatives and polymers.[38] NDTI-based small molecules were obtained from a one-pot direct arylation of **C20-NDTI** (0.1 M) and **BrHF** (molar ratio = 1:10). A mixture of mono-(denoted as **NDTI-HF**) and bi- (denoted as **NDTI-2HF**) substituted products was obtained with yields of 25% and 10%, respectively, which can be attributed to the relatively low reactivity of the NDTI molecule under these direct arylation conditions (**Scheme 2.1**).

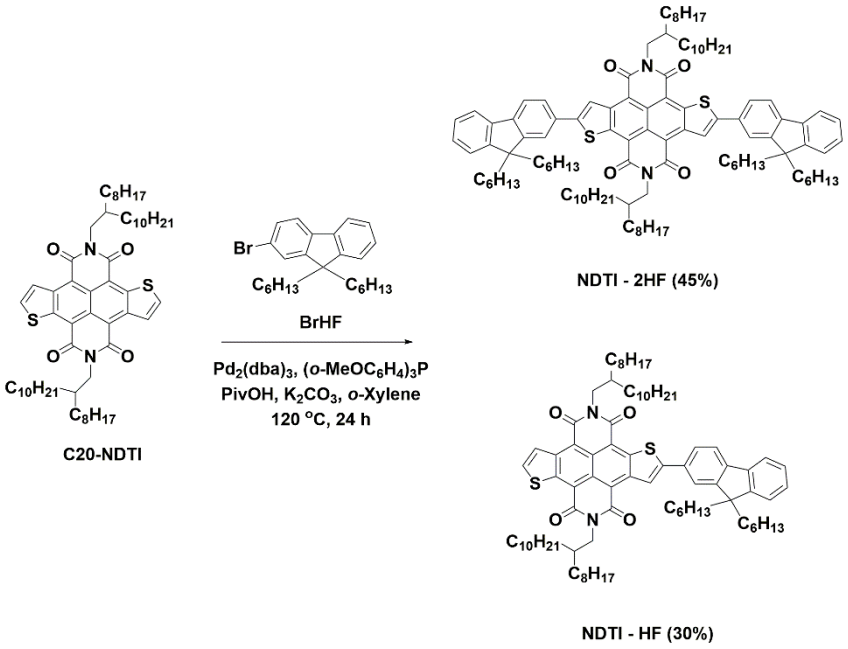

Scheme 2.1 Synthesis of **NDTI-2HF** and **NDTI-HF** via direct arylation.

Increasing the concentration of **C20-NDTI** to 0.2 M improved the yield of **NDTI-2HF** to 45% and **NDTI-HF** to 30%, while 10% of **C20-NDTI** remained unreacted. Although no significant formation of by-products was observed from the activation of the β-H in the NDTI monomer, the presence of unreacted monomers is an indication of the relatively low reactivity of the a-H under these reaction conditions. In addition, the homo-coupling of (**BrHF**) is a possible side reaction that might also contribute to the relatively low yield of NDTI-2HF. The ^{1}H NMR spectra (**Figure 2.1**) of both products (**NDTI-HF** and **NDTI-2HF**)

show a clear peak at 9.15 ppm which could be assigned to the β-proton of the annulated thiophenes. All other peaks could be assigned to protons from the NDTI core and fluorene moieties. The broad peaks in the aromatic region of the ^{1}H NMR spectra (**Figure 2.1**) of **NDTI-HF** and **NDTI-2HF** as well as some other NDTI based small molecules reported by Takimiya and co-workers[40-41] might have originated from inter-molecular aggregation in the solvent at room temperature Such broadening is more serious in the ^{1}H NMR spectra of the NDTI copolymers. as discussed later. The chemical structures of these two products were further confirmed by mass spectroscopy.

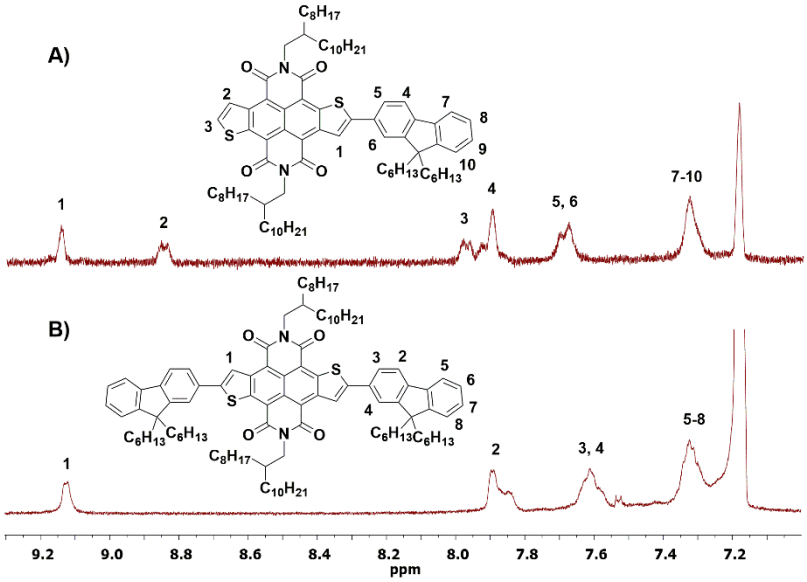

Figure 2.1 ^{1}H NMR (300 MHz) spectra showing the range of aromatic protons in A) NDTI-HF and B) NDTI-2HF.

DAP between **C20-NDTI** and **DBrBTz** or **DBrOF** (**Scheme 2.2**) resulted in the formation of **PNDTI-OF** and **PNDTI-BTz** in moderate yields. Gel permeation chromatography (GPC) traces of NDTI polymers are presented in **Figure 2.2**. **PNDTI-BTz** synthesized yielded low molecular weight polymers as compared to the Suzuki coupling product (M_n = 7.2 kDa) and Stille coupling product (M_n = 14.4 kDa) reported by Takimiya's group.[39] It is speculated that an aromatically stabilized closed-shell structure hinders the deprotonation of NDTI by the carboxylate additive from the NDTI-palladium transition state, thereby

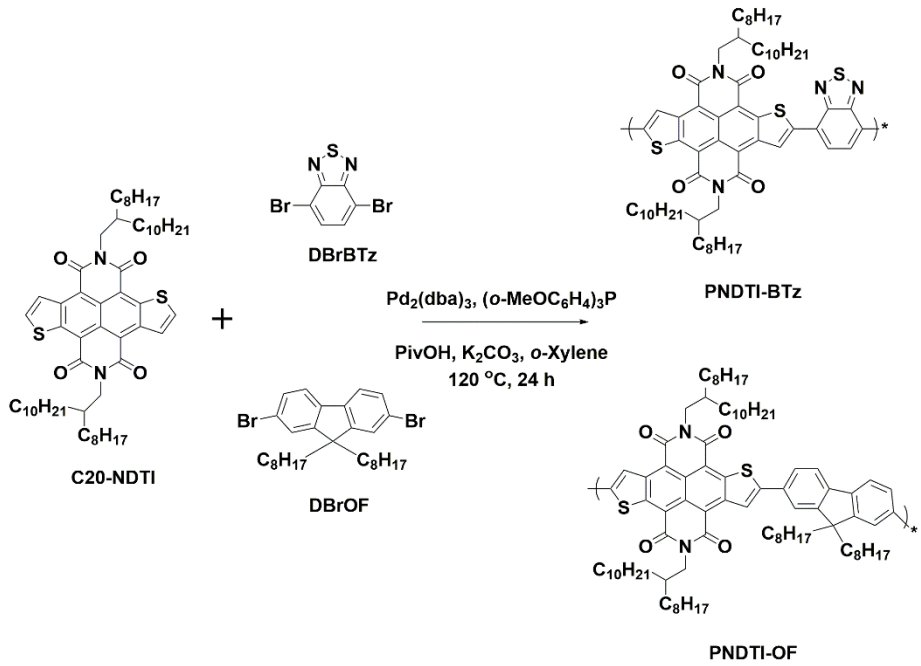

Scheme 2.2 Synthesis of **PDNTI-OF** and **PNDTI-BTz** via direct arylation.

Table 2.1 Summary of the synthesis of NDTI-based small molecules and polymers.

Species [a]	Entry	Concentration (M)	Yield (%)	M_n (kDa)	PDI
NDTI-2HF [b]	1	0.1	10	-	-
	2	0.2	45	-	
PNDTI-OF	3	0.1	50 [c]	3.6 [c]	1.53
	4	0.2	50 [c]	5.2 [c]	1.6
			38 [d]	7.2 [d]	2.16
PNDTI-BTz	5	0.1	45 [c]	3.3 [c]	1.54

[a] All reactions were carried out at 120 ºC for 24 hours. [b] Molecular weight was verified by mass spectroscopy. [c] Results from the hexane fraction. [d] Results the chloroform fraction

rendering the α-carbon inert, which is the target site for aryl–aryl coupling. The relatively low reactivity does not favour the formation of high molecular weight polymers. In effect, the products obtained by DAP at 0.1 M of **C20-NDTI** were

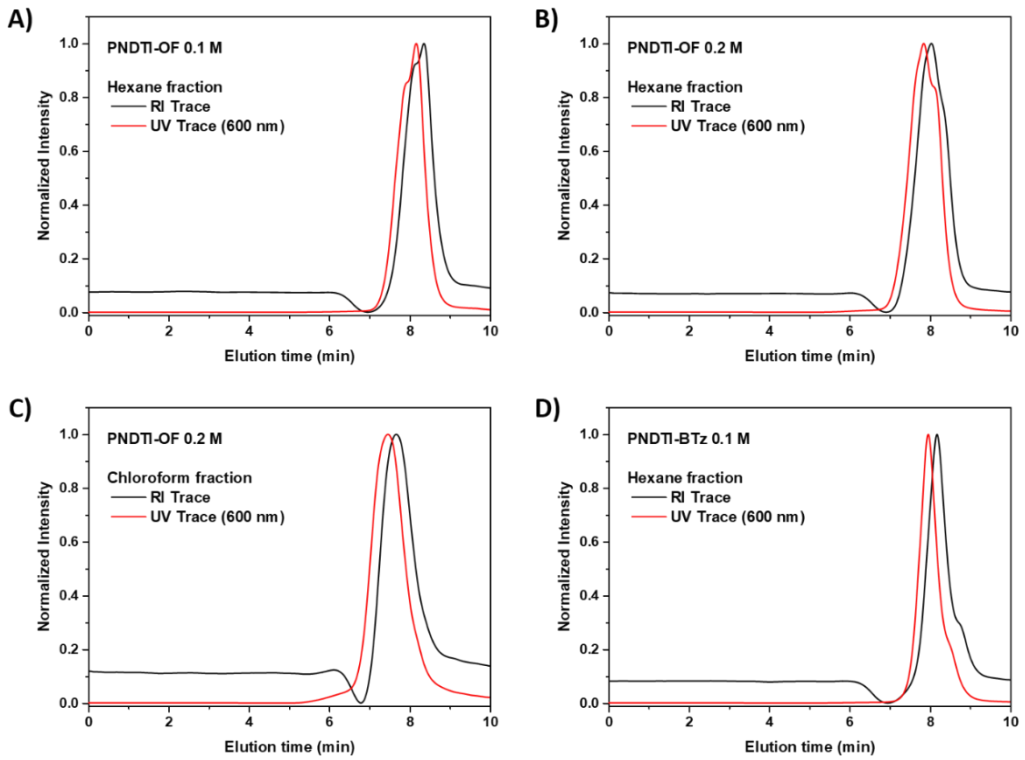

Figure 2.2 GPC **(**RI and UV) traces of a) **PNDTI-OF** (Entry 3), B) **PNDTI-OF** (Entry 4 - Hexane), C) **PNDTI-OF** (Entry 4 - CF) and D) **PNDTI-BTz** at 80^{o} C with chloroform as the eluent.

mainly oligomers. In an attempt to obtain higher molecular weight products, **PNDTI-OF** was synthesized at a higher concentration (0.2 M). It was observed that increasing the concentration afforded higher molecular weight polymers (M_n = 7.21 kDa, **Table 2.1**-Entry 4) from the chloroform fraction as opposed to the previous run at 0.1 M (**Table 2.1**-Entry 3) where polymeric products could only be obtained from the hexane fraction. The GPC traces of **PNDTI-OF**s from entries 3 and 4 (**Figure 2.2a-c**), show unimodal peaks with relatively narrow polydispersity indices. Furthermore, comparison of the hexane fractions showed that, although the yield remained unchanged for Entries 3 and 4, the molecular weight slightly increased to 5.16 kDa for Entry 4. The ^{1}H NMR spectra of all polymers containing fluorene show broad peaks in the aromatic range in $C_2D_2Cl_4$ at 373 K (**Figure 2.3-2.5**), whereas the protons from the polymer backbone and

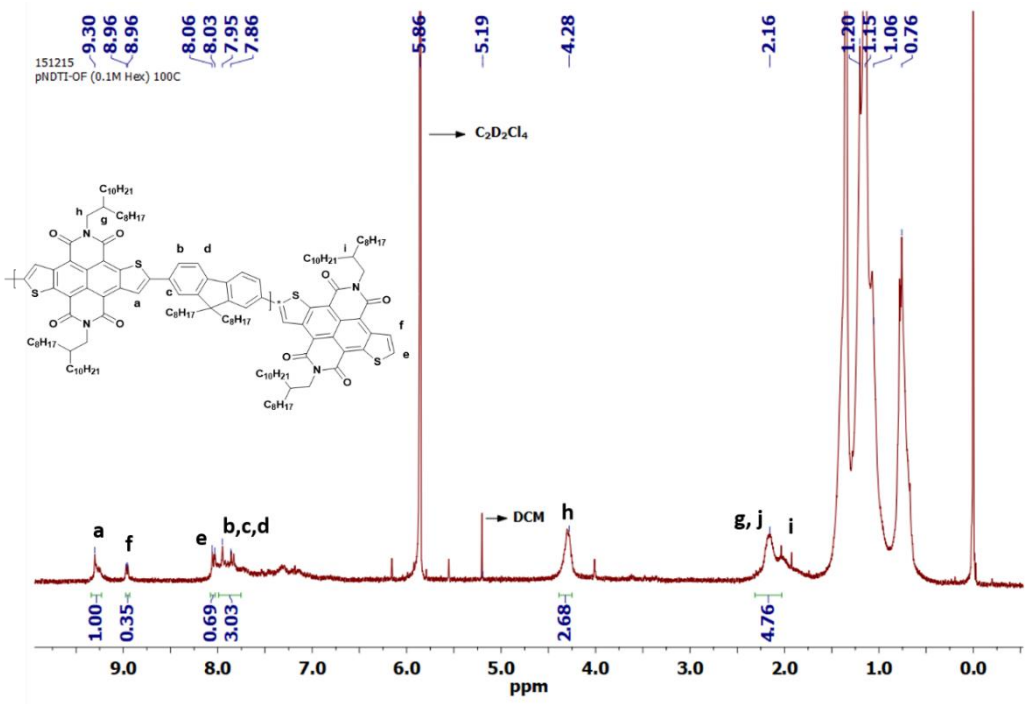

Figure 2.3 ^{1}H NMR spectra of the hexane fraction of **PNDTI-OF** synthesized at a concentration of 0.1 M (300 MHz, $C_2D_2Cl_4$, 373 K).

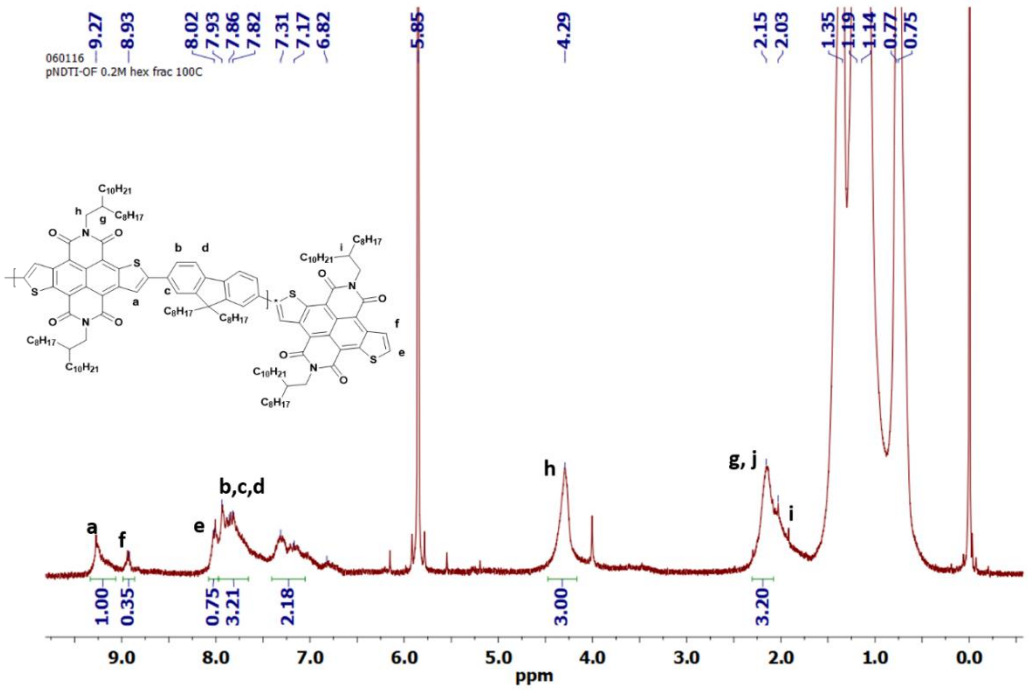

Figure 2.4 ^{1}H NMR spectra of the hexane fraction of **PNDTI-OF** synthesized at a concentration of 0.2 M (300 MHz, $C_2D_2Cl_4$, 373 K).

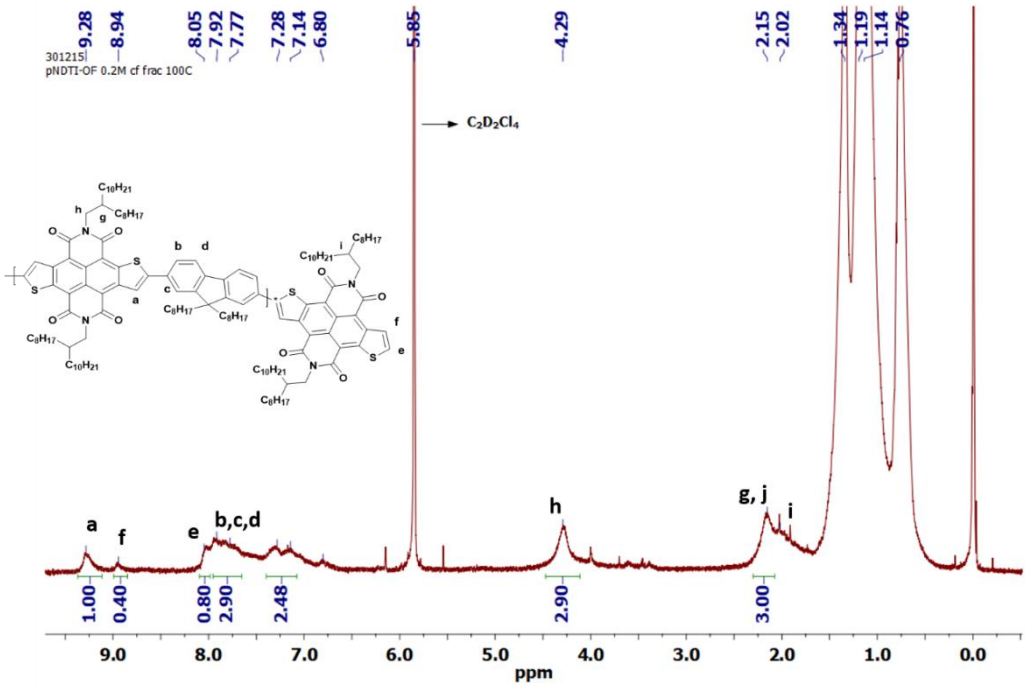

Figure 2.5 ^{1}H NMR spectra of the chloroform fraction of **PNDTI-OF** synthesized at a concentration of 0.2 M (300 MHz, $C_2D_2Cl_4$, 373 K).

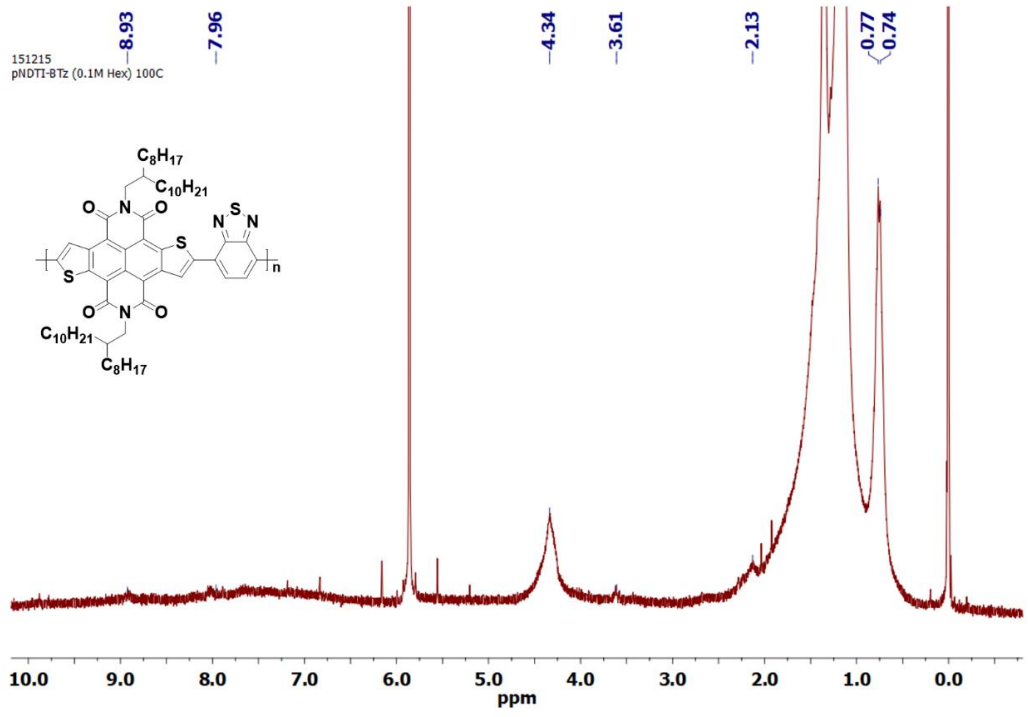

Figure 2.6 ^{1}H NMR spectra of the hexane fraction of **PNDTI-BTz** synthesized at a concentration of 0.1 M (300 MHz, $C_2D_2Cl_4$, 373 K).

NDTI end-group could still be assigned. In contrast, no discernible peaks could be identified from the ^{1}H NMR spectrum of **PNDTI-BTz** (**Figure 2.6**), even in $C_2D_2Cl_4$ at 373 K. A similar phenomenon was also reported in the NDTI-based polymers previously synthesized via Stille coupling.[39]

2.3 Thermal properties

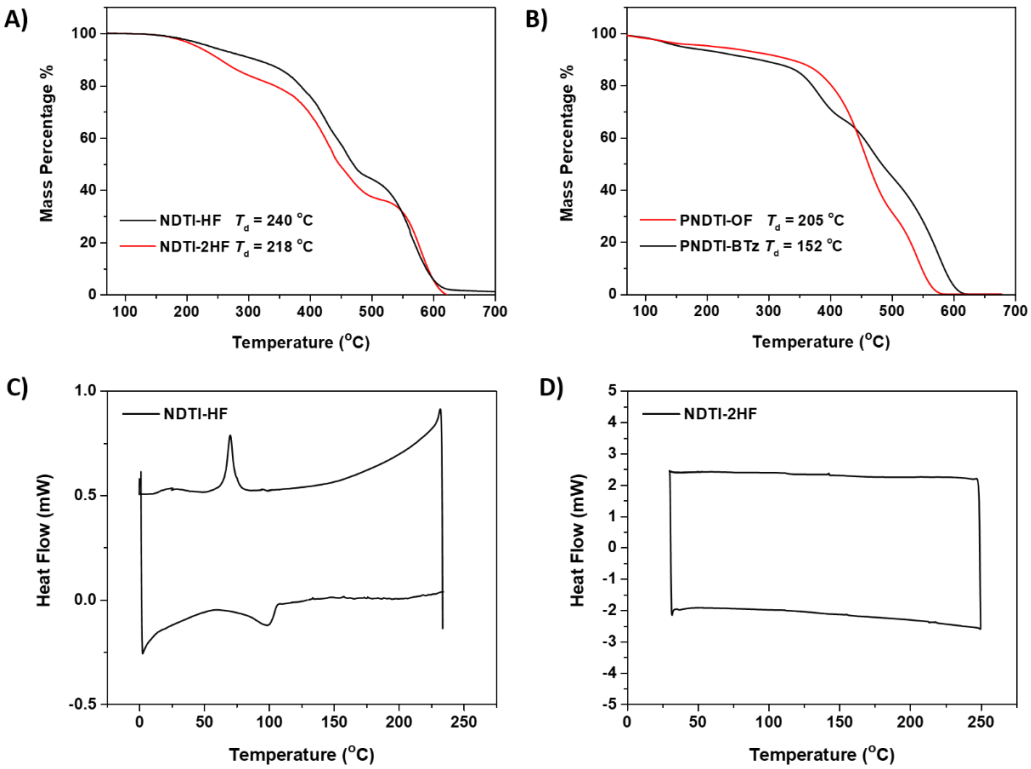

Figure 2.7 Thermogravimetric analysis plots (A, B) of NDTI-based A) small molecules and B) polymers. Differential scanning calorimetry profiles of C) **NDTI-HF** and D) **NDTI-2HF**.

Thermo-gravimetric analysis (TGA) and differential scanning calorimetry (DSC) were used to study the thermal properties of NDTI based small molecules. Both **NDTI-HF** (T_d = 239.6 °C) and **NDTI-2HF** (T_d = 217.5 °C) showed degradation temperatures (corresponding to 5% weight loss) below 250 °C, which is reasonable for small molecules (**Figure 2.7a**). The DSC curves shows that **NDTI-HF** undergoes phase transition at approximately 107 °C in the second endothermic cycle (**Figure 2.7c**). On the contrary, no phase transition

could be observed for **NDTI-2HF**. Hexane fraction of **PNDTI-OF** obtained in entry 4 and **PNDTI-BTz** obtained in entry 5 were also studied of by TGA. Degradation temperatures of 205 ºC and 152 ºC were observed for PNDTI-OF and PNDTI-BTz respectively (**Figure 2.7b**).

2.4 Optical and electrochemical characterizations

The optical properties of small molecules and polymers were studied in solutions and in films. All materials showed strong absorption over the visible range. Upon the addition of fluorene groups to the NDTI moiety, a significant red-shift in absorption maximas was observed from **C20-NDTI** to **NDTI-HF** to **NDTI-2HF** (**Figure 2.8a**). This bathochromatic shift can also be seen in the fluorescence spectra of **NDTI-HF** and **NDTI-2HF** as the maximum emission shifts from 641 to 655 nm. Moreover, conjugation with the fluorene units leads to enhancement of the intensity of the intermolecular charge-transfer (ICT) bands of NDTI core compared to the bands from π–π interaction. It is interesting to note that the absorption edge of **NDTI-2HF** in thin films shifts bathochromatically by 90 nm in comparison to its absorption in solution (**Figure 2.8b**). A more significant bathochromatic shift was observed in thin films of **NDTI-HF**, which suggests strong J-type aggregation in the solid states of these small molecules.

Band-gaps of the NDTI-based small molecules were calculated using absorption onset wavelengths of drop-cast thin films (**Figure 2.8**). As expected, **NDTI-HF** (λ_{onset} = 719 nm, E_g = 1.7 eV) showed a slightly larger bandgap than **NDTI-2HF** (λ_{onset} = 752 nm, E_g = 1.65 eV). The bandgap of **NDTI-2HF** is smaller than other NDTI triads reported by Takimiya and co-workers.[40-41] Energy levels of the small molecules were calculated from their optical bandgap and the oxidation onsets obtained from cyclic voltammetry (**Figure 2.9**). **NDTI-HF** and **NDTI-2HF** exhibit multiple reduction peaks which can be attributed to reduction of the NDTI core. These reversible peaks can be clearly observed in the cyclic voltammogram of **C20-NDTI**. The electron-donating effect of the fluorene units was evident from the negative shift of the reduction onsets in **NDTI-2HF** when compared to **C20-NDTI** (**Figure 2.2**). As expected, the electron affinity or the reducibility of the small molecule decreased with the addition of the fluorene

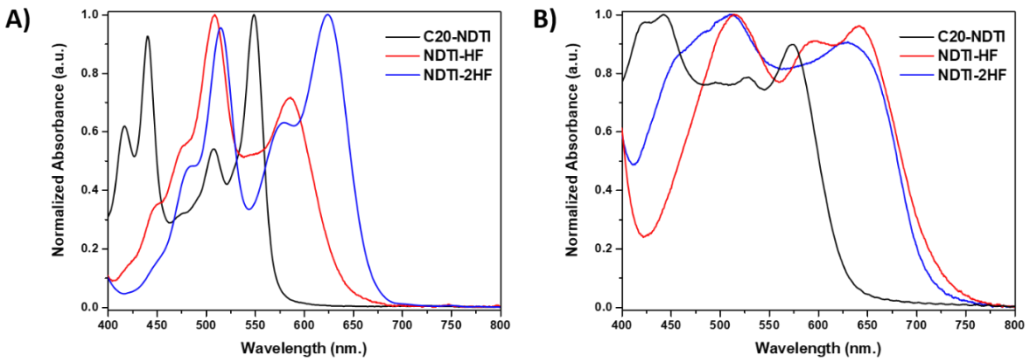

Figure 2.8 UV-Vis spectroscopy of NDTI small molecules in A) chloroform solutions and B) films.

Table 2.2 Electrochemical and optical properties of NDTI small molecules and polymers.

Species	E_{ox}^{onset} (V) [a]	E_{HOMO} (eV) [b]	E_{red}^{onset} (V) [a]	E_{LUMO} (eV) [c]	λ_{edge}^{film} (nm)	E_g^{opt} (eV) [d]
NDTI-2HF	1.61	-6.01	-0.90	-4.34	752	1.65
NDTI-HF	1.66	-6.06	-0.97	-4.34	719	1.72
PNDTI-OF [e]	1.33	-5.72	-0.87	-4.12	775	1.6
PNDTI-BTz	1.18	-5.58	-0.79	-4.01	790	1.57

[a] V vs Ag/AgCl. [b] Empirically calculated from E_{HOMO} (ev) = 4.4 - E_{ox}^{onset}. [c] Estimated from $E_{LUMO} = E_{HOMO} - E_g^{opt}$. [d] Estimated from absorption edge in thin films. [e] Polymer synthesized in entry 3.

units (**Table 2.2**). UV–vis absorption spectra of **PNDTI-OF**s synthesized by DAP are presented in **Figure 2.10**. As expected, the absorption edges of the polymers red shift with increasing molecular weight (Table 2.1-Entry 4 (chloroform) > Table 2.1-Entry 4 (Hexane) > Table 2.1-Entry 3). In addition, all **PNDTI-OF**s have longer absorption wavelengths than their triad analogue, **NDTI-2HF**. **PNDTI-OF**s

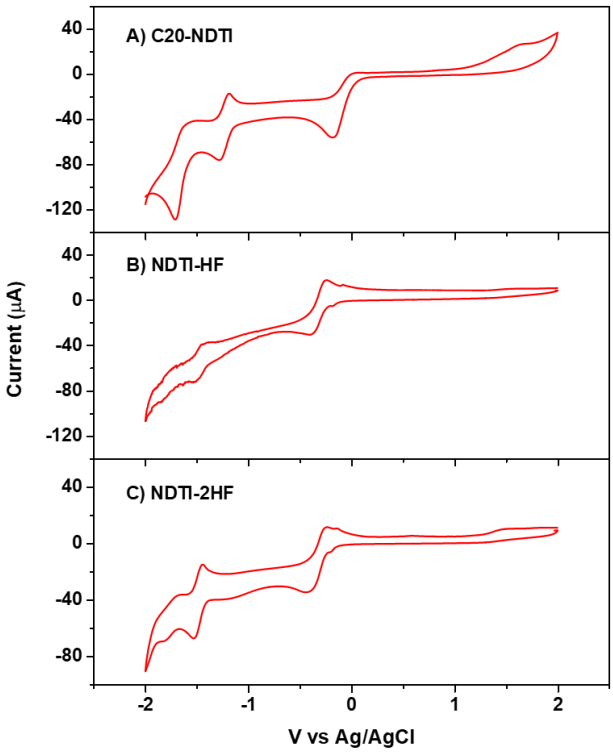

Figure 2.9 Cyclic Voltammograms of A) **C20-NDTI**, B) **NDTI-HF** and D) **NDTI-2HF**.

synthesized at 0.2 M (Table 2.1-Entry 4) have absorption extending beyond 800 nm in film. This can be explained as a direct result of the longer conjugation length in these polymers as compared to **PNDTI-OF** (Table 2.1-Entry 3). UV–vis absorption spectra of **PNDTI-BTz** (**Figure 2.9**) were compared with those of **PNDTI-OF** (Entry 1). **PNDTI-OF** and **PNDTI-BTz** exhibited a strong absorption between 700 and 400 nm with a maximum absorption at 640 and 542 nm, respectively. Moreover, the absorption tail of **PNDTI-BTz** (750 nm) was more red shifted than that of **PNDTI-OF** (725 nm). NDTI-based copolymers synthesized at a concentration of 0.1 M (**Table 2.1**-Entries 3 and 5) were used for comparison of their electrochemical properties. **PNDTI-BTz** (λ_{onset} = 790 nm) was found to have the lowest band gap of 1.57 eV. This is slightly higher than the same polymer reported by Takimiya and co-workers[39] owing to the higher molecular weight and conjugation length. Although LUMO levels of NDTI moieties remain relatively unaffected by comonomers as demonstrated by Takimiya and co-workers,[39-41] the narrow band gap can be explained by the

presence of benzothiadiazole units in the polymer backbone that facilitate planarity and hence good π-orbital overlap. **PNDTI-OF** was found to have a band-gap of 1.6 eV (λ_{onset} = 775 nm) which is comparable to that of **PNDTI-BTz**. Based on the same rationale, the HOMO level of **PNDTI-OF** can be expected to be elevated without significant change in the LUMO energy (**Table 2.2**).

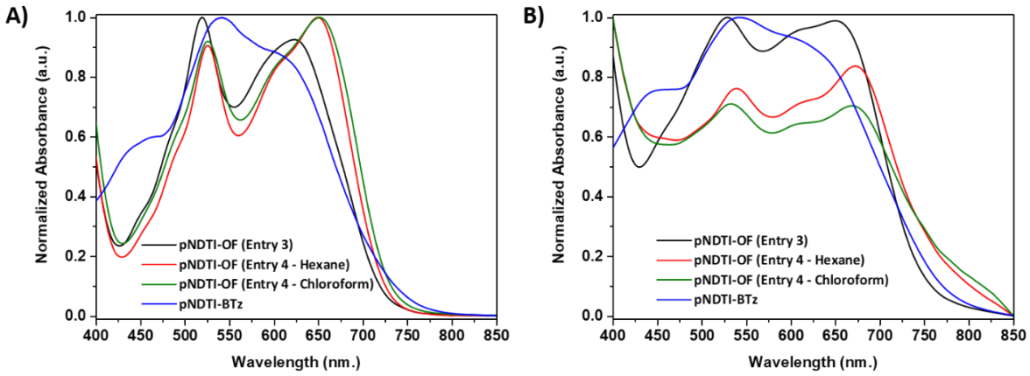

Figure 2.10 UV-Vis spectroscopy of NDTI-based polymers in A) chloroform solutions and B) thin films.

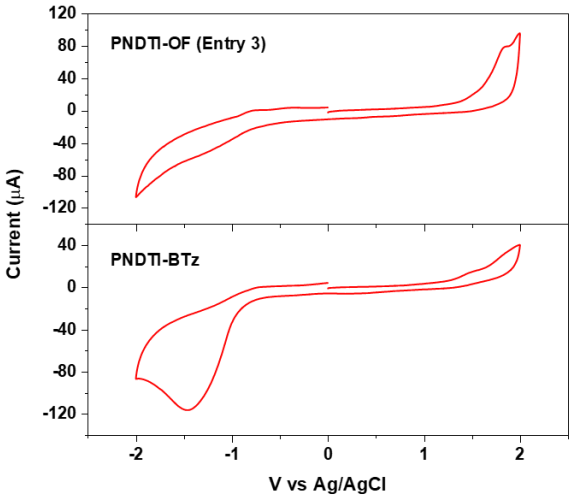

Figure 2.11 Cyclic Voltammograms of NDTI-based polymers.

HOMO and LUMO energy levels were calculated from the oxidation onset of the materials in cyclic voltammograms (**Figure 2.11**) and the optical band gap from thin films. **PNDTI-OF** and **PNDTI-BTz** show strong oxidation and reduction peaks, respectively, in the range of -2 to 2 V. HOMO and LUMO estimated for **PNDTI-OF** from its oxidation onset were -5.72 and -4.12 eV, respectively. These values were consistent with the energy levels of reported NDTI polymers with electron-rich co-monomers.[39] Moreover, the LUMO level of **PNDTI-OF** was slightly higher than that of NDTI (E_{LUMO} = -3.95 eV)[9] indicating the invariant nature of LUMO levels in NDTI polymers. DFT calculations of similar triads[39-41] have proved that the LUMO levels are generally localized over the NDTI core as opposed to the entire structure or the side groups. However, the electron-donating effect of fluorene units in the polymer backbone contributes to the elevation of the HUMO level. This effect is highly suppressed in **NDTI-2HF** (E_{HOMO} = -6 eV) whose HOMO level is only marginally higher than that of NDTI (E_{HOMO} = -6.05 eV). This can be attributed to the smaller conjugation length of **NDTI-2HF** and reduced contribution of electron-rich fluorenes as compared to **PNDTI-OF**. Nonetheless, the HOMO–LUMO levels of **PNDTI-OF** and **NDTI-2HF** show promise for good ambi-polar behaviour as has previously been demonstrated for D–A–D type NDTI polymers[9-10] and triads.[40-41]

2.5 Conclusion

In summary, direct arylation coupling of NDTI systems was demonstrated by synthesizing both small-molecule derivatives and polymers. In particular, a new D–A–D triad consisting of NDTI as the core flanked with 9,9-dihexylfluorene was synthesized. The electrochemical and optical properties of these materials show great promise for applications in optoelectronics. Moreover, with further optimization of the reaction conditions, direct arylation in NDTI systems can yield functional building blocks and high molecular weight polymers. Hence, DAP provides the advantage of being a facile synthetic procedure for synthesis of high-performance n- and p-type polymers.

2.6 Experimental section

2.6.1 Materials and methods

All solvents used are of reagent grade unless stated otherwise. 9,9-Dioctyl-2,7 dibromofluorene (**DBrOF**), 4,7-dibromo-2,1,3-benzothiadiazole (**DBrBT**) were of commercial grade and used as received without further purification. All reactions were performed under a nitrogen atmosphere. 2-Bromo-9,9-dihexyl-9H-fluorene (**BrHF**)[42] and *N*,*N*'-Di(2-octyl)dodecyl-4,5,9,10-naphtho[2,3-*b*:6,7-*b*']dithiophenediimide (**C20-NDTI**)[9] were synthesized according to reported procedures. Gel permeation chromatography was performed on an Agilent 1260 Infinity system at 80 °C/ 55 bar, with polystyrenes as the reference standard and chloroform as an eluent. Nuclear magnetic resonance spectra were recorded on a Bruker AV 300 spectrometer in $CDCl_3$ at room temperature with TMS as internal reference; chemical shifts (δ) were reported in parts per million. Optical properties were studied in chloroform solutions of materials (unless mentioned otherwise) and drop-cast thin films. UV-Vis absorption spectra were recorded on a Shimadzu spectrometer model UV-2450. Emission spectra were recorded on a PerkinElmer LS55 fluorescence spectrometer. Cyclic voltammograms (CVs) were recorded on an CHI Electrochemical Analyzer Model 660D at room temperature in acetonitrile containing 0.1 M tetrabutylammonium hexafluorophosphate (Bu_4NPF_6) as a supporting electrolyte at a scan rate of 100 mV/s. Glassy carbon was used as working electrodes; counter electrodes were made of Pt, and the reference electrode was Ag/AgCl. All the potentials were calibrated with the standard ferrocene/ferrocenium redox couple. Thermo-gravimetric analysis and differential scanning calorimetry were performed on a Pyris Diamond TGA (Perkin Elmer) and Mettler Toledo 822e DSC respectively, at a heating rate of 10^oC/ min under nitrogen. Mass spectroscopy was performed on a ABI 4800 Proteomics Analyzer MALDI TOF/TOF mass spectrometer (Applied Biosystems).

2.6.2 Synthesis of 5,11-bis(9,9-dihexyl-9H-fluoren-2-yl)-N,N'-Bis(2-octyldodecyl)-4,5,9,10-naphtho[2,3-b:6,7-b']dithiophene-4,5,9,10-diimide (NDTI-2HF)

To a microwave vial charged with a stirring bar, **C20-NDTI** (50 mg, 0.053 mmol), 1-bromo-9,9-dihexyl-9H-fluorene (0.53 mmol), $Pd_2(dba)_3$ (2.7 µmol, 2.4 mg), (o-$MeOC_6H_4)_3P$ (5 µmol, 1.7 mg), K_2CO_3 (0.2 mmol, 36.8 mg) and pivalic acid (0.025 mmol, 2.5 mg) were added. *o*-xylene (0.3 mL) was added to the vial inside a glove box and sealed with a rubber cap. The vial was then placed in an oil-bath pre-heated to 120 °C in 24 hours. After cooling to room temperature, the reaction mixture was diluted with chloroform and extracted with aq. NaCl. The extract was dried over $MgSO_4$ and filtered over vacuum to obtain crude product mixture. The product mixture was purified by column chromatography (20% v/v DCM-Hexane) to give **NDTI-2HF** in 45% yield (38.3 mg) and **NDTI-HF** in 30% yield (20 mg).

NDTI-2HF. ^{1}H NMR ($CDCl_3$, 300 MHz) δ ppm: 9.21 (s, 2H), 7.98-7.35 (m, 14H), 4.36 (m, 4H), 2.14 (m, 10H), 1.43-0.77 (m, 120H). EI MS *m/z* (%): 1604 (M^+, 100), 1060 (16), 855 (26).

NDTI-HF. ^{1}H NMR ($CDCl_3$, 300 MHz) δ ppm: 9.19 (s, 1H), 8.9 (d, 1H, J = 6 Hz), 8.03 (d, 1H, J = 6 Hz), 7.88-7.38 (m, 7H), 4.27 (m, 4H), 2.14 (m, 6H), 1.43- 0.77 (m, 98H). EI MS *m/z* (%): 1271(M^+, 100), 1378 (27), 1060 (35), 855 (62).

2.6.3 General synthesis procedure for PNDTIs via direct arylation

To a microwave vial charged with a stirring bar, **C20-NDTI** (50 mg, 0.053 mmol), DBrX (0.053 mmol, as described in **Scheme 2**), $Pd_2(dba)_3$ (2.7 µmol, 2.4 mg), (o-$MeOC_6H_4)_3P$ (5 µmol, 1.7 mg), K_2CO_3 (0.2 mmol, 36.8 mg) and pivalic acid (0.025 mmol, 2.5 mg) were added. *o*-xylene (0.5 mL) was added to the vial inside a glove box and sealed with a rubber cap. The vial was then placed in an oil-bath pre-heated to 120 °C in 24 hours. After cooling to room temperature, the reaction mixture was diluted with chloroform and added dropwise to 100 mL of methanol, filtered through a Soxhlet thimble, and then

subjected to Soxhlet extraction with methanol, acetone, hexane and chloroform sequentially. Hexane and chloroform fractions were concentrated and precipitated in methanol. The precipitates were collected by filtration and dried under vacuum for one day to obtain the target polymers.

2.7 References

1. Zhang, C.; Shi, K.; Cai, K.; Xie, J.; Lei, T.; Yan, Q.; Wang, J.-Y.; Pei, J.; Zhao, D. *Chem. Commun.* **2015,** *51*, 7144-7147.
2. Hwang, Y.-J.; Earmme, T.; Courtright, B. A. E.; Eberle, F. N.; Jenekhe, S. A. *J. Am. Chem. Soc.* **2015,** *137*, 4424-4434.
3. Zitong, L.; Guanxin, Z.; Zhengxu, C.; Xin, C.; Hewei, L.; Yonghai, L.; Jianguo, W.; Deqing, Z. *Adv. Mater.* **2014,** *26*, 6965-6977.
4. Hu, Y.; Gao, X.; Di, C.-a.; Yang, X.; Zhang, F.; Liu, Y.; Li, H.; Zhu, D. *Chem. Mater.* **2011,** *23*, 1204-1215.
5. Xiaohua, H.; Chunyan, G.; Wuqiong, S.; Wei, H.; Shaoliang, L.; Deyue, Y. *J. Polym. Sci., Part A: Polym. Chem.* **2013,** *51*, 1040-1050.
6. Geng, Y.; Huang, J.; Tajima, K.; Zeng, Q.; Zhou, E. *Polymer* **2015,** *63*, 164-169.
7. Zhao, Z.; Zhang, F.; Hu, Y.; Wang, Z.; Leng, B.; Gao, X.; Di, C.-a.; Zhu, D. *ACS Macro Lett.* **2014,** *3*, 1174-1177.
8. Kolhe, N. B.; Ashar, A. Z.; Narayan, K. S.; Asha, S. K. *Macromolecules* **2014,** *47*, 2296-2305.
9. Fukutomi, Y.; Nakano, M.; Hu, J.-Y.; Osaka, I.; Takimiya, K. *J. Am. Chem. Soc.* **2013,** *135*, 11445-11448.
10. Luzio, A.; Fazzi, D.; Nübling, F.; Matsidik, R.; Straub, A.; Komber, H.; Giussani, E.; Watkins, S. E.; Barbatti, M.; Thiel, W.; Gann, E.; Thomsen, L.; McNeill, C. R.; Caironi, M.; Sommer, M. *Chem. Mater.* **2014,** *26*, 6233-6240.
11. Liégault, B.; Lapointe, D.; Caron, L.; Vlassova, A.; Fagnou, K. *J. Org. Chem.* **2009,** *74*, 1826-1834.
12. Lutz, A.; Rubén, V.; R., K. A. *Angew. Chem. Int. Ed.* **2009,** *48*, 9792-9826.
13. Alberico, D.; Scott, M. E.; Lautens, M. *Chem. Rev.* **2007,** *107*, 174-238.

14. Yuta, N.; Junpei, K.; Takeshi, Y.; Liyuan, H.; Takaki, K. *J. Polym. Sci., Part A: Polym. Chem.* **2014,** *52*, 1401-1407.

15. Wei, L.; Junpei, K.; Masahiro, K.; Takaki, K. *J. Polym. Sci., Part A: Polym. Chem.* **2015,** *53*, 1396-1402.

16. Mercier, L. G.; Leclerc, M. *Acc. Chem. Res.* **2013,** *46*, 1597-1605.

17. Okamoto, K.; Zhang, J.; Housekeeper, J. B.; Marder, S. R.; Luscombe, C. K. *Macromolecules* **2013,** *46*, 8059-8078.

18. Kai, W.; Mingfeng, W. *Curr. Org. Chem.* **2013,** *17*, 999-1012.

19. Rudenko Andrey, E.; Thompson Barry, C. *J. Polym. Sci., Part A: Polym. Chem.* **2014,** *53*, 135-147.

20. Facchetti, A.; Vaccaro, L.; Marrocchi, A. *Angew. Chem. Int. Ed.* **2012,** *51*, 3520-3523.

21. Kowalski, S.; Allard, S.; Zilberberg, K.; Riedl, T.; Scherf, U. *Prog. Polym. Sci.* **2013,** *38*, 1805-1814.

22. Nakabayashi, K.; Mori, H. *Chem. Lett.* **2013,** *42*, 717-718.

23. Zhao, H.; Liu, C.-Y.; Luo, S.-C.; Zhu, B.; Wang, T.-H.; Hsu, H.-F.; Yu, H.-h. *Macromolecules* **2012,** *45*, 7783-7790.

24. Liu, S.-Y.; Shi, M.-M.; Huang, J.-C.; Jin, Z.-N.; Hu, X.-L.; Pan, J.-Y.; Li, H.-Y.; Jen, A. K. Y.; Chen, H.-Z. *J. Mater. Chem. A* **2013,** *1*, 2795-2805.

25. Zhang, J.; Kang, D.-Y.; Barlow, S.; Marder, S. R. *J. Mater. Chem.* **2012,** *22*, 21392-21394.

26. Rudenko, A. E.; Thompson, B. C. *Macromolecules* **2015,** *48*, 569-575.

27. Okamoto, K.; Housekeeper, J. B.; Michael, F. E.; Luscombe, C. K. *Polym. Chem.* **2013,** *4*, 3499-3506.

28. Wang, Q.; Takita, R.; Kikuzaki, Y.; Ozawa, F. *J. Am. Chem. Soc.* **2010,** *132*, 11420-11421.

29. Wang, K.; Wang, G.; Wang, M. *Macromol. Rapid Commun.* **2015,** *36*, 2162-2170.

30. Shao, J.; Wang, G.; Wang, K.; Yang, C.; Wang, M. *Polym. Chem.* **2015,** *6*, 6836-6844.

31. Wang, X.; Wang, K.; Wang, M. *Polym. Chem.* **2015,** *6*, 1846-1855.

32. Guo, Q.; Dong, J.; Wan, D.; Wu, D.; You, J. *Macromol. Rapid Commun.* **2013,** *34*, 522-527.

33. Kowalski, S.; Allard, S.; Scherf, U. *ACS Macro Lett.* **2012,** *1*, 465-468.

34. Berrouard, P.; Najari, A.; Pron, A.; Gendron, D.; Morin, P. O.; Pouliot, J. R.; Veilleux, J.; Leclerc, M. *Angew. Chem. Int. Ed.* **2011,** *51*, 2068-2071.

35. Matsidik, R.; Komber, H.; Luzio, A.; Caironi, M.; Sommer, M. *J. Am. Chem. Soc.* **2015,** *137*, 6705-6711.

36. Matsidik, R.; Martin, J.; Schmidt, S.; Obermayer, J.; Lombeck, F.; Nübling, F.; Komber, H.; Fazzi, D.; Sommer, M. *J. Org. Chem.* **2015,** *80*, 980-987.

37. Li, C.-H.; Kettle, J.; Horie, M. *Mater. Chem. Phys.* **2014,** *144*, 519-528.

38. Wang, X.; Wang, M. *Polym. Chem.* **2014,** *5*, 5784-5792.

39. Nakano, M.; Osaka, I.; Takimiya, K. *Macromolecules* **2015,** *48*, 576-584.

40. Nakano, M.; Osaka, I.; Hashizume, D.; Takimiya, K. *Chem. Mater.* **2015,** *27*, 6418-6425.

41. Hu, J.-Y.; Nakano, M.; Osaka, I.; Takimiya, K. *J. Mater. Chem. C* **2015,** *3*, 4244-4249.

42. Shavaleev, N. M.; Monti, F.; Scopelliti, R.; Baschieri, A.; Sambri, L.; Armaroli, N.; Grätzel, M.; Nazeeruddin, M. K. *Organometallics* **2013,** *32*, 460-467.

Chapter 2 is published as Bohra, H.; Shao, J.; Huang, S.; Wang, M., Facile Synthesis of Naphthodithiophenediimide Based Small Molecules and Polymers Via Direct Arylation Coupling. *Tetrahedron Lett.* 2016, *57*, 1497-1501. DOI: 10.1016/j.tetlet.2016.02.081

3. Direct arylation polymerization towards efficient synthesis of benzo[1,2-c:4,5-c′] dithiophene-4,8-dione based donor-acceptor alternating copolymers for organic optoelectronic applications

3.1 Introduction

In recent years, organic solar cells (OSCs) employing the bulk heterojunction (BHJ) architecture – electron donor (polymer or small molecule) and electron acceptor (fullerene or non-fullerenes) blends as the active layer – have been able to achieve power conversion efficiencies (PCEs) in the range of 10-13%.[1-5] Further improving the performance of OSCs would require minimizing losses from contributing factors such as open circuit voltage (V_{oc}) and the short circuit current (J_{sc}). Since V_{oc} is dependent on the difference between the highest occupied molecular orbital (HOMO) of the donor and the lowest occupied molecular orbital (LUMO) of the acceptor,[6-9] developing new donor polymers with deep HOMO levels and broad absorption bands is a good strategy to provide the necessary offset between the frontier orbitals of donors and acceptors. Recently, this strategy has been efficiently employed in a series of moderate band gap benzo[1,2-c:4,5-c′]dithiophene-4,8-dione (BDTD) based polymers which have shown excellent performance in OSCs (PCE > 9%).[4, 10-12] In the previous chapter, we used a core-extended naphthalenediimide derivative – **NDTI** as an acceptor molecule for its unique structural and electrochemical properties to synthesize donor-acceptor (D-A) polymers via direct arylation. Much like **NDTI**, BDTD is another acceptor molecule with a rigid and planar structure which enhances interchain packing and is beneficial in tuning the energy levels of polymers by pairing with appropriate comonomers.[13] However, majority of BDTD polymers have been synthesized via Stille coupling[10-12, 14-16]

which requires tedious pre-functionalization of monomers with highly toxic organotin intermediates.

In the last decade, an alternative coupling method known as direct arylation has been extensively developed for a variety of building blocks to facilitate the direct polymerization of a halogenated (bromo, iodo) and C-H active aromatic monomers thereby providing a synthetically facile and eco-friendly alternative to conventional polymerizations.[17-44] π-conjugated polymers synthesized by direct arylation polymerization (DAP) have shown impressive performance in optoelectronics as well.[25, 45] Recently, Wang and coworkers reported the direct arylation synthesis of a high performance phenylene-*alt*-difluorobenzothiadiazole polymer, PPDT2FBT which gave PCEs upto 7.4%.[46] Most notably, Marks and coworkers reported a benzo[1,2-b;4,5-b']dithiophene-*alt*-fluorothieno[3,4-b]thiophene polymer, PBDTT-FTTE synthesized by DAP which showed PCEs as high as 8.4% - the highest for polymers synthesized by DAP.[47] Structure and OPV performance of PBDTT-FTTE were comparable to its Stille counterpart thereby reinforcing DAP as a promising alternative to conventional coupling reactions. Nonetheless, direct arylation has not been used to synthesize BDTD based polymers so far.

To bridge the gap between high performance OSCs and sustainable synthesis of photovoltaic polymers, here we present a one-step synthetic scheme of direct arylation polymerization between dibrominated **BDTD** (**Scheme 1**) as one electron accepting monomer (A) and three respective thiophene-based electron-donating monomers (D) to synthesize a series of D-A alternating copolymers. To the best of our knowledge, this is the first instance of BDTD-based polymers synthesized by DAP. We have systematically characterized these polymers (**P1-3**) including their chemical structures, optical properties, thermal properties, electrochemical properties, charge-carrier mobilities in thin-film field effect transistors, and their performances as electron donors in bulk heterojunction solar cell devices using a fullerene derivative, $PC_{71}BM$, as the electron partner. Although these polymers only showed moderate performances in the optoelectronic devices, we believe that the "greener" feature of the

synthetic chemistry involved in the polymer synthesis and the structure-property relationship gained from this study will be useful for future design and synthesis of other high-performance semiconducting polymers for a variety of optoelectronic applications.

3.2 Polymer synthesis and structural characterization

The synthetic route to the three donor-acceptor linear polymers reported in this study is shown in **Scheme 3.1**. Polymers are composed of a common acceptor unit, benzo[1,2-c:4,5-c′]dithiophene-4,8-dione (**BDTD**), which, owing to its planar structures imparts a rigid backbone to the polymer. BDTD-based polymers have consistently shown stellar performance in OSCs (PCEs > 8%), which makes it an attractive acceptor molecule for designing new high-performance polymers by direct arylation.[4, 10-11, 13-16, 48-49] **BDTD** was polymerized with a thiophene-fused donor, 4,8-bis((2-ethylhexyl)oxy)benzo[1,2-b:4,5-b']dithiophene (**M1**), and two thiophene-flanked donors, 2,2'-(2,5-bis((2-ethylhexyl)oxy)-1,4-phenylene)dithiophene (**M2**) and 3,3'''-dioctyl-2,2':5',2'':5'',2'''-quaterthiophene (**M3**) to give polymers **P1, P2** and **P3** respectively. It should be noted that a similar analogue of **P1** containing n-hexyl side chains on **BDTD** was previously reported by Aso and coworkers[14] via Stille coupling for application in organic solar cells. However, the polymer suffered from low short circuit current and poor PCE. Polymers **P2** and **P3** both consist of thiophene-flanked donor groups (**M2** and **M3**) as opposed to thiophene-fused structure of **M1**, which enhances the flexibility of the polymer chains due to their non-rigid structure. These structural differences have been especially highlighted in previous reports[12, 16] of BDTD-quarterthiophene polymers which are analogues of **P3**.

A preliminary optimization for the direct arylation of BDTD with C-H active donors was carried out by testing two direct arylation conditions using $Pd_2(dba)_3$ and Hermann's catalyst, respectively, on the synthesis of **P1** and **P2** (**Table 3.1**). Both these conditions have been previously optimized for the C-H activation of thiophene-flanked monomers [28, 50] and have been used for synthesizing a variety of linear[47, 51-59] and 2D/3D conjugated[60-62] networks. **P1**

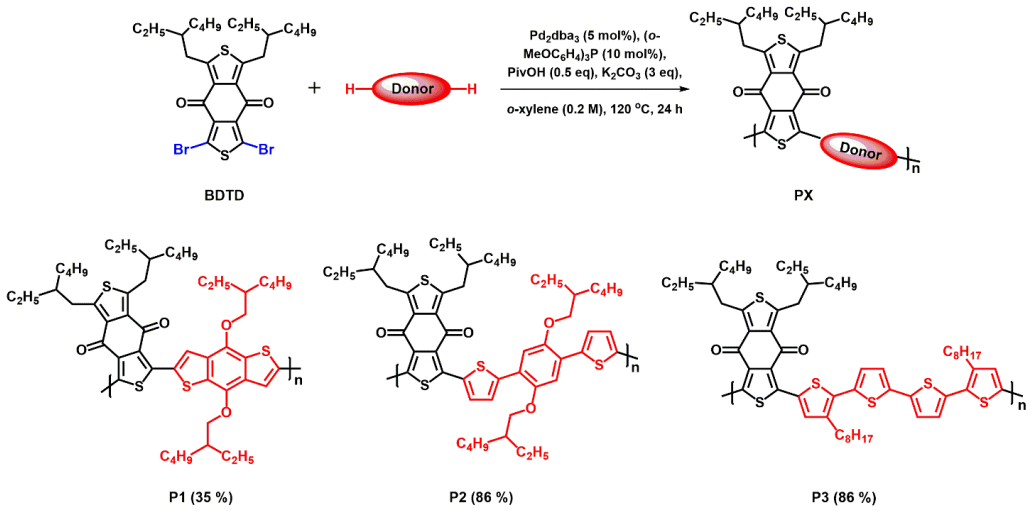

Scheme 3.1 Synthesis of donor-acceptor polymers via direct arylation polymerization.

Table 3.1 Reaction conditions and characteristics of BDTD polymers

Polymer	Entry	[Pd] [a]	Base	*t* (h)	Yield [b]	M_n (*kDa*) [c]	M_w (*kDa*) [c]	PDI [c]
P1	1	$Pd_2(dba)_3$	K_2CO_3	24	35% (57%)	32.0 (9.4)	47.7 (19.4)	1.49 (2.04)
	2	Hermann's catalyst [d]	Cs_2CO_3	48	36% (51%)	41.7 (9.7)	125.0 (22.5)	3.0 (2.31)
P2	3	$Pd_2(dba)_3$	K_2CO_3	24	86% (7.5%)	16.0 (3.0)	26.5 (5.1)	1.65 (1.67)
	4	Hermann's catalyst	Cs_2CO_3	24	61% (38%)	16.0 (6.7)	25.0 (9.3)	1.57 (1.4)
P3	5	$Pd_2(dba)_3$	K_2CO_3	24	86% (-) [e]	23.0 [f]	53.4	2.79

[a] Ligand: (o-$MeOC_6H_4)_3P$, Solvent: *o*-xylene, Temperature: 120 °C. [b] Yield from the chloroform fraction. Number in parentheses corresponds to yield of the hexane fraction. [c] GPC of the chloroform fraction measured in THF at 25 °C. Numbers in parentheses corresponds to the molecular weights and PDI of the hexane fraction. [d] Solvent: Toluene. [e] Data for hexane fraction was not recorded. [f] GPC was carried out in 1,3,5-trichlorobenzene at 150 °C.

was obtained in relatively low yields from both conditions since majority of products were obtained as oligomers in the hexane fraction (**Figure 3.1a** and

3.1c). Although a higher molecular weight polymer could be obtained by using Hermann's catalyst (M_n = 42 kDa, PDI = 3.0, **Figure 3.1d**), **P1** obtained from $Pd_2(dba)_3$ (M_n = 32 kDa, PDI = 1.49, **Figure 3.1b**) was considered to be of higher quality due to its narrower dispersity and shorter reaction time. In contrast, **P2** obtained from $Pd_2(dba)_3$ and Hermann's catalyst had similar molecular weights (M_n = 16 kDa, **Figure 3.2b** and **3.2d**) despite the longer reaction time for the latter condition. Moreover, the yield of **P2** obtained by using $Pd_2(dba)_3$ (Entry 3) was 86% compared to 61% from Hermann's catalyst (Entry 4). Based on the molecular weights and yields for **P1** and **P2** obtained from these trials we deemed $Pd_2(dba)_3$ a more suitable catalyst than Hermann's catalyst for BDTD-based polymers. Subsequently, a DAP protocol using $Pd_2(dba)_3$ as the catalyst gave **P3** with a number-average molecular weight (M_n) of 23 *kDa* (**Figure 3.3**) in 86% yield. It should be noted that the molecular weight of **P3** was measured in 1,3,5-

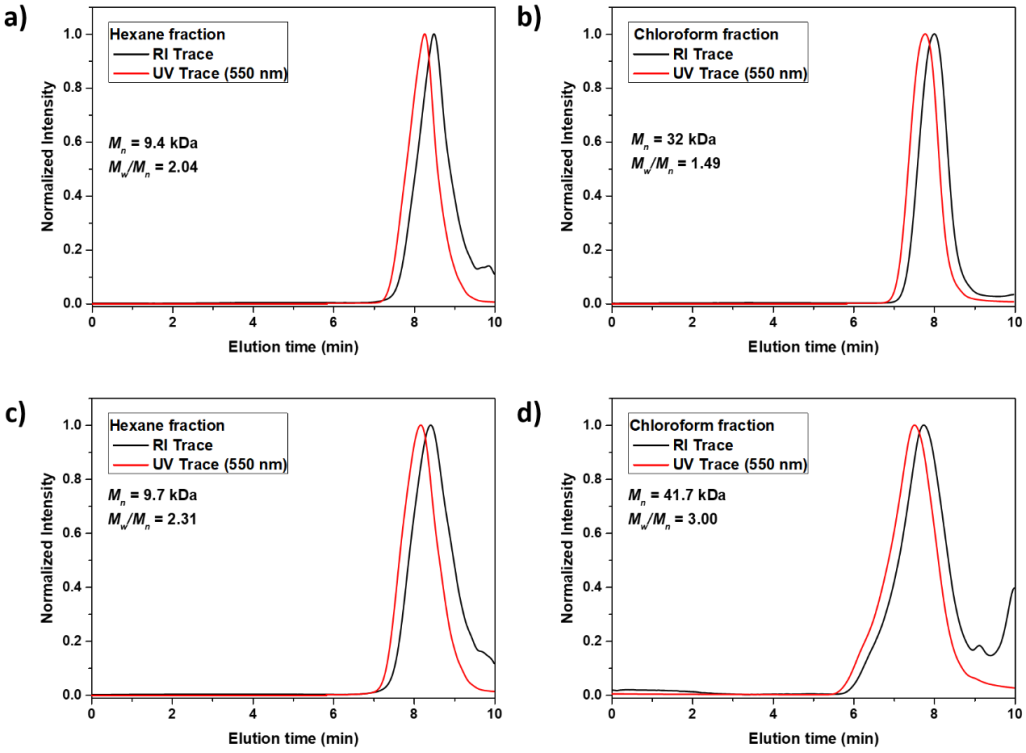

Figure 3.1 GPC traces of hexane (a, c) and chloroform fractions (b, d) of polymer **P1** synthesized using $Pd_2(dba)_3$ (a, b) Hermann's catalyst (c, d) measured in THF at 25 °C.

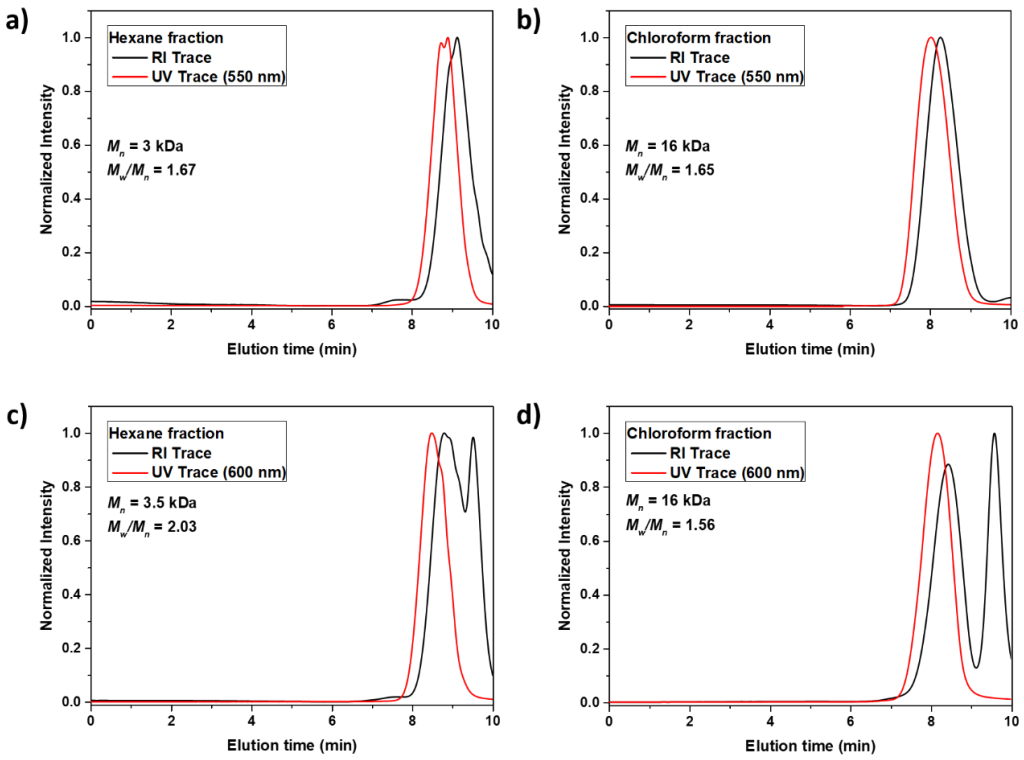

Figure 3.2 GPC traces of hexane (a, c) and chloroform fractions (b, d) of polymer **P2** synthesized using $Pd_2(dba)_3$ (a, b) Hermann's catalyst (c, d) measured in THF at 25 °C.

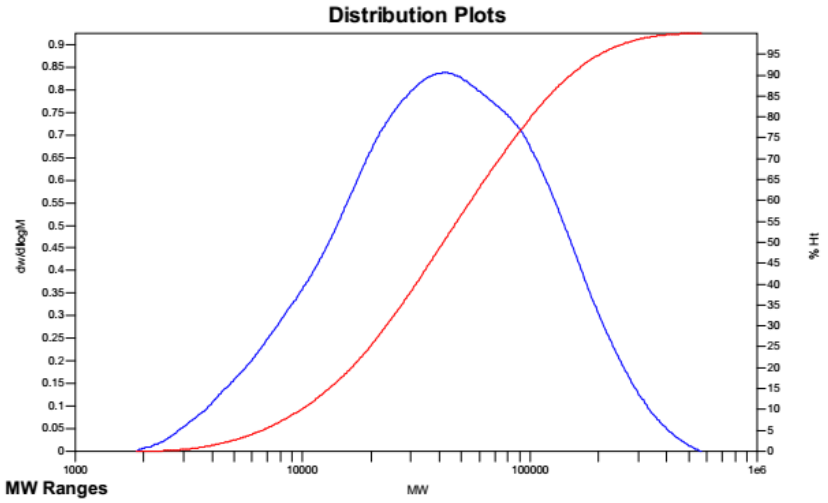

Figure 3.3 GPC traces of polymer **P3** synthesized using $Pd_2(dba)_3$ measure in 1,3,5-trichlorobenzene at 150 °C.

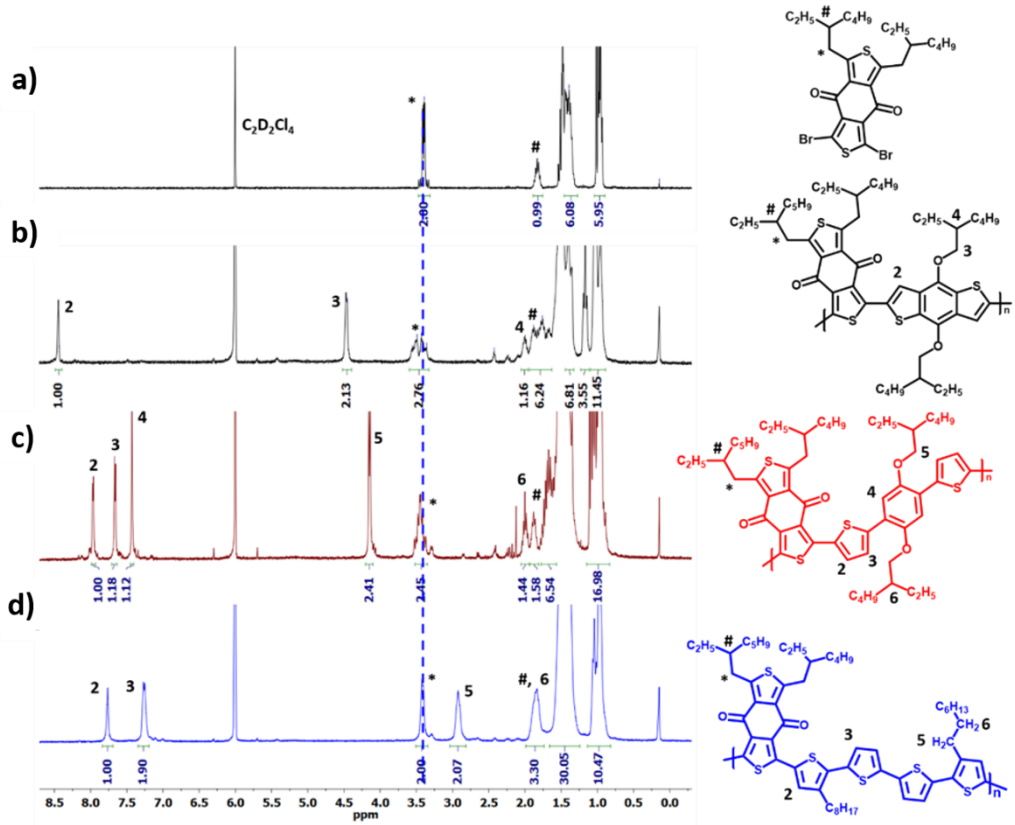

Figure 3.4 Comparison of ^{1}H-NMR spectra of the monomer a) **BDTD** with polymers b) **P1,** c) **P2** and d) **P3.** Spectra of monomers were measured in $CDCl_3$ at room temperature while the spectra of polymers were measured in $C_2D_2Cl_4$ at 100 ^oC.

trichlorobenzene at 150 ^oC due to its poor solubility in THF at room temperature. Only polymers synthesized using $Pd_2(dba)_3$ were used for further characterization.

Structures of all polymers were characterized by ^{1}H-NMR spectroscopy in $C_2D_2Cl_4$ at 100 ^oC (**Figure 3.4**). Peaks from **BDTD** in the polymer backbone were observed around 3.4 ppm and 1.8 ppm and are denoted by '*' and '#', respectively. Weak peaks at 3.25 ppm in the spectra of **P2** (**Figure 3.4c**) and **P3** (**Figure 3.4d**) were assigned to the alkyl protons of the terminal BDTD group. However, no such end-group peaks could be observed for **P1** (**Figure 3.4b**). The peak at 8.43 ppm (denoted by 2) in the spectrum of **P1** is assigned to the β-carbon of **M1** in the polymer backbone. In the spectrum of **P2**, peaks denoted by 2 and

3 (**Figure 3.4c**) correspond to the thiophene protons of **M2** while peak 4 corresponds to the phenyl proton. Several smaller peaks can also be observed in the aromatic region of **P2** which can be attributed to the donor end-groups. For a detailed analysis of these peaks, the aromatic regions of the NMR spectra of polymer **P2** and monomer **M2** were compared (**Figure 3.5a**). Peaks 1' (7.55 ppm), 2' (7.15 ppm) and 3' (7.38 ppm) were assigned to the protons of the chain-

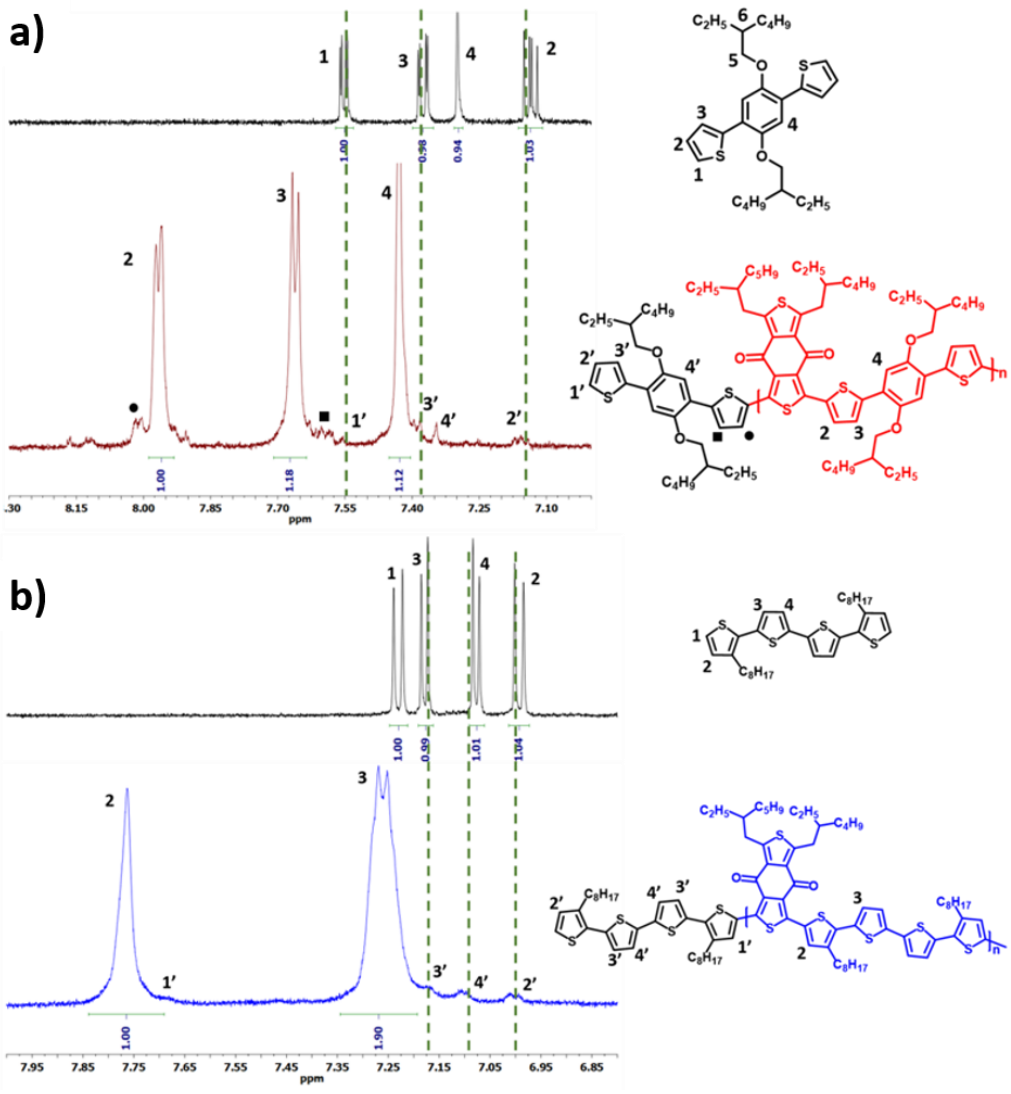

Figure 3.5 End-group analysis of NMR spectra of a) **P2** and b) **P3**. Donor end-group assignment was carried out comparing the NMR spectra of **P2** (red) and **P3** (blue) with spectra of **M1** and **M2** respectively.

end thiophene, while peak 4' (7.34 ppm) corresponds to the phenyl-proton of the donor end-group. The peaks at 8.01 ppm and 7.92 ppm were assigned to the thiophene adjacent to the terminal acceptor group in the polymer backbone.

Similar end-group analysis was carried for **P3** by comparing the aromatic region of its NMR spectrum with that of **M3 (Figure 3.5b).** Peak 2' (7.0 ppm), 3' (7.17 ppm) and 4' (7.09 ppm) was assigned to the terminal thiophenes of the donor group based on the position of the analogous protons in **M3** while 1' (7.68 ppm) was assigned to the thiophene adjacent to the terminal **BDTD** group in **P3**.

3.3 Optical properties

Optical properties of all polymers were studied by UV-Vis absorption and fluorescence spectroscopy both in *o*-dichlorobenzene (DCB) and in chloroform ($CHCl_3$) solutions (**Figure 3.6**). Polymers **P1** and **P2** have similar absorption

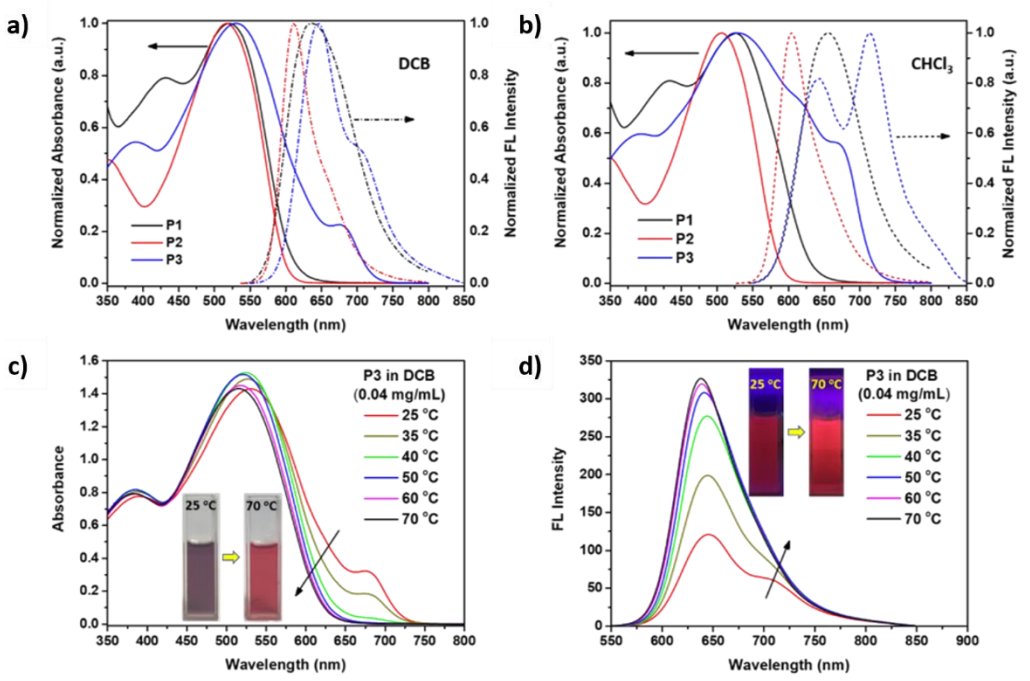

Figure 3.6 UV-vis absorption (solid) and fluorescence emission (dashed) spectra of **P1** (black), **P2** (red) and **P3** (blue) in 0.04 mg/mL a) *o*-dichlorobenzene (DCB) and b) chloroform solutions. Temperature dependent c) UV-Vis absorption and d) fluorescence emission spectroscopy of **P3** in DCB.

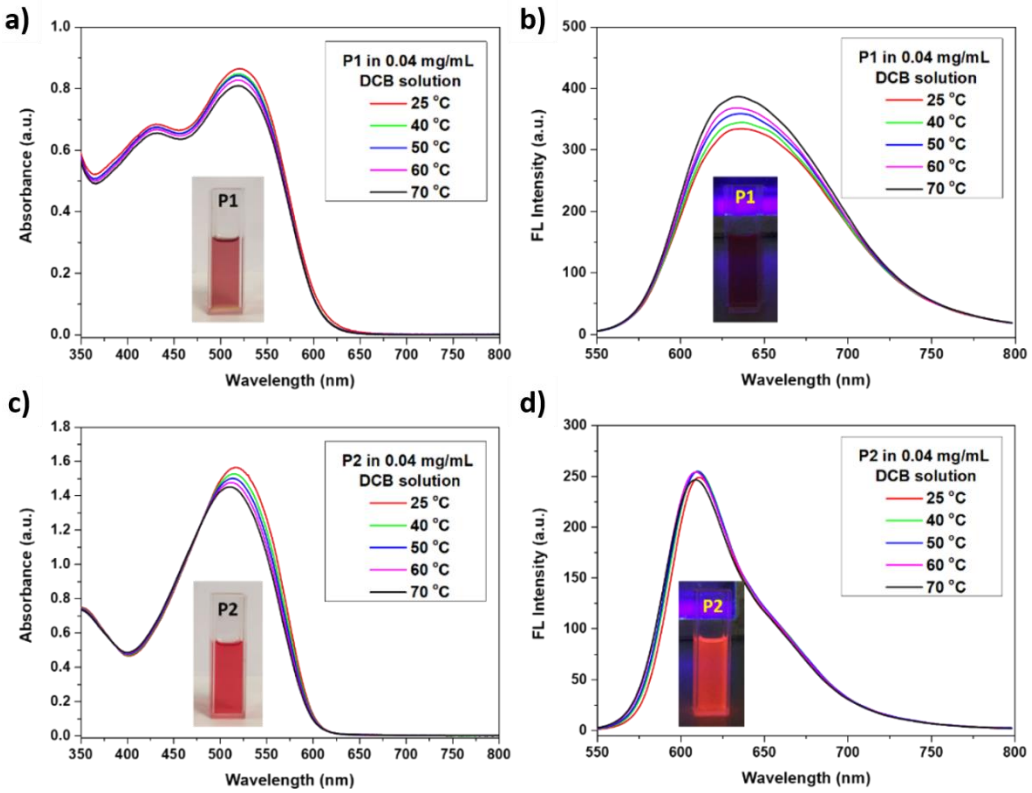

Figure 3.7 Temperature dependent UV-Vis absorption (a, c) and fluorescence (b, d) spectra of **P1** (a, b) and **P2** (c, d) in 0.04 mg/mL 1,2-dichlorobenzene solutions. Inset, digital images of **P1** (a, b) and **P2** (c, d) solutions under room (a, c) and 365 nm UV light (b, d).

profiles in both solvents that show strong absorption between 400 and 600 nm and maxima at 520 nm. Optical bandgaps of **P1** and **P2** were found to be 1.87 eV and 1.89 eV, respectively.

The absorption range of **P3** in DCB solutions (**Figure 3.6a**) extends up to 700 nm and a shoulder band, most likely corresponding to J-aggregation, is also observed at 678 nm which can be attributed to the strong π–π interaction between polymer chains. In fact, the band at 678 nm, appears to be stronger in chloroform and chlorobenzene solutions (**Figure 3.9a**) of **P3** of similar concentrations, implying the presence of aggregation in solution state. Such aggregation in **BDTD** based polymers has been observed by Hou and coworkers earlier,[16] albeit only with fluorinated comonomers. To investigate the effect of temperature on

aggregation, UV-vis absorption and fluorescence spectra of polymers were recorded while increasing temperature stepwise. The absorption and fluorescence profiles of **P1** and **P2** are invariant to temperature (**Figure 3.7**). From **Figure 3.6c,** it can be observed that as temperature increases the vibrionic band in the absorption spectrum of **P3** decreases in intensity till it completely vanishes at 70 ^{o}C as intermolecular π–π interactions are completely suppressed. The absorption edge blue shifts from 725 nm at 25 ^{o}C to 625 nm at 70 ^{o}C thereby confirming the band at 678 nm as a J-aggregation band. A similar effect is seen in the fluorescence spectrum where the shoulder peak at 25 ^{o}C merges into a broad unimodal peak leading to brighter fluorescence of the solution as shown in the digital images (**Figure 3.6d**). Temperature dependent optical characterization of **P3** in chlorobenzene (CB) solutions also yielded similar results **(Figure 3.8c and 3.8d**).

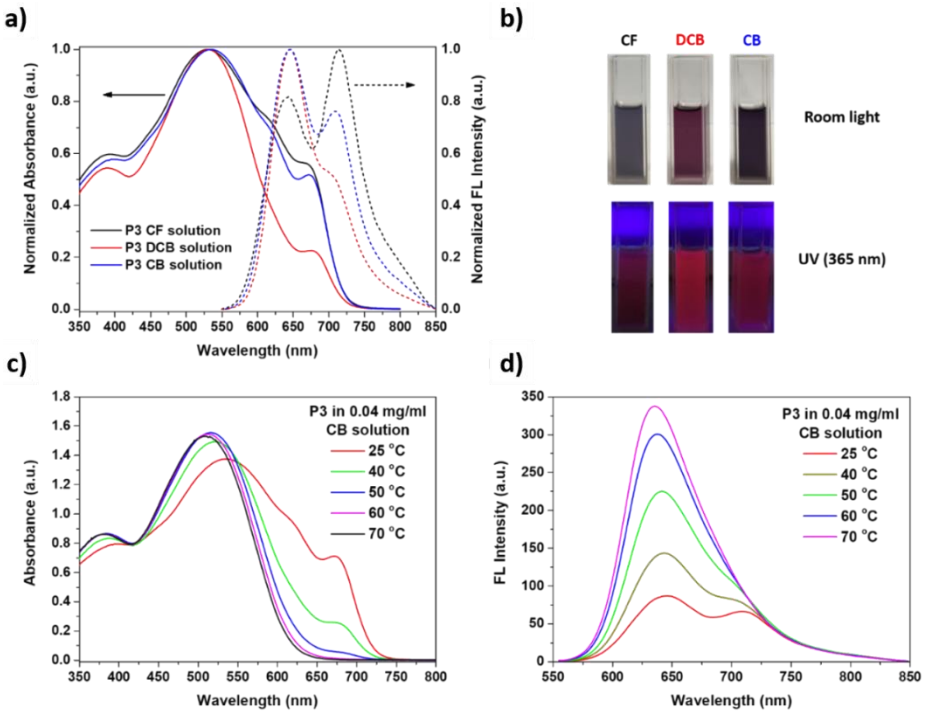

Figure 3.8 a) UV-Vis absorption (solid) and fluorescence (dashed) spectra of **P3** in chloroform (CF), 1,2-dichlorobenzene (DCB) and chlorobenzene (CB). b) Digital images of solutions of **P3** in various solvents under room light and UV light at room temperature. c) Temperature dependent UV-Vis and d) Fluorescence spectroscopy of **P3** in 0.04 mg/mL chlorobenzene solutions.

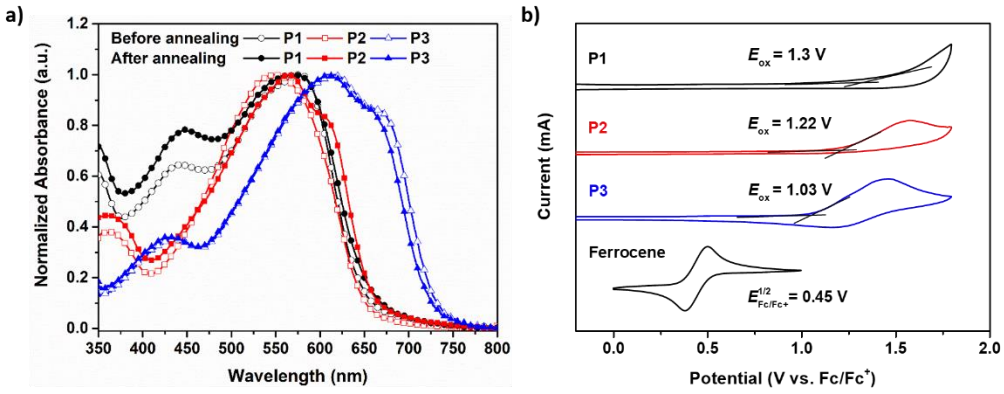

Figure 3.9 a) UV-vis absorption spectra of **P1** (black), **P2** (red) and **P3** (blue) thin films before and after annealing at 150 °C for 10 minutes. b) Cyclic voltammograms of **P1**, **P2**, **P3** and ferrocene standard.

Table 3.2 Optical properties of BDTD-based polymers.

Polymer	$\lambda_{max,abs}^{sol}$ (nm) [a]	$\lambda_{max,em}$ (nm) [a]	$\lambda_{max,abs}^{film}$ (nm)	E_{eg}^{op} (eV) [b]	E_{ox} (V)	E_{HOMO} (eV) [c]	E_{LUMO} (eV) [d]
P1	524	655	570	1.87	1.3	-5.65	-3.78
P2	507	604	546	1.89	1.22	-5.57	-3.68
P3	533	644	616	1.66	1.03	-5.43	-3.77

[a] Measured from spectra in DCB. [b] Determined from the absorption edge of UV-Vis absorption spectra in films. [c] Calculated using the equation, $E_{HOMO} = E_{ox} + (4.8 - E^{1/2}_{Fc/Fc^+})$. [d] $E_{LUMO} = E_{HOMO} - (E_{eg}^{op})$.

Optical absorption of **P1-P3** was also studied in film state (**Figure 3.9a**). As expected, all polymers exhibit a bathochromic shift of the absorption edge in film state and the shoulder peak of **P3** is seen to be higher in intensity. Annealing the polymer films at 150 °C did not lead to significant differences in the absorption spectra of the polymers. The optical characteristics of **BDTD** polymers are summarized in **Table 3.2**.

Electrochemical properties of polymers were studied by cyclic voltammetry (**Figure 3.9b**) and are summarized in **Table 3.2**. Polymers **P1** and **P2** exhibit non-reversible oxidation peaks with onsets at 1.3 V and 1.22 V respectively while **P3** exhibits a quasi-reversible oxidation peak with onset at 1.03 V. The HOMO energy levels calculated from the oxidation onset potentials were found to be -5.65, -5.57 and -5.43 eV for **P1**, **P2** and **P3**, respectively. The relatively higher HOMO level of **P3** can be attributed to the strong electron-donating effect of the quarterthiophene moiety. LUMO levels were determined from the HOMO energy level and the optical bandgaps and were calculated to be -3.78 eV, -3.68 eV and -3.77 eV for **P1**, **P2** and **P3,** respectively. Since the LUMO energy of all polymers lie in the narrow range of -3.78 and -3.68 eV, it can be concluded that the LUMO levels are largely determined by **BDTD** moiety.

3.4 Thermal properties

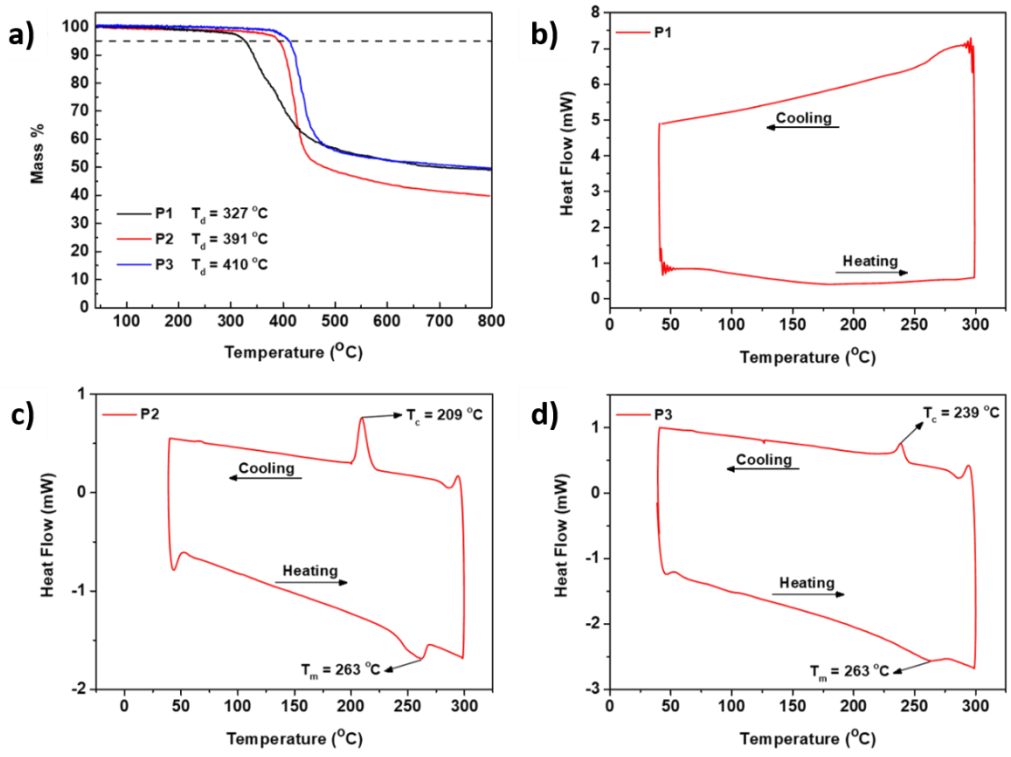

Figure 3.10 a) Thermogravimetric analysis of **BDTD** polymers. Differential scanning calorimetry of b) **P1**, c) **P2** and d) **P3** measured under N_2 at a scan rate of 10 °C min^{-1}.

Thermal properties of **BDTD** polymers were tested by thermogravimetric analyses (TGA) and differential scanning calorimetry (DSC) (**Figure 3.11**). **P3** was found to have the highest decomposition temperature (T_d) of 410 ^{o}C while **P1** and **P2** with T_d at 327 ^{o}C and 391 ^{o}C, respectively. Differential scanning calorimetry (DSC) profiles of **P1** did not exhibit any thermal transitions, suggesting its amorphous nature. **P2** showed a melting temperature (T_m) of 263 ^{o}C and a crystallization temperature (T_c) of 209 ^{o}C. While **P3** has a similar T_m as **P2**, its T_c was found be higher at 239 ^{o}C. These results indicate the semicrystalline nature of **P2** and **P3.**

3.5 Organic field effect transistors (OFETs) and film morphology

Since the hole mobilities of **P1** reported by Aso et. al.[14] were found to be only of order 10^{-7} cm^2 V^{-1} s^{-1}, only polymers **P2** and **P3** were used to fabricate OFET devices to examine their performance in devices. Hole mobilities of these polymers were tested in a bottom-gate/top-contact device architecture and the results are summarized in **Table 3.3**. We found that both **P2** and **P3** showed good hole mobilities (1.84×10^{-3} and 2.4×10^{-4} cm^2 V^{-1} s^{-1}, respectively) from as-spun films. Annealing the devices at 150 ^{o}C increased the mobility of polymer **P3** by an order of magnitude to 1.4×10^{-3} cm^2 V^{-1} s^{-1} (**Figure 3.11g-h**). On the contrary, annealing devices made from **P2** led to a slight decrease in hole mobility (**Figure 3.12c-d**).

Figure 3.12 shows the height and phase images of polymer thin films. From the AFM images, it can be inferred that the morphology of **BDTD**-based polymers is smooth and featureless (**Figure 3.12a-c**) at room temperature. No microphase separation is observed in **P1** and **P3** even after thermal treatment (**Figure 3.13d-f**). Morphology of **P2** (**Figure 3.12e**) shows a significant increase in aggregates after annealing at 150 ^{o}C which agrees with the red shift of the absorption maxima by 20 nm and the appearance of a shoulder band at 605 nm in UV-Vis absorption spectra of **P2** (**Figure 3.9a**) films measured after annealing

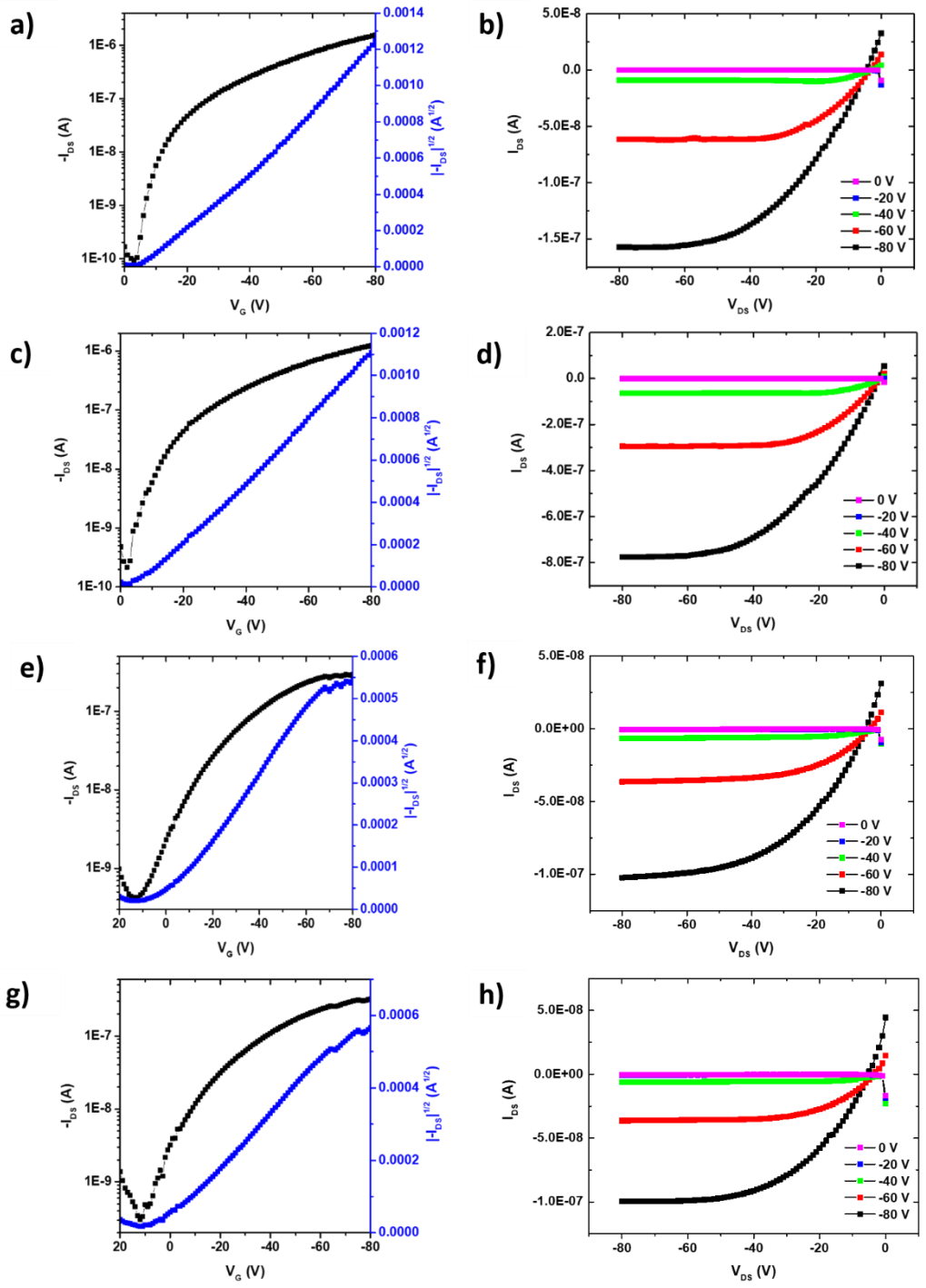

Figure 3.11 Transfer (a, c, e, g) and output curves (b, d, f, h) of OFET devices fabricated from - **P2** thin films with thermal annealing at 150 ^{o}C (a, b), **P2** thin films without thermal annealing (c, d), **P3** thin films with thermal annealing at 150 ^{o}C (e, f) and **P3** thin films without thermal annealing (g, h). Plots were measured at a negative source-drain bias (V_{DS} = -80 V).

Table 3.3 OFET characteristics of **P2** and **P3.**

Polymer	Annealing Temperature (°C)	μ_h (cm^2 V^{-1} s^{-1})	V_{th} (V)	On/off ratio
P2	Without annealing	1.8×10^{-3}	-8	10^3
	150 °C	1.7×10^{-3}	-1.2	10^3
P3	Without annealing	2.4×10^{-4}	13.7	10^2
	150 °C	1.4×10^{-3}	14.4	10^2

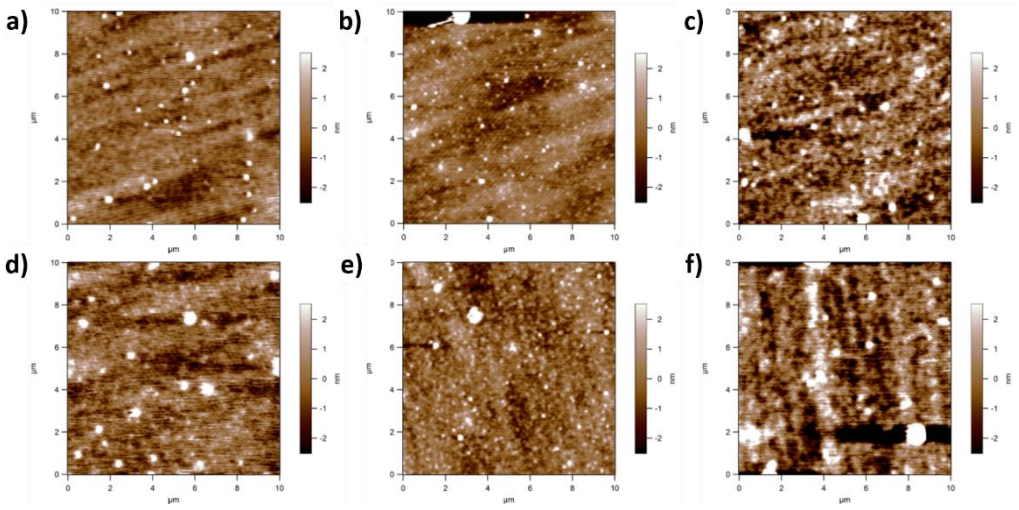

Figure 3.12 Tapping mode AFM height images of polymer thin films before (a-c) and after annealing (d-f) at 150 °C. **P1** (a, d), **P2** (b, e) and **P3** (c, f). The scale of all images is 10 μm x 10 μm.

3.6 Organic solar cells (OSCs)

OSC devices of **BDTD** polymers were fabricated using an inverted architecture (ITO/ ZnO/ polymer: $PC_{71}BM$ (1:1.5, w/w)/ MoO_3/ Ag) with $PC_{71}BM$ as the electron acceptor. Mass ratio of polymer to $PC_{71}BM$ was maintained at 1:1.5. Devices made from **P1** without annealing showed a poor PCE of 0.3%, while thermal and solvent annealing was found to be detrimental to **P1**-based devices (**Figure 3.13a**, **Table 3.4**). In comparison, a similar polymer

with the same conjugated backbone as **P1** but different side chains synthesized by Aso and co-workers[14] via Stille coupling was tested in OSCs in a conventional device architecture using $PC_{61}BM$ as the electron acceptor. Their devices showed a PCE of 0.7% and V_{oc} of 0.87 V, which is better than the **P1** devices fabricated here using an inverted device architecture. **P2**-based devices also exhibited PCEs < 1%, though the efficiency could be improved to 1.1% by solvent annealing (**Figure 3.13c**).

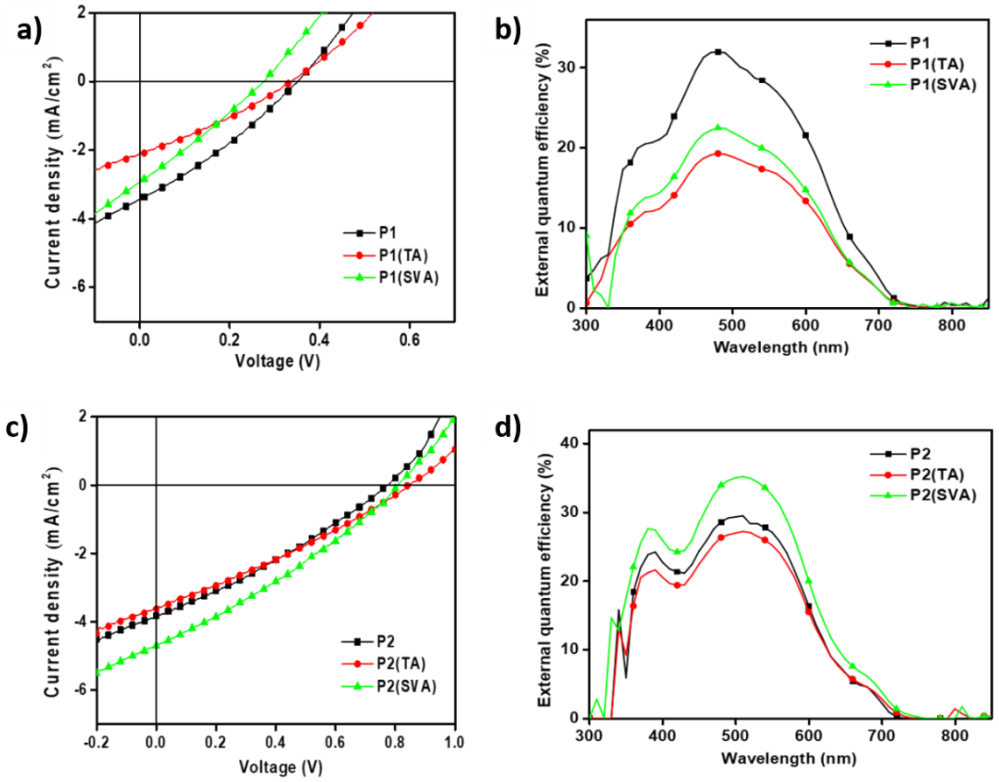

Figure 3.13 *J-V* curves (a, c) of **P1/P2**:$PC_{70}BM$ devices fabricated under different processing conditions and their corresponding EQE spectra (b, d).

The *J-V* and EQE curves of optimal **P3**-based devices are shown in **Figure 3.14c** and **3.14d** and the extracted performance parameters are shown in **Table 3.4**. Devices fabricated from **P3** without thermal annealing or additives showed PCEs of 1.6% which is similar to the maximum efficiencies of **P1** and **P2.** However, a higher J_{sc} value of 6.75 mA cm^{-2} could be observed. Thermal

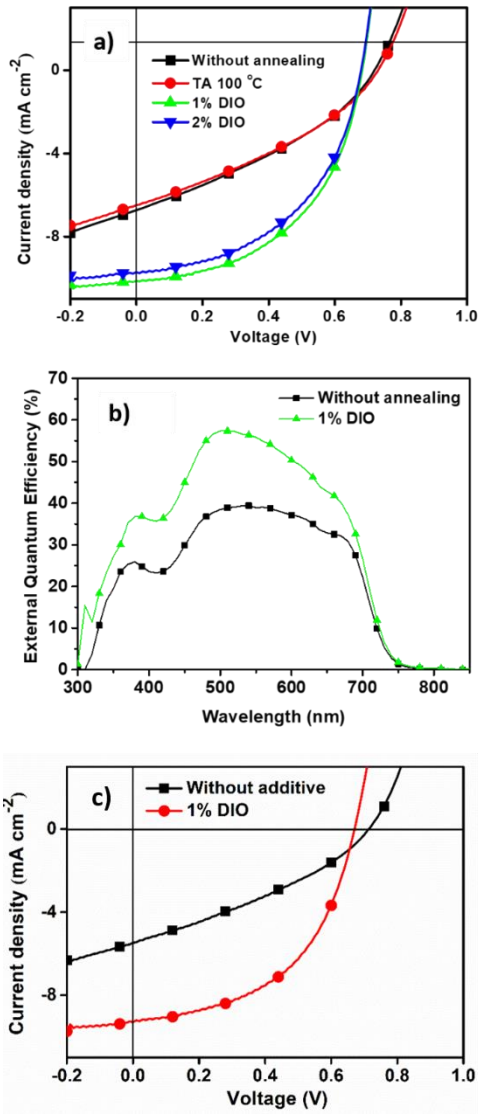

Figure 3.14 a) *J-V* curves of **P3**:$PC_{71}BM$ devices fabricated from chlorobenzene solutions with different processing conditions. b) EQE spectra of the control device and device treated with DIO. c) *J-V* curves of **P3**:$PC_{71}BM$ devices fabricated from *o*-dichlorobenzene solutions with and without DIO.

annealing did not change the performance significantly. Addition of 1 vol % 1,8-diiodooctane (DIO) as an additive to the polymer solution increased the PCE to 3.5% and J_{sc} to 10.5 mA cm^{-2} which is best performance obtained for all the **BDTD** based polymer in this study. The role of solvent additives in enhancing OSC performance has been has been the subject of several studies in the past.[63]

Moreover, several additives have also been screened and DIO has been found to give to promising results in a variety of polymer-fullerene systems.[64-65] From the EQE curves, the device with DIO processing presented a stronger photo-response in the range of 300 to 700 nm,

Table 3.4 OSC data of BDTD polymers fabricated.

Polymer	Annealing [a]	Additive	V_{oc} (V)	J_{sc} (mA cm^{-2})	FF (%)	PCE (%)
P1	No	No	0.35	3.43	30.0	0.3
	Annealed at 100 °C (TA)	No	0.34	2.09	30.3	0.2
	Solvent Vapour Annealed (SVA)	No	0.28	2.93	27.3	0.2
P2	No	No	0.77	3.83	29.7	0.9
	Annealed at 100 °C (TA)	No	0.84	3.62	29.0	0.9
	Solvent Vapour Annealed (SVA)	No	0.81	4.69	30.3	1.1
P3	No (Control)	No	0.72	6.75	34.0	1.6
	Annealed at 100 °C (TA)	No	0.73	6.50	34.3	1.6
	No	1% DIO	0.68	10.16	50.5	3.5
	No	2% DIO	0.68	9.15	49.6	3.1
	No [b]	No	0.71	5.48	33.4	1.3
	No [b]	1% DIO	0.67	9.29	50.8	3.2

[a] Devices were fabricated from chlorobenzene solutions. [b] Devices were fabricated from *o*-dichlorobenzene solutions.

which is the origin of enhanced J_{sc}. But increasing the DIO loading to 2 vol % resulted in a slight decrease of the PCE to 3.1%. Hou and co-workers reported

the device characterization of a **BDTD-*alt*-**quarterthiophene polymer (**PDPP4T**) which is analogous to **P3** with ethylhexyl side chains on the quarterthiophene unit instead of octyl in **P3.**[16] In an inverted device structure, PCEs up to 6.3% were obtained from **PDPP4T**:$PC_{71}BM$ solar cells when 1% DIO was used as a solvent additive. V_{oc} values obtained by Hou (0.66 V) are similar to those obtained from our devices but their J_{sc} (16.06 mA cm^{-2}) is significantly higher which is responsible for the higher efficiency. The difference in J_{sc} values can be attributed to the different alkyl side chains in **PDPP4T** and **P3** and their effect on phase separation in polymer:fullerene blends. In a recent study, Sun and coworkers reported that moderately bulky branched side chains were ideal for obtaining high PCEs from BDTD polymer solar cells while long branched side chains were detrimental due to the excess steric hinderance and reduced π–π stacking.[66] However, no clear comparison of the effect of straight and branched side chains on device performance was discussed by Sun. **P3,** containing straight alkyl chains, exhibits a red shifted absorption maximum in films compared to **PDPP4T**. Moreover, unlike **PDPP4T**, chlorobenzene solutions of **P3** (**Figure 3.8a**) exhibit a distinct band at 675 nm which indicates **P3**'s strong tendency to aggregate in solutions. The effect of aggregation on device performance is observed more clearly when **P3** based devices fabricated with and without solvent additives are compared. In the absence of additives, J_{sc} values of 6.75 mA and 6.50 mA were observed for devices fabricated with and without thermal annealing, respectively, while the addition of 1 vol % DIO increased the J_{sc} to 10.16 mA. Although this increase in J_{sc} can be attributed to the ability of additives to suppress aggregate formation in polymer:fullerene blends, we hypothesize that the strong intermolecular attraction in **P3** containing straight octyl chains leads to the formation of large polymer domains which hinder the diffusion of excitons across the polymer-fullerene interface. A similar phenomenon has been reported by You and coworkers[67] in poly(naphthodithiophene-*alt*-benzothiadiazole) in which both monomers had straight alkyl chains. The corresponding solar cells exhibited low short circuit currents due to formation of large aggregates in films. Highest efficiency was obtained from a polymer containing ethylhexyl side chains on both monomers, which exhibited improved nano-scale phase

separation crucial for charge transport in BHJ solar cells.[68-72] Although these results provide a convincing rationale for selecting branched side chains over straight side chains, they may not be a reliable guideline for side-chain engineering in other polymer systems . For a better understanding of the effect of side chains on device performance in BDTD-based systems, rigorous optimizations with a wide range of side chains in specific BDTD polymers is warranted.

3.7 Conclusion

In conclusion, three BDTD-based polymers were successfully synthesized by direct arylation and their optoelectronic properties were characterized. Bandgap of all polymers lies in the moderate to wide bandgap range. **P3** consisting of a quarterthiophene comonomer exhibited strong aggregation in solution. Polymers **P2** and **P3** were tested in OFET devices and hole mobilities up to 1.7×10^{-3} cm^2 V^{-1} s^{-1} and 1.4×10^{-3} cm^2 V^{-1} s^{-1} respectively were obtained after thermal annealing. Photovoltaic devices for **P1** and **P2** showed maximum PCEs of 0.2% and 1.5% when solvent vapour annealing was employed in an inverted device architecture. Devices made from **P3** films also showed poor performance (PCEs ~ 1.6%) in the absence of additives. Addition of 1% (wt%) DIO in the active layer, however, led to significant improvement of PCEs to 3.5%. We expect that, by engineering the side chains in the polymer backbone and optimizing the nano-morphology of thin films, further improvement in PCEs can be achieved. This study indicates that, with rational monomer selection and side chain engineering, direct arylation can be as efficient as Stille coupling for synthesizing yield high molecular weight and defect-free BDTD polymers. By eliminating the need for pre-functionalization of C-H bonds with toxic reagents, direct arylation has the potential to emerge as the eco-friendly and scalable option for synthesis of photovoltaic polymers.

3.8 Experimental section

3.8.1 Materials and methods

1,3-dibromo-5,7-bis(2-ethylhexyl)benzo[1,2-c:4,5-c']dithiophene-4,8-dione (**BDTD**) was purchased from Derthon Optoelectronic Materials Science and Technology. 4,8-bis((2-ethylhexyl)oxy)benzo[1,2-b:4,5-b']dithiophene **(M1)**,[73] 2,2'-(2,5-bis((2-ethylhexyl)oxy)-1,4-phenylene)dithiophene **(M2)**[74] and 3,3'''-dioctyl-2,2':5',2'':5'',2'''-quaterthiophene (**M3**)[75] were synthesized according to literature procedure. All solvents were obtained from commercial sources and used as received unless otherwise specified. All ^{1}H-NMR were performed on a Bruker AV 300 spectrometer with TMS as internal reference; chemical shifts (δ) are reported in parts per million. Thermo- gravimetric analyses were performed on a Pyris Diamond TGA (Perkin Elmer) instrument, at a heating rate of 10 ^{o}C min^{-1} under N_2 atmosphere from 40 ^{o}C to 800 ^{o}C. Differential scanning calorimetry (DSC) was carried out in a Mettler Toledo 822e DSC under nitrogen. The UV-visible absorption spectra were obtained on a UV-visible spectrophotometer (UV-2450, Shimadzu). Cyclic voltammograms (CVs) were recorded on an CHI Electrochemical Analyzer Model 660D at room temperature using 0.1 M tetrabutylammonium hexafluorophosphate as a supporting electrolyte at a scan rate of 100 mV/s. Glassy carbon was used as working electrode, platinum wire as counter electrode and silver as the reference electrode. CVs of **P1**-**P3** were measured in 0.1 M electrolyte solution in CH_3CN by drop-casting a solution of polymers from chloroform on the glassy carbon electrode. All the potentials were calibrated with the standard ferrocene/ferrocenium redox couple (Fc/Fc^{+}). Atom force microscopy was carried out on Asylum Research MFP-3D AFM. The thin films of AFM samples were prepared by spin coating of polymer solutions (10 mg/mL in chlorobenzene) onto silicon substrates and annealing at 150 ^{o}C for 10 min under N_2 atmosphere. The OFET devices were then characterized using a Keithley SCS-4200 semiconductor parameter analyser under ambient conditions. The Steady-state current-voltage (*J*-*V*) curves were determined on a Keithley 2400 under AM 1.5 solar simulator from a solar simulator (Enlitech.Inc) calibrated by a silicon reference cell (Hamamatsu S1133 color, with KG-5 visible fiith). The EQE was recorded by using an integrated EQE measurement system with Si-photodetector (Enlitech. Inc).

3.8.2 General synthetic procedure for polymers via direct arylation polymerization

A mixture of palladium catalyst, base, phosphine ligand, additive and an equimolar mixture of BDTD and **M1, M2** or **M3** was added to a 5 mL microwave tube charged with a magnetic stir bar. Solvent (1 mL) was added to the mixture inside a glovebox and the tube was sealed with a septum before. The mixture was stirred at room temperature for 5 min and then placed in an oil bath pre-heated to 120 ^{o}C. After certain reaction time, the vial was cooled to room temperature and the reaction mixture was poured into cold methanol. The resulting solids were filtered and subjected to Soxhlet extraction in methanol and hexane sequentially for the removal of low molecular weight materials and impurities. The remaining polymer was extracted with chloroform, precipitated again from cold methanol and dried under vacuum. The detailed reaction conditions for polymers listed in **Table 3.1** are summarized below.

Entry 1: **BDTD** (155 mg, 0.257 mmol), **M1** (115 mg, 0.257 mmol), $Pd_2(dba)_3$ (12 mg, 0.012 mmol), P(*o*-$MeOC_6H_4)_3$ (9 mg, 0.025 mmol), K_2CO_3 (103 mg, 0.747 mmol), PivOH (13 mg, 0.125 mmol) and *o*-xylene (1.3 mL).

Entry 2: **BDTD** (100 mg, 0.173 mmol), **M1** (74 mg, 0.173 mmol), Herrmann's catalyst (6 mg, 0.007 mmol), P(*o*-$MeOC_6H_4)_3$ (5 mg, 0.013 mmol), Cs_2CO_3 (130 mg, 0.4 mmol), PivOH (5 mg, 0.5 mmol) and toluene (0.8 mL).

Entry 3: **BDTD** (101 mg, 0.168 mmol), **M2** (83 mg, 0.168 mmol), $Pd_2(dba)_3$ (8 mg, 0.008 mmol), P(*o*-$MeOC_6H_4)_3$ (6 mg, 0.017 mmol), K_2CO_3 (93 mg, 0.67 mmol), PivOH (9 mg, 0.083 mmol) and *o*-xylene (0.83 mL).

Entry 4: **BDTD** (101 mg, 0.168 mmol), **M2** (83 mg, 0.168 mmol), Herrmann's catalyst (4 mg, 0.004 mmol), P(*o*-$MeOC_6H_4)_3$ (6 mg, 0.016 mmol), Cs_2CO_3 (343 mg, 0.458 mmol), PivOH (6 mg, 0.06 mmol) and *o*-xylene (1 mL).

Entry 5: **BDTD** (80 mg, 0.133 mmol), **M3** (73 mg, 0.133 mmol), $Pd_2(dba)_3$ (6 mg, 0.007 mmol), P(*o*-$MeOC_6H_4)_3$ (5 mg, 0.013 mmol), K_2CO_3 (73 mg, 0.531 mmol), PivOH (7 mg, 0.067 mmol) and *o*-xylene (0.7 mL).

3.8.3 OFET fabrication and characterization

Bottom-gate/top-contact organic field effect transistors (OFETs) were fabricated using heavily doped Si wafer as the bottom gate electrode with 300 nm of SiO_2 layer as the gate dielectric (C_i = 1.08 × 10^{-10} F·cm^{-2}, C_i is the capacitance of SiO_2 dielectric). The substrate was cleaned in acetone and isopropanol, and dried on the hot plate at 80 °C, followed by treating with plasma for 15 min. After that, the substrate was immersed in an octadecyltrichlorosilane (ODTS) solution (Toluene as the solvent) overnight, rinsed with toluene to remove extra ODTS and dried on the hot plate at 110 °C. The polymers were dissolved in chlorobenzene at a concentration of 10 mg/mL by stirring for four days. The polymer films were spin-cast at 2000 rpm and annealed at a designated temperature for 15 min. Finally, gold electrode with 60 nm was thermally evaporated in vacuum through a shadow mask with the following dimensions (length (L) = 200 μm, and channel width (W) = 4.0 mm).

3.8.4 OPV fabrication and characterization

ITO substrates with Sheet Resistance ~ 12 Ω were sonicated in acetone for 10 minutes, then sequentially in detergent, deionized water and isopropyl alcohol respectively for 15 minutes to clear impurities adhering to the ITO surface. This was followed by a desiccation at 90 °C lasting overnight in a vacuum oven. Next, a precursor solution ($Zn(Ac)_2$ solution, 100 mg/mL in 2-methoxyethanol with 2% ethanolamine) to the ZnO interlayer was spin-coated onto pre-cleaned and UV-Ozone-treated ITO substrates, and the substrates were heated at 200 °C for 30 minutes continuously. Polymer and $PC_{71}BM$ in a weight ratio of 1:1.5 were co-dissolved in pure CB solvent such that the total solids concentration was 30 mg mL^{-1}; 1,8-diiodooctane (DIO) was used as an additive. The active layer solutions were stirred at 80 °C for over 3 hours before spin coating. The thickness of active layer spin-coated on the top of ZnO was controlled by the spinning speed from the solutions. Subsequently, 10 nm molybdenum oxide (MoO_3) hole-buffer layer and 100 nm Ag electrode were deposited by thermal evaporation in vacuum (about 1×10^{-4} Pa) through a defined

shadow mask. The effective area of device was 4.5 mm^2 and they were measured in a closed glove box.

3.9 References

1. You, J.; Dou, L.; Yoshimura, K.; Kato, T.; Ohya, K.; Moriarty, T.; Emery, K.; Chen, C.-C.; Gao, J.; Li, G.; Yang, Y. *Nat. Commun.* **2013,** *4*, 1446.
2. Liu, Y.; Zhao, J.; Li, Z.; Mu, C.; Ma, W.; Hu, H.; Jiang, K.; Lin, H.; Ade, H.; Yan, H. *Nat. Commun.* **2014,** *5*, 5293.
3. Zhou, H.; Zhang, Y.; Mai, C.-K.; Collins, S. D.; Bazan, G. C.; Nguyen, T.-Q.; Heeger, A. J. *Adv. Mater.* **2015,** *27*, 1767-1773.
4. Zhao, W.; Li, S.; Yao, H.; Zhang, S.; Zhang, Y.; Yang, B.; Hou, J. *J. Am. Chem. Soc.* **2017,** *139*, 7148-7151.
5. Li, M.; Gao, K.; Wan, X.; Zhang, Q.; Kan, B.; Xia, R.; Liu, F.; Yang, X.; Feng, H.; Ni, W.; Wang, Y.; Peng, J.; Zhang, H.; Liang, Z.; Yip, H.-L.; Peng, X.; Cao, Y.; Chen, Y. *Nat. Photonics* **2016,** *11*, 85.
6. Albrecht, S.; Janietz, S.; Schindler, W.; Frisch, J.; Kurpiers, J.; Kniepert, J.; Inal, S.; Pingel, P.; Fostiropoulos, K.; Koch, N.; Neher, D. *J. Am. Chem. Soc.* **2012,** *134*, 14932-14944.
7. Chen, H.-Y.; Hou, J.; Zhang, S.; Liang, Y.; Yang, G.; Yang, Y.; Yu, L.; Wu, Y.; Li, G. *Nat. Photonics* **2009,** *3*, 649.
8. Zhang, M.; Guo, X.; Ma, W.; Ade, H.; Hou, J. *Adv. Mater.* **2015,** *27*, 4655-4660.
9. Blom, P. W. M.; Mihailetchi, V. D.; Koster, L. J. A.; Markov, D. E. *Adv. Mater.* **2007,** *19*, 1551-1566.
10. Lin, Y.; Zhao, F.; He, Q.; Huo, L.; Wu, Y.; Parker, T. C.; Ma, W.; Sun, Y.; Wang, C.; Zhu, D.; Heeger, A. J.; Marder, S. R.; Zhan, X. *J. Am. Chem. Soc.* **2016,** *138*, 4955-4961.
11. Huo, L.; Liu, T.; Sun, X.; Cai, Y.; Heeger, A. J.; Sun, Y. *Adv. Mater.* **2015,** *27*, 2938-2944.
12. Fan, Q.; Su, W.; Guo, X.; Guo, B.; Li, W.; Zhang, Y.; Wang, K.; Zhang, M.; Li, Y. *Adv. Energy Mater.* **2016,** *6*, 1600430.

13. Qian, D.; Ye, L.; Zhang, M.; Liang, Y.; Li, L.; Huang, Y.; Guo, X.; Zhang, S.; Tan, Z. a.; Hou, J. *Macromolecules* **2012,** *45*, 9611-9617.

14. Ie, Y.; Huang, J.; Uetani, Y.; Karakawa, M.; Aso, Y. *Macromolecules* **2012,** *45*, 4564-4571.

15. Qian, D.; Ma, W.; Li, Z.; Guo, X.; Zhang, S.; Ye, L.; Ade, H.; Tan, Z. a.; Hou, J. *J. Am. Chem. Soc.* **2013,** *135*, 8464-8467.

16. Zhang, S.; Qin, Y.; Uddin, M. A.; Jang, B.; Zhao, W.; Liu, D.; Woo, H. Y.; Hou, J. *Macromolecules* **2016,** *49*, 2993-3000.

17. Ackermann, L.; Vicente, R.; Kapdi, A. R. *Angew. Chem. Int. Ed.* **2009,** *48*, 9792-9826.

18. Schipper, D. J.; Fagnou, K. *Chem. Mater.* **2011,** *23*, 1594-1600.

19. Mercier, L. G.; Leclerc, M. *Acc. Chem. Res.* **2013,** *46*, 1597-1605.

20. Okamoto, K.; Zhang, J.; Housekeeper, J. B.; Marder, S. R.; Luscombe, C. K. *Macromolecules* **2013,** *46*, 8059-8078.

21. Kowalski, S.; Allard, S.; Zilberberg, K.; Riedl, T.; Scherf, U. *Prog. Polym. Sci.* **2013,** *38*, 1805-1814.

22. Kai, W.; Mingfeng, W. *Curr. Org. Chem.* **2013,** *17*, 999-1012.

23. Pouliot, J.-R.; Grenier, F.; Blaskovits, J. T.; Beaupré, S.; Leclerc, M. *Chem. Rev.* **2016,** *116*, 14225-14274.

24. Suraru, S.-L.; Lee, J. A.; Luscombe, C. K. *ACS Macro Lett.* **2016,** *5*, 724-729.

25. Bohra, H.; Wang, M. *J. Mater. Chem. A* **2017,** *5*, 11550-11571.

26. Wakioka, M.; Ichihara, N.; Kitano, Y.; Ozawa, F. *Macromolecules* **2014,** *47*, 626-631.

27. Iizuka, E.; Wakioka, M.; Ozawa, F. *Macromolecules* **2015,** *48*, 2989-2993.

28. Wang, Q.; Takita, R.; Kikuzaki, Y.; Ozawa, F. *J. Am. Chem. Soc.* **2010,** *132*, 11420-11421.

29. Pouliot, J.-R.; Wakioka, M.; Ozawa, F.; Li, Y.; Leclerc, M. *Macromol. Chem. Phys.* **2016,** *217*, 1493-1500.

30. Fujinami, Y.; Kuwabara, J.; Lu, W.; Hayashi, H.; Kanbara, T. *ACS Macro Lett.* **2012,** *1*, 67-70.

31. Lu, W.; Kuwabara, J.; Iijima, T.; Higashimura, H.; Hayashi, H.; Kanbara, T. *Macromolecules* **2012,** *45*, 4128-4133.

32. Choi, S. J.; Kuwabara, J.; Kanbara, T. *ACS Sustainable Chem. Eng.* **2013,** *1*, 878-882.

33. Kuwabara, J.; Kanbara, T. *J. Synth. Org. Chem. Jpn.* **2014,** *72*, 1271-1278.

34. Kuwabara, J.; Yamazaki, K.; Yamagata, T.; Tsuchida, W.; Kanbara, T. *Polym. Chem.* **2015,** *6*, 891-895.

35. Kuwabara, J.; Fujie, Y.; Maruyama, K.; Yasuda, T.; Kanbara, T. *Macromolecules* **2016,** *49*, 9388-9395.

36. Lombeck, F.; Komber, H.; Gorelsky, S. I.; Sommer, M. *ACS Macro Lett.* **2014,** *3*, 819-823.

37. Broll, S.; Nubling, F.; Luzio, A.; Lentzas, D.; Komber, H.; Caironi, M.; Sommer, M. *Macromolecules* **2015,** *48*, 7481-7488.

38. Matsidik, R.; Komber, H.; Luzio, A.; Caironi, M.; Sommer, M. *J. Am. Chem. Soc.* **2015,** *137*, 6705-6711.

39. Lombeck, F.; Komber, H.; Fazzi, D.; Nava, D.; Kuhlmann, J.; Stegerer, D.; Strassel, K.; Brandt, J.; Mendaza, A. D. D.; Muller, C.; Thiel, W.; Caironi, M.; Friend, R.; Sommer, M. *Adv. Energy Mater.* **2016,** *6*.

40. Rudenko, A. E.; Wiley, C. A.; Stone, S. M.; Tannaci, J. F.; Thompson, B. C. *J. Polym. Sci., Part A: Polym. Chem.* **2012,** *50*, 3691-3697.

41. Rudenko, A. E.; Wiley, C. A.; Tannaci, J. F.; Thompson, B. C. *J. Polym. Sci., Part A: Polym. Chem.* **2013,** *51*, 2660-2668.

42. Rudenko, A. E.; Thompson, B. C. *J. Polym. Sci., Part A: Polym. Chem.* **2015,** *53*, 135-147.

43. Livi, F.; Gobalasingham, N. S.; Thompson, B. C.; Bundgaard, E. *J. Polym. Sci., Part A: Polym. Chem.* **2016,** *54*, 2907-2918.

44. Gobalasingham, N. S.; Carlé, J. E.; Krebs, F. C.; Thompson, B. C.; Bundgaard, E.; Helgesen, M. *Macromol. Rapid Commun.* **2017,** *38*, 1700526.

45. Wu, W.; Xin, H.; Ge, C.; Gao, X. *Tetrahedron Lett.* **2017,** *58*, 175-184.

46. Wakioka, M.; Nakamura, Y.; Wang, Q.; Ozawa, F. *Organometallics* **2012,** *31*, 4810-4816.

47. Dudnik, A. S.; Aldrich, T. J.; Eastham, N. D.; Chang, R. P. H.; Facchetti, A.; Marks, T. J. *J. Am. Chem. Soc.* **2016,** *138*, 15699-15709.

48. Sun, D.; Meng, D.; Cai, Y.; Fan, B.; Li, Y.; Jiang, W.; Huo, L.; Sun, Y.; Wang, Z. *J. Am. Chem. Soc.* **2015,** *137*, 11156-11162.

49. Yang, B.; Zhang, S.; Chen, Y.; Cui, Y.; Liu, D.; Yao, H.; Zhang, J.; Wei, Z.; Hou, J. *Macromolecules* **2017,** *50*, 1453-1462.

50. Wang, X.; Wang, M. *Polym. Chem.* **2014,** *5*, 5784-5792.

51. Wang, K.; Wang, G.; Wang, M. *Macromol. Rapid Commun.* **2015,** *36*, 2162-70.

52. Shao, J.; Wang, G.; Wang, K.; Yang, C.; Wang, M. *Polym. Chem.* **2015,** *6*, 6836-6844.

53. Bohra, H.; Shao, J.; Huang, S.; Wang, M. *Tetrahedron Lett.* **2016,** *57*, 1497-1501.

54. Wang, X.; Wang, K.; Wang, M. *Polym. Chem.* **2015,** *6*, 1846-1855.

55. Huang, J.; Wang, K.; Gupta, S.; Wang, G.; Yang, C.; Mushrif, S. H.; Wang, M. *J. Polym. Sci., Part A: Polym. Chem.* **2016,** *54*, 2015-2031.

56. Morin, P.-O.; Bura, T.; Sun, B.; Gorelsky, S. I.; Li, Y.; Leclerc, M. *ACS Macro Lett.* **2015,** *4*, 21-24.

57. Homyak, P.; Liu, Y.; Liu, F.; Russel, T. P.; Coughlin, E. B. *Macromolecules* **2015,** *48*, 6978-6986.

58. Pouliot, J.-R.; Sun, B.; Leduc, M.; Najari, A.; Li, Y.; Leclerc, M. *Polym. Chem.* **2015,** *6*, 278-282.

59. Guo, C.; Quinn, J.; Sun, B.; Li, Y. *Polym. Chem.* **2016,** *7*, 4515-4524.

60. Efrem, A.; Wang, K.; Amaniampong, P. N.; Yang, C.; Gupta, S.; Bohra, H.; Mushrif, S. H.; Wang, M. *Polym. Chem.* **2016,** *7*, 4862-4866.

61. Bohra, H.; Tan, S. Y.; Shao, J.; Yang, C.; Efrem, A.; Zhao, Y.; Wang, M. *Polym. Chem.* **2016,** *7*, 6413-6421.

62. Bohra, H.; Li, P.; Yang, C.; Zhao, Y.; Wang, M. *Polym. Chem.* **2018,** *9*, 1972-1982.

63. McDowell, C.; Abdelsamie, M.; Toney, M. F.; Bazan, G. C. *Adv. Mater.* **2018,** *30*, 1707114.

64. Perez, L. A.; Rogers, J. T.; Brady, M. A.; Sun, Y.; Welch, G. C.; Schmidt, K.; Toney, M. F.; Jinnai, H.; Heeger, A. J.; Chabinyc, M. L.; Bazan, G. C.; Kramer, E. J. *Chem. Mater.* **2014,** *26*, 6531-6541.

65. Kniepert, J.; Lange, I.; Heidbrink, J.; Kurpiers, J.; Brenner, T. J. K.; Koster, L. J. A.; Neher, D. *J. Phys. Chem. C* **2015,** *119*, 8310-8320.

66. Tao, L.; Xuexue, P.; Xiangyi, M.; Yu, L.; Donghui, W.; Wei, M.; Lijun, H.; Xiaobo, S.; Ho, L. T.; Minjuan, H.; Hyosung, C.; Young, K. J.; H., C. W. C.; Yanming, S. *Adv. Mater.* **2017,** *29*, 1604251.

67. Yang, L.; Zhou, H.; You, W. *J. Phys. Chem. C* **2010,** *114*, 16793-16800.

68. Peet, J.; Heeger, A. J.; Bazan, G. C. *Acc. Chem. Res.* **2009,** *42*, 1700-1708.

69. Huang, Y.; Kramer, E. J.; Heeger, A. J.; Bazan, G. C. *Chem. Rev.* **2014,** *114*, 7006-7043.

70. McNeill, C. R.; Watts, B.; Thomsen, L.; Ade, H.; Greenham, N. C.; Dastoor, P. C. *Macromolecules* **2007,** *40*, 3263-3270.

71. Park, S. H.; Roy, A.; Beaupré, S.; Cho, S.; Coates, N.; Moon, J. S.; Moses, D.; Leclerc, M.; Lee, K.; Heeger, A. J. *Nat. Photonics* **2009,** *3*, 297.

72. Li, H.; Zhao, Y.; Fang, J.; Zhu, X.; Xia, B.; Lu, K.; Wang, Z.; Zhang, J.; Guo, X.; Wei, Z. *Adv. Energy Mater.* **2018,** *8*, 1702377.

73. Pawle, R. H.; Agarwal, A.; Malveira, S.; Smith, Z. C.; Thomas, S. W. *Macromolecules* **2014,** *47*, 2250-2256.

74. Guo, H.; Shen, T.; Wu, F.; Hou, R.; Liu, X.; Zhao, B.; Tan, S. *J. Appl. Polym. Sci.* **2016,** *133*, 42982.

75. Odobel, F.; Suresh, S.; Blart, E.; Nicolas, Y.; Quintard, J.-P.; Janvier, P.; Le Questel, J.-Y.; Illien, B.; Rondeau, D.; Richomme, P.; Häupl, T.; Wallin, S.; Hammarström, L. *Chem. Eur. J.* **2002,** *8*, 3027-3046.

4. Narrow bandgap thienothiadiazole-based conjugated porous polymers: from facile direct arylation polymerization to tunable porosities and optoelectronic properties

4.1 Introduction

Conjugated porous polymers (CPPs)[1-5] integrated with high porosity, optoelectronic properties and chemical stability are a class of multifunctional organic materials that have attracted much attention owing to their potential applications such as gas storage,[6-8] chemosensing,[9-12] and photocatalysis.[13-15] In Chapters 2 and 3, we synthesized linear conjugated polymers by choosing high-performance acceptor molecules and polymerizing them with rationally selected donors, thereby providing good control over the optical and electrochemical properties of the polymers, which is crucial for application in optoelectronics. Similar to linear polymers, the design and synthesis of CPPs also follows a modular approach.[16] With careful selection of monomers and polymerization techniques, tunability over a wide range of physical and chemical properties can be achieved.[17-20] In particular, bandgap control is crucial in polymers for energy conversion as well as other light harvesting applications. For instance, incorporation of strong electron-accepting moieties such as benzothiadiazoles and weak electron-donating units such as benzenes and fluorenes in conjugated polymer networks not only reduced the bandgaps, but also improved the photocatalytic activity compared to pure electron-donating networks.[21] A similar donor-acceptor (D-A) strategy was used recently by Bonillo et al. to finely tune the bandgap and emission properties of polyphenylene networks by modifying the monomer ratios of different electron-accepting moieties in a Suzuki–Miyaura polymerization protocol.[22]

Much like linear polymers, traditional synthesis of CPPs involving the aryl C–C bond formation has been carried out by transition-metal catalyzed

reactions such as Sonogashira–Hagihara coupling,[23-24] Yamamoto coupling,[25-26] Suzuki–Miyaura coupling,[17-18, 27] and Stille coupling.[28] Linker-specific polycondensation reactions such as Schiff-base condensation[29] and imidization[30-31] reactions have also been vastly utilized in the synthesis of CPPs. Most of these reactions, nevertheless, involve multiple synthetic steps for the functionalization of comonomers. Moreover, some transition-metal catalyzed reactions such as Stille coupling result in the formation of toxic byproducts which are detrimental to the environment.

Direct arylation polymerization (DAP) as an alternative to conventional polymerization reactions for the synthesis of linear π-conjugated polymers has attracted increasing attention in the last decade.[32-37] DAP, which involves the facile one step coupling of aryl bromides with C–H active arenes without pre-activation of C–H bonds using flammable and/or toxic organometallic reagents, has enabled the synthesis of a myriad of linear conjugated polymers with qualities (regioselectivity, molecular weights, etc.) comparable to or even better than those synthesized by conventional coupling techniques.[38-49] However, DAP as a synthetic tool for conjugated porous polymers has not been investigated until recently.[50-51] For instance, Liu et al. have reported DAP between 1,2,4,5-tetrafluorobenzene and two aryl bromides, 1,3,5-tribomobenzene and tetrakis(4-bromophenyl)methane.[50] Although the resulting polymers showed specific surface areas as high as 1170 $m^2 g^{-1}$, their wide bandgaps limited light absorption in visible and near infrared (NIR) regions. More recently, Wang and coworkers reported a facile one-step DAP using 8,11-dibromodithieno[3,2-*a*:2′,3′-*c*]phenazine as a single monomer, resulting in CPPs with a narrow bandgap of 1.5 eV and hierarchical porosity.[51] However, the scope of CPPs that could be synthesized using the facile DAP scheme remains limited.

In this chapter, we extend the scope of direct arylation from synthesis of conjugated linear polymers to new narrow-bandgap conjugated 2D/3D porous networks. Herein, we present the synthesis of a series of narrow bandgap conjugated porous polymers by DAP of 4,6-di(2- thienyl)thieno[3,4-c][1,2,5]

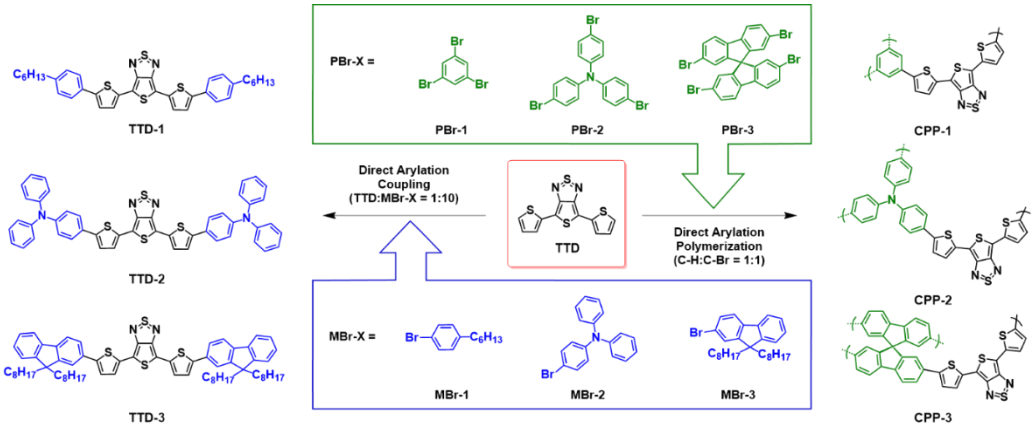

Scheme 4.1 Synthesis of **TTD**-based D–A–D triads and CPPs by direct arylation coupling.

thiadiazole (**TTD**) with multi-topic aryl bromides. **TTD**, composed of a strong electron-accepting core of thienothiadiazole flanked by thiophene groups on both sides, is a coplanar π-conjugated narrow bandgap monomer. We speculated that the electron-deficient nature of the thienothiadiazole core could result in effective cleavage of the acidic C–H bonds in the thiophene groups. To understand the reactivity and regioselectivity of **TTD**, C–H direct arylation coupling between **TTD** and three mono-brominated reagents (**MBr-1–3**, **Scheme 4.1**) was examined, resulting in three donor-acceptor-donor (D-A-D) triads that are easier to purify and characterize than CPPs. Then three representative electron rich/neutral aryl bromides, 1,3,5 tribromobenzene,[20-21] 2,2′,7,7′-tetrabromo-9,9′-spirobifluorene[26, 52] and tris(4-bromophenyl)amine[53-54] were used as comonomers in DAP with **TTD**. The structure–property relationships of **TTD**-based CPPs were studied through systematic characterization using nuclear magnetic resonance (NMR) spectroscopy, Fourier transform infrared spectroscopy (FTIR), elemental analysis, electron microscopy, porosity analysis and UV-Vis-NIR absorption spectroscopy.

4.2 Direct arylation synthesis and structural characterization: from TTD-based small molecules to conjugated porous polymers (CPPs)

4.2.1 TTD-based small molecules

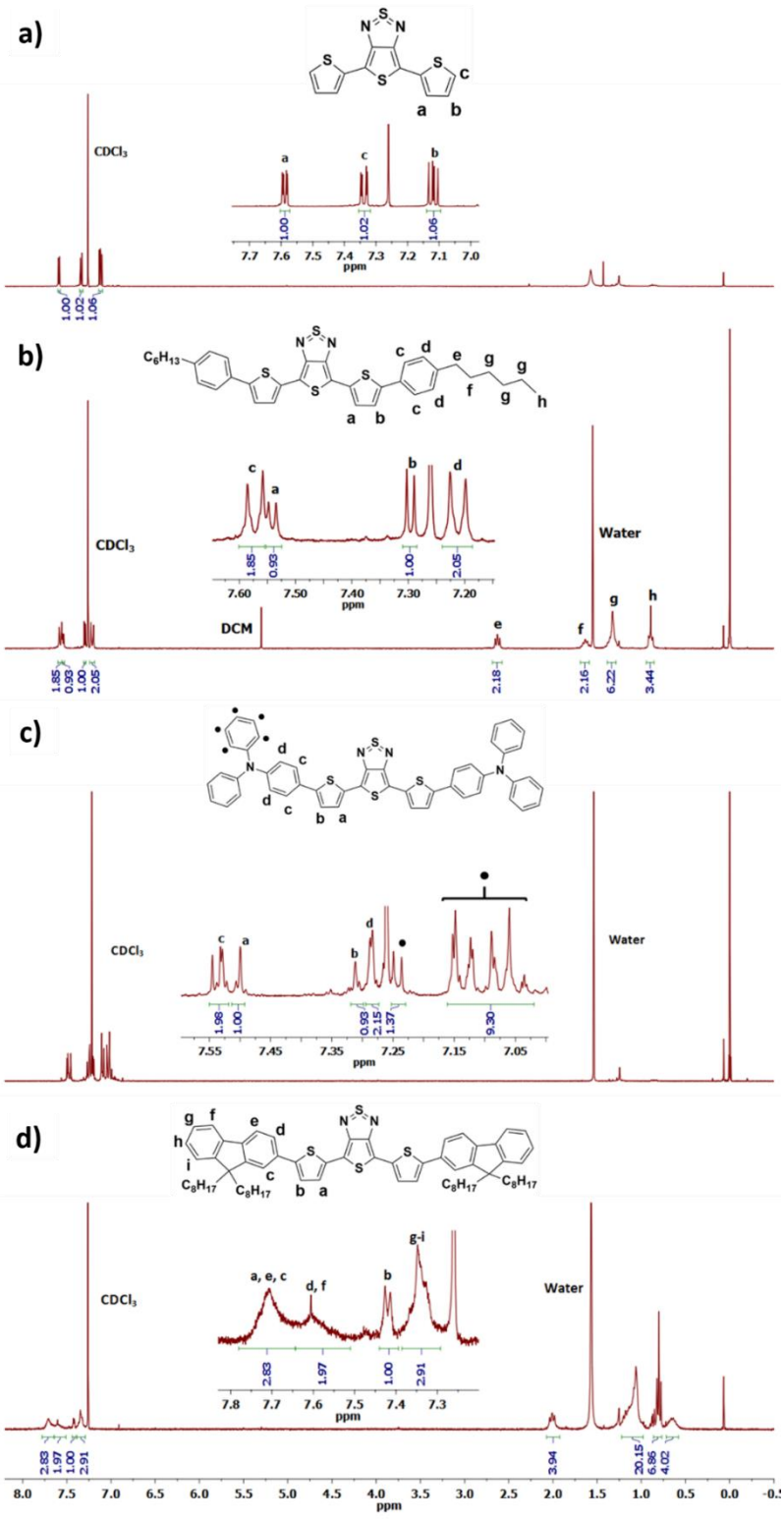

Figure 4.1 ^{1}H-NMR spectra of a) **TTD**, b) **TTD-1**, c) **TTD-2** and d) **TTD-3** in $CDCl_3$ at 298 K with complete assignment of protons.

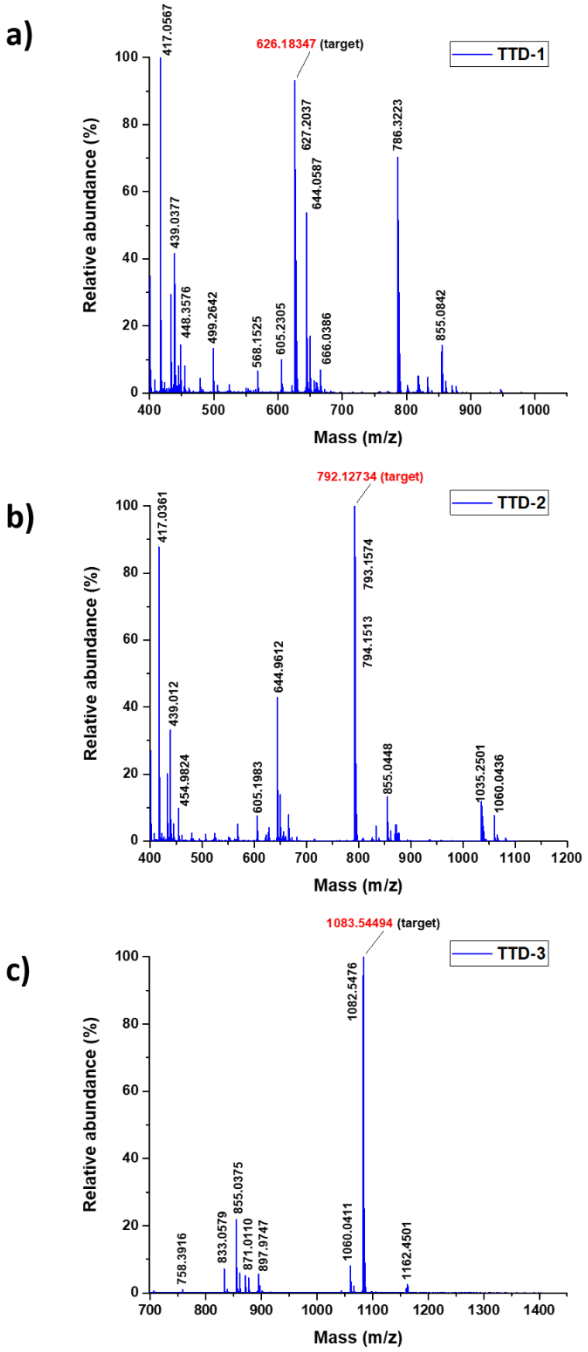

Figure 4.2 Mass spectra of a) **TTD-1**, b) **TTD-2** and c) **TTD-3.**

The synthetic routes to the **TTD**-based small molecular D-A-D triads and CPPs are shown in **Scheme 4.1**. These triads serve as model compounds for the respective conjugated polymer networks. A Pd(0) catalyst, $Pd_2(dba)_3$, in combination with (o-$MeOC_6H_4)_3P$ was used in a carboxylate-mediated direct

arylation coupling to produce **TTD-(1–3)**.[45] The reaction was carried out at 120 °C for 24 hours. All triads were obtained in high yields – 95% for **TTD-1**, 80% for **TTD-2** and 83% for **TTD-3**. ^{1}H-NMR spectra of the triads (**Figure 4.1**) show the peak from the β-proton of the **TTD** core at 7.30 ppm in **TTD-1**, 7.31 ppm in **TTD-2** and 7.41 ppm in **TTD-3**, respectively, suggesting good regioselectivity of **TTD** under the present reaction conditions. The chemical structures of the triads were further confirmed by mass spectroscopy (**Figure 4.2**). The relatively high reactivity and regioselectivity of **TTD** observed in these model reactions are crucial for the following DAP to obtain structurally defined CPPs.

4.2.2 TTD-based conjugated porous polymers (CPPs)

TTD-based near infrared conjugated porous polymers (**CPP-** (**1**–**3**)) were synthesized using the same reaction conditions as for the synthesis of **TTD-1–3** triads, except for the reaction time and monomer ratio. The DAP reaction condition[45] used here was found efficient for the synthesis of benzodithiophene-based linear polymers and the C–H activation of a variety of thiophene-flanked acceptor molecules[45-48] including thienothiadiazole[49] for the synthesis of donor–acceptor linear polymers. A molar ratio of 1:1 between C–H and C–Br bonds of the monomers was maintained, and all the polymerization reactions were carried out for 48 hours to ensure as complete a reaction as possible. Polymers were purified by washing thoroughly with organic (methanol, chloroform and THF) and aqueous solvents (water and diluted HCl) to remove all oligomeric products as well as any byproducts of DAP. The CPPs obtained here appear as green powders that are insoluble in common organic solvents such as THF, chloroform, toluene and chlorobenzene. Characterization of the chemical structures of **CPP-(1–3)** was first carried out using FTIR spectroscopy (**Figure 4.3**). A band at 1489 cm^{-1} in the FTIR spectra of **TTD**, which is assigned to the symmetric stretch of the aromatic C=C bond of thiophene, is clearly present in the spectra of all CPPs. The symmetric C=C stretching bands of their respective aryl bromide comonomers appear at 1583 cm^{-1} in **CPP-1**, 1480 cm^{-1} in **CPP-2** and 1465 cm^{-1} in **CPP-3**, respectively. Stretching vibrations of thiophene rings in **TTD** were also detected as weak bands in the frequency range between 840 and 860 cm^{-1}.

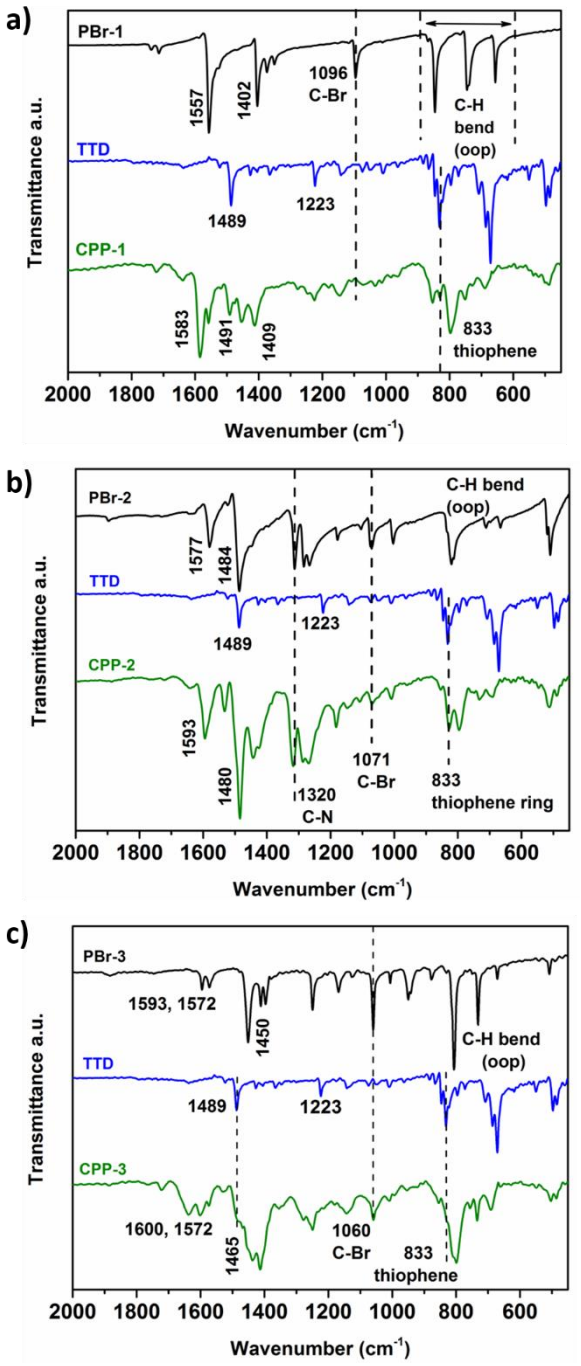

Figure 4.3 Comparison of FTIR spectra (fingerprint region) of (a) **CPP-1**, (b) **CPP-2** and (c) **CPP-3** shown in green with **TTD** (blue) and their respective aryl bromide comonomers (black).

CPP-2 showed the characteristic stretching bands of aromatic C–N bonds at 1320 cm^{-1} (**Figure 4.3b**). The obvious attenuation of the C–Br stretch band at 1096

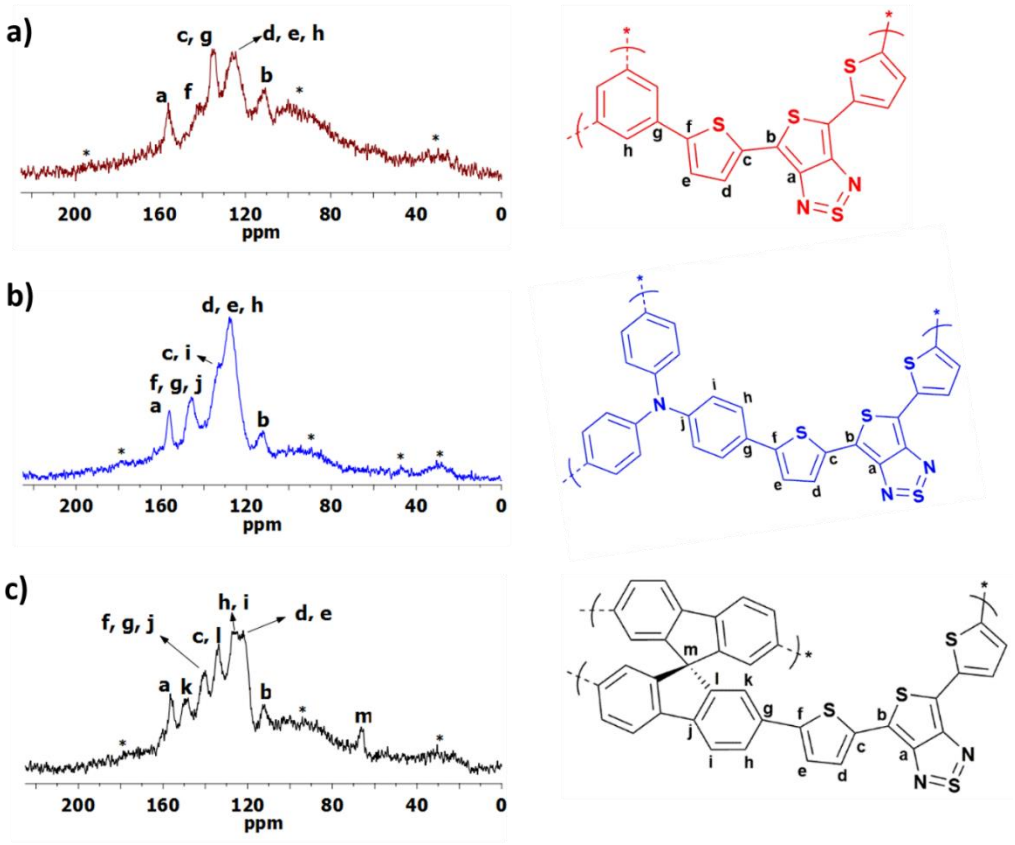

Figure 4.4 ^{13}C CP/MAS spectra of **CPP-1** (a), **CPP-2** (b) and **CPP-3** (c).

cm^{-1} in **CPP-1** suggests the highly efficient direct arylation reaction and the large extent of polymerization. In contrast to **CPP-1**, small peaks at1071 and 1060 cm^{-1} corresponding to the C–Br stretch band were still observed in **CPP-2** and **CPP-3**, respectively, suggesting the lower extent of polymerization in the latter two polymers than the former.

CPP-(1–3) were further characterized by solid state ^{13}C CP/ MAS NMR spectroscopy to confirm their structures. ^{13}C NMR spectra of all polymers with complete peak assignments are shown in **Figure 4.4**. A sharp peak around 156 ppm and a broad peak around 112 ppm, which are assigned to the carbons of the thienothiadiazole moiety of **TTD**, are observed in the spectra of all CPPs. In **CPP-1**, the broad peaks observed at 141.7 and 135.5 ppm could be attributed to

the substituted carbons of the **TTD** (α-carbon) and the phenyl repeating unit, respectively (**Figure 4.4a**). In addition, the peaks of unsubstituted carbons (C–H) of these monomers overlap into a broad peak located at 125.8 ppm. In **CPP-2**, the carbon signal from the tertiary amine (C–N) group appears at 145.8 ppm and overlaps with the signals of the substituted carbons of triphenylamine and **TTD** units (**Figure 4.4b**). Unsubstituted carbons of **CPP-2** are assigned to the broad peak at 128 ppm and its shoulder at 132.6 ppm. In **CPP-3**, the signals from the phenyl rings of spirobifluorene appear as broad peaks between 150 and 124 ppm, as shown in **Figure 4.4c**. The sharp peak at 66.5 ppm is assigned to the quaternary carbon of spirobifluorene. The ^{13}C-NMR results discussed above, which are complementary to the FTIR results, further prove the chemical structures of the target **CPP-1–3** obtained under the present direct arylation scheme.

Elemental analysis of CPPs showed some inconsistency between the theoretical (neglecting the contribution of bromide end groups) and experimental values, which is typical for porous solids and can be attributed to due to the presence of trace impurities trapped in the pores.[51] A better match between the theoretical and experimental mass percentages was observed in **CPP-1** compared to **CPP-2** and **CPP-3**. These results are consistent with the

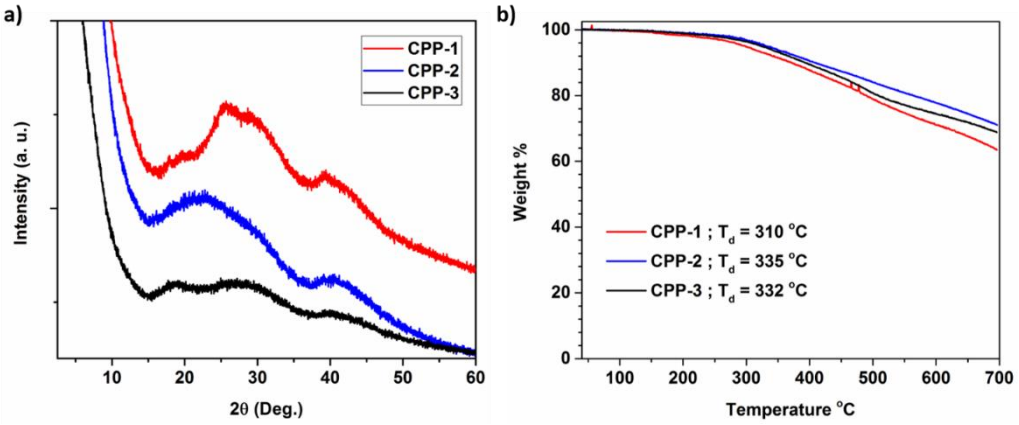

Figure 4.5 a) Powder X-ray diffraction patterns of **TTD**-based CPP. b) TGA plots of CPPs recorded under N2 atmosphere at a heating rate of 10 °C/ min.

FTIR spectra of **CPP-2** and **CPP-3** (**Figure 4.3b and 4.3c**) where the appearance of a weak C–Br band indicates their lower extent of polymerization.

Powder X-ray diffraction (XRD) patterns of all CPPs exhibit broad peaks in the range $2\theta = 5 – 60°$, indicating the amorphous nature of these polymers (**Figure 4.5a**). Thermogravimetric analysis shows that all CPPs (**Figure 4.5b**) are stable up to 300 °C under nitrogen atmosphere, a characteristic of the good thermal stability of such covalent polymer networks.

4.3 Morphology of TTD-based CPPs

Morphologies of **CPP-(1–3)** were studied by scanning electron microscopy (SEM) and transmission electron microscopy (TEM). From the SEM image of **CPP-1** (**Figure 4.6a**), dense networks of thin fibres can be observed most likely due to aggregation of the individual strands. The thickness of the fibres estimated from the SEM images is ~30 nm. Both **CPP-2** and **CPP-3** appear as microspheres with different sizes as seen from their SEM images (**Figure 4.6b** and **4.6c**). The particles of **CPP-3** are approximately twice as large as those of **CPP-2**. Moreover, the micro-spheres of **CPP-2** have a smooth surface, in contrast to the granular and relatively rough surface of **CPP-3** (**Figure 4.6b** inset). While the high-resolution TEM images clearly show the microporous structures of **CPP-2** (**Figure 4.6d**) and **CPP-3** (**Figure 4.6f**), the microporous nature is not obvious in **CPP-1** (**Figure 4.6b**), presumably due to its smaller pore sizes and tighter π–π stacking caused by the relatively small and flat phenyl repeating unit in **CPP-1**.

4.4 Surface area and porosity of TTD-based CPPs

Porosities of **CPP-1**, **CPP-2** and **CPP-3** were studied in physisorption experiments using nitrogen as the sorbate molecule. Sorption isotherms of CPPs measured at 77 K are shown in **Figure 4.7**. All polymers show a combination of Type II and Type IV sorption isotherms according to IUPAC classification. The uptake of N_2 at relatively low pressures $p/p_o < 0.1$ is much lower compared to previously reported porous organic polymers,[4, 8, 16] suggesting the relatively low microporosity in these polymers. In contrast, a sharp increase of N_2-uptake was

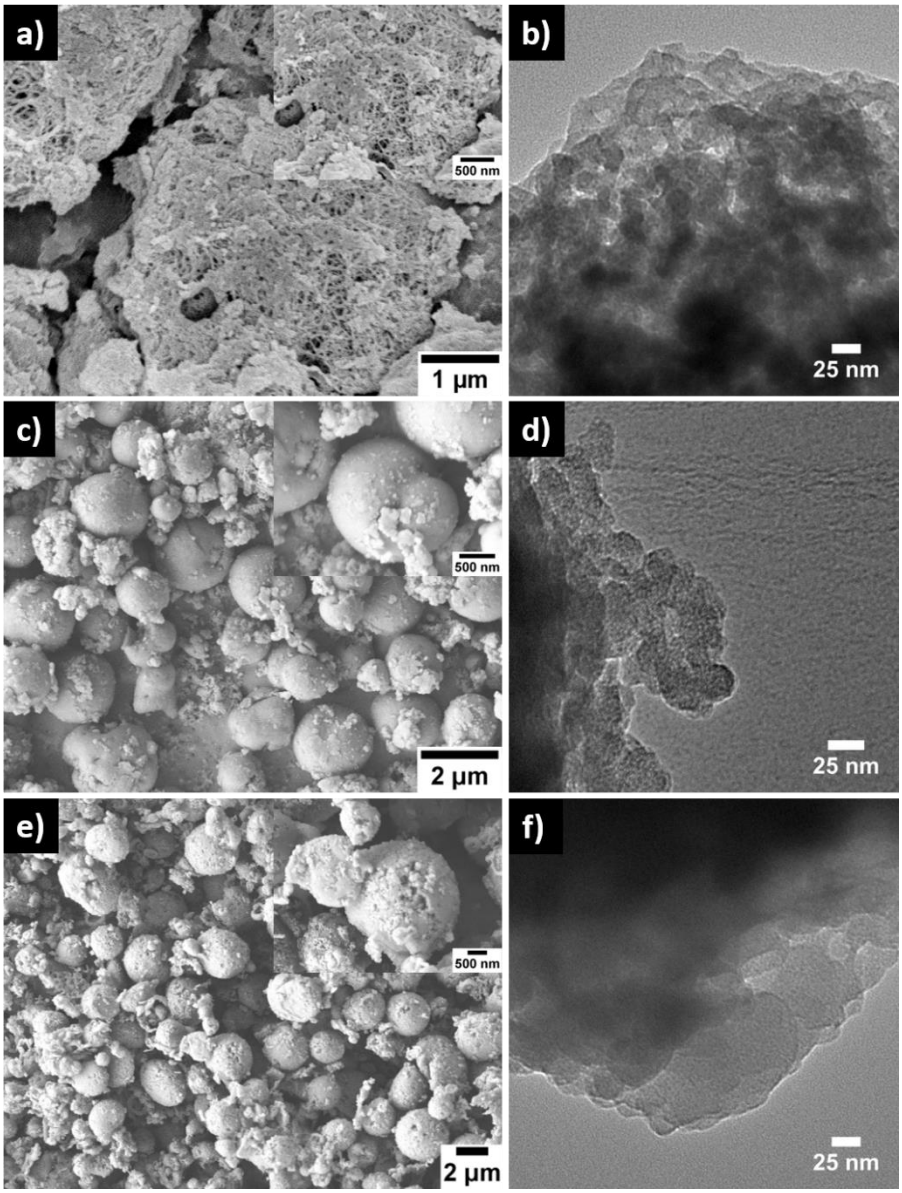

Figure 4.6 SEM (a, c, e) and TEM (b, d, f) images of **CPP-1** (a, b), **CPP-2** (c, d) and **CPP-3** (e, f). Magnified SEM images (inset) of a) **CPP-1**, b) **CPP-2** and c) **CPP-3**.

observed at $p/p_o = 0.9 – 1$, an indication of the presence of dominating meso- and macropores from the interparticular voids in these polymers. A small degree of hysteresis was observed in the isotherms of **CPP-1** in the relatively high-pressure range ($0.5 < p/p_o < 0.99$). This can be explained by the presence of pores with narrow openings that restrict the access of nitrogen molecules. Alternatively, this could also be attributed to the swelling of the polymer framework due to the

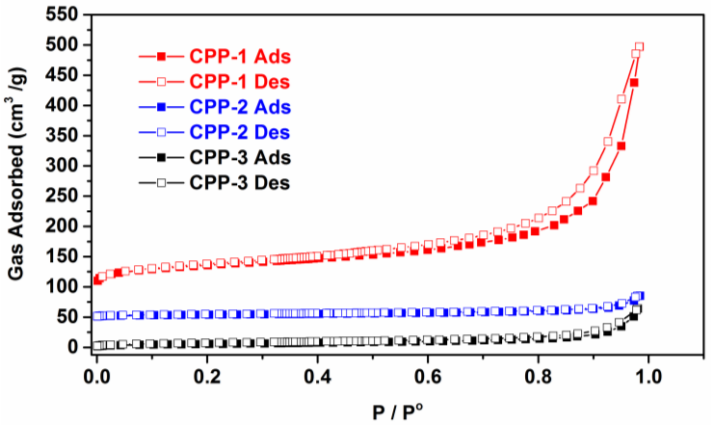

Figure 4.7 N_2 adsorption–desorption isotherms of **CPP-(1–3)** measured at 77 K. For clarity, the isotherms of **CPP-1** and **CPP-2** were shifted vertically by 50 $cm^3\ g^{-1}$, respectively.

Table 4.1 N_2 adsorption characteristics of **CPP-(1–3).**

Species	S_{BET} ($m^2\ g^{-1}$) [a]	S_{DFT} ($m^2\ g^{-1}$) [b]	V_{micro} ($cm^3\ g^{-1}$) [c]	$V_{tot,\ DFT}$ ($cm^3\ g^{-1}$)
CPP-1	128.3	95.3	0	0.52
CPP-2	14.2	10.9	0	0.04
CPP-3	20.6	17.2	0	0.08

[a] Specific surface area calculated from the adsorption branch of the N_2 isotherm using the BET method. [b] Specific surface area calculated using the NL-DFT method for slit pores with equilibrium model. [c] Micro-pore volume calculated from the adsorption branch of the N_2 isotherm using the t-plot method

dissolution of the adsorbate into the non-porous sections of polymer during the adsorption cycle.[55]

Key porosity properties of CPPs are listed in **Table 4.1**. Among the three polymers, **CPP-1** with fibrillar networks shows the largest Brunauer–Emmett–Teller (BET) surface area of 128.3 $m^2\ g^{-1}$, which is significantly higher than those of the **CPP-2** (14.2 $m^2\ g^{-1}$) and **CPP-3** (20.63 $m^2\ g^{-1}$) microspheres. Pore size distribution (PSD) profiles of CPPs were calculated using the NL-DFT method (**Figure 4.8d-f**). All CPPs have a broad PSD ranging from 14 Å to well beyond

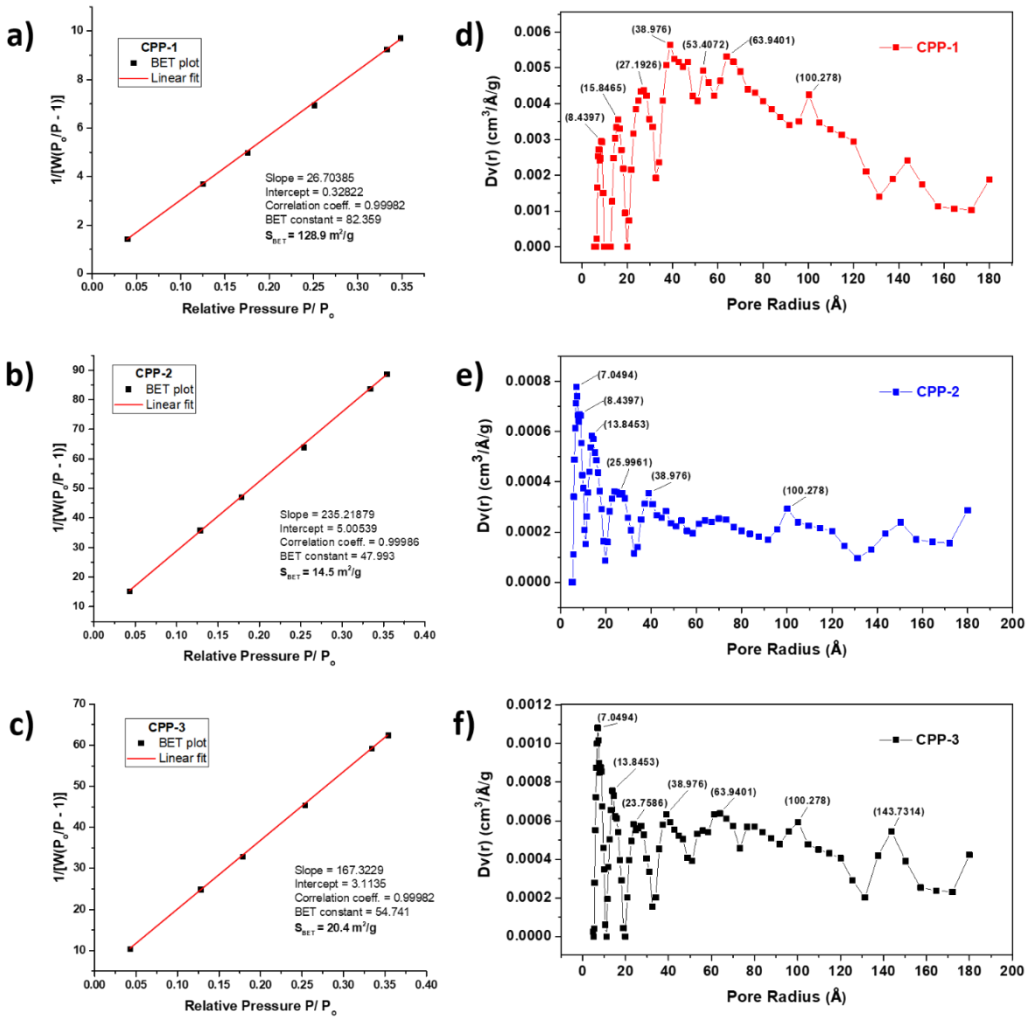

Figure 4.8 BET specific surface area plots (a-c) and pore size distributions (d-f) of **CPP-1** (a, b), **CPP-2** (c, d) and **CPP-3** (e, f). Pore size distributions were calculated using the NL-DFT method of CPPs.

200 Å. The structure– porosity relationship that we observed here in **CPP-1–3** is similar to that in previously reported conjugated microporous polymers (CMPs).[19-20, 23-24, 56-57] For instance, the lower surface area of **CPP-2** as compared to **CPP-1**, which is consistent with the morphologies of these polymers as shown in the SEM images (**Figure 4.7**), may be attributed to the larger size of the triphenylamine moiety. Cooper and co-workers also reported that increasing the size of monomers in an A2 + B3 synthetic model led to polymers with lower surface areas.[20]

4.5 Optical properties of TTD-based small molecules and CPPs

Optical properties of **TTD**-based triads were studied in chlorobenzene by UV-Vis-NIR absorption spectroscopy (**Figure 4.9a**). Absorption maxima of all triads show a significant red shift when compared to the spectrum of **TTD**, which is mainly attributed to the donor–acceptor interaction between **TTD** and its donor partner. It can be observed that the extent of the redshift is proportional to the electron donating strength of the donor. Among the three D-A-D triads, **TTD-2** – **TTD** coupled with two triphenylamine moieties, absorbs at the longest wavelength and has the smallest optical bandgap (E_g^{opt} = 1.38 eV), whereas **TTD-1** consisting of phenyl groups has the largest optical bandgap (E_g^{opt} = 1.48 eV). The decrease of the bandgap in the order of **TTD-2** < **TTD-3** < **TTD-1** is consistent with the increasing strength of the electron donating groups (triphenylamine > fluorene > phenyl) in the triads.

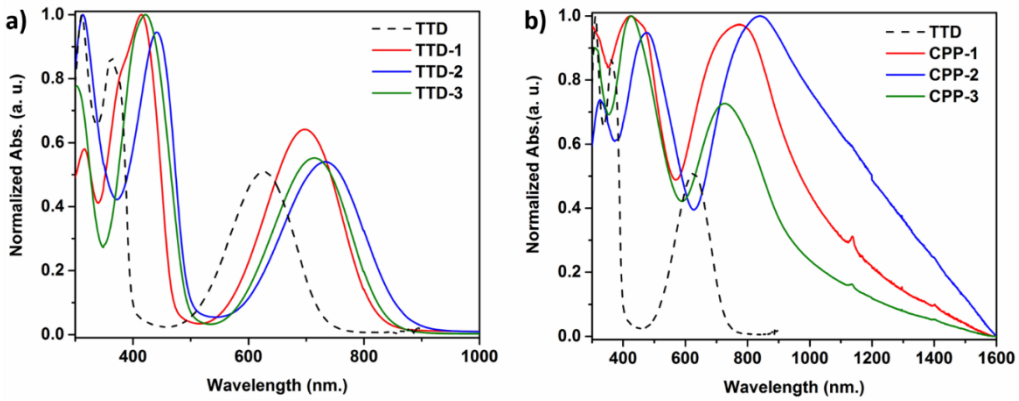

Figure 4.9 a) UV-Vis-NIR absorption spectra of **TTD-(1–3)** in chlorobenzene solutions. b) UV-Vis-NIR absorption spectra of **CPP-(1–3)** in chlorobenzene dispersions. UV-Vis spectrum of TTD is plotted for comparison.

Optical properties of CPPs in chlorobenzene dispersions were studied by UV-Vis-NIR spectroscopy (**Figure 4.9b**). Compared to the absorption spectra of the D–A–D triads, all the three polymers (**CPP-**(**1**–**3**)) show a broad absorption across the visible and the near infrared regions. Despite some light scattering effect of the polymer dispersions which made it difficult to estimate the

wavelength of the onset absorption, the band edge absorption peaks of **CPP-1–3** at 772, 840 and 727 nm, respectively, remain well-resolved. The optical bandgaps of **CPP-1–3** follow the trend of **CPP-2** < **CPP-1** ≈ **CPP-3** (**Table 4.2**). **CPP-2** absorbs at the longest wavelength in the NIR region and has the smallest bandgap, largely attributed to the strong donor–acceptor interactions between triphenylamine and **TTD**. The slightly larger bandgap of **CPP-3** vs. **CPP-1** could be attributed to its lowest extent of polymerization as reflected from the FTIR spectrum (**Figure 4.3**).

Table 4.2 Summary of electrochemical properties of **TTD-(1–3)** and **CPP-(1–3).**

Species	E_{ox}^{onset} (V)	E_{red}^{onset} (V)	E_{HOMO} (eV)[a]	E_{LUMO} (eV)[b]	E_g^{Elec} (eV)	λ_{edge} (nm)	E_g^{opt} (eV)
TTD-1	0.74	-0.69	-5.54	-4.11	1.43	838	1.48
TTD-2	0.59	-0.70	-5.39	-4.09	1.30	898	1.38
TTD-3	0.72	-0.67	-5.52	-4.13	1.39	855	1.45
CPP-1	0.68	-0.73	-5.48	-4.07	1.41	1055 [c]	1.17 [c]
CPP-2	0.65	-0.69	-5.45	-4.11	1.34	-	-
CPP-3	0.74	-0.77	-5.54	-4.03	1.51	943[c]	1.31[c]

[a] $E_{HOMO} = -(E_{ox}^{onset} + 4.8)$. [b] $E_{LUMO} = -(E_{red}^{onset} + 4.8)$. [c] Optical bandgaps of **CPP-1** and **CPP-3** were determined by a rough estimation of the onset wavelengths. Onset of **CPP-2** is too steep for determination of an onset wavelength.

Electrochemical properties of CPPs vs. TTD-based triads were evaluated by cyclic voltammetry (CV). While all triads showed reversible oxidation and quasi-reversible reduction peaks (**Figure 4.10a**), irreversible oxidation and reduction peaks were observed in all the three CPPs (**Figure 4.10b**). Oxidation and reduction potentials of CPPs provide further insight into their electronic structures. Oxidation potential (E_{ox}) of **CPP-3** at 0.74 V was the highest among the three CPPs, followed by **CPP-1** (E_{ox}^{onset} = 0.68 eV) and **CPP-2** (E_{ox}^{onset} = 0.65 eV). The HOMO levels of **CPP-1–3** estimated from the CV results are -

5.48, -5.45 and -5.54 eV, respectively. A similar trend was observed for the reduction potential as well, resulting in the LUMO levels which are -4.07, -4.11 and -4.03 eV for **CPP-1–3**, respectively. These results imply that the extended conjugation of TTD with an electron-donor led to a cathodic shift of the oxidation potentials and therefore an increase of their HOMO energy levels. The extent of the shift is proportional to the strength of the donor. As a consequence, the push–pull effect between **TTD** and donor moieties results in a systematic narrowing of the HOMO–LUMO gaps of CPPs such that the electrochemical bandgaps follow the order of **CPP-2** < **CPP-1** < **CPP-3** (**Table 4.2**). The larger bandgap and the lower HOMO energy level of **CPP-3** compared to **CPP-1** can be explained by the lower degree of polymerization in the former. These results are consistent with the optical bandgaps of these **CPP** polymers.

While **TTD**-based linear narrow-bandgap polymers have shown potential applications for organic NIR photodetectors and field effect transistors,[58-59] we expect that the 2D/3D **TTD** conjugated porous networks described above would find applications such as photocatalysis to harvest light in the NIR region.

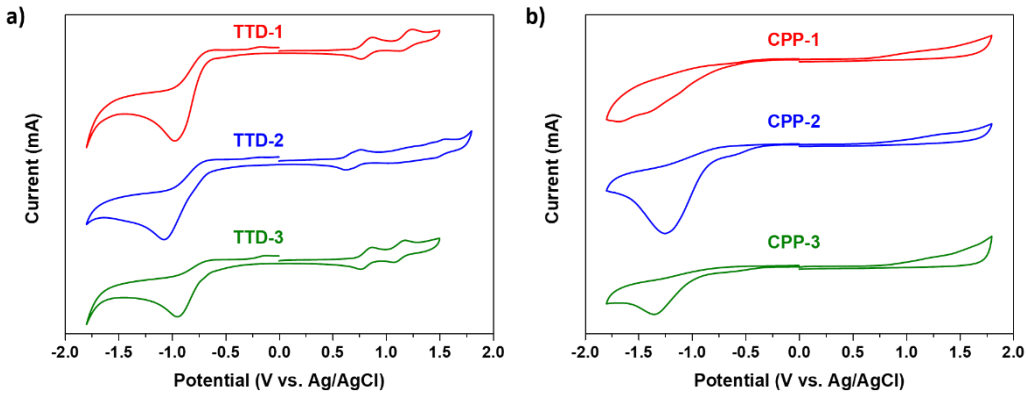

Figure 4.10 Cyclic voltammograms of a) **TTD-(1-3)** with a 0.1 M solution of Bu_4NPF_6 as the supporting electrolyte in dry CH_2Cl_2. Cyclic voltammograms of b) **CPP-(1-3)** in 0.1 M solution of Bu_4NPF_6 in dry CH_3CN as the supporting electrolyte.

Moreover, incorporation of strong acceptor molecules in polymer networks of π-conjugated porous polymers have been demonstrated as an efficient strategy for improving their performance as heterogeneous photocatalysts.[21, 60-61] **TTD**-based polymers with weak electron donors may prevent the fast recombination of excitons favouring the formation of a triplet state.

4.6 Conclusion

In summary, three narrow bandgap conjugated porous polymers (CPPs) have been synthesized by direct arylation polymerization of thiophene-flanked thienothiadiazole (**TTD**) – a low bandgap electron-accepting building block – with polytropic aryl bromides of various geometries. Direct arylation coupling between **TTD** and a series of mono-brominated aryls resulted in small molecular D–A–D triads in high yields, suggesting the relatively high reactivity and regioselectivity of **TTD**. Under the same polymerization conditions, the morphologies and porosities of the CPPs were determined by the structure of the aryl monomers. Specifically, DAP coupling between **TTD** and 1,3,5-tribomobenzene resulted in fibrillar networks that showed significantly higher porosity than the other two CPPs with 2,2′,7,7′-tetrabromo-9,9′-spirobifluorene and tris(4-bromophenyl)amine as comonomers, respectively. The bandgaps of the CPPs were determined by the D–A intramolecular charge transfer. Among the three CPPs, **CPP-2** composed of **TTD** and triphenylamine as repeating units showed the narrowest bandgap below 1.3 eV due to the largest extent of D–A charge transfer. These experimental results demonstrate that a rational selection of monomers enables the synthesis of a series of narrow bandgap conjugated porous polymers with tunable porosities, morphologies and optoelectronic properties.

4.7 Experimental section

4.7.1 Materials and methods

1,3,5-tribromobenzene (**PBr-1**), tris-(4-bromophenyl)amine (**PBr-2**) and 2,2',7,7'-tetrabromo-9,9'-spirobifluorene (**PBr-3**) were purchased from Sigma Aldrich. 1-Bromo-4-hexylbenzene (**MBr-1**) was purchased from Alfa Aesar. 2-

Bromo-9,9-dioctyl-9H-fluorene[62] (**MBr-3**), 4-bromotriphenylamine[63] (**MBr-2**) and 4,6-di(2- thienyl)thieno[3,4-c][1,2,5]thiadiazole[49] (**TTD**) were synthesized according to reported procedures. All solvents were obtained from commercial sources and used as received unless otherwise specified. ^{1}H-NMR was performed on a Bruker AV 300 spectrometer in deuterated chloroform $CDCl_3$ at room temperature with TMS as internal reference; chemical shifts (δ) are reported in parts per million. Solid state ^{13}C magic-angle spinning nuclear magnetic resonance (MAS NMR) spectra were collected by a JEOL ECA 400 spectrometer. FTIR spectra were recorded on a Perkin Elmer Spectrum One FTIR spectrometer. Thermogravimetric analyses were performed on a Pyris Diamond TGA (Perkin Elmer) instrument, at a heating rate of 10 ^{o}C/ min under N_2 atmosphere from 40 ^{o}C to 700 ^{o}C. SEM imaging was carried out using a JEOL JSM 6701F SEM (Scanning Electron Microscope) operating in scanning mode. Samples were prepared by depositing dry samples on aluminium stubs using an adhesive high purity carbon tape. TEM images were obtained using a Carl Zeiss Libra 120 Plus transmission electron microscope (TEM). Samples were prepared by depositing polymers from an ethanol dispersion onto a copper grid coated with ultra-thin carbon film. Nitrogen sorption isotherms were obtained at 77 K using Quantachrome Instruments Autosorb-iQ (Boynton Beach, Florida USA) with extra-high pure gases. Surface areas were calculated in the relative pressure (p/p_o) range from 0.04 to 0.35 of the adsorption branch. UV-Vis- NIR absorption spectra were measured on a Cary 5000 UV-Vis-NIR (Varian) spectrometer. Cyclic voltammograms (CVs) were recorded on an CHI Electrochemical Analyzer Model 660D at room temperature using 0.1 M tetrabutylammonium hexafluorophosphate (Bu_4NPF_6) as a supporting electrolyte at a scan rate of 100 mV/s. Glassy carbon was used as working electrode, Pt wire as counter electrode and silver wire as the reference electrode. CVs of **CPP-**(**1**-**3**) were measured in 0.1 M Bu_4NPF_6 solution in CH_3CN by drop-casting a suspension of CPPs in Nafion on the glassy carbon electrode. CVs of **TTD-**(**1**-**3**) were measured in solution state by dissolving the small molecules in 0.1 M solution of Bu_4NPF_6 in CH_2Cl_2 All the potentials were calibrated with the standard ferrocene/ferrocenium redox couple (Fc/Fc^{+}). Powder X-ray diffraction patterns

were obtained at 40 kV and 40 mA on a Bruker Advanced D8 XRD using Cu-Kα radiation (λ = 1.5418 Å) over 2θ range of 5 ^{o} – 60 ^{o} at room temperature. Elemental analysis was carried out on a Vario EL III CHNS Elemental Analyser. Mass spectroscopy was performed on a ABI 4800 Proteomics Analyzer MALDI TOF/TOF mass spectrometer (Applied Biosystems)

4.7.2 General synthesis procedure for TTD-Xs via direct arylation coupling

TTD (80 mg, 0.2614 mmol), **MBr-1**, **-2** or **-3** (2.61 mmol), $Pd_2(dba)_3$ (0.013 mmol, 11.9 mg), (o-$MeOC_6H_4)_3P$ (0.02614, 9.2 mg), K_2CO_3 (1.045 mmol, 144.3 mg) and PivOH (0.137 mmol, 13.3 mg) were added into a reaction vial equipped with a magnetic stirring bar. *o*-xylene (1.3 ml, 0.2 M) was added inside a glovebox and the vial was sealed. The reaction was carried out for 24 hours in an oil bath preheated to 120 °C. After completion, the reaction mixture was diluted with 30 mL chloroform and filtered to remove any insoluble matter. Solvent was removed under vacuum and the crude product was separated over silica gel. The pure product was obtained by precipitation in methanol.

TTD-1: **MBr-1** = 1-bromo-4-hexylbenzene (629.4 mg). Yield: 110.9 mg (95%). ^{1}H NMR ($CDCl_3$, 300 MHz) δ ppm: 7.57 (d, 4H, J = 8.3 Hz), 7.54 (d, 2H, J = 4.1 Hz), 7.30 (d, 2H, J = 4.0 Hz), 7.21 (d, 4H, J = 8.3 Hz), 2.69–2.58 (m, 4H), 1.62 (d, 4H, J = 7.9 Hz), 1.62 (s, 12H), 0.89 (t, 6H, J = 6.9 Hz). EI-MS *m/z* (%): 626 (M^+, 93), 605 (10), 568 (8), 499 (13).

TTD-2: **MBr-2** = 4-bromotriphenylamine (846.1 mg). Yield: 130.6 mg (80%). ^{1}H NMR ($CDCl_3$, 300 MHz) δ ppm: 7.55–7.52 (m, 4H), 7.50 (d, 2H, J = 2.0 Hz), 7.54 (d, 2H, J = 4.1 Hz), 7.31 (d, 2H, J = 2.0 Hz), 7.29 (d, 4H, J = 1.2 Hz), 7.24 (d, 2H, J = 7.9 Hz), 7.16–7.02 (m, 18H). EI-MS *m/z* (%): 792 (M^+, 100), 644 (47), 605 (8), 456 (10).

TTD-3: **MBr-3** = 2-bromo-9,9-dioctyl-9H-fluorene (1.22 g). Yield: 121 mg (83%). ^{1}H NMR ($CDCl_3$, 300 MHz) δ ppm: 7.57 (s, 6H, br), 7.61 (s, 4H, br), 7.42 (d, 2H, J = 3.8 Hz), 7.35 (s, 6H), 2.07–1.92 (m, 8H), 1.22–0.98 (m, 40H), 0.8 (t, 12H, J = 1 Hz), 0.64 (s, 8H). EI-MS *m/z* (%): 1083 (M^+, 100), 1060 (8), 897.97 (6), 855 (21).

4.7.3 General synthesis procedure for CPP-Xs via direct arylation polymerization

TTD, PBr-X (C–H:C–Br = 1:1), $Pd_2(dba)_3$ (5 mol%), (o-$MeOC_6H_4)_3P$ (10 mol%), K_2CO_3 (400 mol%) and PivOH (50 mol%) were added to a reaction vial charged with a magnetic stirring bar. *o*-xylene (0.2 M) was added inside a glovebox and the vial was sealed with a rubber cap. The reaction was carried out at 120 ℃ in an oil bath for 48 hours. After cooling to room temperature, the reaction mixture was diluted with THF and filtered under vacuum. The solids were washed with methanol, water, dilute HCl and THF and then subjected to Soxhlet extraction with methanol and THF for 24 hours, respectively. The residual solids were collected and dried at 100 °C under vacuum to obtain the final product.

CPP-1: 1,3,5-tribromobenzene (70 mg), **TTD** (102 mg), $Pd_2(dba)_3$ (15.27 mg), (o-$MeOC_6H_4)_3P$ (11.74 mg), K_2CO_3 (184.37 mg), PivOH (17.14 mg) and *o*-xylene (1.67 mL). Yield: 110.9 mg (94%). IR (KBr cm^{-1}): 3059, 1583, 1555, 1491, 1408, 856, 833, 792. Solid state ^{13}C NMR (400 MHz) δ ppm: 156, 141.7, 135.5, 125.8, 112.3. Elemental Analysis (%) for $C_{48}H_{18}N_6S_{12}$. Calculated: C, 54.24; H, 1.69; N, 7.91; S, 36.16. Found: C, 51.34; H, 1.88; N, 5.89; S, 26.05.

CPP-2: tris(4-bromophenyl)amine (126 mg), **TTD** (120 mg), $Pd_2(dba)_3$ (17.95 mg), (o-$MeOC_6H_4)_3P$ (13.816 mg), K_2CO_3 (216.75 mg), PivOH (20.15 mg) and *o*-xylene (1.96 mL). Yield: 130.6 mg (71%). IR (KBr cm^{-1}): 3054, 3021, 1593, 1529, 1480, 1429, 1320, 1266, 847, 829, 792. Solid state ^{13}C NMR (400 MHz) δ ppm:156, 145.8, 132.6, 128, 112.3. Elemental Analysis (%) for $C_{72}H_{36}N_8S_{12}$. Calculated: C, 61.89; H, 2.58; N, 8.02; S, 27.51. Found: C, 58.65; H, 2.576; N, 6.468; S, 21.09.

CPP-3: 2,2′,7,7′-tetrabromo-9,9′-spirobifluorene (105.4 mg), **TTD** (102.06 mg), $Pd_2(dba)_3$ (15.27 mg), (o-$MeOC_6H_4)_3P$ (11.74 mg), K_2CO_3 (184.37 mg), PivOH (17.14 mg) and *o*-xylene (1.67 mL). Yield: 121 mg (79%). IR (KBr cm^{-1}): 3058, 1636, 1600, 1572, 1527, 1435, 1410, 1249, 1139, 1055, 854, 792. Solid state ^{13}C NMR (400 MHz) δ ppm: 156.2, 150, 140.7, 134.3, 127.2, 121.5,

112.3, 66.5. Elemental Analysis (%) for $C_{49}H_{20}N_4S_8$. Calculated: C, 63.88; H, 2.19; N, 6.08; S, 27.85. Found: C, 57.26; H, 1.98; N, 4.4; S, 19.93.

4.8 References

1. Arne, T. *Angew. Chem. Int. Ed.* **2010,** *49*, 8328-8344.
2. McKeown, N. B.; Budd, P. M. *Macromolecules* **2010,** *43*, 5163-5176.
3. Liu, Q.; Tang, Z.; Wu, M.; Zhou, Z. *Polym. Int.* **2013,** *63*, 381-392.
4. Dawson, R.; Cooper, A. I.; Adams, D. J. *Prog. Polym. Sci.* **2012,** *37*, 530-563.
5. Slater, A. G.; Cooper, A. I. *Science* **2015,** *348*.
6. Hug, S.; Stegbauer, L.; Oh, H.; Hirscher, M.; Lotsch, B. V. *Chem. Mater.* **2015,** *27*, 8001-8010.
7. Robert, D.; I, C. A.; J, A. D. *Polym. Int.* **2013,** *62*, 345-352.
8. Xiang, Z.; Cao, D. *J. Mater. Chem. A* **2013,** *1*, 2691-2718.
9. Xiang, L.; Zhu, Y.; Gu, S.; Chen, D.; Fu, X.; Zhang, Y.; Yu, G.; Pan, C.; Hu, Y. *Macromol. Rapid Commun.* **2015,** *36*, 1566-1571.
10. Gu, C.; Huang, N.; Gao, J.; Xu, F.; Xu, Y.; Jiang, D. *Angew. Chem. Int. Ed.* **2014,** *53*, 4850-4855.
11. Bandyopadhyay, S.; Pallavi, P.; Anil, A. G.; Patra, A. *Polym. Chem.* **2015,** *6*, 3775-3780.
12. Ma, H.; Li, F.; Li, P.; Wang, H.; Zhang, M.; Zhang, G.; Baumgarten, M.; Müllen, K. *Adv. Funct. Mater.* **2016,** *26*, 2025-2031.
13. Luo, J.; Zhang, X.; Zhang, J. *ACS Catal.* **2015,** *5*, 2250-2254.
14. Gu, C.; Huang, N.; Chen, Y.; Qin, L.; Xu, H.; Zhang, S.; Li, F.; Ma, Y.; Jiang, D. *Angew. Chem. Int. Ed.* **2015,** *54*, 13594-13598.
15. Wang Zi, J.; Ghasimi, S.; Landfester, K.; Zhang Kai, A. I. *Adv. Mater.* **2015,** *27*, 6265-6270.
16. Xu, Y.; Jin, S.; Xu, H.; Nagai, A.; Jiang, D. *Chem. Soc. Rev.* **2013,** *42*, 8012-31.
17. Xie, Z.; Yoon, S.-J.; Park Soo, Y. *Adv. Funct. Mater.* **2010,** *20*, 1638-1644.
18. Xu, Y.; Nagai, A.; Jiang, D. *Chem. Commun.* **2013,** *49*, 1591-1593.

19. Dawson, R.; Laybourn, A.; Khimyak, Y. Z.; Adams, D. J.; Cooper, A. I. *Macromolecules* **2010,** *43*, 8524-8530.

20. Jiang, J.-X.; Su, F.; Trewin, A.; Wood, C. D.; Niu, H.; Jones, J. T. A.; Khimyak, Y. Z.; Cooper, A. I. *J. Am. Chem. Soc.* **2008,** *130*, 7710-7720.

21. Zhang, K.; Vobecka, Z.; Tauer, K.; Antonietti, M.; Vilela, F. *Chem. Commun.* **2013,** *49*, 11158-11160.

22. Bonillo, B.; Sprick, R. S.; Cooper, A. I. *Chem. Mater.* **2016,** *28*, 3469-3480.

23. Stockel, E.; Wu, X.; Trewin, A.; Wood, C. D.; Clowes, R.; Campbell, N. L.; Jones, J. T. A.; Khimyak, Y. Z.; Adams, D. J.; Cooper, A. I. *Chem. Commun.* **2009**, 212-214.

24. Jiang, J.-X.; Su, F.; Trewin, A.; Wood Colin , D.; Campbell Neil , L.; Niu, H.; Dickinson, C.; Ganin Alexey , Y.; Rosseinsky Matthew , J.; Khimyak Yaroslav , Z.; Cooper Andrew , I. *Angew. Chem. Int. Ed.* **2007,** *46*, 8574-8578.

25. Xiao, Y.; Shuwen, Y.; Miao, Y.; Jia-Xing, J. *Macromol. Rapid Commun.* **2014,** *35*, 834-839.

26. Schmidt, J.; Werner, M.; Thomas, A. *Macromolecules* **2009,** *42*, 4426-4429.

27. Cheng, G.; Hasell, T.; Trewin, A.; Adams Dave, J.; Cooper Andrew, I. *Angew. Chem. Int. Ed.* **2012,** *51*, 12727-12731.

28. Peng-Fei, L.; B., S. T.; S., S. D. *Angew. Chem. Int. Ed.* **2015,** *54*, 9361-9366.

29. Zhu, Y.; Long, H.; Zhang, W. *Chem. Mater.* **2013,** *25*, 1630-1635.

30. Liebl, M. R.; Senker, J. *Chem. Mater.* **2013,** *25*, 970-980.

31. Weber, J.; Su, Q.; Antonietti, M.; Thomas, A. *Macromol. Rapid Commun.* **2007,** *28*, 1871-1876.

32. Bohra, H.; Wang, M. *J. Mater. Chem. A* **2017,** *5*, 11550-11571.

33. Pouliot, J. R.; Grenier, F.; Blaskovits, J. T.; Beaupre, S.; Leclerc, M. *Chem. Rev.* **2016,** *116*, 14225-14274.

34. Rudenko Andrey, E.; Thompson Barry, C. *J. Polym. Sci., Part A: Polym. Chem.* **2014,** *53*, 135-147.

35. Kowalski, S.; Allard, S.; Zilberberg, K.; Riedl, T.; Scherf, U. *Prog. Polym. Sci.* **2013,** *38*, 1805-1814.

36. Okamoto, K.; Zhang, J.; Housekeeper, J. B.; Marder, S. R.; Luscombe, C. K. *Macromolecules* **2013,** *46*, 8059-8078.

37. Mercier, L. G.; Leclerc, M. *Acc. Chem. Res.* **2013,** *46*, 1597-1605.

38. Berrouard, P.; Najari, A.; Pron, A.; Gendron, D.; Morin, P.-O.; Pouliot, J.-R.; Veilleux, J.; Leclerc, M. *Angew. Chem. Int. Ed.* **2012,** *51*, 2068-2071.

39. Lu, W.; Kuwabara, J.; Kanbara, T. *Macromolecules* **2011,** *44*, 1252-1255.

40. Wang, Q.; Takita, R.; Kikuzaki, Y.; Ozawa, F. *J. Am. Chem. Soc.* **2010,** *132*, 11420-11421.

41. Se´vignon, M.; Papillon, J.; Schulz, E.; Lemaire, M. *Tetrahedron Lett.* **1999,** *40*, 5873-5876.

42. Morin, P.-O.; Bura, T.; Sun, B.; Gorelsky, S. I.; Li, Y.; Leclerc, M. *ACS Macro Lett.* **2015,** *4*, 21-24.

43. Pouliot, J.-R.; Sun, B.; Leduc, M.; Najari, A.; Li, Y.; Leclerc, M. *Polym. Chem.* **2015,** *6*, 278-282.

44. Matsidik, R.; Komber, H.; Luzio, A.; Caironi, M.; Sommer, M. *J. Am. Chem. Soc.* **2015,** *137*, 6705-11.

45. Wang, X.; Wang, K.; Wang, M. *Polym. Chem.* **2015,** *6*, 1846-1855.

46. Wang, K.; Wang, G.; Wang, M. *Macromol. Rapid Commun.* **2015,** *36*, 2162-2170.

47. Huang, J.; Wang, K.; Gupta, S.; Wang, G.; Yang, C.; Mushrif, S. H.; Wang, M. *J. Polym. Sci., Part A: Polym. Chem.* **2016,** *54*, 2015-2031.

48. Bohra, H.; Shao, J.; Huang, S.; Wang, M. *Tetrahedron Lett.* **2016,** *57*, 1497-1501.

49. Shao, J.; Wang, G.; Wang, K.; Yang, C.; Wang, M. *Polym. Chem.* **2015,** *6*, 6836-6844.

50. Liu, D.-P.; Chen, Q.; Zhao, Y.-C.; Zhang, L.-M.; Qi, A.-D.; Han, B.-H. *ACS Macro Lett.* **2013,** *2*, 522-526.

51. Efrem, A.; Wang, K.; Amaniampong, P. N.; Yang, C.; Gupta, S.; Bohra, H.; Mushrif, S. H.; Wang, M. *Polym. Chem.* **2016,** *7*, 4862-4866.

52. Chen, Q.; Wang, J.-X.; Yang, F.; Zhou, D.; Bian, N.; Zhang, X.-J.; Yan, C.-G.; Han, B.-H. *J. Mater. Chem.* **2011,** *21*, 13554-13560.

53. Wang, D.; Li, L.; Yang, W.; Zuo, Y.; Feng, S.; Liu, H. *RSC Adv.* **2014,** *4*, 59877-59884.

54. Hua, C.; Rawal, A.; Faust, T. B.; Southon, P. D.; Babarao, R.; Hook, J. M.; D'Alessandro, D. M. *J. Mater. Chem. A* **2014,** *2*, 12466-12474.

55. Weber, J.; Schmidt, J.; Thomas, A.; Böhlmann, W. *Langmuir* **2010,** *26*, 15650-15656.

56. Kim, B.; Park, N.; Lee, S. M.; Kim, H. J.; Son, S. U. *Polym. Chem.* **2015,** *6*, 7363-7367.

57. Ren, S.; Dawson, R.; Adams, D. J.; Cooper, A. I. *Polym. Chem.* **2013,** *4*, 5585-5590.

58. Yuen, J. D.; Kumar, R.; Seifter, J.; Valouch, S.; Zakhidov, D.; Moses, D.; Lemmer, U.; Heeger, A. J.; Wudl, F. *J. Am. Chem. Soc.* **2011,** *133*, 19602-19605.

59. Gong, X.; Tong, M.; Xia, Y.; Cai, W.; Moon, J. S.; Cao, Y.; Yu, G.; Shieh, C.-L.; Nilsson, B.; Heeger, A. J. *Science* **2009,** *325*, 1665-1667.

60. Kai, Z.; Daniel, K.; H., S. P.; Markus, A.; Filipe, V. *Angew. Chem. Int. Ed.* **2013,** *52*, 1432-1436.

61. Wang, Z. J.; Ghasimi, S.; Landfester, K.; Zhang, K. A. I. *Chem. Commun.* **2014,** *50*, 8177-8180.

62. Shavaleev, N. M.; Monti, F.; Scopelliti, R.; Baschieri, A.; Sambri, L.; Armaroli, N.; Grätzel, M.; Nazeeruddin, M. K. *Organometallics* **2013,** *32*, 460-467.

63. Wang, H.-Y.; Chen, G.; Xu, X.-P.; Chen, H.; Ji, S.-J. *Dyes Pigm.* **2011,** *88*, 358-365.

Chapter 4 is published as Bohra, H.; Tan, S. Y.; Shao, J.; Yang, C.; Efrem, A.; Zhao, Y.; Wang, M., Narrow Bandgap Thienothiadiazole-Based Conjugated Porous Polymers: From Facile Direct Arylation Polymerization to Tunable Porosities and Optoelectronic Properties. *Polym. Chem.* 2016, *7*, 6413-6421. DOI: 10.1039/c6py01453d

5. Thiophene-flanked building blocks for the synthesis of conjugated porous polymers by direct arylation polymerization

5.1 Introduction

Incorporating π-conjugated building blocks in the polymer structure has been explored as an efficient strategy to synthesize functional conjugated porous polymers (CPPs) with tunable properties.[1-3] For instance, in the previous chapter we synthesized three narrow-bandgap (< 1.5 eV) CPPs with varying morphologies by polymerizing thiophene-flanked thienothiadiazole monomer (**TTD)** with polytopic aryl bromides. In a recent study, Cooper and workers demonstrated excellent control over the bandgap and quantum yield of conjugated microporous polymers by varying the stoichiometric ratio of monomers such as benzothiadiazole and perylenediimide.[4] In fact, a library of benzothiadiazole-based CPPs[5] has been developed for applications ranging from photocatalysis of a variety of redox reactions[6-7] including water splitting[8] to antimicrobial photodynamic therapy.[9] Diketopyrrolopyrrole is another chromophore that has been widely used to develop organic photovoltaic materials.[10] However, very few examples of its incorporation in a porous polymer network have been reported. Diketopyrrolopyrrole-based CPPs were first synthesized by Tieke and coworkers by Yamamoto and Sonogashira polymerization of N-arylated phenyl-flanked DPP.[11] Owing to their microporous structure and solid-state fluorescence, Bi et. al. have used phenyl flanked-diketopyrrolopyrrole-based CPPs for fluorescence ion sensing.[12]

Alternating electron-donating and electron-accepting groups in the polymer chain allows excellent control over its photo-physical properties. Thiophene-flanked D-A-D monomers which are frequently used in the synthesis of conjugated linear polymers for organic electronics, are an example of this strategy.[13] A vast library of such monomers has been developed since it combines

the functional properties of acceptors such as benzothiadiazole or diketopyrrolopyrrole with the synthetic compatibility of thiophene with various coupling reactions. Hence, it is imperative to develop a synthetic route for 2D/3D polymers which allows the facile incorporation of these building-blocks in the polymer structure.

Nonetheless, majority of the thiophene-based CPPs reported in literature have been synthesized by conventional C-C coupling reactions such as ferric chloride catalyzed oxidative coupling[14-19] and Sonogashira-Hagihara polymerization.[20-22] Despite its moderate reaction conditions, oxidative coupling has been reported to yield chlorinated polymers[15] with residual iron salts.[23] whereas Sonogashira polymerization is limited to monomers containing terminal ethynyl groups. Moreover, very few thiophene-based CPPs containing functional π-blocks such as bithiophene,[21] benzothiadiazole[24] and diketopyrrolopyrrole have been reported. Direct arylation polymerization (DAP) is an eco-friendly alternative to conventional coupling reactions since it does not require pre-functionalization of C-H bonds with toxic and flammable reagents such as organoboranes and organosilanes which is necessary in Suzuki and Sonogashira polymerizations.[25] Over the past few years, we have used direct arylation for the synthesis of a broad range of π-conjugated small molecules, linear polymers and porous polymers.[26-35] Despite its versatility, DAP has not been studied extensively for the synthesis of thiophene-based CPPs.

In Chapter 4, we presented the direct arylation synthesis of narrow band-gap conjugated porous polymers containing a thiophene-flanked monomer – **TTD** as the C-H active building block.[30] By changing the geometry of the brominated monomer, we observed that polymers with various morphologies and porosities could be obtained. In this chapter, we extend the library of thiophene-containing CPPs by polymerizing tri- (A3) and tetra-brominated (A4) aryls with ditopic (B2) thiophene-flanked monomers – 2,2'-bithiophene (**BT**), 4,7-di(thiophen-2 -yl) benzo[c] [1,2,5] thiadiazole (**DTBT**) and 2,5-bis(2-octyl dodecyl)-3, 6-di(thiophen-2-yl)-2,5- pyrrolo[3,4-c] pyrrole-1,4(2H, 5H)- dione (DPP). While the terminal thiophenes provide active C-H bonds for direct arylation polymerization

(DAP), addition of functional π-blocks such as benzothiadiazole or diketopyrrolopyrrole between the thiophene units allows us to simultaneously modify the geometry and electronic structure of the monomers. This modular design has allowed us to study the effect of thiophene monomers on the morphology, porosity and optical properties of the CPPs. Bandgaps of thiophene containing polymers range from 1.51 eV – 2.38 eV. Morphology of **BT**- and **DTBT**-based polymers appears as microspheres under the SEM whereas all **DPP**-based polymers appear as layered structures.

5.2 Design and synthesis of thiophene-containing CPPs by direct arylation

5.2.1 Molecular design and synthesis

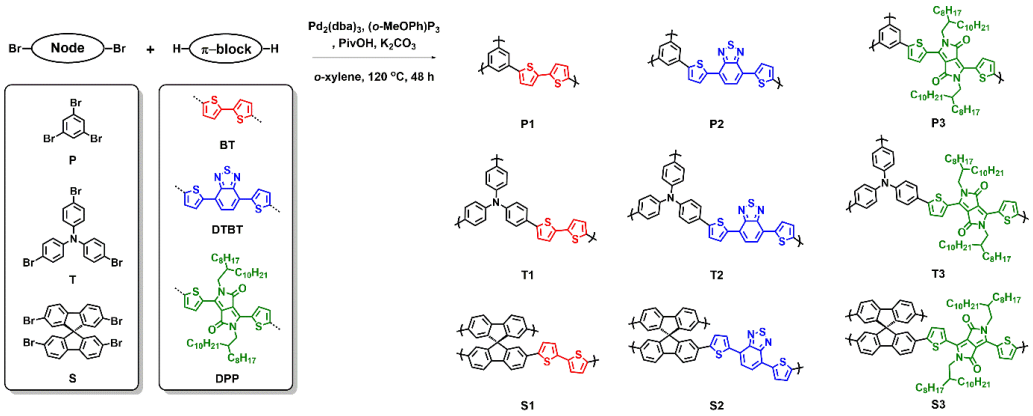

Scheme 5.1 Direct arylation synthesis of conjugated porous polymers and a schematic diagram of the polymer sub-structure. Structures and schematic representations of the brominated monomers (nodes) and the thiophene-flanked monomers (struts) are presented in red and blue respectively.

Structures of the brominated (A_3 and A_4) and thiophene (B_2) monomers are presented in **Scheme 1.** The brominated monomers act as nodes in the CPP structure which allow a controlled extension of conjugation from each reactive site while thiophene monomers act as linkers or struts that connect the nodes to each other. **BT** is the simplest thiophene monomer while **DTBT** and 2,5-bis(2-octyldodecyl)-3,6-di(thiophen-2-yl)-2,5-pyrrolo[3,4-c]pyrrole-1,4(2H,5H)-

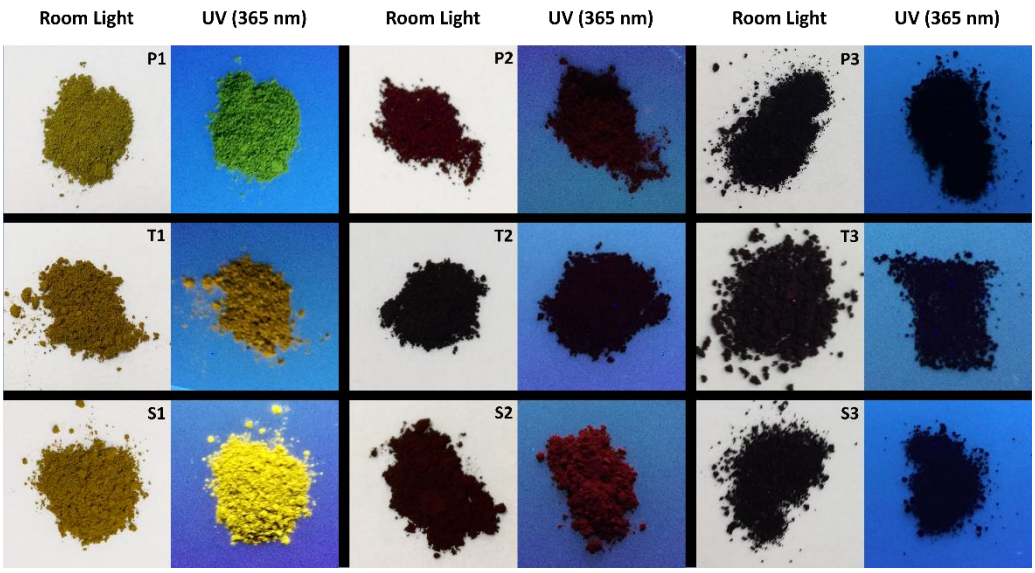

Figure 5.1 Digital images of conjugated porous polymers containing thiophene monomers under room light and UV light (365 nm).

dione **DPP** are relatively larger monomers due to the benzothiadiazole and diketopyrrolopyrrole π-block between two thiophene units. Reactive C-H bonds of thiophene-flanked monomers make them ideal candidates for DAP.

Previously, our group has reported the synthesis of several linear[27-29, 32-36] and porous network[26, 30-31] polymers via C-H activation of thiophene-flanked monomers including **DTBT** and **DPP**. However, in this report polymerization was carried out using conditions pre-optimized for **DTBT**.[33] C-H:C-Br ratio of 1:1 was maintained and reaction time was increased to 48 hours to ensure complete polymerization. It is interesting to note that, while all the polymers precipitated from the reaction media as powders, all **DPP**-based polymers gelated within 15 minutes of reaction time. Nonetheless, the reactions were carried out for 48 hours. We believe that this phenomenon resembles the one observed by Cooper and coworkers[37] at high monomer concentrations although our polymers did not disintegrate into powders even after drying. As a result, the final texture of all DPP-based polymers is hard and granular as opposed to the fine powders obtained from the synthesis of **BT**- and **DTBT**-based polymers (**Figure 5.1**).

5.2.2 Structural characterization

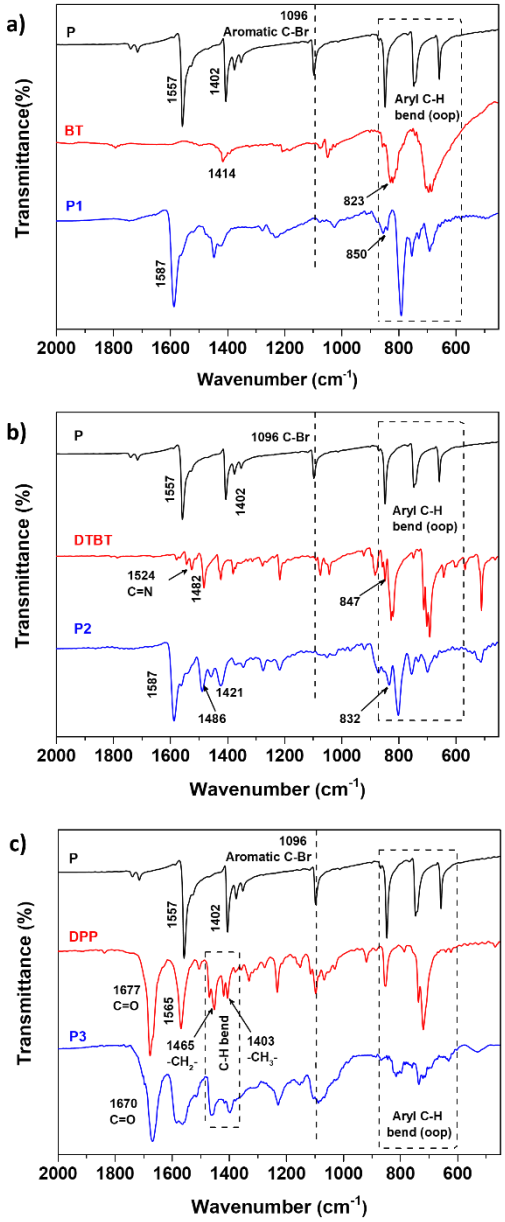

Figure 5.2 Comparison of FT-IR spectra of a) **P1,** b) **P2** and c) **P3** with their constituent monomers.

Incorporation of monomers in the polymer network was tested by IR spectroscopy (**Figure 5.2** and **Figure 5.3**). In all polymers, bands between 1400cm^{-1} and 1600 cm^{-1} are assigned to the C=C stretching vibration from the

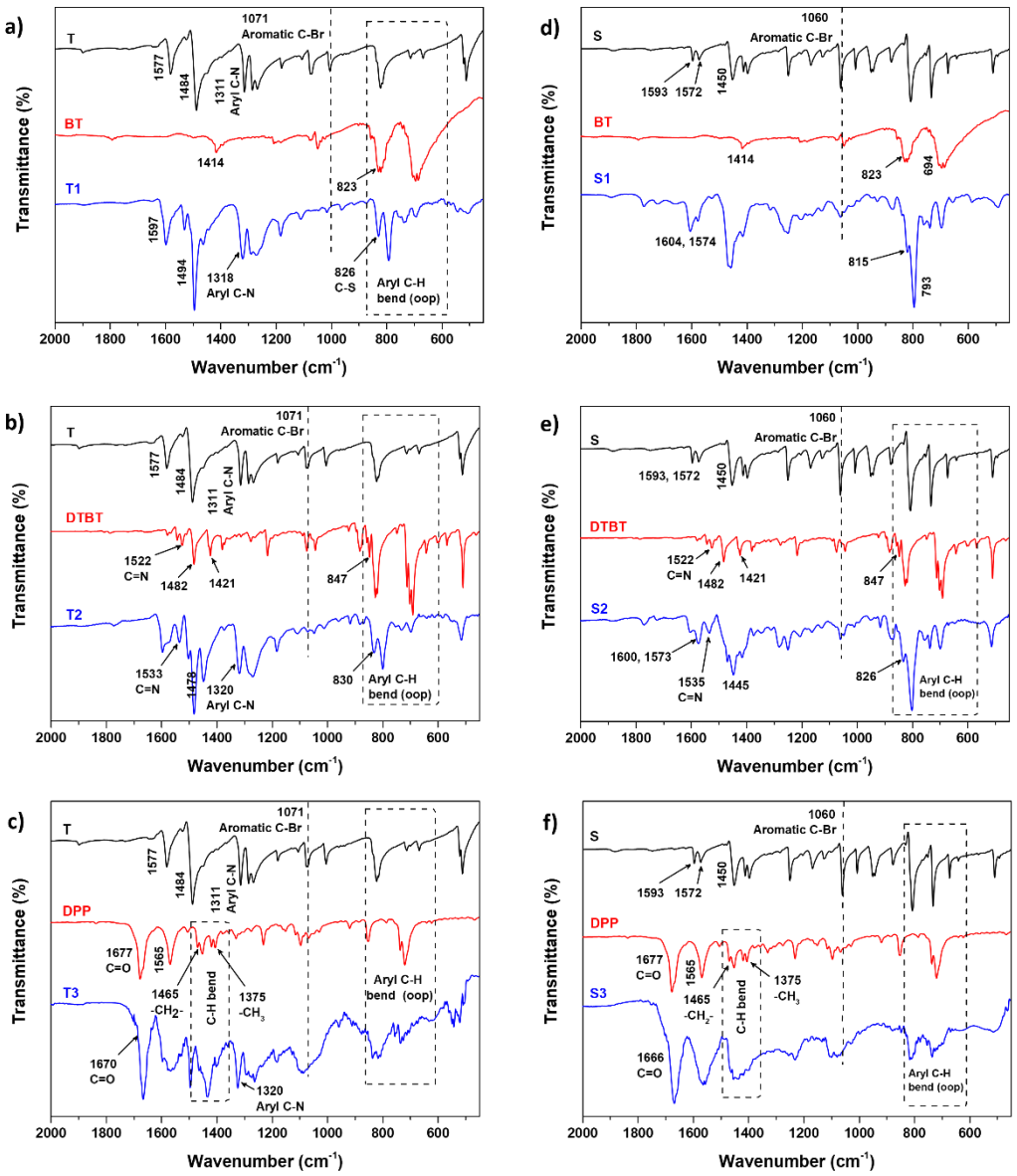

Figure 5.3 Comparison of FT-IR spectra of a) **T1,** b) **T2** c) **T3,** d) **S1,** e) **S2** and f) **S3** with their constituent monomers.

aromatic rings occur while the bands between 600 cm^{-1} and 875 cm^{-1} are assigned to C-H out of plane (oop) bending vibrations. In **BT**-based polymers, C-S stretching vibration from thiophene which occurs at 823 cm^{-1} in **BT** is observed at 850 cm^{-1} in **P1** (**Figure 5.2a**), at 826 cm^{-1} in **T1** (**Figure 5.3a**) and 815 cm^{-1} in **S1** (**Figure 5.3d**). This difference in position of similar stretching bands between monomers to polymers can be attributed to the extensive conjugation in

polymers. The sharp band occurring at 1320 cm^{-1} can be assigned to the C-N stretch of triphenylamine. In the spectra of **DTBT**-based polymers – **P2**, **T2** and **S2**, the thiophene ring vibration occurs consistently around 830 cm^{-1} while the band occurring at 1535 cm^{-1} is assigned to the C=N stretch from the benzothiadiazole moiety. **P3** (**Figure 5.2c**), **T3** (**Figure 5.3c**) and **S3** (**Figure 5.3f**), containing the **DPP** moiety, exhibit a characteristic band at 1670 cm^{-1} which can be assigned to the C=O stretch of the carbonyl group. The stretching vibrations of alkyl chains in **DPP** occur as distinct bimodal peaks at 1451 cm^{-1} and 1400 cm^{-1} whereas, these vibrations occur as broad peaks around 1430 cm^{-1} in the spectra of polymers.

Further analysis of the polymer structure was conducted by solid state ^{13}C NMR spectroscopy. DPP-based polymers – **P3**, **T3** and **S3**, owing to their coarse texture and large grain size, could not be efficiently packed in the rotor and hence their spectra could not be obtained by magic angle spinning NMR spectroscopy. NMR spectra of the remaining polymers are presented in **Figure 5.4**. From the spectra of polymers **P1**, **T1** and **S1 (Figure 5.4a-c**), one can see that the peaks of the **BT** moiety occur consistently at 135 ppm and 124 ppm which correspond to the substituted (a, d) and the non-substituted carbons (b, c) respectively of bithiophene. In the spectra of **P2**, **T2** and **S2 (Figure 5.4d-f**), the peaks from the **DTBT** occur around 140 ppm (b, c) and 152 ppm (a), the latter corresponding to the carbon in the thiadiazole bridge. In **P1 (Figure 5.4a)**, the peak at 143 ppm is assigned to the substituted carbon (f) from the phenyl monomer while the non-substituted carbon (e) occurs at 127 ppm. The peaks from the triphenylamine moiety occur around at 145 ppm and 127 ppm in spectra of **T1** and **T2 (Figure 5.4b and 5.4e)** corresponding to the carbon adjacent to nitrogen and the non-substituted carbons of triphenylamine respectively. In the spectra of **S1 and S2 (Figure 5.4c and 5.4f),** most peaks from the spirobifluorene unit occur around 124 ppm and 141 ppm, with the exception of the sp^3 carbon which occurs at around 67 ppm.

Thermal stability of the polymers was tested by thermogravimetric analysis. All polymers can retain 95% of the original mass up to 300 ^oC

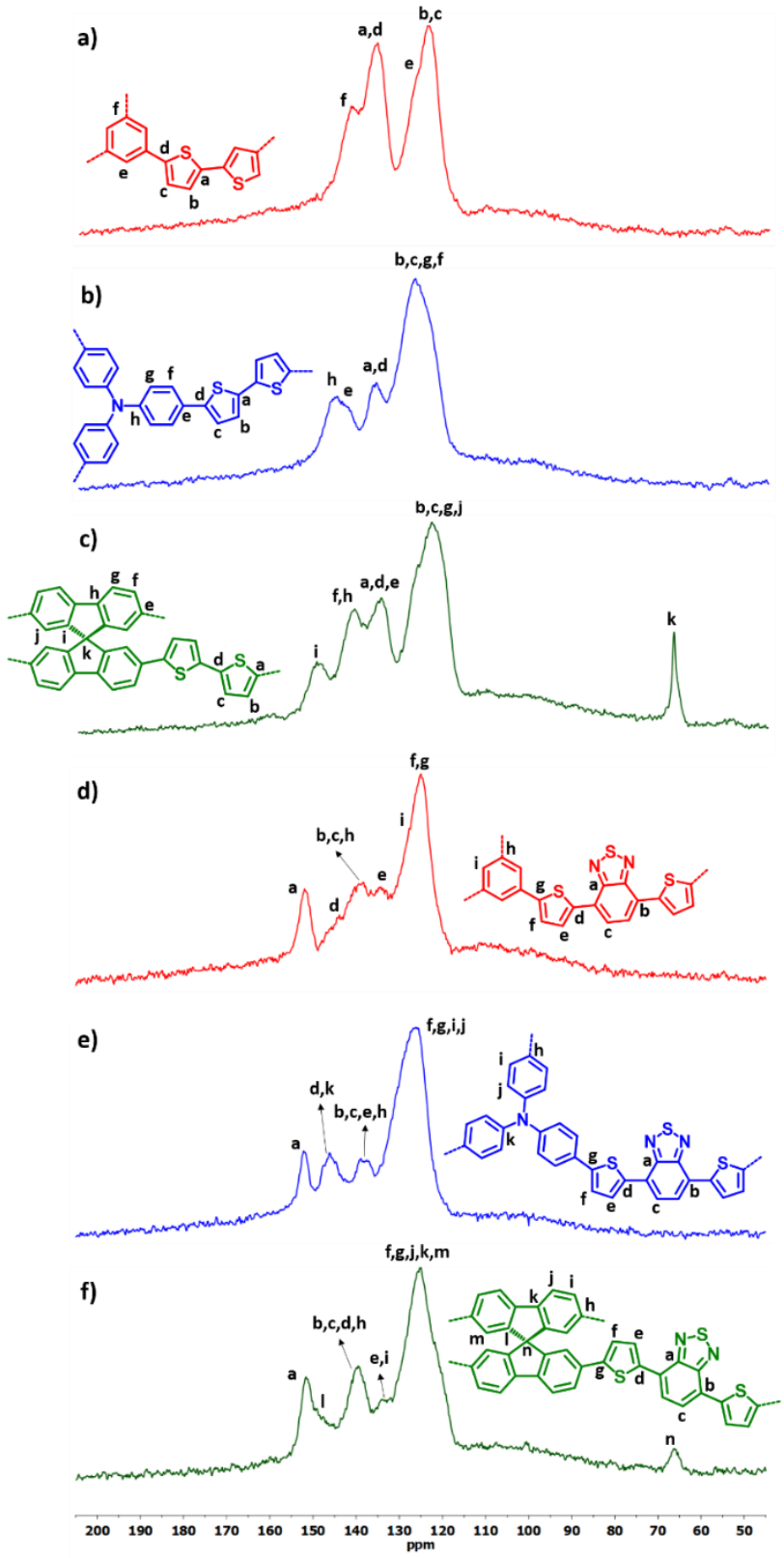

Figure 5.4 Solid state ^{13}C NMR spectra of a) **P1**, b) **T1**, c) **S1,** d) **P2**, e) **T2** and f) **S2**.

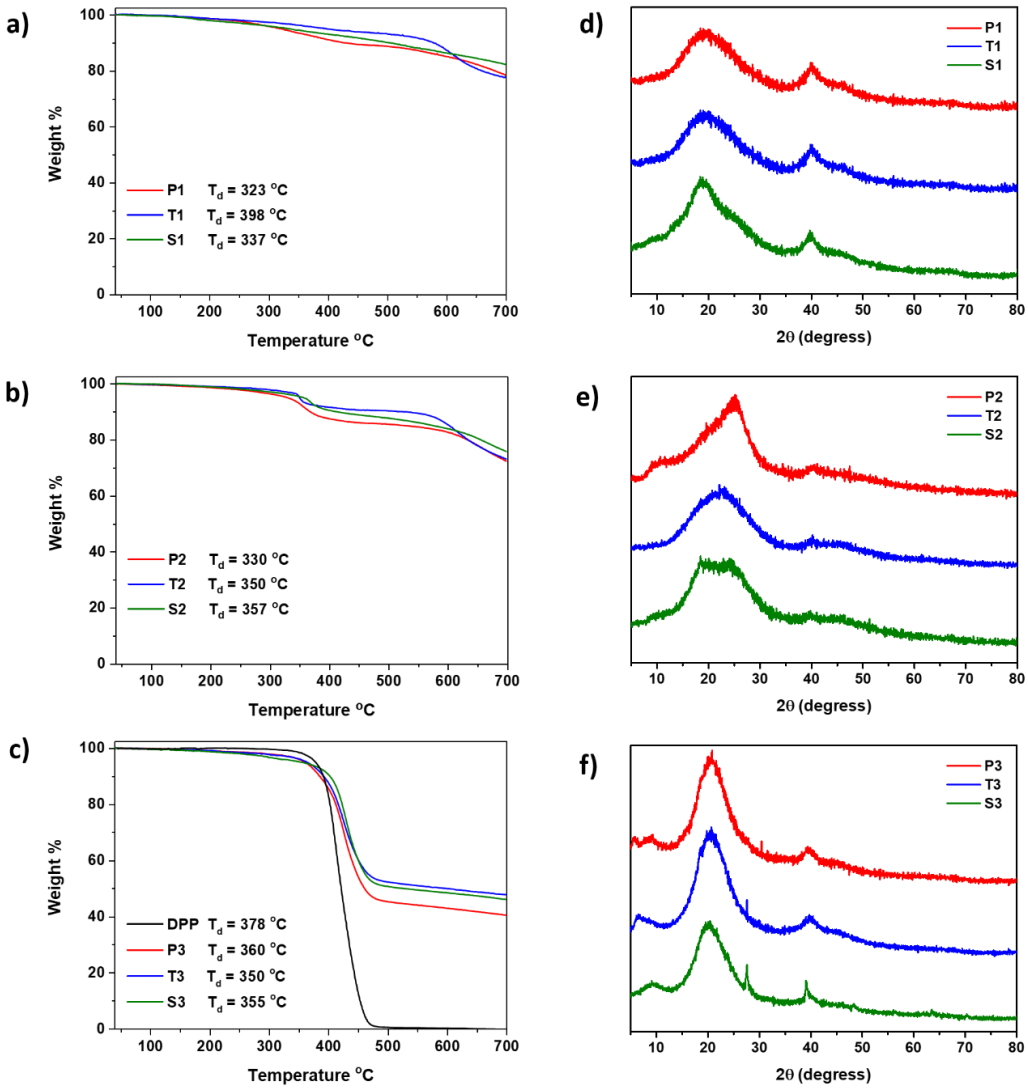

Figure 5.5 TGA plots (a-c) and PXRD patterns (d-f) of **BT**-based polymers – **P1, T1** and **S1** (a, d), **DTBT**-based polymers – **P2, T2** and **S2** (b, e) and **DPP**-based polymers – **P3, T3** and **S3** (c, f). TGA plot of monomer **DPP** (c) is also shown for comparison.

(**Figure 5.5a-c**). Polymers containing the same thiophene monomers exhibit very similar degradation profiles. Most notable trend is the drastic mass loss in the profiles of **P3**, **T3** and **S3** (**Figure 5.5c**) which can be attributed to the degradation of the long alkyl chains since **DPP** exhibits a similar trend as well. Even at 700 ^{o}C, **P1-3**, **T1-3** and **S1-3** do not degrade completely, leaving behind significant amount (> 40%) of residue which is typical for extended covalent networks. Powder X-ray diffraction patterns (**Figure 5.5d-f**) of all polymers exhibit broad

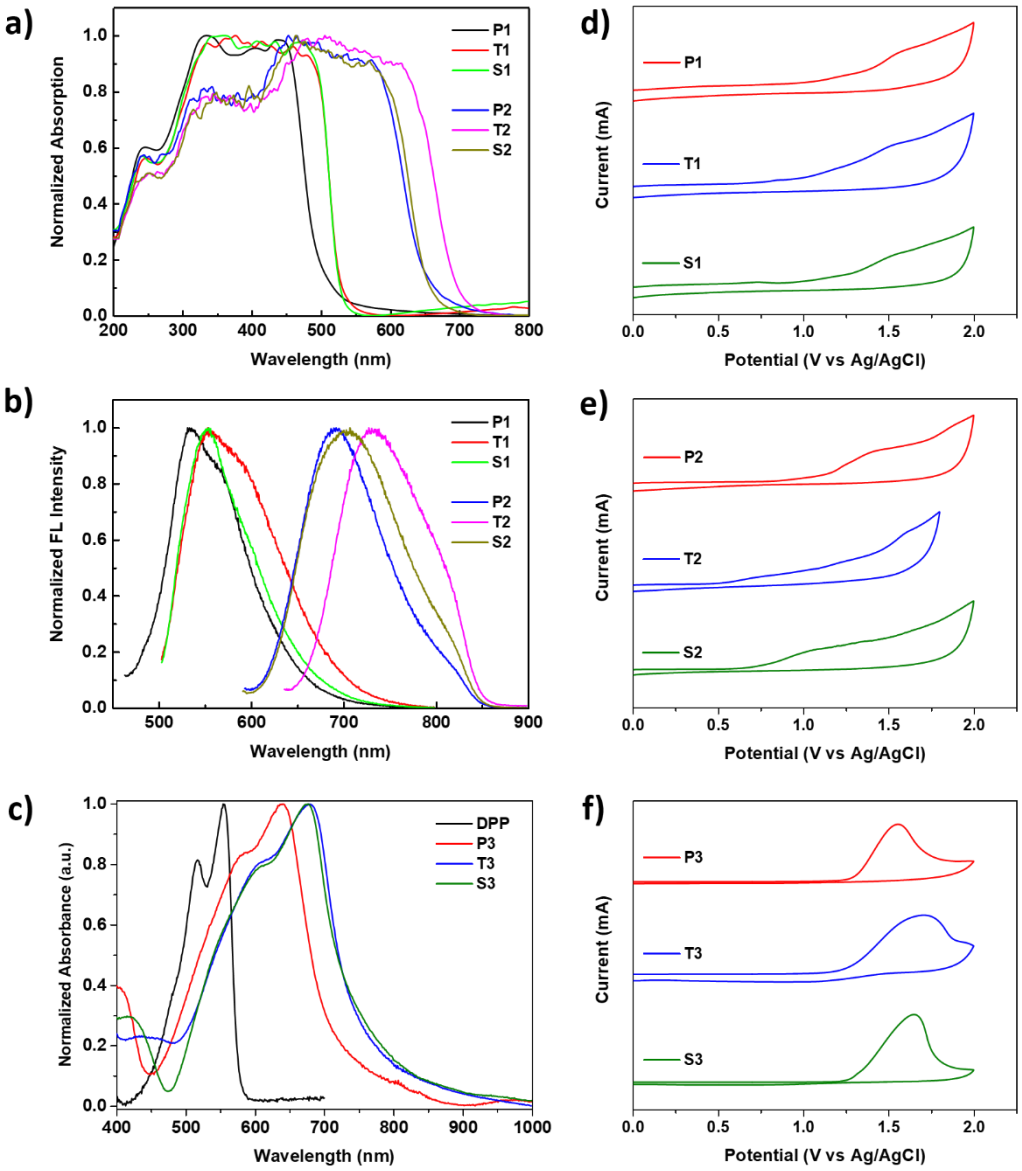

Figure 5.6 Normalized a) diffuse-reflectance UV-Vis spectroscopy and b) fluorescence spectroscopy in solid state of **BT**-based polymers – **P1, T1** and **S1** and **DTBT**-based polymers – **P2**, **T2** and **S2**. Maximum absorption wavelength was used as the excitation wavelength (λ^{ex}). c) Normalized UV-Vis-NIR absorption spectra of **DPP** in *o*-dichlorobenzene solution and **DPP**-based polymers – **P3**, **T3** and **S3** in *o*-dichlorobenzene. Cyclic voltammetry of **BT**-based polymers – d) **P1**, **T1** and **S1**, DTBT-based polymers – e) **P2**, **T2** and **S2** and **DPP**-based polymers – f) **P3**, **T3** and **S3.**

Table 5.1 Optical and electrochemical properties of CPPs.

Polymer	λ^{abs}_{onset} (nm)	λ^{em}_{max} (nm)	E^{opt}_{eg} (eV) [a]	E^{ox}_{onset} (V) [b]	E_{HOMO} (eV) [c]	E_{LUMO} (eV) [d]
P1	520	534	2.38	1.25	-6.05	-3.67
T1	547	554	2.26	1.05	-5.85	-3.59
S1	540	554	2.29	1.14	-5.94	-3.65
P2	680	691	1.82	0.95	-5.75	-3.93
T2	708	706	1.75	0.62	-5.42	-3.67
S2	675	730	1.84	0.72	-5.52	-3.81
P3	828	-	1.49	1.24	-6.04	-4.55
T3	856	-	1.44	1.15	-5.95	-4.51
S3	883	-	1.40	1.22	-6.02	-4.62

[a] Calculated from the absorption onset. [b] Potentials vs. Ag/Ag+ determined by cyclic voltammetry by using 0.1 M tetrabutylammonium hexafluorophosphate (Bu_4NPF_6) in acetonitrile as the supporting electrolyte. [c] $E_{HOMO} = -[E^{ox}_{onset} + 4.8]$ eV. [d] $E_{LUMO} = [E_{HOMO} + E^{opt}_{eg}]$ eV.

peaks at $2\theta = 20^o$ and 40^o which is indicative of their amorphous carbon-based structures.

5.3 Optical and electrochemical properties

Optical properties of **BT**-based polymers (**P1**, **T1** and **S1**) and the **DTBT**-based polymers (**P2**, **T2** and **S2**) were measured by diffuse-reflectance UV-Vis spectroscopy (**Figure 5.6a**) and fluorescence spectroscopy in solid state (**Figure 5.6b**). **P1**, **T1** and **S1** show strong absorption between 200 nm and 500 nm and their bandgaps are found to be in the range of 2.38 - 2.29 eV whereas the absorption edge of polymers containing benzothiadiazole stretch up to 700 nm and their bandgaps lie between 1.75 eV and 1.84 eV**,** which is expected since bandgap of monomer **DTBT** is lower than that of **BT**. A similar trend is observed in the fluorescence spectra of these polymers, which is evident from the shift of the emission maximum wavelengths listed in **Table 5.1.** Optical properties of **P3**, **T3** and **S3** were studied in dispersions of *o*-dichlorobenzene **(Figure 5.6c**) rather than in solid state due to their inability to form compact films. Owing to the narrow bandgap and extensive conjugation in the polymers, **P3**, **T3** and **S3** show

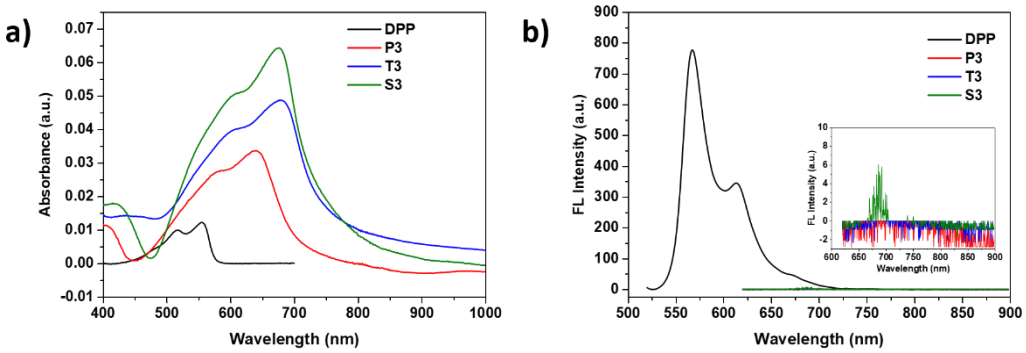

Figure 5.7 Comparison of non-normalized a) absorption and b) fluorescence spectra of **DPP**-based polymers – **P3**, **T3** and **S3** (λ^{ex} = 600 nm) with monomer **DPP** (λ^{ex} = 500 nm) in *o*-dichlorobenzene solutions. Inset shows the magnified fluorescence spectra of **P3**, **T3** and **S3**.

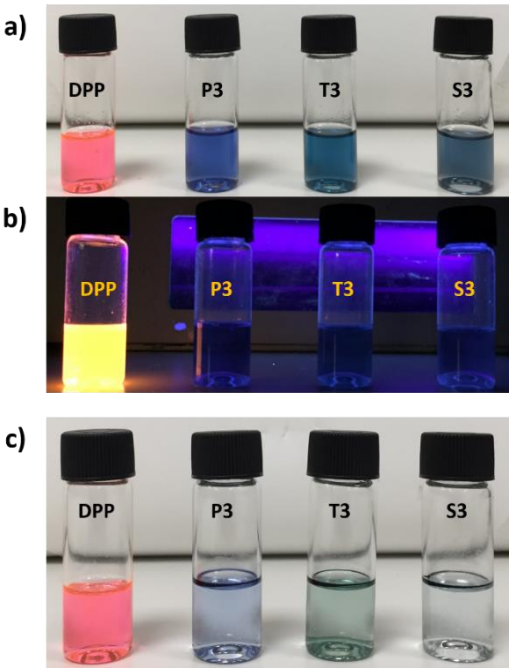

Figure 5.8 Digital images of (l-r) **DPP** solution in *o*-dichlorobenzene, dispersions of **P3**, **T3** and **S3** in *o*-dichlorobenzene under a) room light and b) UV light (365 nm).c) Digital images of dispersions after 3 days.

a strong and broad absorption over the whole visible range as well as the near-infrared region up to 880 nm – a trend commonly seen in **DPP**-based linear polymers. Such red shift of the absorption maximas of **P3**, **T3** and **S3** (**Figure 5.6c**) compared to the monomer **DPP** suggests the extended conjugation in the polymer networks. Fluorescence of the **DPP**-based polymers (**Figure 5.7b**) is drastically quenched compared to the **DPP** monomer which can be attributed to the rigid packing and strong π–π interaction of **DPP** in the polymer.

Electrochemical properties of polymers **P1-3**, **T1-3** and **S1-3** were measured by cyclic voltammetry (**Figure 5.6d-f**). Highest occupied molecular orbital (HOMO) energy levels of the polymers lie between -6.05 and -5.42 eV. It should be noted that the energy levels of the lowest unoccupied molecular orbital (LUMO) of **DPP**-based polymers – **P3**, **T3** and **S3** are the lowest while those of **BT**-based polymers are the highest (**Table 5.1**) possibly due to the strong electro withdrawing effect of **DPP** which results in deeper LUMO levels.

5.4 Morphology

Morphologies of all thiophene-containing CPPs were studied by scanning electron microscopy (SEM) and transmission electron microscopy (TEM). From the SEM images of **BT**-containing polymers (**Figure 5.9a-c**), we observe that all polymers exhibit non-uniform spherical morphologies. **P1** occurs as a dense cluster of irregular spheres of approximately 500 nm in diameter. TEM image of **P1** (**Figure 5.10a**) confirms the presence of microspheres. **T1** (**Figure 5.9b**) and **S1** (**Figure 5.9c**) also exhibit distinct spherical morphologies, however we also observed fibrillar structures surrounding the microspheres which can be seen more clearly from their TEM images (**Figure 5.10b-c**). Moreover, the microspheres of **T1** and **S1**, with an approximate diameter of 2.5 μm and 1.5 μm respectively, are relatively larger than those of **P1**.

Polymers containing **DTBT** all exhibit uniform spherical morphologies abundant with surface defects - **P2** (**Figure 5.9d**) has a rough and irregular surface, while the microspheres of **T2** (**Figure 5.9e**) and **S2** (**Figure 5.9f**) are relatively smoother. Like the **BT**-containing polymers, the larger size of **T2** and

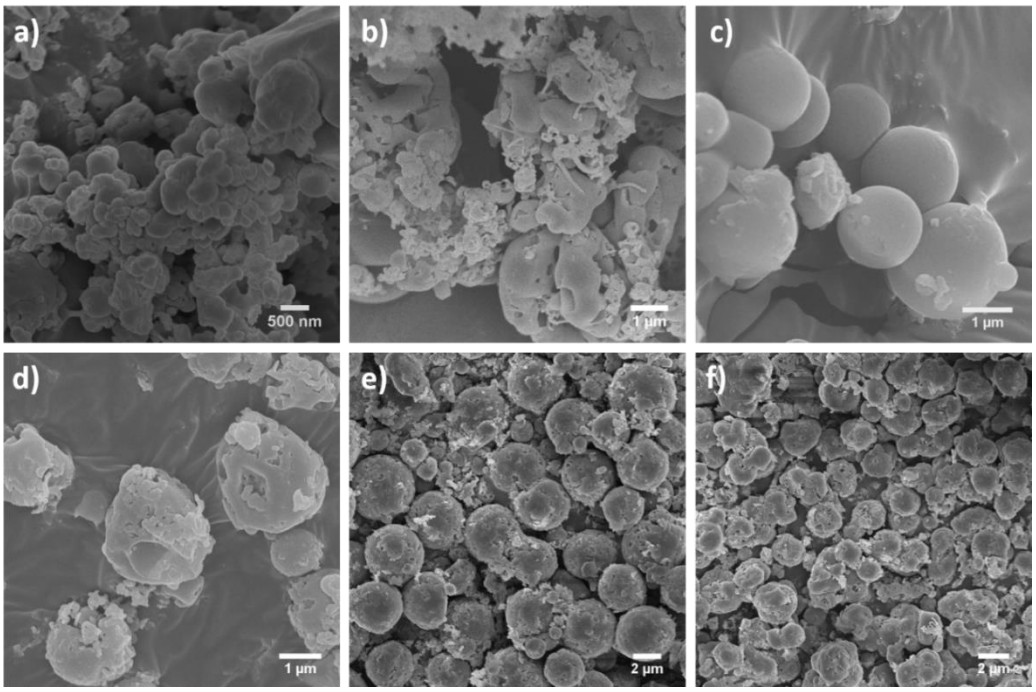

Figure 5.9 SEM images of **BT**-based polymers – a) **P1**, b) **T1**, c) **S1** and **DTBT**-based polymers – d) **P2**, e) **T2**, f) **S2**.

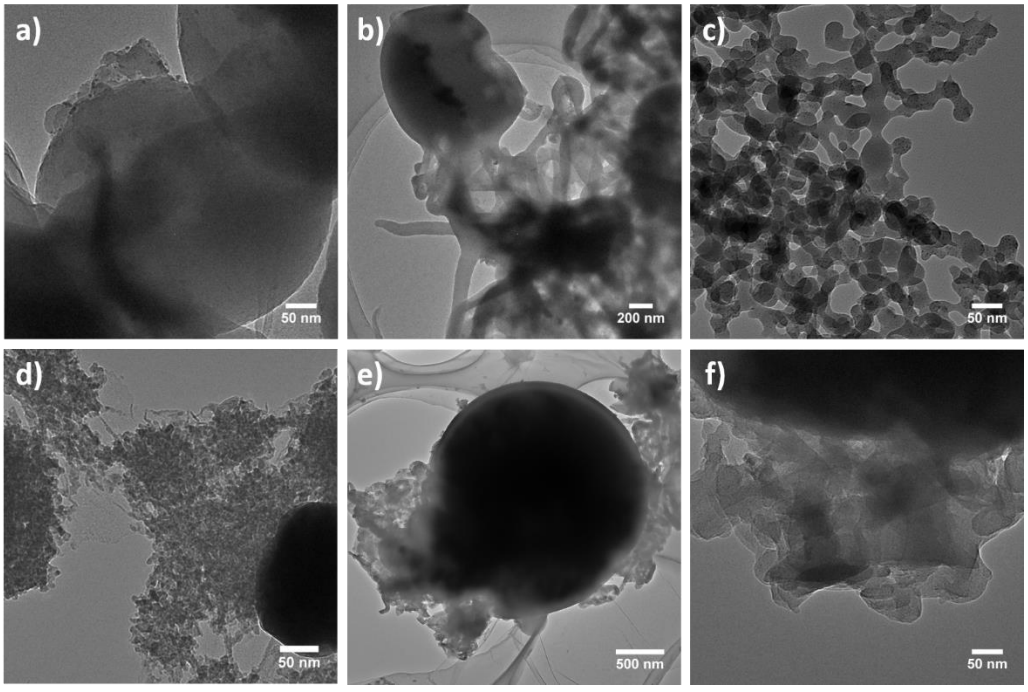

Figure 5.10 TEM images of **BT**-based polymers – a) **P1**, b) **T1**, c) **S1** and **DTBT**-based polymers – d) **P2**, e) **T2**, f) **S2**.

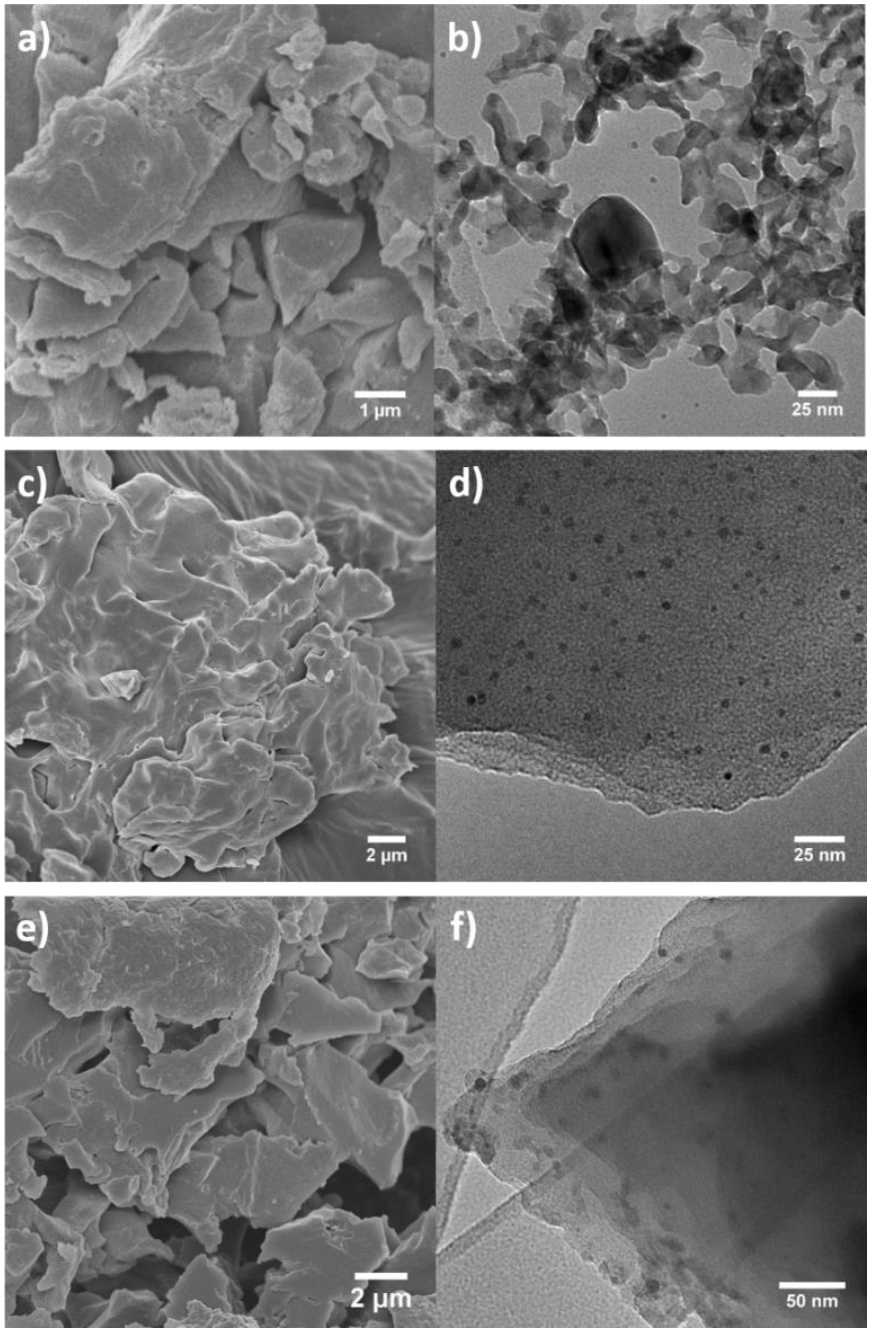

Figure 5.11 SEM (a, c, e) and TEM (b, d, f) images of **DPP**-based polymers **P3** (a, b)**, T3** (c, d) and **S3** (e, f).

S2 compared to **P2** is apparent in the **DTBT** containing polymers as well. Moreover, the microspheres of **DTBT**-based polymers are larger than their **BT**-based counterparts consisting the same node.

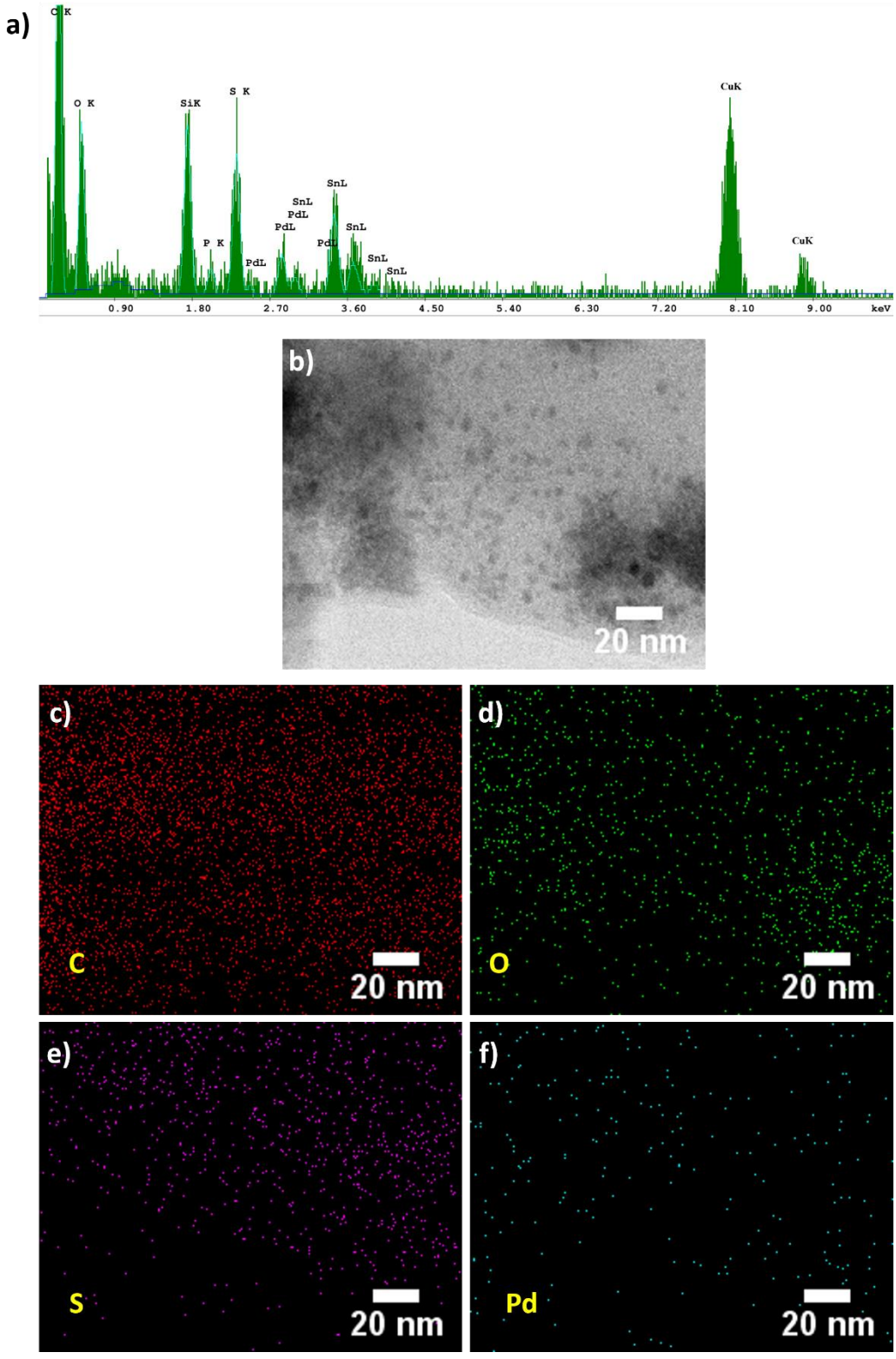

Figure 5.12 a) Energy dispersive X-ray (EDX) spectrum of **T3**. b) HR-TEM image of **T3** and the EDX mapping of elements c) C, d) O, e) S and d) Pd.

In contrast to the spherical morphology of **BT-** and **DTBT**-based polymers, **DPP**-based polymers appear as flat, uncharacteristic monoliths with smooth surfaces. A very similar morphology was observed for conjugated microporous polymers containing alkylated thiophene reported by Li and coworkers which also exhibited flat and 'wrinkled' surfaces.[20] SEM images of **P3** (**Figure 5.11a**), **T3** (**Figure 5.11c**) and **S3** (**Figure 5.11e**) exhibit a discernible layered structure which was exfoliated into sheets by dispersing the **DPP**-based polymers in *o*-dichlorobenzene (DCB) at 120 ^{o}C. After exfoliation, stacks of thin polymer sheets were observed from the TEM images of **T3** (**Figure 5.11d**) and **S3 (Figure 5.11f)**. In contrast, dispersing **P3** in DCB lead to the formation of thin irregular strips (**Figure 5.11b**). We also observed the presence of spherical nanoparticles in the TEM images of **T3** and **S3.** These particles were presumed to correspond to residual palladium catalyst from the direct arylation reaction. To analyze the nanoparticles, energy dispersive X-ray (EDX) mapping of **T3** was carried out (**Figure 5.12**). In addition to carbon, oxygen and sulfur, the EDX spectrum as well as mapping (**Figure 5.12f**) showed the presence of palladium in **T3** which confirmed our hypothesis.

5.5 Porosity and gas adsorption characteristics

Porosities of thiophene-containing polymers were studied by N_2 adsorption experiments and the results are summarized in **Table 5.2**. **Figure 5.13** presents the BET adsorption isotherms and BJH pore size distributions of **BT** and **DTBT** based CPPs. Isotherms of **P1** and **T1** (**Figure 5.13a**) show negligible gas uptake in the low-pressure range and a sudden increase in uptake as p/p_o approaches 1, which is characteristic of Type III adsorption. In contrast, the isotherm of **S3** exhibits typical Type II behavior – moderate uptake in the low-pressure range followed by a plateau and an increased uptake in high-pressure range. As a result, the BET surface areas of **P1** and **T1** are 12 m^2 g^{-1} and 24 m^2 g^{-1} respectively while surface area of **S1** is 407 m^2 g^{-1}. **P1** and **T1** exhibit broad pore size distributions with peaks centered at 1.8 and 2.2 nm for **P1** and 2.6 nm for **T1** while **S1** exhibits a unimodal distribution with a relatively larger pore diameter of 3.9 nm. Both the pore volumes and pore diameters of **BT** containing

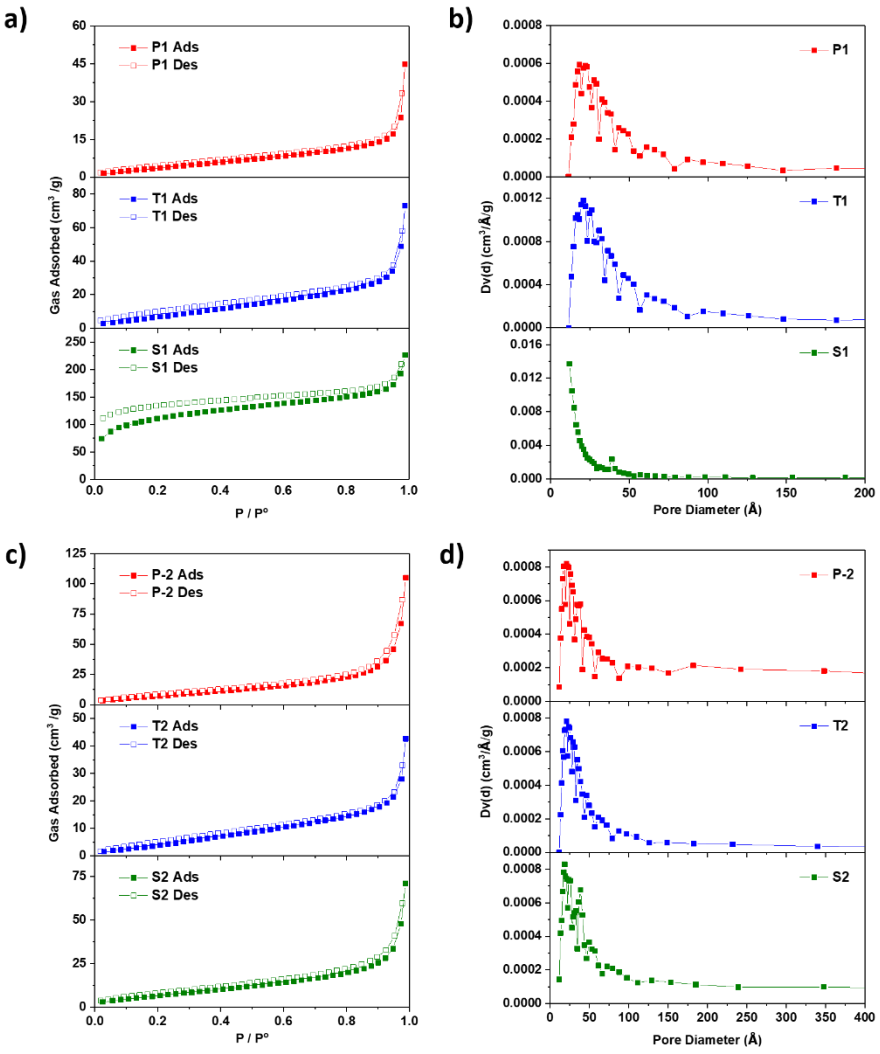

Figure 5.13 N_2 adsorption isotherms (a, c) and BJH pore size distribution (b, d) of **BT** based polymers (a, b) and **DTBT** based polymers (**c, d**).

polymers follow the trend **P1** < **T1** < **S1** which can be explained by the increasing size of the nodes (**P** < **T** < **S**).

All **DTBT** containing polymers show similar adsorption characteristics – their isotherms exhibit Type III behavior (**Figure 5.13c**) and all polymers have broad pore size distributions (**Figure 5.13d**) with pore sizes lying between 1.8 nm and 2.5 nm. BET surface areas of **DTBT** containing polymers lie in a narrow range of 15 $m^2\ g^{-1}$ and 24 $m^2\ g^{-1}$ and their pore volumes range form 0.06 – 0.16 $cm^3\ g^{-1}$. Despite the larger size of the **DTBT** strut, the pore volumes and pore

Table 5.2 Adsorption characteristics of thiophene-containing conjugated porous polymers.

Polymer	S^{BET} ($m^2\ g^{-1}$) [a]	$S^{Langmuir}$ ($m^2\ g^{-1}$) [b]	Pore Diameter (nm)	Pore Volume ($cm^3\ g^{-1}$) [c]
P1	12	34	1.8, 2.2	0.069
T1	24	91	2.0, 2.6	0.11
S1	407	535	3.9	0.35
P2	24	46	1.8, 2.1, 2.6	0.162
T2	15	41	2.0, 2.4	0.066
S2	22	50	1.8, 2.5	0.11
P3	10	16	2.5	0.097
T3	0	0	-	0.03
S3	0	0	-	0.048

[a] Specific surface area calculated from the adsorption branch of the N_2 isotherm using the BET method. [b] Specific surface area calculated from the adsorption branch of the N_2 isotherm using the Langmuir method. [c] Calculated at p/p_o = 0.99.

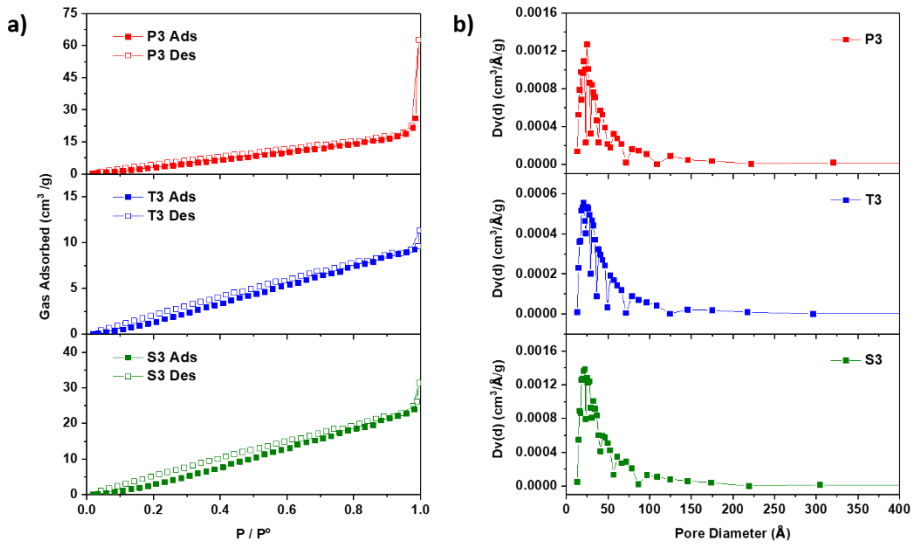

Figure 5.14 a) N_2 adsorption isotherms and b) BJH pore size distribution of **DPP** based polymers **P3**, **T3** and **S3**.

sizes of DTBT-based polymers do not increase with monomer size. Ren et. al. reported the Suzuki polymerization synthesis of **T2** and obtained a slightly higher

BET surface area of 50 m^2/g, however did not observe a systematic increase in porosity when the size of benzothiadiazole-based increased.[24] Isotherms of **DPP** containing polymers (**Figure 5.14a**) show very poor gas uptake in the entire pressure range which results in poor adsorption characteristics. **P3** has a BET surface of 10 $m^2\ g^{-1}$while **T3** and **S3** were found to be completely non-porous. Negligible of porosities of **P3**, **T3** and **S3** can be attributed to the interpenetration of long alkyl chains in to the structural unit of the polymer (**Scheme 5.1**) which prevents the formation of porous structures.

5.6 Conclusion

In conclusion, a series of conjugated porous polymers were synthesized by the direct arylation polymerization of tri- and tetra- brominated monomers with three C-H active, thiophene-flanked monomers containing the bithiophene, benzothiadiazole and diketopyrrolopyrrole moiety. Optical properties of the polymers show that the band gaps and energy levels of CPPs can be fine-tuned by careful selection of thiophene-based monomers. Except for **S1** which has a BET surface of 407 $m^2\ g^{-1}$, all thiophene-containing CPPs poor porosities and low BET surfaces areas. DPP-containing polymers were found to have interesting layered structures which could be exfoliated in to thin sheets. Overall, these results demonstrate the ability of direct arylation to synthesize a broad scope of thiophene-based conjugated porous polymers without tedious pre-activation of C-H bonds in arene monomers. Bandgap, porosity and morphology of CPPs can be controlled by careful selection of monomers, allowing for the synthesis of new π-conjugated polymers for a variety of applications such as photocatalysis and beyond.

5.7 Experimental section

5.7.1 Materials and methods

1,3,5-Tribromobenzene (**P**), tris-(4-bromophenyl)amine (**T**), 2,2',7,7'-tetrabromo-9,9' spirobifluorene (**S**) and 2,2'-bithiophene (**BT**) were purchased from Sigma Aldrich. 4,7-di(thiophen-2-yl)benzo[c][1,2,5]thiadiazole (**DTBT**)[33] and 2,5-bis(2-octyldodecyl)-3,6-di(thiophen-2-yl)-2,5-pyrrolo[3,4-c]pyrrole-

1,4(2H,5H)-dione (**DPP**)[38] were prepared according to reported procedures. All solvents were obtained from commercial sources and used as received unless otherwise specified. Solid state ^{13}C magic angle spinning nuclear magnetic resonance (MAS NMR) spectra were collected by a JEOL ECA 400 spectrometer. FT-IR spectra were recorded on a Perkin Elmer Spectrum One FT-IR spectrometer. Thermo- gravimetric analyses were performed on a Pyris Diamond TGA (Perkin Elmer) instrument, at a heating rate of 10 ^{o}C min^{-1} under N2 atmosphere from 40 ^{o}C to 700 ^{o}C. SEM imaging was carried out using a JEOL JSM 6701F SEM (Scanning Electron Microscope) operating in scanning mode. Samples were prepared by depositing dry samples on aluminium stubs using an adhesive high purity carbon tape. TEM images were obtained using a Carl Zeiss Libra 120 Plus transmission electron microscope (TEM). Samples were prepared by depositing polymers from an ethanol dispersion onto a copper grid coated with ultra-thin carbon film. Nitrogen sorption isotherms were obtained at 77 K using Quantachrome Instruments Autosorb-6 with extra high purity gases. All samples were degassed at 110 ^{o}C for 16 h in vacuum before analysis. Surface areas were calculated in the relative pressure (p/p_o) range from 0.05 to 0.35 of the adsorption branch. Pore size distribution was obtained by the Barrett–Joyner–Halenda (BJH) method using the adsorption curve of the isotherm. The total pore volume was estimated by the amount of nitrogen adsorbed at the relative pressure of 0.99. The UV-visible absorption spectra were obtained on a UV-visible spectrophotometer (UV-2450, Shimadzu). Cyclic voltammograms (CVs) were recorded on an CHI Electrochemical Analyzer Model 660D at room temperature using 0.1 M tetrabutylammonium hexafluorophosphate (Bu_4NPF_6) solution in CH_3CN as a supporting electrolyte at a scan rate of 100 mV/s. Glassy carbon was used as working electrode, platinum wire as counter electrode and silver as the reference electrode. Samples were prepared by drop-casting a slurry of polymers in Nafion on the glassy carbon electrode. All the potentials were calibrated with the standard ferrocene/ferrocenium redox couple (Fc/Fc+). Powder X-ray diffraction patterns were obtained at 40 kV and 40 mA on a Bruker Advanced D8 XRD using Cu-Kα radiation (λ = 1.5418 Å) over 2θ range of 5.0° - 6 0° at room temperature. Elemental analysis was carried out on a Vario EL III CHNS Elemental Analyzer.

5.7.2 General synthetic scheme for 2-D CPPs.

To a microwave vial charged with a magnetic stirring bar, monomers A and X (C-H:C-Br = 1:1), $Pd_2(dba)_3$ (5 mol%), (o-$MeOC_6H_4)_3P$ (10 mol%), K_2CO_3 (400 mol%) and PivOH (50 mol%) were added. *o*-xylene (0.2 M) was added inside a glove-box and vial was sealed with a rubber cap. The vial was placed in an oil bath preheated to 120 °C and the reaction was carried out for 48 hours. After cooling to room temperature, the reaction mixture was diluted with THF and filtered over vacuum. The precipitate was washed with methanol, water, dil. HCl and THF and then subjected to Soxhlet extraction sequentially with methanol, chloroform and THF for 24 hours each. The residual solids were collected and dried at 100 ^oC under vacuum to obtain the final product.

P1: **P** (100 mg), **BT** (79.22 mg), $Pd_2(dba)_3$ (21.9 mg), (o-$MeOC_6H_4)_3P$ (16.78 mg), K_2CO_3 (263.37 mg), PivOH (24.4 mg) and *o*-xylene (2.4 mL). Yield: 103.6 mg. IR (KBr cm^{-1}): 3061, 1587, 1445, 850, 788, 750, 686. Solid state ^{13}C NMR (400 MHz) δ: 141.6, 135.8, 123.8. Elemental Analysis (%) Calculated for $C_{36}H_{18}S_6$: C, 67.28; H, 2.8; N, 0.0; S, 29.90. Found: C, 62.43; H, 1.07; N, 0.04; S, 23.47.

P2: **P** (50 mg), **DTBT** (71.6 mg), $Pd_2(dba)_3$ (10.9 mg), (o-$MeOC_6H_4)_3P$ (8.39 mg), K_2CO_3 (131.17 mg), PivOH (12.16 mg) and *o*-xylene (1.16 mL). Yield: 77.5 mg. IR (KBr cm^{-1}): 3067, 2913, 1587, 1486, 1421, 1559, 832, 801, 753, 696. Solid state ^{13}C NMR (400 MHz) δ: 152, 143.9, 138.3, 133.8, 127.7, 125, 121.1. Elemental Analysis (%) for $C_{54}H_{24}N_6S_9$. Calculated: C, 62.07; H, 2.29; N, 8.05; S, 27.58. Found: C, 55.52; H, 1.36; N, 5.93; S, 20.63.

P3: **P** (24.33 mg), **DPP** (100 mg), $Pd_2(dba)_3$ (5.3 mg), (o-$MeOC_6H_4)_3P$ (4.08 mg), K_2CO_3 (64.1 mg), PivOH (5.96 mg) and *o*-xylene (0.58 mL). Yield: 171.7 mg. IR (KBr cm^{-1}): 3081, 2921, 2850, 1670, 1564, 1459, 1394, 805. Elemental Analysis (%) for $C_{174}H_{264}N_6O_6S_6$. Calculated: C, 79.45; H, 10.04; N, 3.19; S, 7.31. Found: C, 72.96; H, 6.39; N, 2.85; S, 7.02.

T1: T (153.3 mg), **BT** (79.22 mg), $Pd_2(dba)_3$ (21.8 mg), (o-$MeOC_6H_4)_3P$ (16.78 mg), K_2CO_3 (263.37 mg), PivOH (24.4 mg) and *o*-xylene (2.4 mL). Yield:

160.5 mg. IR (KBr cm^{-1}): 3061, 3024, 1597, 1494, 1318, 826, 789, 729, 692. Solid state ^{13}C NMR (400 MHz) δ: 145.1, 142.5, 136.6, 127.2. Elemental Analysis (%) for $C_{60}H_{36}N_2S_6$. Calculated: C, 73.77; H, 3.69; N, 2.87; S, 19.67. Found: C, 70.13; H, 1.70; N, 2.50; S, 15.92.

T2: **T** (144.8 mg), **DTBT** (140 mg), $Pd_2(dba)_3$ (21.2 mg), (o-$MeOC_6H_4)_3P$ (16.32 mg), K_2CO_3 (256 mg), PivOH (13.6 mg) and *o*-xylene (2.36 mL). Yield: 130 mg. IR (KBr cm^{-1}): 3022, 1592, 1478, 1440, 1533, 1320, 830, 796, 693. Solid state ^{13}C NMR (400 MHz) δ: 152, 143.9, 138.3, 133.8, 127.7, 125, 121.1. Solid state ^{13}C NMR (400 MHz) δ: 152.2, 147.7, 146.2, 138.9, 137.6, 126.2. Elemental Analysis (%) for $C_{78}H_{42}N_8S_9$. Calculated: C, 67.92; H, 3.04; N, 8.12; S, 20.89. Found: C, 63.88; H, 1.64; N, 6.48; S, 15.89.

T3: T (37.2 mg), **DPP** (100 mg), $Pd_2(dba)_3$ (5.3 mg), (o-$MeOC_6H_4)_3P$ (4.08 mg), K_2CO_3 (64.1 mg), PivOH (5.96 mg) and *o*-xylene (0.58 mL). Yield: 218.14 mg. IR (KBr cm^{-1}): 3098, 2918, 2854, 1662, 1566, 1492, 1320, 832, 728. Elemental Analysis (%) for $C_{198}H_{282}N_8O_6S_6$. Calculated: C, 79.72; H, 9.75; N, 3.88; S, 6.64. Found: C, 75.18; H, 6.34; N, 3.41; S, 6.10.

S1: S (150.8 mg), **BT** (79.22 mg), $Pd_2(dba)_3$ (21.8 mg), (o-$MeOC_6H_4)_3P$ (16.78 mg), K_2CO_3 (263.37 mg), PivOH (24.4 mg) and *o*-xylene (2.4 mL). Yield: 170.9 mg. IR (KBr cm^{-1}): 3058, 1604, 1574, 1453, 815, 793, 691. Solid state ^{13}C NMR (400 MHz) δ: 150.4, 141, 138.7, 134.7, 66.9. Elemental Analysis (%) for $C_{41}H_{20}S_4$. Calculated: C, 76.86; H, 3.13; N, 0.0; S, 20.0. Found: C, 70.87; H, 1.12; N, 0.01; S, 15.11.

S2: S (104.63 mg), **DTBT** (100 mg), $Pd_2(dba)_3$ (15.16 mg), (o-$MeOC_6H_4)_3P$ (11.66 mg), K_2CO_3 (183.17 mg), PivOH (17.018 mg) and *o*-xylene (1.65 mL). Yield: 103.5 mg. IR (KBr cm^{-1}): 3010, 2840, 1600, 1573, 1445, 1535, 1060, 797, 734, 693, 826. Solid state ^{13}C NMR (400 MHz) δ: 151.6, 149.2, 139.5, 125.5, 65.9. Elemental Analysis (%) for $C_{53}H_{24}N_4S_6$. Calculated: C, 70.04; H, 2.64; N, 6.16; S, 21.14. Found: C, 64.09; H, 1.49; N, 4.79; S, 16.88.

S3: S (36.63 mg), **DPP** (100 mg), $Pd_2(dba)_3$ (5.3 mg), (o-$MeOC_6H_4)_3P$ (4.08 mg), K_2CO_3 (64.1 mg), PivOH (5.96 mg) and *o*-xylene (0.58 mL). Yield:

138.7 mg. IR (KBr cm^{-1}): 2923, 2851, 1666. 1567, 1439, 1060, 805, 697. Elemental Analysis (%) for $C_{133}H_{184}N_4O_4S_4$. Calculated: C, 81.26; H, 9.36; N, 2.85; S, 6.52. Found: C, 73.91; H, 6.018; N, 2.43; S, 5.94.

5.7.3 Sample preparation for UV-Vis-NIR and Infrared spectroscopy of DPP-based polymers – P3, T3 and S3

Stock solutions for UV-Vis-NIR spectroscopy were prepared by dispersing 2 mg of DPP polymers in 4 mL *o*-dichlorobenzene and stirring at 120 ^oC for 24 hours under N_2 atmosphere. Samples for infrared spectroscopy were prepared by mixing DPP polymers with small amounts of KBr in chloroform and stirring at 80 ^oC under N_2 atmosphere. After 24 hours the solvent was evaporated, and the samples were dried at 80 ^oC under vacuum. The dried solids were used directly for analysis.

5.8 References

1. Slater, A. G.; Cooper, A. I. *Science* **2015,** *348*.
2. Xu, Y.; Jin, S.; Xu, H.; Nagai, A.; Jiang, D. *Chem. Soc. Rev.* **2013,** *42*, 8012-8031.
3. Vilela, F.; Zhang, K.; Antonietti, M. *Energy Environ. Sci.* **2012,** *5*, 7819.
4. Bonillo, B.; Sprick, R. S.; Cooper, A. I. *Chem. Mater.* **2016,** *28*, 3469-3480.
5. Li, R.; Byun, J.; Huang, W.; Ayed, C.; Wang, L.; Zhang, K. A. I. *ACS Catal.* **2018,** *8*, 4735-4750.
6. Kai, Z.; Daniel, K.; H., S. P.; Markus, A.; Filipe, V. *Angew. Chem. Int. Ed.* **2013,** *52*, 1432-1436.
7. Jun, W. Z.; Kim, G.; Saman, G.; Katharina, L.; I., Z. K. A. *ChemSusChem* **2015,** *8*, 3459-3464.
8. Xu, Y.; Mao, N.; Zhang, C.; Wang, X.; Zeng, J.; Chen, Y.; Wang, F.; Jiang, J.-X. *Appl. Catal. B: Environ.* **2018,** *228*, 1-9.
9. Palai, A. K.; Kumar, A.; Sim, K.; Kwon, J.; Shin, T. J.; Jang, S.; Cho, S.; Park, S.-U.; Pyo, S. *New J. Chem.* **2016,** *40*, 385-392.
10. Chandran, D.; Lee, K.-S. *Macromol. Res.* **2013,** *21*, 272-283.

11. Zhang, K.; Tieke, B.; Vilela, F.; Skabara Peter, J. *Macromol. Rapid Commun.* **2011,** *32*, 825-830.

12. Bi, S.; Li, Y.; Zhang, S.; Hu, J.; Wang, L.; Liu, H. *J. Mater. Chem. C* **2018,** *6*, 3961-3967.

13. Guo, X.; Baumgarten, M.; Müllen, K. *Prog. Polym. Sci.* **2013,** *38*, 1832-1908.

14. Xue, W.; Chong, Z.; Yunfeng, X.; Qian, H.; Pan, M.; Yu, C.; Jinghui, Z.; Feng, W.; Jia-Xing, J. *Macromol. Chem. Phys.* **2018,** *219*, 1700524.

15. Sun, C.-J.; Wang, P.-F.; Wang, H.; Han, B.-H. *Polym. Chem.* **2016,** *7*, 5031-5038.

16. Sun, C.-J.; Zhao, X.-Q.; Wang, P.-F.; Wang, H.; Han, B.-H. *Sci. China Chem.* **2017,** *60*, 1067-1074.

17. Yali, L.; Buyi, L.; Wei, W.; Kangbing, W.; Bien, T. *Adv. Mater.* **2012,** *24*, 5703-5707.

18. Liu, H.; Li, Q.; Li, Q.; Jin, W.; Li, X.; Hameed, A.; Qiao, S. *Polym. Chem.* **2017,** *8*, 6733-6740.

19. Palma-Cando, A.; Brunklaus, G.; Scherf, U. *Macromolecules* **2015,** *48*, 6816-6824.

20. Feng, R.; Fei, W.; Yu, P.; Hanxue, S.; Zhaoqi, Z.; Chonghua, M.; Chaohu, X.; Weidong, L.; Lihua, C.; An, L. *Macromol. Mater. Eng.* **2018,** *303*, 1700619.

21. Ren, F.; Zhu, Z.; Qian, X.; Liang, W.; Mu, P.; Sun, H.; Liu, J.; Li, A. *Chem. Commun.* **2016,** *52*, 9797-9800.

22. Qin, L.; Xu, G.-j.; Yao, C.; Xu, Y.-h. *Polym. Chem.* **2016,** *7*, 4599-4602.

23. Vangeneugden, D. L.; Vanderzande, D. J. M.; Salbeck, J.; van Hal, P. A.; Janssen, R. A. J.; Hummelen, J. C.; Brabec, C. J.; Shaheen, S. E.; Sariciftci, N. S. *J. Phys. Chem. B* **2001,** *105*, 11106-11113.

24. Ren, S.; Dawson, R.; Adams, D. J.; Cooper, A. I. *Polym. Chem.* **2013,** *4*, 5585-5590.

25. Pouliot, J.-R.; Grenier, F.; Blaskovits, J. T.; Beaupré, S.; Leclerc, M. *Chem. Rev.* **2016,** *116*, 14225-14274.

26. Bohra, H.; Wang, M. *J. Mater. Chem. A* **2017,** *5*, 11550-11571.

27. Wang, K.; Chen, H.; Wei, X.; Bohra, H.; He, F.; Wang, M. *Dyes Pigm.*

28. Kai, W.; Mingfeng, W. *J. Polym. Sci., Part A: Polym. Chem.* **2017,** *55*, 1040-1047.

29. Wang, K.; Wang, G.; Wang, M. *Macromol Rapid Commun* **2015,** *36*, 2162-70.

30. Bohra, H.; Tan, S. Y.; Shao, J.; Yang, C.; Efrem, A.; Zhao, Y.; Wang, M. *Polym. Chem.* **2016,** *7*, 6413-6421.

31. Efrem, A.; Wang, K.; Amaniampong, P. N.; Yang, C.; Gupta, S.; Bohra, H.; Mushrif, S. H.; Wang, M. *Polym. Chem.* **2016,** *7*, 4862-4866.

32. Shao, J.; Wang, G.; Wang, K.; Yang, C.; Wang, M. *Polym. Chem.* **2015,** *6*, 6836-6844.

33. Wang, X.; Wang, K.; Wang, M. *Polym. Chem.* **2015,** *6*, 1846-1855.

34. Wang, X.; Wang, M. *Polym. Chem.* **2014,** *5*, 5784-5792.

35. Bohra, H.; Shao, J.; Huang, S.; Wang, M. *Tetrahedron Lett.* **2016,** *57*, 1497-1501.

36. Huang, J.; Wang, K.; Gupta, S.; Wang, G.; Yang, C.; Mushrif, S. H.; Wang, M. *J. Polym. Sci., Part A: Polym. Chem.* **2016,** *54*, 2015-2031.

37. Jia-Xing, J.; Fabing, S.; Abbie, T.; D., W. C.; L., C. N.; Hongjun, N.; Calum, D.; Y., G. A.; J., R. M.; Z., K. Y.; I., C. A. *Angew. Chem. Int. Ed.* **2007,** *46*, 8574-8578.

38. Huo, L.; Hou, J.; Chen, H.-Y.; Zhang, S.; Jiang, Y.; Chen, T. L.; Yang, Y. *Macromolecules* **2009,** *42*, 6564-6571.

6. “Greener” and modular synthesis of triazine-based conjugated porous polymers via direct arylation polymerization: structure-function relationship and photocatalytic application

6.1 Introduction

Conjugated porous polymers (CPPs) represent an emerging type of multifunctional materials that combine microporosity and high surface areas with π-extended conjugation, making them ideal for versatile applications such as gas adsorption and separation,[1-2] catalysis[3] and energy storage[4-5]. CPPs have been largely synthesized by traditional transition-metal catalyzed reactions and a few linker-specific polycondensation reactions.[1, 6-9] Hence, a modular synthetic tool that allows facile incorporation of versatile building blocks with diverse chemical functionalities in the polymer network is highly desired.[9] From the synthesis of narrow bandgap CPPs in Chapter 4 and the construction of a series of thiophene-containing polymers in Chapter 5, we have established that direct arylation is one such synthetic tool for the efficient synthesis of CPPs. The use of thiophene-flanked building blocks has also been demonstrated as an effective strategy to incorporate a variety of functional monomers, which has allowed us to tune the optical, morphological and surface area characteristics of the resultant polymers.

Recently, 1,3,5-triazine-containing π-conjugated systems have been used as functional materials in a wide variety of applications due to their high electron deficiency, planar structure and more importantly, their high nitrogen content. Nitrogen doping has been demonstrated to enhance the supercapacitance of energy storage materials by improving the electrochemically active surfaces.[10-12] Recently, a covalent triazine framework (CTF) was used as a bipolar electrode in a sodium ion battery to achieve high specific energy densities up to 500 W h kg^{-1} over 7000 cycles.[13] Triazine-based porous organic polymers are also ideal candidates for selective CO_2 separation owing to the strong dipole-quadrupole

interactions between nitrogen and CO_2.[14-15] Porous nature and high electron affinity of triazine-based polymers make them efficient and inexpensive redox active catalysts for key reactions such as water splitting and some selective oxidation reactions.[16-17]

Despite the versatile applications of triazine-containing polymers in CO_2 capture,[15] energy storage[13] and catalysis,[17] these polymers have been most commonly synthesized under thermally and chemically harsh reaction conditions which are often energy intensive and require corrosive reagents. For instance, ionothermal[18] and solvothermal[19-20] cyclotrimerization of aryl nitriles has been used most commonly for the synthesis of triazine frameworks.[9, 21] Ionothermal reactions require high temperatures and stoichiometric amounts of $ZnCl_2$ which are difficult to remove from the polymer while solvothermal reactions are carried out in highly corrosive 'superacids' such as triflic acid. Other conventional C-C coupling reactions such as Sonogashira polymerization have also been reported by Cooper and co-workers for the synthesis of triazine-based CPPs, but such reaction schemes are limited to only ethynyl-containing monomers.[22] Recently Hayashi et. al. reported the synthesis of triazine-containing CPPs via direct arylation coupling between 2,4,6-tris(4-bromophenyl)-1,3,5-triazine and two fluoroarenes (1,2,4,5-tetrafluorobenzene and 1,3,5-trifluorobenzene), respectively. The resulting polymers showed moderate capacities for CO_2 uptake, albeit neither the optical and morphological characterization nor the photocatalytic applications of these polymers have been reported.[23]

We have been exploring a "greener" C-C coupling approach so called direct arylation polymerization (DAP) for facile synthesis of a broad scope of π-conjugated small molecules, linear donor-acceptor alternating copolymers, and 2D/3D networks.[24-33] In contrast to Suzuki coupling and Stille coupling, DAP does not require tedious pre-activation of C-H bonds in arene monomers, and does not involve flammable organometallic agents such as butyl lithium and highly toxic stannyl agents that are often used in Stille coupling. Nevertheless, DAP has been rarely used for synthesis of triazine-containing 2D/3D networks as a new type of π-conjugated porous polymers.

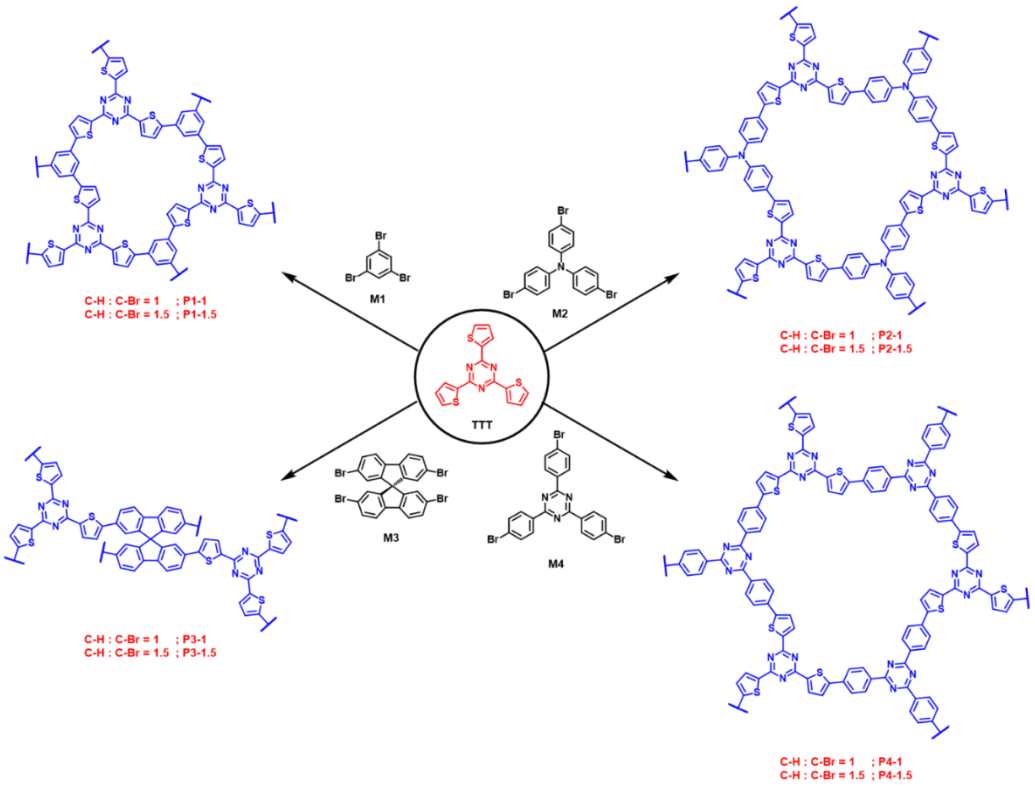

Scheme 6.1 Triazine-based conjugated porous polymers synthesized by direct arylation polymerization (DAP) with different monomers and stoichiometric ratios under a general reaction condition: $Pd_2(dba)_3$ (5 mol %), (o-$MeOC_6H_4)_3P$ (10 mol %), PivOH (0.5 eq), K_2CO_3 (3 eq), o-xylene (0.2 M), 120 °C, 48 h.

In this chapter, we present the synthesis and characterization of a new series of triazine-core polymers (**Scheme 6.1**) through direct arylation polymerization of 2,4,6-(tri-2-thienyl)-1,3,5-triazine (**TTT**) (A_3 type) and multi-topic brominated monomers (B_3 and B_4 type). **TTT** is a star-shaped molecule consisting of a triazine core and three thiophene groups on the 2, 4 and 6 positions which provide the active C-H bonds for direct arylation. Much like **TTD** (Chapter 4), **BT**, **DTBT** and **DPP** (Chapter 5), the functional unit of **TTT** – triazine is flanked by thiophene moieties which make triazine more accessible via direct arylation. The planarity of **TTT** also promotes the extended π-conjugation in CPPs.[34] We expected to establish a structure-function relationship of these triazine-containing CPPs by rational choice of the monomers and examination of the following two effects: 1) The effect of the different geometries and electronic

structures of aryl bromides; 2) The effect of varying the molar ratio of a given aryl bromide on the properties of the resultant polymers. Morphology of the CPPs is greatly influenced by the monomers and varies from nanofiber bundles to featureless aggregates. The BET specific surface areas of the polymers range from 43 to 222 m^2 g^{-1}. We also found that the optical and electrochemical properties could be tuned by rational selection of monomers, but the band structures remained invariant within the same family of polymers irrespective of the monomer ratio used. Triazine-based CPPs were used as catalysts for the visible-light catalysed oxidation of benzylamine. Polymers containing the highest fraction of triazine units showed the highest conversion (99% for **P4-1**) at relatively lower catalyst loadings and reaction times as short as 5 hours.

6.2 Molecular design of building blocks and synthesis of CPPs

As mentioned in Introduction, we chose 2,4,6-(tri-2-thienyl)-1,3,5-triazine (**TTT**) as the essential monomer to introduce the triazine moiety in the multidimensional polymeric network, due to the presence of reactive C-H bonds in the thiophene units. The inherent planarity of **TTT** promotes donor-acceptor interaction between thiophene and triazine and consequently enhances π-conjugation in the polymer network.[34] Due to the relatively poor reactivity of aryl chlorides under certain conditions of direct arylation,[35-36] we synthesized **TTT** via an established route of Stille coupling[34] using cyanuric chloride and 2-(tributylstannyl)thiophene instead of direct arylation. At the same time we note that **TTT** can be also synthesized through other routes such as the cyclotrimerization of 2-thiophenecarbonitrile in the presence of triflic acid.[37-38] Tritopic (**M1**, **M2** and **M4)** and tetratopic (**M3**) aryl bromides were used as comonomers for **TTT** in the direct arylation scheme. Their extended aromatic structures are most suited for the formation of rigid polymer networks.[1] Moreover, these aryl bromides have been successfully employed in the synthesis of several conjugated microporous polymers.[22, 39]

A schematic presentation of the network structures of triazine CPPs, in particular **P1**-, **P2**- and **P4**-type CPPs, is given in **Scheme 6.1**. It should be noted that the actual conformation of the polymer network may be different due to the

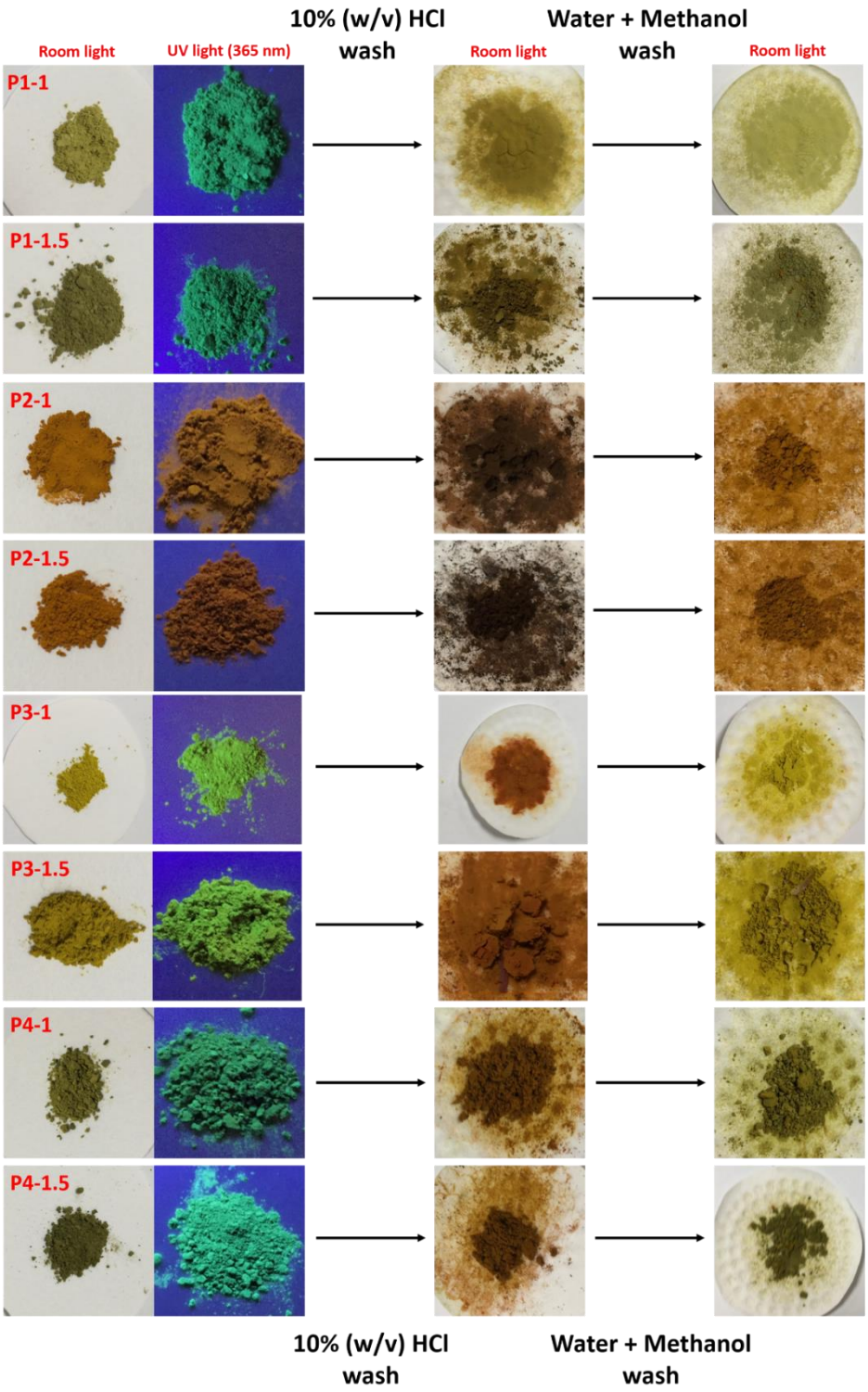

Figure 6.1 Digital images of pristine polymers under room light and UV (365 nm) light (left column); after washing with 10% (w/v) HCl (center column) and after washing with water and methanol (right column).

lack of long-range order in CPPs, particularly for **P3** due to the twisted configuration in the spirobifluorene unit.

Direct arylation synthesis for triazine-core CPPs was carried out using reaction conditions that were optimized for benzo[1,2-*b*:4,5-*b*']dithiophene-based linear polymers[33] and have been used for synthesizing a variety of linear[24, 28-30, 32] and 2D/3D conjugated networks.[25, 27] $Pd_2(dba)_3$/(*o*- $MeOC_6H_4)_3P$ was used as the catalyst/ligand system together with pivalic acid as a proton shuttle[40] and K_2CO_3 as the base. More details of the polymerizations are described in the Experimental section. All the polymers were obtained as insoluble solids that precipitated out of the reaction media. Washing with 10% (w/v) HCl caused color change of the polymers which could be reversed by washing with water and methanol (**Figure 6.1**). Such pH-responsive color change could be attributed to the protonation of the triazine ring which leads to a bathochromic shift of the absorption edge.[41] Two series of triazine polymers were synthesized by varying the ratio of the C-H and C-Br bonds. In the PX-1 series, a molar ratio of C-H:C-Br = 1:1 is maintained between **TTT** and the corresponding brominated comonomer (X-Br) whereas the ratio is increased to 1.5:1 in the PX-1.5 series. Effect of varying monomer ratio is evident from the elemental analyses of the polymers. For instance, increasing the C-H:C-Br ratio from 1:1 to 1.5:1 results in an expected increase in the nitrogen content from 8.6% in **P1-1** to 9.6% in **P1-1.5**.

6.3 Structural characterization of CPPs

Incorporation of monomers in the polymer networks was confirmed by FTIR spectroscopy. Stretching vibrations around 1500, 1370 and 800 cm^{-1} were observed in IR spectra of all polymers (**Figure 6.2**) which are characteristic of the triazine moiety in **TTT**. Characteristic bands of thiophene in **TTT** can also be seen at 1030, 860 and 712 cm^{-1} in the spectra of all polymers, but at a slightly smaller wavenumber due to extended conjugation in the polymers. Attenuation of the aromatic C-Br band occurring in the IR spectra of polymers suggest the high degree of polymerization after the direct arylation cross-coupling. Effect of varying monomer ratios was not evident from the FTIR spectra of PX-1 and PX-

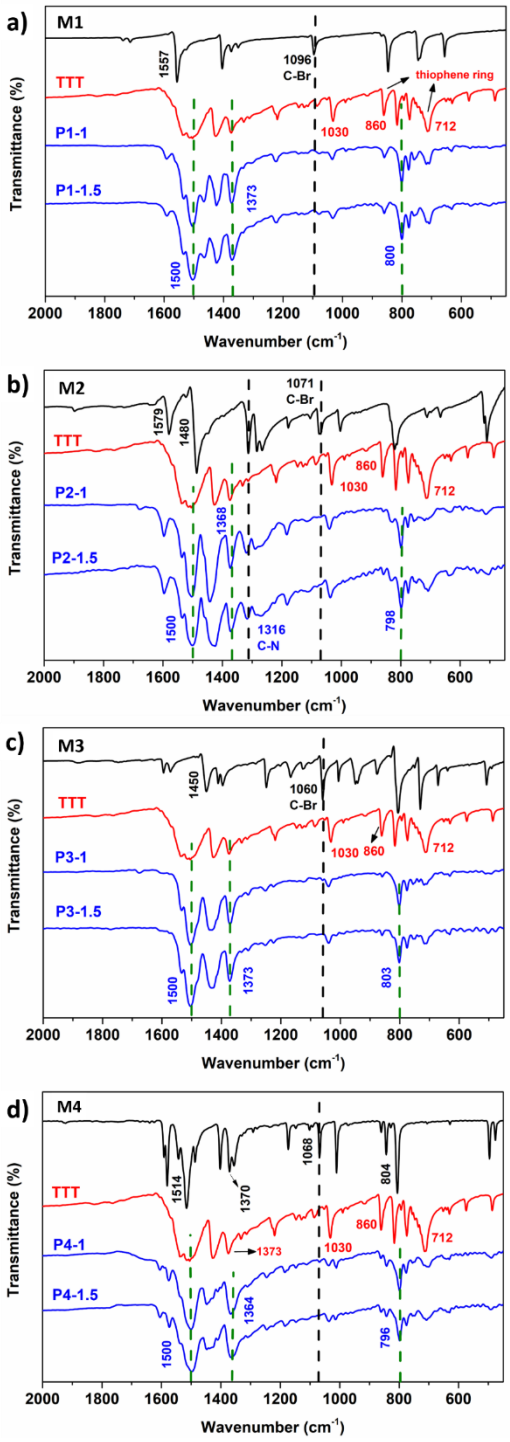

Figure 6.2 Comparison of the fingerprint region of FTIR spectra of a) **P1**, b) **P2**, c) **P3** and d) **P4** type triazine-core CPPs (blue) and their constituent monomers.

1.5 polymers since the intensity of the characteristic triazine bands (green dotted line) are comparable.

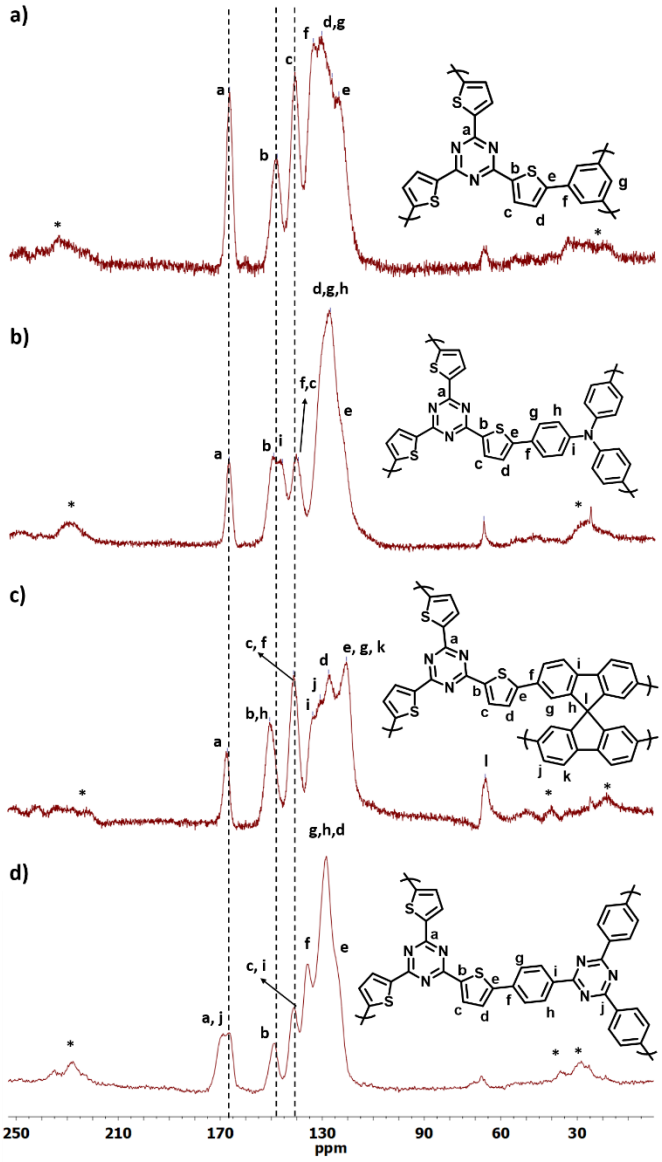

Figure 6.3 Solid-state ^{13}C/MAS NMR spectra of a) **P1-1**, b) **P2-1**, c) **P3-1** and d) **P4-1.** Peaks marked with * correspond to spinning sidebands.

CPPs synthesized with a C-H:C-Br ratio of 1:1, i.e. **P1-1**, **P2-1**, **P3-1** and **P4-1** were chosen as representative polymers for structural analysis by solid-state CP/MAS ^{13}C-NMR spectroscopy (**Figure 6.3**). The peak corresponding to the carbon in the triazine ring appears consistently at 167 ppm in all polymers. The thiophene-C adjacent to the triazine ring appears between 148 and 151 ppm while the peak corresponding to the α-carbon of the trithienyltriazine (**TTT**) unit

appears between 139 and 141 ppm. The peak of α-carbon of the phenyl unit in **P1-1** (**Figure 6.3a**) appears at 134 ppm while the peak of non-substituted carbons (2,4,6- positions) in the phenyl unit overlaps with the peak of non-substituted β-carbon of the trithienyltriazine unit at 126.7 ppm. The peak of the C-N carbon in the triphenylamine unit of **P2-1** (**Figure 6.3b**) appears at 146 ppm and the peak of the α-carbon overlaps with the α-carbon of the **TTT** unit at 140 ppm. In the NMR spectrum of **P3-1** (**Figure 6.3c**), the peak at 65 ppm can be assigned to the sp^3 carbon of the spirobifluorene moiety while the broad peak between 120 and 140 ppm is assigned to the remaining carbons of spirobifluorene. Peaks from both triazine units in the spectrum of **P4-1** were also successfully assigned (**Figure 6.3d**). These NMR spectra, together with the FTIR spectra (**Figure 6.2**) described earlier, confirm the chemical structures of the resulting target polymers.

6.4 Thermal properties

Thermal stability of the polymers synthesized above was tested by thermogravimetric analyses (**Figure 6.4a-d**). All the polymers are stable up to 350 ^oC after which significant mass loss (> 5%) occurs. Even at 700 ^oC, triazine-core CPPs retain more than 50% mass, indicating very high thermal stability which is characteristic of such covalently linked conjugated networks. The powder X-ray diffraction (PXRD) patterns of triazine CPPs (**Figure 6.4e-h**) show broad peaks in the range of $2\theta = 10^o - 25^o$, which indicates their amorphous nature. Interestingly, sharp peaks at 28^o and 40^o were observed in the PXRD patterns of **P4-1**. These peaks could correspond to the ordered arrangement of two adjacent two-dimensional polymer domains.[42]

6.5 Morphological characterization of CPPs

We studied morphologies of **P1**-**P4** polymers with scanning electron microscopy (SEM) and transmission electron microscopy (TEM). The effect of monomer ratio on the morphologies is most significant for triazine CPPs containing phenyl (**P1-1**, **P1-1.5**) and triphenylamine (**P2-1**, **P2-1.5**) groups. For instance, **P1-1** (**Figure 6.5a**) exhibits short and irregular fibres with an

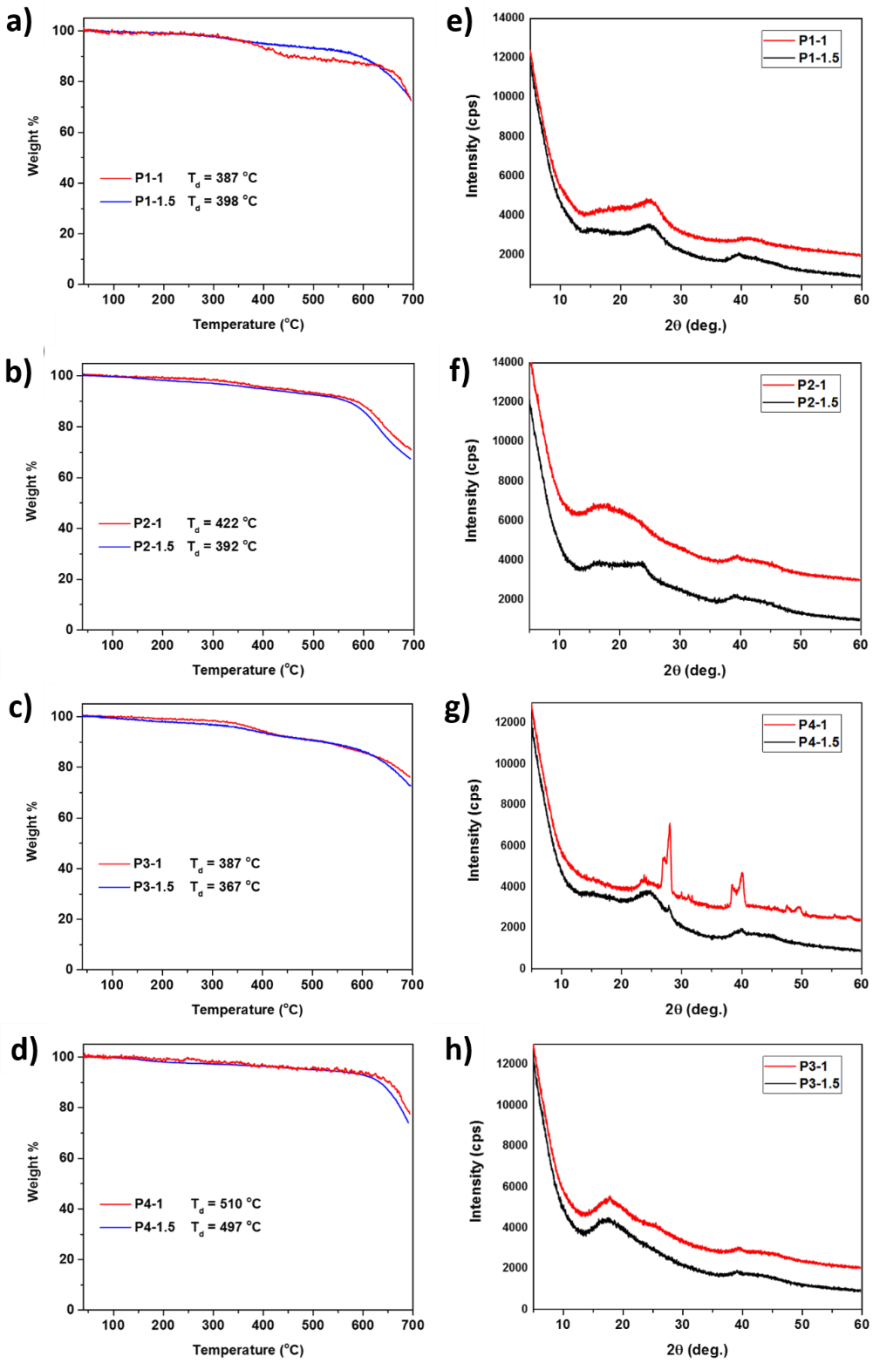

Figure 6.4 TGA plots (a-d) and powder X-ray diffraction patterns (e-h) of triazine polymers synthesized by direct arylation.

approximate width of 20-30 nm that are clearly visible from the TEM image (**Figure 6.5b**). In contrast, fibres of **P1-1.5** (**Figure 6.5c**) are longer and thinner (~15 nm) than those of **P1-1** and seem to be well dispersed. Interestingly, one

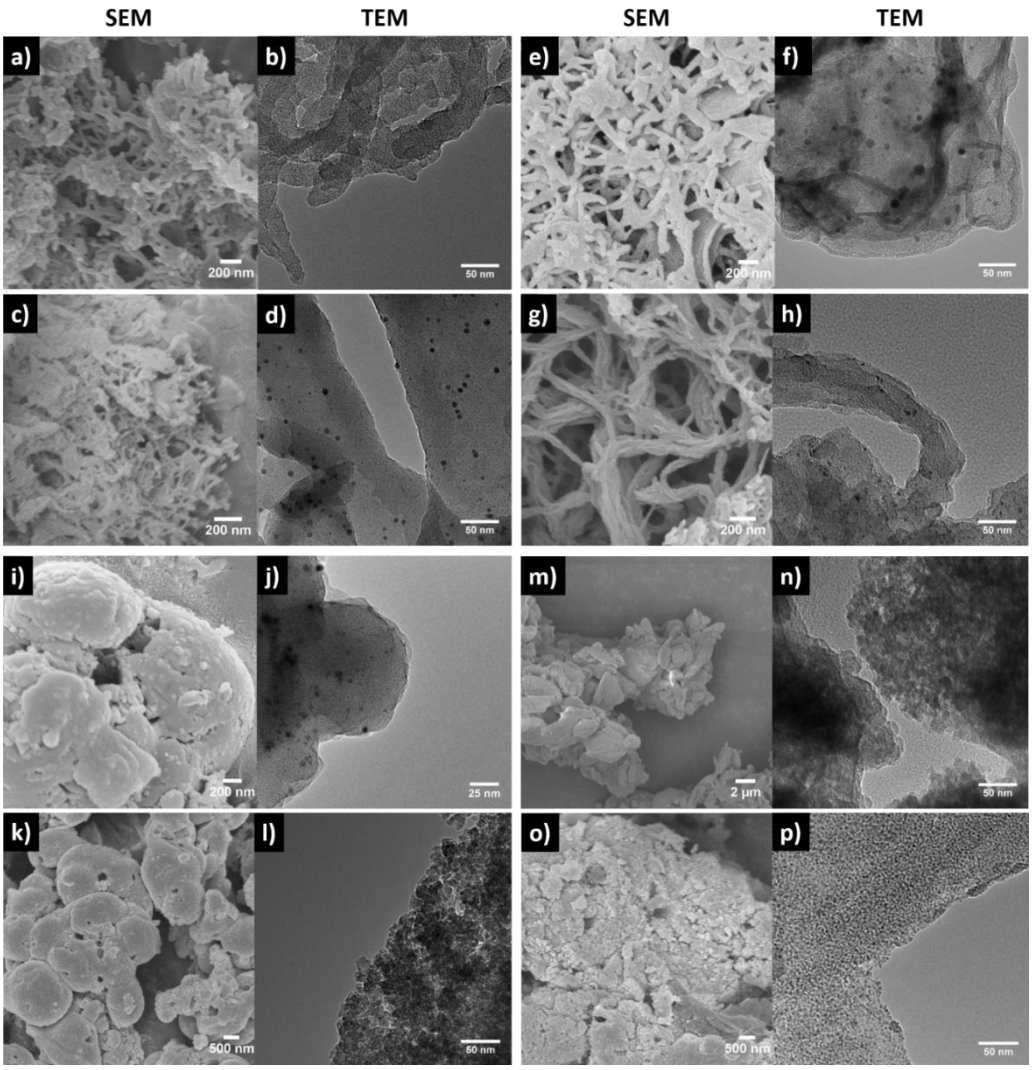

Figure 6.5 SEM (column 1 and 3) and TEM (column 2 and 4) images of **P1-1** (a, b), **P1-1.5** (c, d), **P2-1** (e, f), **P2-1.5** (g, h), **P3-1** (i, j), **P3-1.5** (k, l), **P4-1** (m, n) and **P4-1.5** (o, p).

can see some tiny spherical nanoparticles with an average diameter around 5 nm, which are well dispersed in the polymeric matrices of **P1-1.5** (**Figure 6.5d**). Similar nanoparticles can also be observed in TEM micrographs of **P2-1 (Figure 6.5f)**, **P2-1.5 (Figure 6.5h)** and **P3-1 (Figure 6.5j)**. These nanoparticles presumably correspond to the residual palladium (Pd) catalyst from the DAP reaction. A similar result was reported by both Cooper's group[43] and Yu's

group[42] where residual Pd from Suzuki polycondensation was quantified and the metallic particles in the TEM were attributed to Pd.

P2-1 (**Figure 6.5e**) under SEM appears as an aggregation of short, flat and non-uniform strips approximately 100 nm thick. In comparison, **P2-1.5** (**Figure 6.5g**) exists as an entwined network of relatively thin and uniform fibres. Moreover, each individual fibre of **P2-1.5** appears to be composed of even thinner thread-like structures (~20 nm) bundled together (**Figure 6.5h**). The evolution of **P2-1.5** nano-fibres was also studied as a function of reaction time and is detailed in the next section.

The effect of monomer ratio is negligible in polymers containing spirobifluorene units (**Figure 6.5i and 6.5k**) - which appear as irregular semi-spheroids with uneven surfaces and microscopic pores. **P4-1** appears as non-uniform aggregates of particles with no characteristic morphology. It is interesting to note that, even though **P1**, **P2** and **P4** polymers have been synthesized from A_3+B_3 type building blocks, only **P1** (**P1-1**, **P1-1.5**) and **P2** (**P2-1**, **P2-1.5**) polymers show distinct fibre like morphologies. Hence, it is difficult to predict the morphology based on the geometry of the monomers alone.

6.6 Morphological evolution of P2-1.5 and effect of reaction solvent

Morphology of **P2-1.5** was found to be an intricate network of relatively uniform nano-fibers. Such morphology has been rarely observed for amorphous conjugated polymer networks synthesized by Pd-catalyzed polycondensation reactions. To investigate the formation of these fibers, **P2-1.5** was synthesized with various reaction times and the morphology of the polymers thus obtained was monitored by SEM. **Figure 6.6** shows the SEM images of **P2-1.5** synthesized under similar reaction conditions as reported earlier but with different reaction periods. From the SEM images, it is evident that the length and uniformity of the fibers increases as the reaction time is increased. **P2-1.5** synthesized for 3 hours (**Figure 6.6a**) contains short fibers mixed with some featureless irregular domains. No significant change of the morphology was observed when the reaction time was increased from 3 to 6 hours (**Figure 6.6b**). One can observe

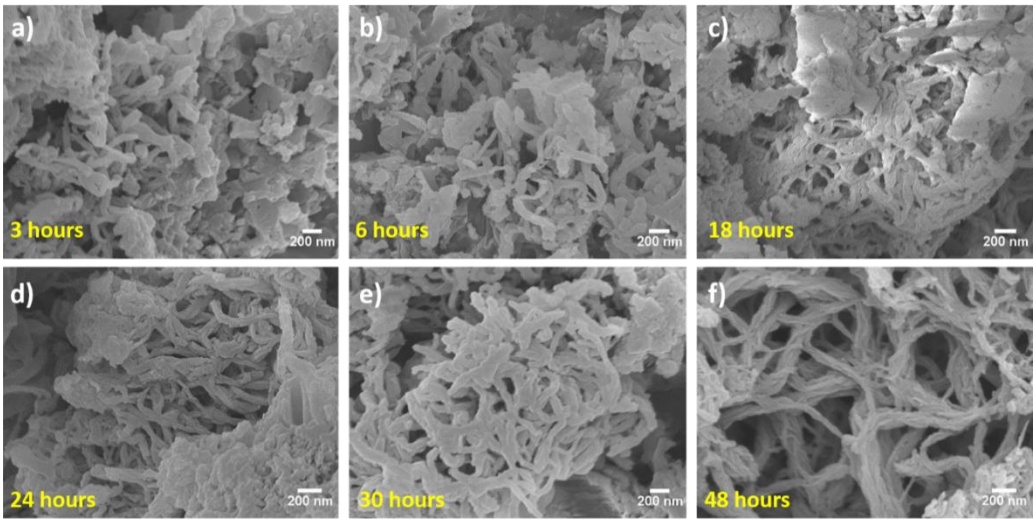

Figure 6.6 SEM images of **P2-1.5** synthesized at reaction times of a) 3, b) 6, c) 18, d) 24 and e) 30 hours. f) SEM image of **P2-1.5** obtained after a complete reaction time of 48 hours (same as **Figure 6.5g**).

relatively longer fibers in **P2-1.5** synthesized over 18 hours (**Figure 6.6c**) than that obtained after 3 hours, accompanied by some featureless structures. After 24 hours, the average length of the fibers slightly increases as compared to **P2-1.5** synthesized after 18 hours. After 30 hours, the fibers obtained are uniform in shape and the individual fibers are distinguishable.

To understand the effect of reaction medium on the morphology of **P2-1.5**, polymerization was also carried out in chloroform (CF), tetrahydrofuran (THF) and *o*-dichlorobenzene (DCB) as the reaction media respectively. Reactions in CF and THF were carried at 80 ^{o}C whereas the reaction in DCB was carried out at 120 ^{o}C. All other reaction conditions were kept the same. **P2-1.5_CF** (**Figure 6.7a**) and **P2-1.5_THF** (**Figure 6.7b**) show fiber-like morphologies similar to **P2-1.5** synthesized in *o*-xylene (**Figure 6.5g**). Moreover, the FTIR spectra of **P2-1.5_CF** (**Figure 6.7d**) and **P2-1.5_THF** (**Figure 6.7e**) did not show any sign of unreacted C-Br bonds. These results suggest that the morphology of **P2-1.5** remains uninfluenced over a small range of solvent polarity and even reaction temperature. In contrast, **P2-1.5_DCB** exhibits an uncharacteristic morphology without nanoscale features (**Figure 6.7c**). This

could be a result of the undesired activation of C-Cl bonds of DCB under direct arylation conditions which alters the chemical structure and the resulting morphology of the polymer. To examine this hypothesis, a test reaction between **TTT** and DCBs was carried out by excluding **M2** from the synthesis of **P2-1.5_DCB** while keeping other conditions the same. After 24 hours, three highly

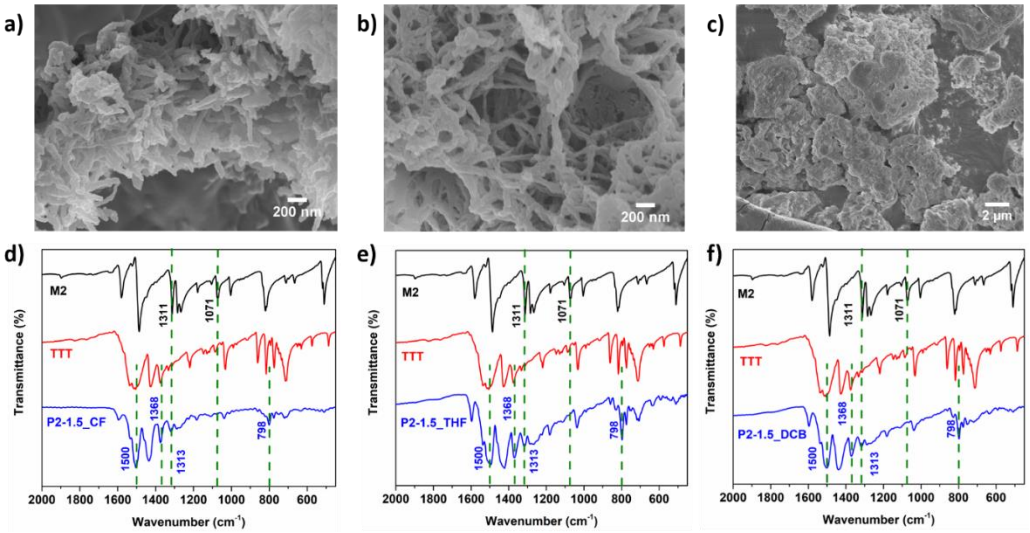

Figure 6.7 SEM images (a-c) and FTIR spectra (d-e) of **P2-1.5** synthesized in chloroform (a, d), tetrahydrofuran (b, e) and dichlorobenzene (c, f).

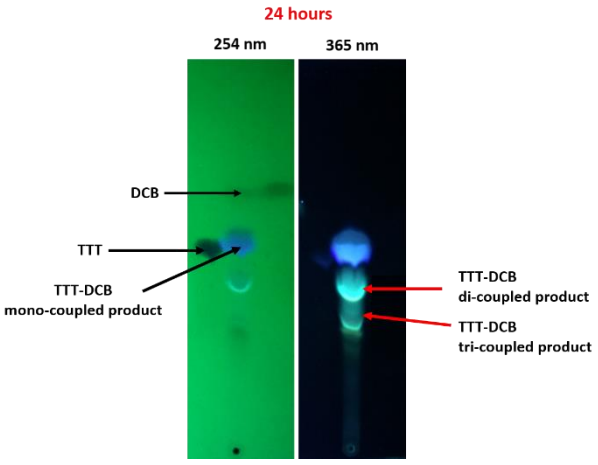

Figure 6.8 TLC results of TTT-DCB coupling reaction after 24 hours under 254 nm (left) and 365 nm (right) UV light.

fluorescent spots were observed on the TLC (**Figure 6.8**), which were assigned as mono-, di-, and tri-coupled products of TTT and DCB. These results indicate that TTT-DCB side reactions are indeed possible in the synthesis of **P2-1.5_DCB**.

6.7 Gas Sorption and Porosity

Polymer surface areas and pore size distributions were measured by nitrogen adsorption and desorption at 77.3 K. All polymers exhibited a Type II adsorption isotherm and a broad pore size distribution. A summary of gas adsorption characteristics of triazine polymers is presented in **Table 6.1**. Polymers **P1-1** and **P1-1.5** showed similar adsorption behaviour in the low-pressure region (**Figure 6.9a**). A sudden rise in gas uptake is observed for both **P1-1** and **P1-1.5** which is characteristic of Type II behaviour. However, a higher volume is adsorbed by **P1-1.5** than **P1-1** at $p/p_o \sim 0.99$. Pore size distribution of **P1-1** (**Figure 6.9b**) suggests small populations of mesopores and micropores. In contrast, the distribution in **P1-1.5** is relatively narrower and focused in the mesopore region. Unlike **P1** polymers, the adsorption isotherms of **P2-1** and **P2-1.5** (**Figure 6.9c**) are significantly different. **P2-1** exhibits a steady increase in gas uptake as the relative pressure increases in the adsorption cycle. Strong H3 type hysteresis is observed in the desorption cycle which persists even at relatively low pressures and ends in an open loop. This could possibly be a consequence of strong interaction of N_2 with the polymer surface or swelling of the polymers network. A similar trend is observed in **P2-1.5** although the hysteresis is relatively weaker compared to **P2-1**. Gas uptake of **P2-1.5** is also relatively lower over the entire pressure range. As a result, BET surface area of **P2-1** (195 $m^2 g^{-1}$) is significantly higher than that of **P2-1.5** (43.3 $m^2 g^{-1}$). On the other hand, **P2-1.5** exhibits a multimodal distribution over the mesopore range which extends into the macropore region (**Figure 6.9d**). Polymers **P3-1** and **P3-1.5** both exhibit strong hysteresis in the desorption cycle. Both polymers have open loop isotherms which are indicative of expansion/swelling of the polymer network as seen in **P2-1**. BET surface areas of **P3-1** and **P3-1.5** are 210 and 162 $m^2 g^{-1}$, respectively. Polymers **P4-1** and **P4-1.5** exhibit higher gas uptake over

the entire pressure range compared to other triazine CPPs in this work as is evident from their isotherms. Both polymers exhibit hysteresis over the entire pressure range. The desorption profile of **P4-1** runs parallel to the adsorption

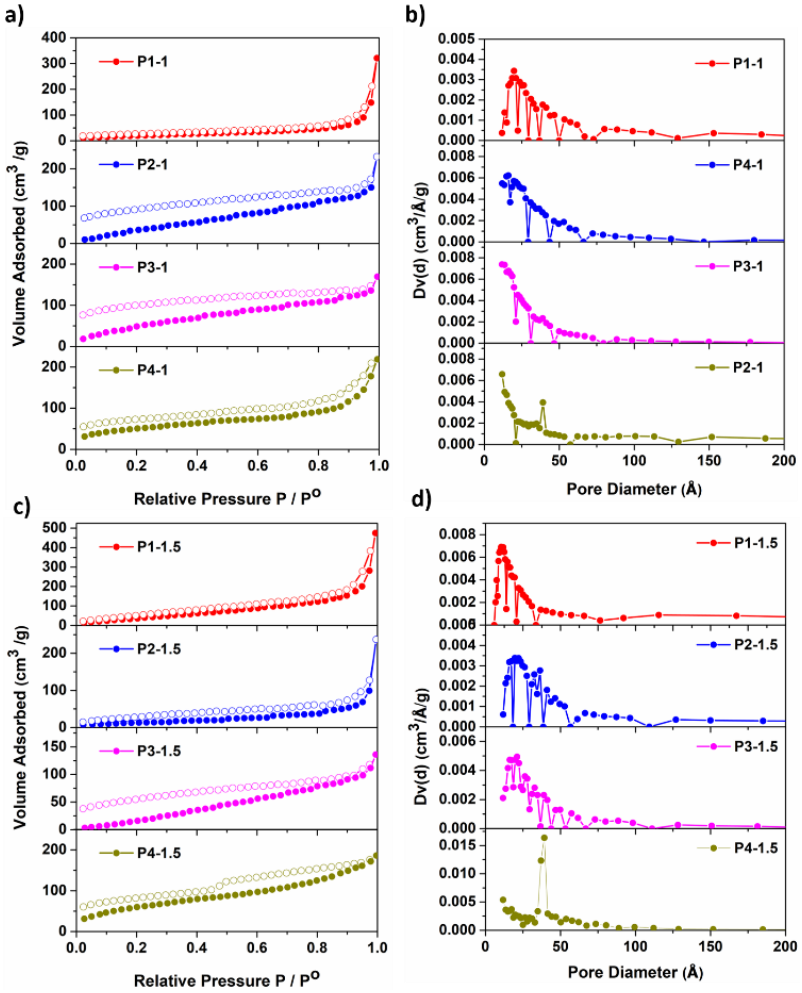

Figure 6.9 Comparison of N_2 adsorption isotherms (a, c) and pore size distributions calculated from BJH desorption model (b, d) of triazine CPPs synthesized in a C-H:C-Br ratio of 1:1 (a, b) and 1:1.5 (c, d). The dark and open circles in a) and c) represent the adsorption and desorption cycles respectively.

curve, suggesting slit like pores in the polymer that irreversibly expand due to N_2 adsorption. **P4-1.5** exhibits a distinguishable H4 type hysteresis in the high-pressure range, indicating pores with narrow openings (ink-bottle shaped) which require higher energy to be completely vacated in the desorption cycle.

Table 6.1 Adsorption characteristics of triazine-based CPPs

	S.A. $_{BET}$ ($m^2 g^{-1}$) [a]	**S.A.** $_{Langmuir}$ ($m^2 g^{-1}$) [b]	**Pore Size BJH** (nm)	**Total Pore Volume** ($cm^3 g^{-1}$) [c]
P1-1	74.9	124	1.7, 3.9	0.496
P1-1.5	192.8	514	1.5, 2.3, 3.1	0.734
P2-1	195	565	1.9, 3.1, 5.1	0.359
P2-1.5	43.3	52.7	1.6, 2.2, 3.7	0.367
P3-1	210.6	457	1.2, 2.3, 3.7	0.262
P3-1.5	162	100	1.6, 2.1	0.210
P4-1	162.4	276	3.8	0.372
P4-1.5	222	412	3.9	0.278

[a] Specific surface area calculated from the adsorption branch of the N_2 isotherm using the BET method. [b] Specific surface area calculated from the adsorption branch of the N_2 isotherm using the Langmuir method. [c] calculated at $p/p_o = 0.99$.

Comparison of the BET specific surface areas of all polymers (**Table 6.1**) reveals that changing the monomer ratio does not necessarily lead to an increase in surface area of the polymer. For instance, BET surface areas of **P4-1** and **P4-1.5** are 162 and 222 $m^2 g^{-1}$, respectively. This contrasts with the trend observed by Cooper and coworkers, wherein increasing the ratio of ethynyl to bromide monomers in Sonogashira polymerization schemes led to systematic improvement in porosity.[44] We also expected the pore sizes of **P1-**, **P2-** and **P4-**type CPPs to increase systematically with increasing size of their monomers (phenyl < triphenylamine < triphenyltriazine) but no apparent increase in pore size could be observed. In fact, **P1-** and **P2-**type polymers show very similar multi-modal behaviour with significant populations at 2.2 nm whereas the pore size distribution of **P4-**type polymers is centred at 3.8 nm. These results, along with the low surface areas of triazine core CPPs, can be attributed to the formation of closely packed networks in the direct arylation reaction which leads

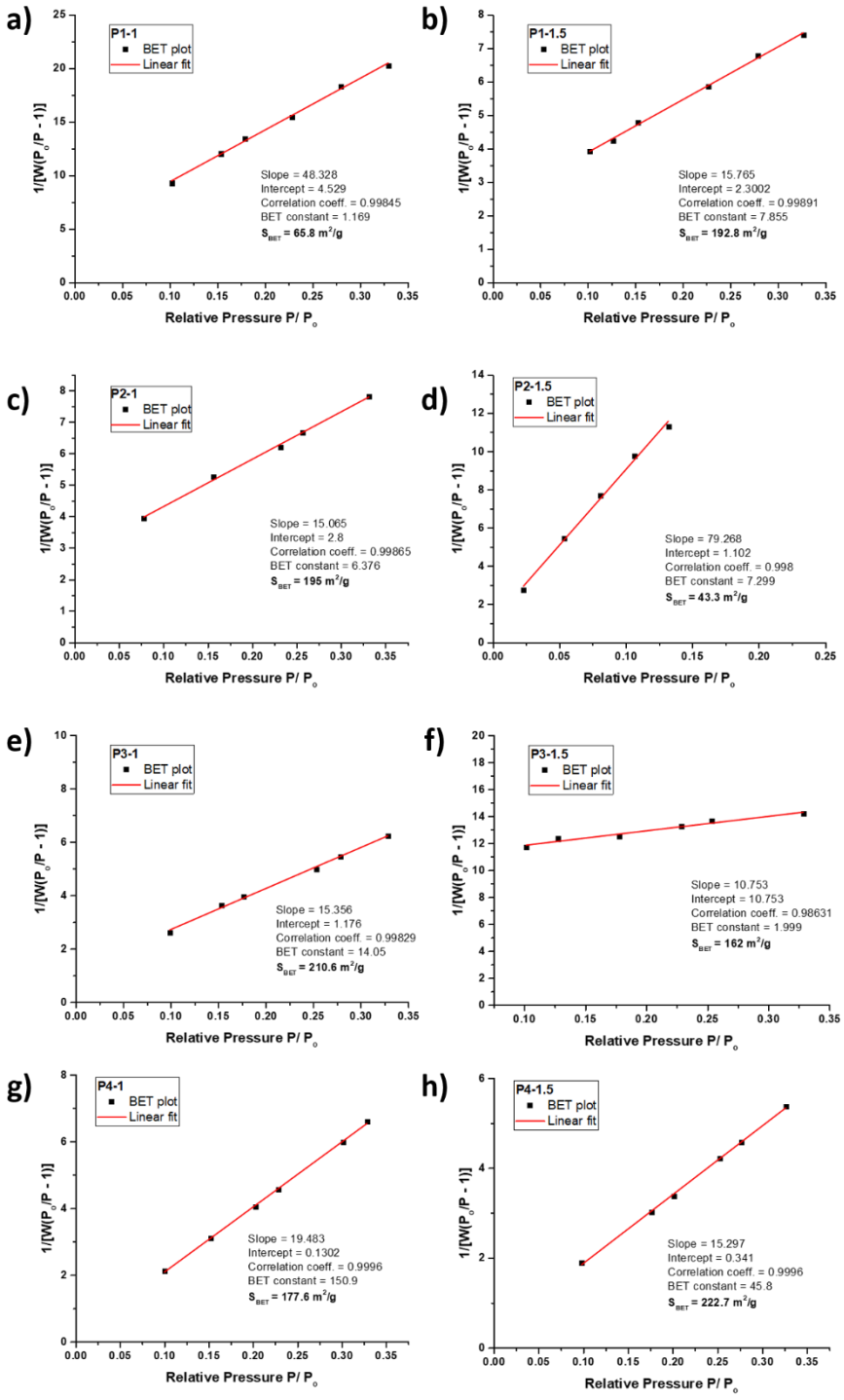

Figure 6.10 BET specific surface area plots of triazine-based CPPs.

to interpenetration of the polymer chains in the pores therefore inhibiting the accessibility of the microporous structures to sorbents such as N_2 gas.

A facile method for enhancing the porosity of network polymers is the use of porous silica supports. Recently, Huang and co-workers reported the cyclotrimerization synthesis of a covalent triazine framework with **TTT** as the repeating unit, by coating the monomers on mesoporous silica.[45] BET surfaces areas of 543 $m^2 g^{-1}$ were obtained but the surface areas dropped to 57 $m^2 g^{-1}$ once the silica support was removed. Kim et. al. reported that the porosity of conjugated microporous polymers synthesized by Sonogashira coupling could be enhanced by choosing ligands with appropriate cone angles.[46] This strategy may not be feasible for direct arylation polymerization since changing the ligand could render the reaction condition ineffective and optimization of new DAP conditions with new catalyst/ligand pairs can be tedious. Another potentially effective strategy to improve the porosity of CPPs would be to choose monomers with rigid conformations which impart long range order to the polymer network.[47]

6.8 Optical and Electrochemical properties

The optical properties of triazine CPPs were studied by diffuse-reflectance UV-vis spectroscopy (**Figure 6.11a**) and fluorescence spectroscopy (**Figure 6.11b**). All triazine polymers show strong absorption between 300 and 500 nm and the optical bandgaps lie between 2.17 and 2.53 eV (**Table 6.2**). From the UV-Vis absorption and fluorescence spectra, it is evident that the absorption edge and emission maxima of triazine polymers synthesized using a C-H:C-Br ratio of 1:1 do not differ significantly from those synthesized using a ratio of 1.5. The optical bandgaps of triazine CPPs follow the order **P1** > **P4** > **P3** > **P2**, which is consistent with the increasing strength of electron donating groups of the comonomers described in **Scheme 6.1** (**M1** < **M4** < **M3** < **M2**). Hence, a rational choice of monomers allows for facile and systematic tuning of the optical properties of CPPs which are crucial to their application in photocatalysis. Oxidation potentials and the HOMO/LUMO energy levels of the CPPs were determined by cyclic voltammetry (**Figure 6.12**). HOMO levels of CPPs lie in between -5.51 and -6.32 eV. As expected, the highest HOMO levels were obtained for **P2-1** (-5.51 eV) and **P2-1.5** (-5.66 eV) due to the presence of strongest electron donor – triphenylamine, in the polymer structure.

6.9 Photocatalytic activity

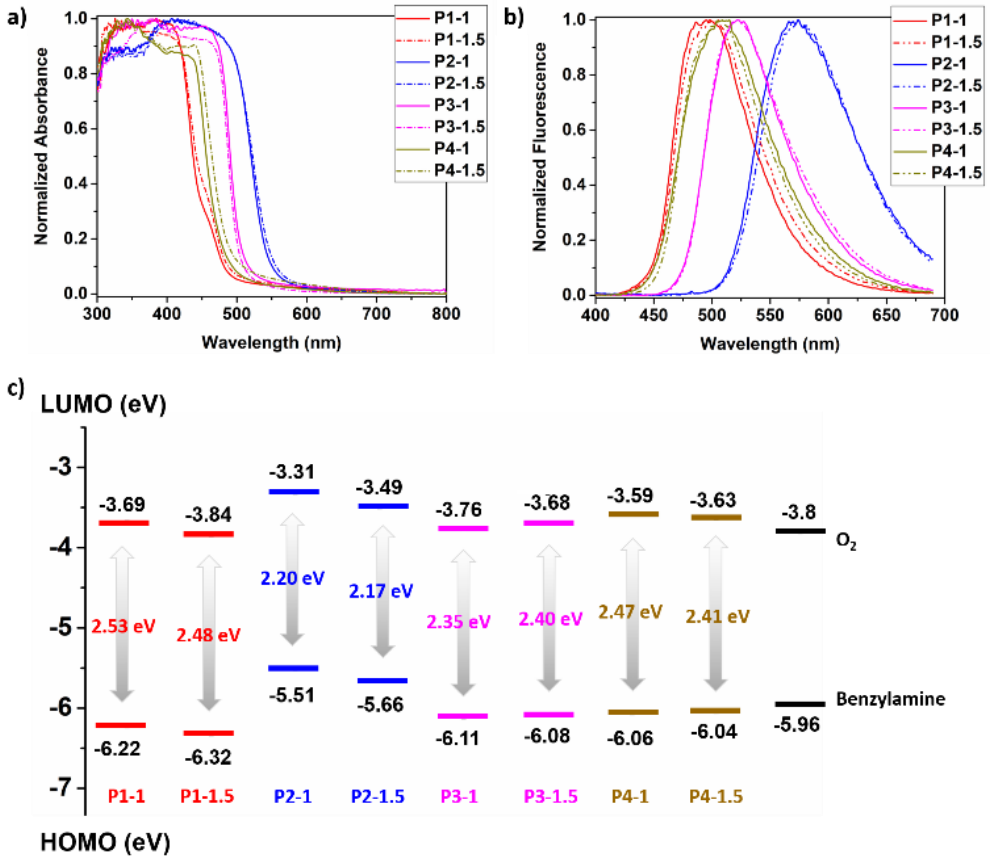

Figure 6.11 a) Diffuse reflectance UV-Vis and b) fluorescence spectra of triazine-based conjugated porous polymers. c) Schematic representation of the HOMO/LUMO energy levels of triazine-core CPPs. HOMO level of benzylamine and LUMO level of O_2 are presented for comparison.

Imine chemistry is integral to synthesis of precursors for N-heterocyclic compounds and intermediates via non-toxic reagents in the pharmaceutical industry.[48-50] Only few metal-free catalysts have been reported for oxidation of benzylamine.[51-58] Moreover, the established mechanism of this reaction makes it a facile model for demonstration of photocatalytic activity. Here, we examined the application of the triazine-core CPPs synthesized and characterized above to catalyse the selective oxidation of benzylamine under light irradiation.

Table 6.2 Summary of optical and electrochemical properties of triazine-based CPPs.

Polymer	λ_{edge}^{abs} (nm)	λ_{max}^{em} (nm)	E_{eg}^{opt} (eV) [a]	E_{ox}^{onset} (V) [b]	E_{HOMO} (eV) [c]	E_{LUMO} (eV) [d]
P1-1	489	495	2.53	1.42	-6.22	-3.69
P1-1.5	498	504	2.48	1.52	-6.32	-3.84
P2-1	563	569	2.20	0.71	-5.51	-3.31
P2-1.5	570	574	2.17	0.86	-5.66	-3.49
P3-1	527	523	2.35	1.31	-6.11	-3.76
P3-1.5	515	520	2.40	1.28	-6.08	-3.68
P4-1	500	507	2.47	1.26	-6.06	-3.59
P4-1.5	514	507	2.41	1.24	-6.04	-3.63

[a] Calculated from the absorption onset. [b] Potentials vs Ag/Ag^+ determined by cyclic voltammetry by using 0.1 M tetrabutylammonium hexafluorophosphate (Bu_4NPF_6) in acetonitrile as the supporting electrolyte. [c] $E_{HOMO} = -[E_{ox}^{onset} + 4.8]$ eV. [d] $E_{LUMO} = [E_{HOMO} + E_{eg}^{opt}]$ eV.

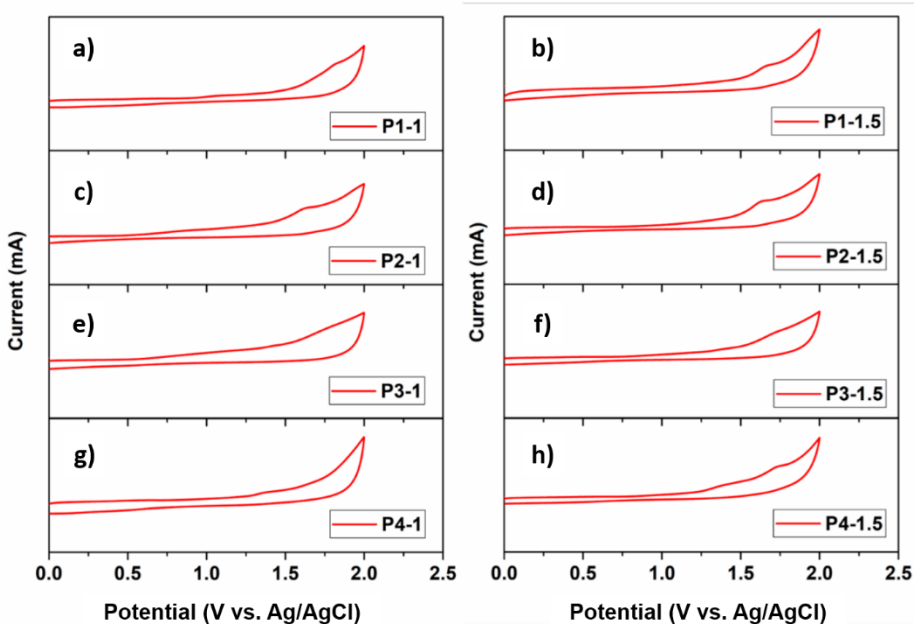

Figure 6.12 Cyclic voltammograms of a) **P1-1**, b) **P1-1.5**, c) **P2-1**, d) **P2-1.5**, e) **P3-1**, f) **P3-1.5**, g) **P4-1** and h) **P4-1.5**.

Table 6.3 Photocatalyzed oxidative coupling of benzylamine by triazine-based CPPs.

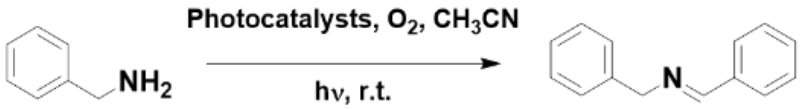

Photocatalyst [a]	Reaction time (hrs)	Conversion [b]
P4-1	3	68%
P4-1	5	> 99%
P4-1*	5	99%
P4-1.5	5	94%
P3-1	5	88%
P3-1.5	5	86%
P2-1	5	37%
P2-1.5	5	45%
P1-1	5	80%
P1-1.5	5	55%

[a] Reaction Conditions: 6 mg of polymer and 1 mmol of benzylamine were added to 3 mL of CH_3CN. Mixture was bubbled with O_2 and irradiated with 20 W white LED light. [b] Conversion was determined by ^{1}H-NMR.

with **P4-1** as the photocatalyst and a reaction time of 3 hours, the conversion was found to be 68%. When the reaction time was increased to 5 hours, complete conversion of benzylamine was achieved although traces of an over oxidised product, benzaldehyde were observed in the NMR spectrum (**Figure 6.13**). **P4-1** in comparison to reported photocatalysts showed a remarkable photocatalytic performance of complete conversion at a relatively lower catalyst loading,[56-57] in shorter reaction times[55] and by using low-power light sources.[54] Similar reaction conditions were used for photocatalysis trials with **P4-1.5** and the remaining (**P3**, **P2** and **P1** type) polymers. Among all the polymers tested here as the photocatalyst, **P4-1** and **P4-1.5** give the highest conversion (> 90%). Stability of **P4-1** was tested by recycling the catalyst over 5 photocatalytic cycles.

Conversion upto 80% could be obtained from the 5th cycle, indicating the good reusability of **P4-1** in the photocatalytic reaction (**Figure 6.14d**).

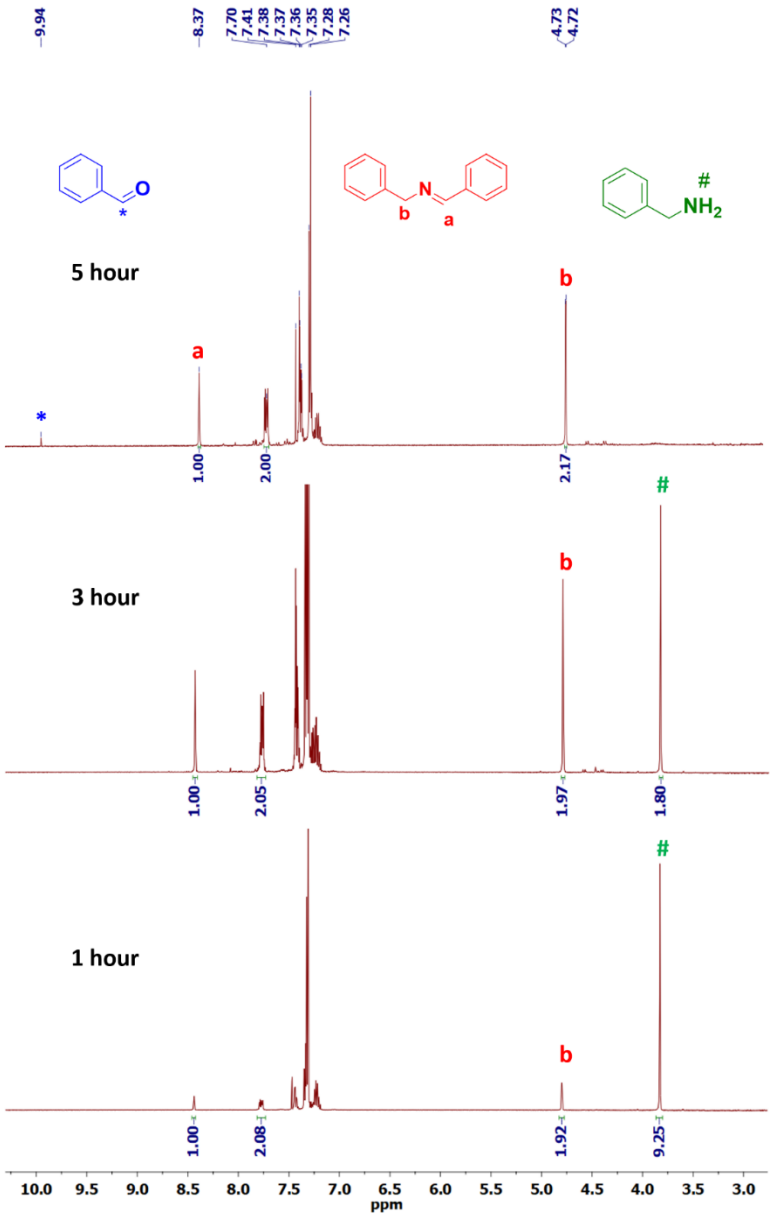

Figure 6.13 ^{1}H-NMR (300 MHz, $CDCl_3$) spectra of the crude product mixture at different reaction times for the photocatalysis of benzylamine using **P4-1** as the photo-catalyst.

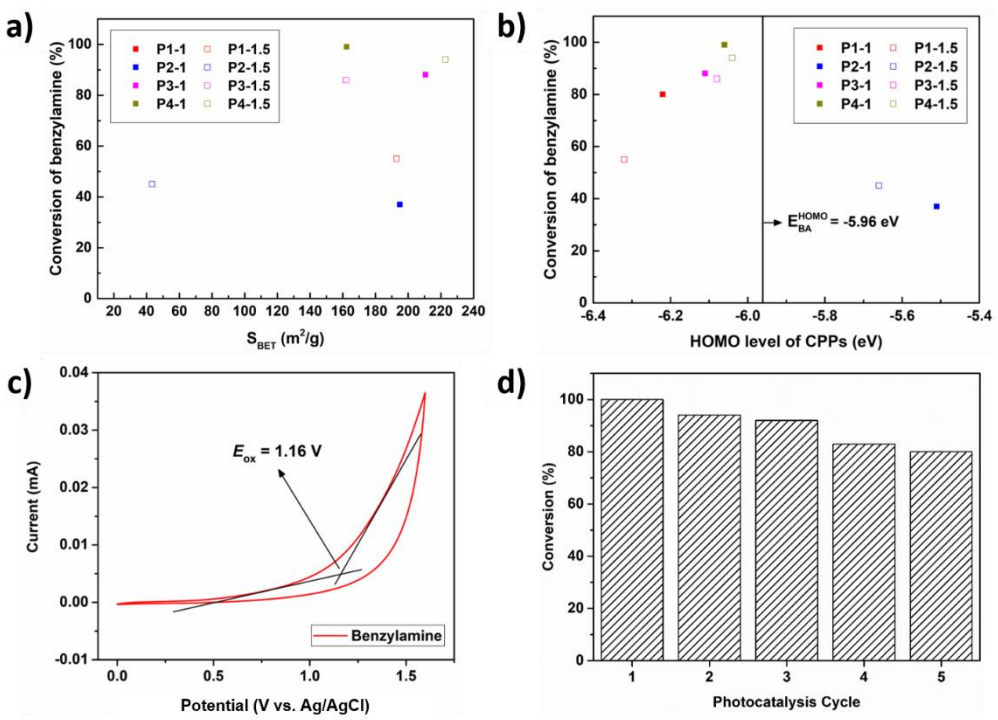

Figure 6.14 Correlation of the a) BET surface area and b) the HOMO level of triazine-based CPPs with the conversion of benzylamine. c) Cyclic voltammogram of benzylamine. d) Cycling experiments of the aerobic photocatalyzed oxidative coupling of benzylamine by **P4-1**.

the polymers tested here as the photocatalyst, **P4-1** and **P4-1.5** give the highest conversion (> 90%). Stability of **P4-1** was tested by recycling the catalyst over 5 photocatalytic cycles. Conversion upto 80% could be obtained from the 5th cycle, indicating the good reusability of **P4-1** in the photocatalytic reaction (**Figure 6.14d**).

We observed that triazine-core CPPs consisting similar building blocks gave similar conversion for benzylamine irrespective of the monomer ratio. Exceptions to this trend were **P1-1** and **P1-1.5** which gave conversions of 80% and 55%, respectively. No correlation between the performance of triazine-based CPPs as catalysts and their specific surface area could be found from our experiments (**Figure 6.14a**). For instance, **P2-1** with specific surface area of 195 m^2 g^{-1} gave a poor conversion value of 37% which is significantly lower than

those achieved by polymers such as **P1-1** (51%, S_{BET} = 75 m^2 g^{-1}) with smaller BET surface areas.

The superior performance of **P4-1** and **P4-1.5** can be attributed to the higher content of pyridinic nitrogen in the polymer structure, arising from the triazine rings in both constituent monomers. Similar enhancement of the photocatalytic activity has been observed in N-doped graphene quantum dots in the coupling of primary amines.[59] In addition, the potentials of the HOMO and LUMO levels of triazine CPPs relative to the energy potentials of benzylamine play the most crucial role in determining the photocatalytic performance. From previous reports,[51, 54, 56] it is known that the photo-oxidation of benzylamines proceeds by the formation of an excited state, CPP*, which in turn reduces molecular oxygen into its photo-generated active species – superoxide radical ($O_2^{\cdot-}$) and singlet oxygen ($^1O_2$) leaving behind CPP^+. Benzylamine is oxidized by CPP^+ to form a cationic intermediate and thereby regenerating CPP. Energy levels of triazine CPPs calculated by cyclic voltammetry are shown in **Table 6.2**. The LUMO levels of all polymers are higher than that of oxygen (-3.8 eV).[60] Therefore, photo-generated electron transfer from CPP* to O_2 is possible. Except for **P2-1** and **P2-1.5**, the HOMO levels of all polymers are lower than that of benzylamine (**Figure 6.14b**), which implies that the oxidation of benzylamine is feasible. Therefore, the low conversion of **P2-1** and **P2-1.5** can be mainly attributed to their higher HOMO level (lower oxidation potential) with respect to benzylamine which inhibits the oxidation reaction.

To analyse the effect of residual palladium (Pd) on the photocatalytic activity of triazine-based CPPs, we employed inductively coupled plasma-optical emission spectroscopy (ICP-OES) to measure the palladium content of CPPs that gave the highest (**P4-1**) and lowest (**P2-1**) conversion in the photo-oxidation of benzylamine (**Table 6.3**). We also treated **P4-1** with NH_4OH (28% in water) and ethylenediamine-tetraacetic acid (EDTA) according to a reported procedure[61] to lower the Pd content and the purified polymer was labelled **P4-1*.** The mean Pd content in **P4-1** and **P2-1** was found to be 2.7 ± 0.18 ppm and 4.0 ± 0.01 ppm, respectively, while the purified polymer **P4-1*** exhibited a Pd content of 1.5 ±

0.01 ppm. Moreover, the photocatalytic activity of purified polymer **P4-1*** was similar to that of **P4-1** (**Table 6.3**), implying insignificant effect of the residual Pd on the photocatalytic activity of the CPPs.

6.10 Conclusion

In summary, a series of triazine-based conjugated porous polymers were synthesized by direct arylation polymerization of 2,4,6-tri(2-thienyl)-1,3,5-triazine with tri- and tetra- brominated aryls using two C-H:C-Br ratios – 1:1 and 1.5:1. Optical properties of the polymers show that rational choice of monomers can be effective in systematically tuning the optical absorption of the polymers. Morphology of the polymers was found to vary with the choice and the molar ratio of the comonomers. In particular, **P2-1.5** exhibits an intricate morphology that evolves from non-uniform fibrillar structures to well-defined but bundled nano-fibres over the course of the reaction. Selective oxidation of benzylamine was used as a model reaction to demonstrate the photocatalytic activity of triazine-core CPPs. Conversions up to 99% were obtained when **P4-1** was used with relatively small catalyst loadings than organic photocatalysts reported in literature. Overall, these results demonstrate the ability of direct arylation coupling to synthesize robust, amorphous and nitrogen-rich conjugated porous polymers which can be used as redox active photocatalysts by reacting nitrogen containing building blocks with polytopic aryls. This modular approach towards the synthesis of CPPs offers much space to tune their optoelectrochemical properties and porosities that determine their performances as organic photocatalysts.

6.11 Experimental Section

6.11.1 Materials and Methods

1,3,5-Tribromobenzene (**M1**), tris-(4-bromophenyl)amine (**M2**) and 2,2',7,7'-tetrabromo-9,9'- spirobifluorene (**M3**) were purchased from Sigma Aldrich. 2,4,6-tri(thiophen-2-yl)-1,3,5-triazine **(TTT)**[34] and 2,4,6-tri(4-bromophenyl)-1,3,5-triazine **(M4)**[62] were synthesized according to literature procedure. All solvents were obtained from commercial sources and used as

received unless otherwise specified. ^{1}H-NMR was performed on a Bruker AV 300 spectrometer in deuterated chloroform ($CDCl_3$) at room temperature with TMS as internal reference; chemical shifts (δ) are reported in parts per million. Solid state ^{13}C magic-angle spinning nuclear magnetic resonance (MAS NMR) spectra were collected by a JEOL ECA 400 spectrometer. FTIR spectra were recorded on a Perkin Elmer Spectrum One FTIR spectrometer. Thermo-gravimetric analyses were performed on a Pyris Diamond TGA (Perkin Elmer) instrument, at a heating rate of 10 ^{o}C min^{-1} under N_2 atmosphere from 40 ^{o}C to 700 ^{o}C. SEM imaging was carried out using a JEOL JSM 6701F SEM (Scanning Electron Microscope) operating in scanning mode. Samples were prepared by depositing dry samples on aluminium stubs using an adhesive high purity carbon tape. TEM images were obtained using a Carl Zeiss Libra 120 Plus transmission electron microscope (TEM). Samples were prepared by depositing polymers from an ethanol dispersion onto a copper grid coated with ultra-thin carbon film. Nitrogen sorption isotherms were obtained at 77 K using Quantachrome Instruments Autosorb-6 with extra-high purity gases. All samples were degassed at 110 ^{o}C for 16 h in vacuum before analysis. Surface areas were calculated in the relative pressure (p/p_o) range from 0.05 to 0.35 of the adsorption branch. Pore size distribution was obtained by the Barrett–Joyner–Halenda (BJH) method using the adsorption curve of the isotherm. The total pore volume was estimated by the amount of nitrogen adsorbed at the relative pressure of 0.99. The UV-visible absorption spectra were obtained on a UV-visible spectrophotometer (UV-2450, Shimadzu). Cyclic voltammograms (CVs) were recorded on an CHI Electrochemical Analyzer Model 660D at room temperature using 0.1 M tetrabutylammonium hexafluorophosphate (Bu_4NPF_6) solution in CH_3CN as a supporting electrolyte at a scan rate of 100 mV/s. Glassy carbon was used as working electrode, platinum wire as counter electrode and silver as the reference electrode. Samples were prepared by drop-casting a slurry of polymers in Nafion on the glassy carbon electrode. All the potentials were calibrated with the standard ferrocene/ferrocenium redox couple (Fc/Fc^+). Powder X-ray diffraction patterns were obtained at 40 kV and 40 mA on a Bruker Advanced D8 XRD using Cu-Kα radiation (λ = 1.5418 Å) over 2θ range of 5.0° - 60° at room temperature.

Elemental analysis was carried out on a Vario EL III CHNS Elemental Analyzer. Palladium content was measured by inductively coupled plasma-optical emission spectrometer ICP-OES using Prodigy High Dispersion ICP. Samples were prepared by digesting the 10 mg of polymers in a solution of HNO_3 (70 %)/HCl (37 %) (2.5/0.5 v/v) at 120 ^oC for 2 days.[63]

6.11.2 General synthetic procedure of triazine based CPPs – PX-1

Measured quantities of **TTT** and **MX** (C-H : C-Br = 1:1), $Pd_2(dba)_3$ (5 mol %), (*o*-$MeOC_6H_4)_3P$ (10 mol %), K_2CO_3 (400 mol %) and PivOH (50 mol%) were added to a reaction vial charged with a magnetic stirring bar. *o*-xylene (0.2 M w.r.t. **TTT**) was added inside a glove-box and vial was sealed with a rubber cap. The reaction was carried out at 120 °C in an oil bath for 48 hours. After cooling to room temperature, the reaction mixture was diluted with THF and filtered under vacuum. The precipitates were washed with excess THF followed by 10% (w/v) HCl, water and finally methanol to remove soluble by-products. The precipitates were then subjected to Soxhlet extraction with chloroform and THF sequentially for 24 hrs with each solvent. The residual solids were collected and dried at 100 ^oC under vacuum to obtain the final product. **PX-1.5** was synthesized using the same synthetic procedure with a molar ratio of C-H:C-Br = 1.5:1 maintained between the corresponding two monomers.

P1-1 (65.5 mg, 53%): **M1** (96.2 mg, 0.305 mmol), **TTT** (100 mg, 0.306 mmol), $Pd_2(dba)_3$ (13.9 mg), (*o*-$MeOC_6H_4)_3P$ (10.8 mg), K_2CO_3 (168.5 mg), PivOH (15.8 mg) and *o*-xylene (1.52 mL). IR (KBr, cm^{-1}): 3075, 1537, 1500, 1466, 1373, 1032, 800, 776, 707 Solid state ^{13}C NMR (400 MHz) δ ppm: 167, 148, 140.5, 134, 130.5, 126.7. Elemental Analysis (%) Calculated for $C_{21}H_9N_3S_3$**:** C, 63.2; H, 2.3; N, 10.5; S, 24.1. Found: C, 59.5; H, 1.2; N, 8.6; S, 19.6.

P1-1.5 (110 mg, 90%) was synthesized using the same synthetic procedure with 64 mg (0.203 mmol) of **M1**. IR (KBr, cm^{-1}): 3075, 1537, 1500, 1466, 1373, 1032, 800, 776, 707. Elemental Analysis (%) Calculated for $C_{28.5}H_{12}N_{4.5}S_{4.5}$**:** C, 61; H, 2.1; N, 11.2; S, 25.7. Found: C, 59.5; H, 1.3; N, 9.6; S, 21.9.

P2-1 (155 mg, 89%): **M2** (147.39 mg, 0.305 mmol), **TTT** (100 mg, 0.306 mmol), $Pd_2(dba)_3$ (13.9 mg), (o-$MeOC_6H_4)_3P$ (10.8 mg), K_2CO_3 (168.5 mg), PivOH (15.8 mg) and *o*-xylene (1.52 mL). IR (KBr, cm^{-1}): 3025, 1594, 1537, 1439, 1500, 1368, 1316, 1037, 798, 770, 702. Solid state ^{13}C NMR (400 MHz) δ ppm: 167, 148, 146, 140, 126, 122. Elemental Analysis (%) Calculated for $C_{33}H_{18}N_4S_3$**:** C, 70.0; H, 3.2; N, 9.9; S, 17.0. Found: C, 66.7; H, 1.4; N, 8.3; S, 14.3.

P2-1.5 (134 mg, 75%) was synthesized using the same synthetic procedure with 97.9 mg (0.203 mmol) of **M2**. IR (KBr, cm^{-1}): 3025, 1594, 1537, 1422, 1500, 1368, 1316, 1037, 798, 770, 702. Elemental Analysis (%) Calculated for $C_{40.5}H_{21}N_{5.5}S_{4.5}$**:** C, 66.8; H, 2.9; N, 10.6; S, 19.8. Found: C, 66.7; H, 1.6; N, 9.0; S, 16.4.

P3-1 (141 mg, 83%): **M3** (144.91 mg, 0.229 mmol), **TTT** (100 mg, 0.306 mmol), $Pd_2(dba)_3$ (13.9 mg), (o-$MeOC_6H_4)_3P$ (10.8 mg), K_2CO_3 (168.5 mg), PivOH (15.8 mg) and *o*-xylene (1.52 mL). IR (KBr, cm^{-1}): 3063, 1500, 1436, 1373, 1039, 774, 713, 803. Solid state ^{13}C NMR (400 MHz) δ ppm: 168, 150.5, 140.5, 134, 126.5, 120, 65. Elemental Analysis (%) Calculated for $C_{135}H_{60}N_{12}S_{12}$: C, 72.6; H, 2.7; N, 7.5; S, 17.2. Found: C, 66.5; H, 1.5; N, 6.0; S, 13.6.

P3-1.5 (115 mg, 67%) was synthesized using the same synthetic procedure with 96.3 mg (0.152 mmol) of **M3**. IR (KBr, cm^{-1}): 3063, 1500, 1436, 1373, 1039, 774, 713, 803. Elemental Analysis (%) Calculated for $C_{165}H_{72}N_{18}S_{18}$: C, 68.8; H, 2.5; N, 8.8; S, 20.0. Found: C, 65; H, 1.3; N, 7.0; S, 15.8.

P4-1 (205 mg, 71%)**: M4** (250 mg, 0.457 mmol), **TTT** (150 mg, 0.457 mmol), $Pd_2(dba)_3$ (21 mg), (o-$MeOC_6H_4)_3P$ (16 mg), K_2CO_3 (252 mg), PivOH (23.3 mg) and *o*-xylene (2.3 mL). IR (KBr, cm^{-1}): 3074, 1603, 1576, 1447, 1500, 1364, 1039, 796, 773, 713. Solid state ^{13}C NMR (400 MHz) δ ppm: 170, 168, 149.5, 135.5, 128, 124. Elemental Analysis (%) Calculated for $C_{36}H_{18}N_6S_3$: C, 68.6; H, 2.9; N, 13.3; S, 15.2. Found: C, 65.4; H, 1.5; N, 11.1; S, 12.7.

P4-1.5 (245 mg, 85 %) was synthesized using the same synthetic procedure with 167 mg (0.306 mmol) of **M4**. IR (KBr, cm^{-1}): 3074, 1603, 1576,

1447, 1500, 1364, 1039, 796, 773, 713. Elemental Analysis (%) Calculated for $C_{43.5}H_{21}N_{7.5}S_{4.5}$: C, 66; H, 2.7; N, 13.3; S, 18.2. Found: C, 63.2; H, 1.3; N, 11.5; S, 16.0.

6.11.3 General procedure for photocatalyzed oxidative coupling of benzylamine

A 15 cm pyrex tube (1 cm dia.) was charged with 107 mg (1 mmol) benzylamine, 6 mg photocatalyst and 3 mL CH_3CN. The tube was sealed with a rubber septum and oxygen was bubbled into the solution at 1 atm. The tube was placed in a water bath and irradiated with 20W white LED lights for 5 hours. To test the stability of the photocatalyst, the polymers were recycled by first diluting the reaction mixture with THF and sonicating the solution for 5 minutes. The solution was then centrifuged at 8000 rpm for 8 minutes after which the solvent was decanted. This process was repeated three times to ensure removal of all reactants and products. The catalyst was then dried at 60^o C and reused for the next cycle.

6.11.4 Calculation of conversion of benzylamine from ^{1}H-NMR spectra

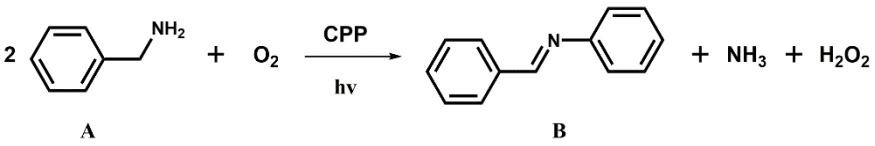

The above reaction can be reduced to the following:

$$2A \rightarrow B$$

For a ^{1}H-NMR spectrum of a mixture of two compounds A and B, the molar ratio of A to B (n_A/n_B) can be written as

$$\frac{n_A}{n_B} = \frac{(\text{Integral of A})/N_A}{(\text{Integral of B})/N_B} = \theta$$

Where, n_A and n_B are the moles of A and B in the product mixture,

while N_A and N_B are the number of protons represented by the peaks chosen.

Conversion (C) of A is defined as the ratio of moles of A reacted (n_A^R) to the initial number of moles of A in the reaction (n_A^0).

Therefore, $C = n_A^R / n_A^0$

Since 2 moles of A react to give one mole of B,

$n_A^R = 2n_B$, and $n_A^0 = 2n_B + n_A$

Hence, $C = \frac{2n_B}{2n_B + n_A}$

$$\frac{1}{C} = \frac{2n_B + n_A}{2n_B}$$

$$\frac{1}{C} = 1 + \frac{n_A}{2n_B}$$

$$\frac{1}{C} = 1 + \frac{\theta}{2}$$

$$C = \frac{2}{(2 + \theta)}$$

Conversion % =

$$C\% = \frac{2}{(2 + \theta)} * 100$$

6.12 References

1. Dawson, R.; Cooper, A. I.; Adams, D. J. *Prog. Polym. Sci.* **2012,** *37*, 530-563.

2. Xie, Y.; Wang, T.-T.; Liu, X.-H.; Zou, K.; Deng, W.-Q. *Nat. Commun.* **2013,** *4*, 1960.

3. Kaur, P.; Hupp, J. T.; Nguyen, S. T. *ACS Catal.* **2011,** *1*, 819-835.

4. Xu, F.; Chen, X.; Tang, Z.; Wu, D.; Fu, R.; Jiang, D. *Chem. Commun.* **2014,** *50*, 4788-4790.

5. Xiang, Z.; Cao, D. *J. Mater. Chem. A* **2013,** *1*, 2691-2718.

6. Xiang, Z.; Cao, D.; Dai, L. *Polym. Chem.* **2015,** *6*, 1896-1911.

7. Das, S.; Heasman, P.; Ben, T.; Qiu, S. *Chem. Rev.* **2017,** *117*, 1515-1563.

8. Slater, A. G.; Cooper, A. I. *Science* **2015,** *348*, aaa8075.

9. Xu, Y.; Jin, S.; Xu, H.; Nagai, A.; Jiang, D. *Chem. Soc. Rev.* **2013,** *42*, 8012-31.

10. Hao, L.; Ning, J.; Luo, B.; Wang, B.; Zhang, Y.; Tang, Z.; Yang, J.; Thomas, A.; Zhi, L. *J. Am. Chem. Soc.* **2015,** *137*, 219-225.

11. Zhu, J.; Zhuang, X.; Yang, J.; Feng, X.; Hirano, S.-i. *J. Mater. Chem. A* **2017,** *5*, 16732-16739.

12. Xie, J.; Gu, P.; Zhang, Q. *ACS Energy Letters* **2017,** *2*, 1985-1996.

13. Sakaushi, K.; Hosono, E.; Nickerl, G.; Gemming, T.; Zhou, H.; Kaskel, S.; Eckert, J. *Nat. Commun.* **2013,** *4*, 1485.

14. Vogiatzis, K. D.; Mavrandonakis, A.; Klopper, W.; Froudakis, G. E. *ChemPhysChem* **2009,** *10*, 374-383.

15. Hug, S.; Stegbauer, L.; Oh, H.; Hirscher, M.; Lotsch, B. V. *Chem. Mater.* **2015,** *27*, 8001-8010.

16. Wang, K.; Yang, L. M.; Wang, X.; Guo, L.; Cheng, G.; Zhang, C.; Jin, S.; Tan, B.; Cooper, A. *Angew. Chem. Int. Ed.* **2017,** *56*, 14149-14153.

17. Puthiaraj, P.; Lee, Y.-R.; Zhang, S.; Ahn, W.-S. *J. Mater. Chem. A* **2016,** *4*, 16288-16311.

18. Bhunia, A.; Vasylyeva, V.; Janiak, C. *Chem. Commun.* **2013,** *49*, 3961-3963.

19. Wang, X.; Zhang, C.; Zhao, Y.; Ren, S.; Jiang, J.-X. *Macromol. Rapid Commun.* **2016,** *37*, 323-329.

20. Ren, S.; Bojdys, M. J.; Dawson, R.; Laybourn, A.; Khimyak, Y. Z.; Adams, D. J.; Cooper, A. I. *Adv. Mater.* **2012,** *24*, 2357-2361.

21. Feng, X.; Ding, X.; Jiang, D. *Chem. Soc. Rev.* **2012,** *41*, 6010-6022.

22. Ren, S.; Dawson, R.; Laybourn, A.; Jiang, J.-x.; Khimyak, Y.; Adams, D. J.; Cooper, A. I. *Polym. Chem.* **2012,** *3*, 928-934.

23. Hayashi, S.; Togawa, Y.; Ashida, J.; Nishi, K.; Asano, A.; Koizumi, T. *Polymer* **2016,** *90*, 187-192.

24. Bohra, H.; Shao, J.; Huang, S.; Wang, M. *Tetrahedron Lett.* **2016,** *57*, 1497-1501.

25. Bohra, H.; Tan, S. Y.; Shao, J.; Yang, C.; Efrem, A.; Zhao, Y.; Wang, M. *Polym. Chem.* **2016,** *7*, 6413-6421.

26. Bohra, H.; Wang, M. *J. Mater. Chem. A* **2017,** *5*, 11550-11571.

27. Efrem, A.; Wang, K.; Amaniampong, P. N.; Yang, C.; Gupta, S.; Bohra, H.; Mushrif, S. H.; Wang, M. *Polym. Chem.* **2016,** *7*, 4862-4866.

28. Huang, J.; Wang, K.; Gupta, S.; Wang, G.; Yang, C.; Mushrif, S. H.; Wang, M. *J. Polym. Sci., Part A: Polym. Chem.* **2016,** *54*, 2015-2031.

29. Shao, J.; Wang, G.; Wang, K.; Yang, C.; Wang, M. *Polym. Chem.* **2015,** *6*, 6836-6844.

30. Wang, K.; Wang, G.; Wang, M. *Macromol Rapid Commun* **2015,** *36*, 2162-70.

31. Wang, K.; Wang, M. *Curr. Org. Chem.* **2013,** *17*, 999-1012.

32. Wang, X.; Wang, K.; Wang, M. *Polym. Chem.* **2015,** *6*, 1846-1855.

33. Wang, X.; Wang, M. *Polym. Chem.* **2014,** *5*, 5784-5792.

34. Leriche, P.; Piron, F.; Ripaud, E.; Frère, P.; Allain, M.; Roncali, J. *Tetrahedron Lett.* **2009,** *50*, 5673-5676.

35. Liégault, B.; Petrov, I.; Gorelsky, S. I.; Fagnou, K. *J. Org. Chem.* **2010,** *75*, 1047-1060.

36. Lombeck, F.; Matsidik, R.; Komber, H.; Sommer, M. *Macromol. Rapid Commun.* **2015,** *36*, 231-237.

37. Kundu, S. K.; Bhaumik, A. *ACS Sustainable Chem. Eng.* **2016,** *4*, 3697-3703.

38. Wang, Z.; Liu, J.; Fu, Y.; Liu, C.; Pan, C.; Liu, Z.; Yu, G. *Chem. Commun.* **2017,** *53*, 4128-4131.

39. Hauser, B. G.; Farha, O. K.; Exley, J.; Hupp, J. T. *Chem. Mater.* **2013,** *25*, 12-16.

40. Lafrance, M.; Fagnou, K. *J. Am. Chem. Soc.* **2006,** *128*, 16496-16497.

41. Meier, H.; Karpuk, E.; Christof Holst, H. *Eur. J. Org. Chem.* **2006,** *2006*, 2609-2617.

42. Li, L.; Cai, Z.; Wu, Q.; Lo, W.-Y.; Zhang, N.; Chen, L. X.; Yu, L. *J. Am. Chem. Soc.* **2016,** *138*, 7681-7686.

43. Sprick, R. S.; Jiang, J.-X.; Bonillo, B.; Ren, S.; Ratvijitvech, T.; Guiglion, P.; Zwijnenburg, M. A.; Adams, D. J.; Cooper, A. I. *J. Am. Chem. Soc.* **2015,** *137*, 3265-3270.

44. Jiang, J.-X.; Su, F.; Trewin, A.; Wood, C. D.; Niu, H.; Jones, J. T. A.; Khimyak, Y. Z.; Cooper, A. I. *J. Am. Chem. Soc.* **2008,** *130*, 7710-7720.

45. Huang, W.; Ma, B. C.; Lu, H.; Li, R.; Wang, L.; Landfester, K.; Zhang, K. A. I. *ACS Catal.* **2017,** *7*, 5438-5442.

46. Kim, B.; Park, N.; Lee, S. M.; Kim, H. J.; Son, S. U. *Polym. Chem.* **2015,** *6*, 7363-7367.

47. Ascherl, L.; Sick, T.; Margraf, J. T.; Lapidus, S. H.; Calik, M.; Hettstedt, C.; Karaghiosoff, K.; Döblinger, M.; Clark, T.; Chapman, K. W.; Auras, F.; Bein, T. *Nat. Chem.* **2016,** *8*, 310-316.

48. Baumann, M.; Baxendale, I. R. *Beilstein J. Org. Chem.* **2013,** *9*, 2265-2319.

49. Martin, S. F. *Pure Appl. Chem.* **2009,** *81*, 195-204.

50. Wu, J.-S.; Cheng, S.-W.; Cheng, Y.-J.; Hsu, C.-S. *Chem. Soc. Rev.* **2015,** *44*, 1113-1154.

51. Su, F.; Mathew, S. C.; Möhlmann, L.; Antonietti, M.; Wang, X.; Blechert, S. *Angew. Chem. Int. Ed.* **2011,** *50*, 657-660.

52. Park, J. H.; Ko, K. C.; Kim, E.; Park, N.; Ko, J. H.; Ryu, D. H.; Ahn, T. K.; Lee, J. Y.; Son, S. U. *Org. Lett.* **2012,** *14*, 5502-5505.

53. Huang, L.; Zhao, J.; Guo, S.; Zhang, C.; Ma, J. *J. Org. Chem.* **2013,** *78*, 5627-5637.

54. Wang, Z. J.; Garth, K.; Ghasimi, S.; Landfester, K.; Zhang, K. A. I. *ChemSusChem* **2015,** *8*, 3459-3464.

55. Wang, Z. J.; Ghasimi, S.; Landfester, K.; Zhang, K. A. I. *Adv. Mater.* **2015,** *27*, 6265-6270.

56. Kang, N.; Park, J. H.; Ko, K. C.; Chun, J.; Kim, E.; Shin, H.-W.; Lee, S. M.; Kim, H. J.; Ahn, T. K.; Lee, J. Y.; Son, S. U. *Angew. Chem. Int. Ed.* **2013,** *52*, 6228-6232.

57. Su, C.; Tandiana, R.; Tian, B.; Sengupta, A.; Tang, W.; Su, J.; Loh, K. P. *ACS Catal.* **2016,** *6*, 3594-3599.

58. Dong, C.-p.; Higashiura, Y.; Marui, K.; Kumazawa, S.; Nomoto, A.; Ueshima, M.; Ogawa, A. *ACS Omega* **2016,** *1*, 799-807.

59. Jeon, S.-J.; Kang, T.-W.; Ju, J.-M.; Kim, M.-J.; Park, J. H.; Raza, F.; Han, J.; Lee, H.-R.; Kim, J.-H. *Adv. Funct. Mater.* **2016,** *26*, 8211-8219.

60. Li, Q.; Batchelor-McAuley, C.; Lawrence, N. S.; Hartshorne, R. S.; Compton, R. G. *J. Electroanal. Chem.* **2013,** *688*, 328-335.

61. Bracher, C.; Yi, H.; Scarratt, N. W.; Masters, R.; Pearson, A. J.; Rodenburg, C.; Iraqi, A.; Lidzey, D. G. *Org. Electron.* **2015,** *27*, 266-273.

62. Tanaka, H.; Shizu, K.; Nakanotani, H.; Adachi, C. *Chem. Mater.* **2013,** *25*, 3766-3771.

63. Ashoka, S.; Peake, B. M.; Bremner, G.; Hageman, K. J.; Reid, M. R. *Anal. Chim. Acta* **2009,** *653*, 191-199.

Chapter 6 is published as Bohra, H.; Li, P.; Yang, C.; Zhao, Y.; Wang, M., "Greener" and Modular Synthesis of Triazine-Based Conjugated Porous Polymers Via Direct Arylation Polymerization: Structure–Function Relationship and Photocatalytic Application. *Polym. Chem.* 2018, *9*, 1972-1982. DOI: 10.1039/C8PY00025E

7. Summary and outlook

7.1 Summary

In this thesis, we have applied direct arylation polymerization to various π-conjugated building blocks to synthesize new linear polymers and conjugated porous polymers. Although the monomers chosen in this research work had been used in literature to synthesize high-performance materials for optoelectronic and photocatalytic applications, their synthesis involved tedious prefunctionalization and harsh chemical conditions. By using pre-optimized direct arylation conditions, we were able to incorporate these monomers in conjugated polymer systems and study their structure-function relationships. Detailed structural, optical and electrochemical characterization of all polymers was carried out. Moreover, we have also studied the morphology and surface area characteristics of conjugated porous polymers. Selected polymers were tested for optoelectronic and photocatalytic application and their performances were found to be comparable to materials synthesized through conventional coupling reactions.

We have demonstrated direct arylation coupling of a new acceptor molecule – naphthothiophenediimide (**NDTI**) by synthesizing small molecules and linear polymers using $Pd_2(dba)_3$ and (o-$MeOC_6H_4)_3P$ as the catalyst-ligand pair (Chapter 2). A donor-acceptor-donor (D-A-D) triad containing 9,9-dihexylfluorene as the donor was synthesized to test the regioselectivity of **NDTI**. Alternating polymers with fluorene and benzothiadiazole were also synthesized and their structural, optical and electrochemical characterization was presented. Although, the C-H activation of **NDTI** was successful under these preoptimized conditions, it should be noted that the molecular weights of **PNDTI-OF** and **PBDTI-BTz** obtained via DAP were lower than that of **NDTI**-based polymers synthesized by Stille and Suzuki coupling. To address the poor reactivity of **NDTI**, we propose a systematic and rigorous optimization of direct arylation reaction conditions with different catalyst-ligand pairs. Polymers

obtained from each trial should be tested for structural defects such as β-coupling to ensure the regioselectivity of **NDTI**.

In another linear polymer system, we used direct arylation to synthesize three polymers containing the new acceptor molecule – **BDTD** (Chapter 3). Molecular weights of **BDTD-**based polymers with benzodithiophene (**P1**) and quarterthiophene (**P3**) moieties were larger than their Stille coupling counterparts. OFET fabricated **P3** showed mobilities up to 1.4×10^{-3} cm^2 V^{-1} s^{-1} devices Photovoltaic devices for **P1** and **P2** showed maximum PCEs of 0.22% and 1.15% when solvent vapour annealing was employed in an inverted device architecture. **P3** devices also showed poor PCEs in the absence of additives (1.6%). However, addition of 1% DIO improved the PCE to 3.5%. We attributed the lower PCE of **P3** compared to an analogous polymer reported by Hou and co-workers, to the straight alkyl chains of **P3** which led to strong aggregation in thin films. To confirm this hypothesis, an analogue of **P3** containing ethylhexyl side chains should be synthesized and devices performances of the two polymers should be compared. Since **BDTD**-based polymers have consistently exhibited PCEs over 10%, a systematic study of the effect of chain length on device characteristic would be beneficial. To this end, a series of BDTD-quarterthiophene polymers with both straight and branched alkyl chains of varying lengths should be synthesized by DAP and the effect of chain length on V_{oc} and J_{sc} should be studied.

In this thesis, we have also demonstrated direct arylation as an efficient synthetic tool for conjugated porous polymers (CPPs). Thiophene-flanked monomers containing active C-H bonds were reacted with tri- and tetra-brominated aryls to give a series of conjugated polymers. In Chapter 4, we used a narrow bandgap electron-accepting building block ‑ thiophene-flanked thienothiadiazole (**TTD**), to synthesize three narrow bandgap CPPs by polymerizing with 1,35-tribromobenzene (**CPP-1**), tetrakis-4-bromophenylamine (**CPP-2**) and 2,2′,7,7′-tetrabromo-9,9′-spirobifluorene (**CPP-3**). Morphologies and porosities of the polymers were determined by the geometry of the monomer. **CPP-2** showed the narrowest bandgap below 1.3 eV

due to the largest extent of D‑A charge transfer between **TTD** and triphenylamine. These experimental results demonstrated that a rational selection of monomers enables the synthesis of a series of narrow bandgap conjugated porous polymers with tunable porosities, morphologies and optoelectronic properties.

Next, we expanded the library of CPPs synthesized by direct arylation by choosing three thiophene-flanked monomers ‑ 2,2’-bithiophene **(BT)**, 4,7-di(thiophen-2-yl) benzo[c][1,2,5] thiadiazole (**DTBT)** and 2,5-bis(2-octyldodecyl)-3,6-di(thiophen- 2-yl)-2,5-pyrrolo [3,4-c]pyrrole-1,4 (2H, 5H)-dione (**DPP)** (Chapter 5). These monomers were reacted with polytopic aryl bromides under direct arylation conditions similar to those used for TTD-based polymers and structure-function relationships of the resulting polymers were studied. All polymers exhibited poor specific surface areas except **S3** which had a BET surface area of 407 m^2 g^{-1}. Optical properties of the polymers showed that the band gaps and energy levels of CPPs can be fine-tuned by careful selection of thiophene-based monomers. DPP-based polymers exhibited layered structures which were exfoliated into thin sheets by dispersing the polymers in *o*-dichlorobenzene. These results demonstrate that bandgap, porosity and morphology of CPPs can be controlled by careful selection of monomers, allowing for the synthesis of new π-conjugated polymers for a variety of applications. In particular, the sheet-like morphology of DPP-based polymers such as **T3** make them potential candidates for optoelectronic materials. An extended 2D donor-acceptor polymer network assembled in a layered structure provides the ideal morphology for inter-molecular charge transfer while the dispersibility of **DPP**-based polymers in organic solvents makes the otherwise insoluble CPP solution processable.

Lastly, we synthesized triazine-based CPPs by reacting 2,4,6-tri(2-thienyl)-1,3,5-triazine (**TTT**) with tri- and tetra-brominated monomers using two C-H:C-Br ratios ‑ 1:1 and 1.5:1 (Chapter 6). Morphology of the polymers was found to vary with the choice and the molar ratio of the comonomers. In particular, **P2-1.5** exhibited an intricate morphology that evolved from non-

uniform fibrillar structures to well-defined but bundled nano-fibres over the course of the reaction. Selective oxidation of benzylamine was used as a model reaction to demonstrate the photocatalytic activity of triazine-core CPPs. Conversions up to 99% were obtained when **P4-1** was used with relatively small catalyst loadings than organic photocatalysts reported in literature. Overall, these results demonstrate the ability of direct arylation coupling to synthesize robust, amorphous and nitrogen-rich conjugated porous polymers which can be used as redox active photocatalysts by reacting nitrogen containing building blocks with polytopic aryls.

In summary, we have demonstrated that direct arylation is a facile and atom-efficient alternative to conventional coupling reactions for incorporating a wide variety of building blocks in linear (1D) and network (2D/3D) conjugated polymers.

7.2 Outlook

It is evident that direct C-H arylation coupling has been established as a mainstream synthetic technique for conjugated small molecules and polymers. Comparison of structural and optical properties reveals that polymeric products of direct arylation are comparable with those synthesized by conventional reactions.[1-5] Circumvention of tedious synthetic steps and absence of toxic organometallic byproducts make direct arylation a lucrative alternative to Stille and Suzuki coupling reactions.

Nevertheless, some challenges remain in improving this synthetic technique. Two decades after its first report, direct arylation has been established by various researchers as an efficient, defect-free[6-14] and broadly applicable C-C coupling reaction but a promising demonstration of its commercial applicability is yet to be seen. To become the synthetic tool of choice for photovoltaic materials, a seamless integration of direct arylation chemistry in the roll-to-roll device fabrication pipeline is crucial. This implies that the research focus should shift from new material development in one pot reactions and reaction optimization, to adapting the synthesis of existing high-performance materials

for large-scale continuous processes. Leclerc's group reported the first application of continuous flow method to DAP by synthesizing an isoindigo-*alt*-ethylenedioxythiophene polymer which showed moderate performance in solar cells (PCE = 3%).[15] Further development of the direct arylation protocol to facilitate continuous flow production is expected.

Typically, direct arylation reactions are catalyzed by expensive palladium catalysts in the presence of phosphine ligands, bases and aromatic solvents under inert conditions. For instance, $Pd_2(dba)_3$/P(*o*-$MeOC_6H_4)_3$ as the catalyst-ligand system and nonpolar (e.g. toluene, *o*-xylene) solvents as the reaction media has been proven to be highly efficient in synthesis of a broad range of well-defined D-A alternating copolymers.[16-17] Use of greener alternatives to aromatic solvents has already been demonstrated[18-19] but very few alternatives to palladium catalysts are known. Hence, development of relatively cheaper transition metal alternatives to palladium would greatly benefit the cost and scalability of direct arylation.

There is no doubt that DAP will continue growing as a promising, economic, and eco-friendly tool for the synthesis of a broad range of high performance π-conjugated polymers with tunable structures and properties for optoelectronic applications and beyond.

7.3 References

1. Marzano, G.; Kotowski, D.; Babudri, F.; Musio, R.; Pellegrino, A.; Luzzati, S.; Po, R.; Farinola, G. M. *Macromolecules* **2015,** *48*, 7039-7048.
2. Marzano, G.; Carulli, F.; Babudri, F.; Pellegrino, A.; Po, R.; Luzzati, S.; Farinola, G. M. *J. Mater. Chem. A* **2016,** *4*, 17163-17170.
3. Gruber, M.; Jung, S.-H.; Schott, S.; Venkateshvaran, D.; Kronemeijer, A. J.; Andreasen, J. W.; McNeill, C. R.; Wong, W. W. H.; Shahid, M.; Heeney, M.; Lee, J.-K.; Sirringhaus, H. *Chem. Sci.* **2015,** *6*, 6949-6960.
4. Berrouard, P.; Najari, A.; Pron, A.; Gendron, D.; Morin, P.-O.; Pouliot, J.-R.; Veilleux, J.; Leclerc, M. *Angew. Chem. Int. Ed.* **2012,** *51*, 2068-2071.

5. Livi, F.; Gobalasingham, N. S.; Thompson, B. C.; Bundgaard, E. *J. Polym. Sci., Part A: Polym. Chem.* **2016,** *54*, 2907-2918.

6. Pouliot, J. R.; Grenier, F.; Blaskovits, J. T.; Beaupre, S.; Leclerc, M. *Chem. Rev.* **2016,** *116*, 14225-14274.

7. Huang, J.; Wang, K.; Gupta, S.; Wang, G.; Yang, C.; Mushrif, S. H.; Wang, M. *J. Polym. Sci., Part A: Polym. Chem.* **2016,** *54*, 2015-2031.

8. Wang, X.; Wang, M. *Polym. Chem.* **2014,** *5*, 5784-5792.

9. Wang, X.; Wang, K.; Wang, M. *Polym. Chem.* **2015,** *6*, 1846-1855.

10. Shao, J.; Wang, G.; Wang, K.; Yang, C.; Wang, M. *Polym. Chem.* **2015,** *6*, 6836-6844.

11. Wakioka, M.; Kitano, Y.; Ozawa, F. *Macromolecules* **2013,** *46*, 370-374.

12. Wang, Q.; Takita, R.; Kikuzaki, Y.; Ozawa, F. *J. Am. Chem. Soc.* **2010,** *132*, 11420-11421.

13. Pouliot, J.-R.; Wakioka, M.; Ozawa, F.; Li, Y.; Leclerc, M. *Macromol. Chem. Phys.* **2016,** *217*, 1493-1500.

14. Morin, P.-O.; Bura, T.; Sun, B.; Gorelsky, S. I.; Li, Y.; Leclerc, M. *ACS Macro Lett.* **2015,** *4*, 21-24.

15. Grenier, F.; Aïch, B. R.; Lai, Y.-Y.; Guérette, M.; Holmes, A. B.; Tao, Y.; Wong, W. W. H.; Leclerc, M. *Chem. Mater.* **2015,** *27*, 2137-2143.

16. Gobalasingham, N. S.; Thompson, B. C. *Prog. Polym. Sci.* **2018,** *83*, 135-201.

17. Bohra, H.; Wang, M. *J. Mater. Chem. A* **2017,** *5*, 11550-11571.

18. Pankow, R. M.; Ye, L.; Gobalasingham, N. S.; Salami, N.; Samal, S.; Thompson, B. C. *Polym. Chem.* **2018,** *9*, 3885-3892.

19. Su, Y.-X.; Deng, Y.-H.; Ma, T.-T.; Li, Y.-Y.; Sun, L.-P. *Green Chem.* **2012,** *14*, 1979-1981.

APPENDIX

LIST OF ABBREVIATIONS AND ACRONYMS

(*o*-$MeoC_6H_4)_3P$	tris(*o*-methoxyphenyl)phosphine
AFM	atomic force microscopy
BDTD	benzo[1,2-c:4,5-c′]dithiophene-4,8-dione
BET	Brunauer-Emmet-Teller
BHJ	bulk heterojunction
BT	2,2'-bithiophene
Bu_4NPF_6	tetrabutylammonium hexafluorophosphate
CF	chloroform
CP	cross polarization
CPP	conjugated porous polymers
CV	cyclic voltammetry
D-A	donor-acceptor
DAP	direct arylation polymerization
DCB	*o*-dichlorobenzene
DIO	1,8-diiodooctane
DPP	3,6-di(thiophen-2-yl)-2,5-pyrrolo[3,4-c]pyrrole-1,4(2H,5H)-dione
DSC	differential scanning calorimetry
DTBT	4,7-di(thiophen-2-yl)benzo[c][1,2,5]thiadiazole
EDX	energy-dispersive X-ray
EI-MS	electron ionization mass spectroscopy
Fc/Fc^+	ferrocene/ferrocenium redox couple
FF	fill factor
FL	fluorescence
FTIR	Fourier-Transform infrared
GPC	gel permeation chromatography
Hermann's Catalyst	*trans*-Bis(acetato)bis[o-(di-o-tolylphosphino)benzyl]dipalladium(II)

HOMO	highest occupied molecular orbital
ICP	inductively coupled plasma
ITO	indium tin oxide
J_{sc}	short circuit current
LUMO	lowest unoccupied molecular orbital
m/z	mass-to-charge ratio
M^+	parent molecular ion
MAS	magic angle spinning
M_n	number-average molecular weight
M_w	weight-average molecular weight
NDTI	naphtho[2,3-b:6,7-b]- dithiophenediimide
NIR	near-infrared
NMR	nuclear magnetic resonance
OFET	organic field effect transistors
OPV	organic photovoltaic
OSC	organic solar cells
p/p_o	relative pressure
PCE	power conversion efficiency
$Pd_2(dba)_3$	tris(dibenzylideneacetone)dipalladium(0)
PDI	polydispersity index
PivOH	pivalic acid
PSD	pore size distribution
PXRD	powder X-ray diffraction
SEM	scanning electron microscopy
t	time
T_c	crystallization temperature
T_d	decomposition temperature
TEM	transmission electron microscopy
TGA	thermogravimetric analysis
THF	tetrahydrofuran
T_m	melting point

TTD	4,6-di(2- thienyl)thieno[3,4-c][1,2,5]thiadiazole
UV-Vis	ultraviolet-visible
V_{oc}	open circuit voltage

LIST OF SCHEMES

LIST OF FIGURES

LIST OF TABLES

LIST OF PUBLICATIONS

1. Bohra, H.; Li, P.; Yang, C.; Zhao, Y.; Wang, M., "Greener" and Modular Synthesis of Triazine-Based Conjugated Porous Polymers Via Direct Arylation Polymerization: Structure–Function Relationship and Photocatalytic Application. *Polym. Chem.* **2018**, *9*, 1972-1982. DOI: 10.1039/c8py00025e

2. Bohra, H.; Wang, M., Direct C-H Arylation: A "Greener" Approach Towards Facile Synthesis of Organic Semiconducting Molecules and Polymers. *J. Mater. Chem. A* **2017**, *5*, 11550-11571. DOI: 10.1039/c7ta00617a

3. Bohra, H.; Tan, S. Y.; Shao, J.; Yang, C.; Efrem, A.; Zhao, Y.; Wang, M., Narrow Bandgap Thienothiadiazole-Based Conjugated Porous Polymers: From Facile Direct Arylation Polymerization to Tunable Porosities and Optoelectronic Properties. *Polym. Chem.* **2016**, *7*, 6413-6421. DOI: 10.1039/c6py01453d

4. Bohra, H.; Shao, J.; Huang, S.; Wang, M., Facile Synthesis of Naphthodithiophenediimide Based Small Molecules and Polymers Via Direct Arylation Coupling. *Tetrahedron Lett.* **2016,** *57*, 1497-1501. DOI: 10.1016/j.tetlet.2016.02.081

5. Wang, K.; Chen, H.; Wei, X.; Bohra, H.; He, F.; Wang, M., Over 7% Photovoltaic Efficiency of a Semicrystalline Donor-Acceptor Polymer Synthesized Via Direct Arylation Polymerization. *Dyes Pigm.* **2018**, *158*, 183-187. DOI: 10.1016/j.dyepig.2018.05.036

6. Efrem, A.; Wang, K.; Amaniampong, P. N.; Yang, C.; Gupta, S.; Bohra, H.; Mushrif, S. H.; Wang, M., Direct Arylation Polymerization Towards Narrow Bandgap Conjugated Microporous Polymers with Hierarchical Porosity. *Polym. Chem.* **2016**, *7*, 4862-4866. DOI: 10.1039/c6py00719h